Engineering Biomaterial Properties for T Cell Immunotherapy

by

John W Hickey

A dissertation submitted to Johns Hopkins University in conformity with the requirements for the degree of Doctor of Philosophy.

Baltimore, Maryland

February 2019

Abstract

Immune cell therapies have revolutionized our idea of a drug. Essentially they are a living drug becoming increasingly used because of their specificity (antigen targeting), durability (memory cells), and success seen in the clinic. Yet immune cell therapies, such as T cell immunotherapies, face substantial challenges for widespread adoption, including difficulty in target identification, complexity, cost, and inability to maintain and control cell function ex vivo. To solve issues facing T cell immunotherapies I engineered several novel biomaterials. I engineered magnetic particles to enrich and detect antigen-specific T cells in high-throughput which extends our capability to detect hundreds of antigen-specific T cells at once. This enables a greater understanding of the adaptive immune responses and also facilitates tailoring a precision medicine approach to antigen-specific T cell therapies. I also engineered extracellular matrix hydrogels for *ex vivo* and for *in vivo* stimulation, which preserves and improves cellular function and reduces the cost and labor, decreasing barriers to patients in the future. Finally, the engineering process for optimal properties of these biomaterials also revealed key biology of T cells such as nanoscale receptor organization and mechanical and environmental influences of T cell activation.

Thesis Committee

Jonathan P. Schneck, M.D. Ph.D. (primary adviser, *reader)*

Professor, Department of Pathology

Johns Hopkins University School of Medicine

Hai-Quan Mao, Ph.D. (*reader*)

Professor, Department of Materials Science and Engineering

Johns Hopkins University

Jordan J. Green, Ph.D.

Professor, Department of Biomedical Engineering

Johns Hopkins University School of Medicine

Andrea Cox, M.D. Ph.D.

Professor, Department of Medicine

Johns Hopkins University School of Medicine

Acknowledgements

I am incredibly grateful to have had the opportunity to do a PhD. My success is the result of hundreds of people and institutions whom have supported me in my journey and education. This acknowledgement section will thus be horribly incomplete, but I will do my best to thank and recognize all who have supported me specifically during my time at Johns Hopkins University.

First, the Johns Hopkins Biomedical Engineering Department has been behind me 100% of the time and supportive of me every step of the way. One of the reasons that I decided to come to Johns Hopkins University was because I recognized that the Department actually cares about their students' wellbeing and their students' success. I have to say that a lot of this is because of Hong Lan who is the most excellent BME PhD Program manager that I know. I do not know how she accomplishes all she does for each one of us (more than 200 of us I think) and still make each one of us feel special. Thank you Hong for all of your help over the past 5.5 years.

One of the things the Department helped me out with was the ability to rotate with different advisers. This was another critical factor in deciding to come to Johns Hopkins because I had little idea to the research I wanted to spend the next several years of my life dedicating myself to. Here I need to acknowledge that what was supporting my rotations was an NIH T32 training grant and I am very grateful to the NIH for these programs and the money that is spent in developing students to become researchers. Beyond this support I was also given an INBT (Institute for Nanobiotechnology) cancer research training grant to work together with Dr. Hai-Quan Mao and Dr. Jonathan Schneck being co-advised, which though unusual allowed me to have advice, mentoring, flexibility, and

resources from both laboratories during my time at Johns Hopkins University. Then with their help, I was able to write a successful NSF graduate fellowship which then funded the last three years of my PhD. I now strongly support the generous support of the U.S. government to young scientists because this fellowship allowed me to be more innovative and independent in the projects I pursued during my PhD rather than just working on established projects. These awards have snowballed and resulted in an ARCS foundation scholarship. This scholarship was generously given by private donors and was for traveling and presenting at conferences, going to mini-courses, and professional development. This single award helped me to a) establish and publish my research in academic, commercial, and clinical settings, b) understand what I wanted to do in the future, and c) help me network for a postdoctoral fellowship. I am very grateful for generous individuals that give and for the ARCS foundation which coordinates these efforts. Finally, I received a Siebel Scholar award, which has allowed our family to not worry about finances so much as we have been finishing up the PhD and searching for a postdoctoral fellowship position.

In the same vein I should say that one of the reasons that I have been able to receive all of these awards is because of Johns Hopkins University. The reputation carries a lot of weight with donors, but also there is an incredible support staff that seeks out these opportunities and creates even more for the students who attend. Indeed one such opportunity JHU has produced has been my involvement with the group *Medical and Educational Perspectives*. This is a non-profit group which focuses on helping students commercialize the products or research they complete both with medical applications in the developing world and in the developed world. The Provost's office at JHU sponsored

a grant that funded this group and allowed me to take a class in medical device commercialization for developing countries, and then travel with a team of biomedical engineers to India to work on a new material for affordable prosthetic legs. This was a once-in-a-lifetime experience and I am so grateful that I could go and for what I learned. Maybe even more so, I am grateful for the friends that I developed through this course and trip: Carmen Kut and Akhila Denduluri—both leaders of the *MEP* organization. I then joined the team leadership and continued on from there in our escapades to improve student entrepreneurship education at JHU, public health campaigns, and high-school outreach. Along the way we added others to the team—Meg Chow, Alina Predescu—all are incredibly talented, academically acclaimed, but most of all good friends and I thoroughly enjoyed working with and learning from during my time at JHU.

Needless to say, those from *MEP* were not the only people that I admired or was mentored by. In fact because Hopkins offers so many different activities and opportunities, I had many. One of my passions is teaching. The Center for Educational Resources at JHU had just started a program called the *Preparing Future Faculty* program. Kelly Clark and Mike Reese really have spearheaded these efforts. I joined at the end of my first year because of my interest in teaching and completed the program within a year. Through the process I was amazed at the time and energy that went into such a program, which is something not directly recognized as being any one person's responsibility at the school. Nevertheless, all events were excellent and helped to shape the way I teach and approach teaching as more of an experiment and a science project. Kelly was exceptionally good at creating new opportunities and letting me know about them as well. She put together the first *Teaching as Research* cohort which I joined. It

was the first time I did a research project and she spent a lot of time with me and others to help us understand how to develop a project and present one as well. She also put together the first ever *Teaching Shark Tank* which I also entered and won. This then started a cascade of events where she was very involved in helping me to create the app *Tcrunch* for improved student teacher communication and is still helping me. She always has impressed me as someone fully competent and very intelligent but mostly cares about the students at JHU.

In line with teaching mentors, I was also very fortunate to have a teaching assistantship under Dr. Eileen Haase. I like to think of her as the heart of the JHU BME teaching program that pumps life into the whole department because of all the courses she has developed and manages for the entire curriculum. After observing her teaching in the course I TA'd with her, she observed also my love of teaching as I had created and taught two undergraduate *Immunoengineering* courses, one for the developing world and the other for the developed world. She offered to me to develop an online *Immunoengineering* Master's level course. This, being a 3-credit course created from scratch, in an online environment that I had never encountered, was daunting, yet with her encouragement I pursued this alongside Elana Ben-Akiva—another BME PhD graduate student. Dr. Haase was extremely patient with both of us as it took us nearly two times as long to develop the content than we had promised and also worked closely giving us personalize feedback and advice for how to develop the course and how to arrange and present the content. I have and will look up to Dr. Haase as a teacher for inspiration in my own teaching in the future.

Beyond extracurricular activities that JHU offers, JHU provides an extremely fertile soil for research. One of the best things that it does is bring the brightest individuals to lead research and train other scientists in the process. I can comfortably say that the members of my thesis committee—Dr. Jonathan Schneck, Dr. Hai-Quan Mao, Dr. Jordan Green, and Dr. Andrea Cox—are among some of the brightest and nicest people at JHU. They have been instrumental in helping to originally steer me to focus my original research interests and later keep me focused on the most interesting aspects of my projects and helping provide additional professional advice for my career. I am extremely grateful for the time that they take out of their busy work schedules to support the development of students and their projects including my own.

Indeed my thesis advisers Dr. Hai-Quan Mao and Dr. Jonathan Schneck have done the most for me at JHU; they have been like research fathers to me. First, Dr. Mao. I am incredibly grateful that I was able to meet Dr. Mao at the JHU BME PhD interview weekend. Dr. Mao was one of the nicest people that I met that weekend and felt like I immediately resonated with and was another reason that I chose to do my PhD at JHU. For this reason I knew that I wanted to first rotate with Dr. Mao. Even though I thought that I wanted to do a tissue engineering research project, he had the foresight to convince me to work on an immunoengineering malaria vaccine nanoparticle project. If Dr. Mao had not done this, I would not have fallen in love with immunology and have taken the medical school *Immunology* course that Dr. Schneck leads. This move essentially changed my entire career. I am grateful for his foresight and advice. What's more, once I fell in love with immunology, Dr. Mao was open and even encouraged me to do rotations in more immunology-focused laboratories including Dr. Schneck's lab instead of keeping

me on the malaria vaccine project which he may have needed students to continue. This was very unselfish and another reason I am grateful to have Dr. Mao as a mentor where he is always looking out for me as a student first. After rotating, I am incredibly glad that he was alright with being a co-adviser and also starting a brand new project with Dr. Schneck. Looking back it must have taken a lot of trust to allow a 2nd year BME graduate student to start a project that I had come up with myself between a new lab and not keeping me to himself. I am grateful for his trust and patience with my progress over the past 5.5 years. One thing that surprised me about PhD research was how long everything took, especially biological experiments, and I definitely thought that I would achieve more progress in my projects than I have, but I am glad that Dr. Mao was also patient when things did not originally work out or come to fruition and he worked with me carefully to try and troubleshoot the problems we were encountering. One of the most important things that has helped me during my PhD is the confidence he has always exuded in me. Even when it was hard for me to believe in myself, Dr. Mao always had good things to say about me. This has helped me move forward when I was bogged down with research dead-ends. I have thoroughly enjoyed working with Dr. Mao and hope to keep that friendship and mentor relationship in the future. Thank you Dr. Mao for everything.

I can also not say how grateful I am to Dr. Jonathan Schneck. He allowed me to do a rotation in the laboratory even though I had very minimal biology background coming from an undergraduate degree in chemical engineering. I immediately recognized the time and effort that he puts in to create and maintain a wonderful lab culture that felt like a lab family. I felt at home in the lab environment and was one of the reasons I

decided to join the lab after I had completed the rotation projects. I have enjoyed this environment and the people that he has brought and kept in the lab since that time. This alone probably has increased my basal sanity and happiness in lab in order to focus on my research. I was excited as a young graduate student to contribute and it is incredible to look back and understand how naïve I was in my rotation project, yet Dr. Schneck was still very encouraging. I remember I went into his office to present my results from different types of chemical conjugations to particle surfaces of antibodies and their use as aAPCs and I had produced a cost-comparison for how much each aAPC would be and also their relative efficacies. I remembered him laughing but congratulating me thinking like an engineer even though that was definitely not the focus of the project or research in general where we were more focused on the T cell. He helped guide me then and through the years of what a scientific question is, what appropriate controls to think of, how to dissect it through experiments, and how to thoroughly analyze the results to probe more about biology and not necessarily just produce a new technology. He has definitely made research more than a routine or optimization process as I might have more done without his guidance. He also did this with little micro-managing which I can imagine is not the natural tendency for most bosses. He gave me the freedom and space that I really needed to grow into someone who could ask and answer independent questions and has given me the confidence I need in going forward with an aim to become a professor myself. This involved letting me tinker around in lab, and delaying when he saw the data even though this was probably frustrating at times. Despite being more hands-off with my daily experiments, I am also grateful for how available he made himself through the years. I can understand that life as a PI can be incredibly busy with all the grants, papers,

university service, classes, and corporate commitments that might come with that. I loved it when he would stop in lab and check up on us to talk about science, our families, or his own family. I also could not ask for a more understanding adviser. There are countless examples that I could give, but I will limit to four major ones. First, my wife and I added two young children to our family while I was a PhD student and Dr. Schneck's response when he found out was "Congratulations!" and not necessarily "Why now?" like many others may have been. He has been supportive of my role as father which means an incredible amount to me. Second, as I already mentioned I love teaching, and with teaching being an elective part of the BME PhD program he could have hesitated to let me do 1 or 2 or even the 7 classes that I taught while I was here, but he never objected but encouraged me to pursue what interested me. Third, I have loved to mentor and he has been supportive of me having sometimes up to four extra students in the lab following me around and working towards our projects. Fourth, when I was going to set my thesis defense time he was flexible for me to do that earlier so my parents could attend even if it would mean me graduating earlier than when I am leaving. What's more, I have learned so much from Dr. Schneck of how to be a mentor, as he has taken the time to work with me through papers, grants, and the inner-workings of university life. These insights have been priceless to my future career and not necessarily a programmed curriculum of a PhD student. Additionally, Dr. Schneck has always supported me in my applications to a myriad of opportunities and always spoke highly of me in his recommendation letters so that I could receive several awards while at JHU. Dr. Schneck is an incredible person, and while he is always saying that I might postpone my

graduation until 2020, I truly feel that it will be a sad day when I am not a student in his lab anymore. Thank you Dr. Schneck for everything.

I could not thank Dr. Schneck without thanking the Schneck lab. Everyone has been not only a fantastic help to me, but also a good friend and like a lab family to me. I was always happy to see Norma, she always asked about me and my boys. I think that I showed her more pictures of my sons than anyone and she never told me to stop, which is impressive. I am grateful for all the meetings she helped me to schedule and taking care of all the administrative things—she never complained no matter how many times I knocked on her door and always had time for me. Her and Joanie were like the "lab moms" and always took care of us. I was also so grateful to have Joanie as a cubicle buddy even though she probably was annoyed daily with my big chair, dozens of undergraduates, and stuff everywhere. It was so nice to have someone to talk to about experiments or reagents or children that she had years of experience with—she was definitely the Wikipedia of the group and also the baker. I am also grateful for the core group of PhD students in the lab: Alyssa Kosmides, Ami Bessell, and Ariel Isser who have been excellent friends and people to work with these past several years. I am extremely grateful for Alyssa and Ami for training me in "immunology" and its techniques in the lab. They were also so helpful in bouncing ideas off of to get whether they really sounded crazy and how to approach problems I was having with my projects. They helped time pass in the tissue culture room while waiting for cells to centrifuge with our conversations. Now this includes Ariel who has been an excellent addition to the team and has helped tremendously with his mathematical and computational approaches to problems and within my thesis work. I am also grateful for the other people and

students I have met while in the lab: Kristy Chu, Christian Schultz, Juan Varela, Carl Harupt, NK, Joe Sabatino, JW Sidholm, and Bo-yi Sung.

I am also grateful for the chance to mentor so many students while I have been at Johns Hopkins University. I started out in my first year where I mentored four high school students and it ballooned from there. My first undergraduate was Fernando, and I am also grateful for his patience, enthusiasm, and commitment which was required because I was such a naïve mentor. I learned a lot of things from doing the wrong thing as a mentor with him—thank you Fernando. From that experience I loved mentoring undergraduates so much that I continued after he left with Kayla Gee, Sebastian Salathe, Wasamah Shaikh, Jae Chung, Manjari Sriparna, and Giacomo Taylor. I have enjoyed each of these relationships and grateful for their help on my projects. Additionally, I was similarly able to mentor and work with rotation graduate students while at JHU: Ariel Isser, Mary Omootoso, Natalie Livingston, Ian Bettencourt, Yi Dong, Meng-Hsuan Hsiao, and Mekha Thomas. I am grateful for the relationships that we were able to develop and the help that they provided me in my research.

In addition, my research has benefited from the collaborative environment that JHU promotes. I am grateful for Dr. Jordan Green and his group for all the time that we worked together on the PLGA/PBAE and shape particle projects and for the opportunity to talk about science at a table of sometimes up to 9 scientists to discuss avenues to push the science forward. Also, more recently I am grateful to Dr. Sharon Gerecth and Hawley Pruitt for their collaborative work in imaging T cells with our hydrogels. The collaborations have helped me learn how to work more efficiently with others and to learn the value of working together on multidisciplinary projects.

I could not finish these acknowledgements without thanking my parents. They have sacrificed so much so that I could have not only a childhood to explore my talents and interests, but also a fun childhood. This helped down the road when I had to choose a direction for a career and my father was helping me to look through majors in realizing I loved science and math. The environment they created for me was incomparable and priceless and I would not trade it for anything. They have also been incredibly supportive even though I live thousands of miles away with their only grandchildren, I have never heard them complain about this. I am most grateful for their love throughout the years, where I have felt validated no matter how well I did in school or now during my PhD, I knew that they loved me. This is an incredible force; and it is an actionable force where they acted on it. My dad would often check that I was taking care of myself and keeping a broader perspective and maintaining a good work-life balance. My mom would often ask about my research even if she did not know what was going on and be thrilled with even the littlest of accomplishments helping me feel valued. They are the best parents that I could have asked for and I would not have been able to succeed without the foundation they created for me and within me as a child. Thank you mom and dad. I am also so grateful for all the rest of my family including my siblings, in-laws, and grandparents for their support and cheering me on through this process.

Finally, I have to most thank my wife Jenna. This PhD should also be hers for the amount of encouragement, support, inspiration, energy, sacrifice, and help she has given to me. It was her who got me interested in biology when we were first dating at our undergraduate institution when she would tell me everything she was learning about in her Neuroscience major. She also inspired me and encouraged me to not accept a stable,

high-paying job offered to me directly out of undergrad doing chemical engineering, but to go to pursue my dream of becoming a professor in doing biomedical engineering research, mentoring, and teaching. In the process, she also sacrificed a lot. She sacrificed a relatively straightforward financial way of life with this career as opposed to the chemical engineering career for one of many years of graduate student stipend reduced through family health care costs in a more expensive city. Also, we did not get into our top graduate schools of choice in the same location and she gave up her top choices and reapplied in the places that I had been accepted for graduate school. Her selflessness is unsurpassable. After finishing her Master's degree, she gave birth to our son James, an impressive task in itself, but then modified her teaching schedule to only teach one section of Biology as an Adjunct Professor at nights so she could take care of him during the day, and now taken a break from working in taking care of James and Benjamin (our second son). I appreciate so much her role in our family as a mother where she most expertly nurtures and teaches our children important, meaningful life lessons and principles which will guide them and benefit them throughout their life, while also taking care of countless dirty diapers, tantrum toddlers, dirty clothes, dinners, late nights with babies, and taking care of me after long days of lab where all my experiments failed and encourages and inspires me to be a better scientist, mentor, teacher, and to do all of the things for the right reasons. For this reason, thoughts of her and our boys inspire me often to work harder and more diligently at my research. Just one of the million examples of her continued support and sacrifice was that she was okay with me traveling this past year to nearly 10 different conferences, courses, or interviews, while she had our boys alone at home. I could not and would not have made it this far without her, and am so

incredibly grateful to her for her support and love in this process and cannot fully express it and so happy we will always be a team in the future.

In summary it is hard to sum up the contributions of people you love and who love you for the past 5.5 years in just several pages. But truly I am grateful to you all and I would not be the person I am now nor have reached the position I have without all of you!

Table of Contents

List of Figures

Chapter 1. Summary and Organization of the Dissertation

The organization of the dissertation is as follows:

Chapter 2 provides an overview of the importance of T cells in the adaptive immune response and their current clinical importance. Furthermore, it focuses as a broad introduction to the field of what has been done in terms of engineering T cells with techniques such as biomaterials. Finally, it distills critical design constraints to consider when designing and engineering a platform to interact or modulate T cells. This was published as a book chapter with the following information: “Hickey, John W., Alyssa K. Kosmides, and Jonathan P. Schneck. "Engineering Platforms for T Cell Modulation." International review of cell and molecular biology 341 (2018): 277-362.”

Chapter 3 is the manuscript: Hickey, John W., et al. "Biologically inspired design of nanoparticle artificial antigen-presenting cells for immunomodulation." Nano letters 17.11 (2017): 7045-7054. The data and story center around using information about nano-scale organization of cell receptors and designing effective cell-modulating/signaling nanoparticles. More specifically, we engineered artificial antigen presenting cells (aAPCs) by both size and ligand density that can activate antigen-specific CD8+ T cells for immunotherapeutic applications.

Chapter 4 is the manuscript: Hickey, John W., et al. "Efficient magnetic enrichment of antigen-specific T cells by engineering particle properties." Biomaterials 187 (2018): 105-116. The data and story center around probing the nanoparticle biomaterial design space (size, ligand density, ligand choice, concentration) to increase

antigen-specific T cell enrichment while considering T cell biology. Here we create nanoparticle artificial antigen-presenting cells (aAPCs) that both enrich and expand antigen-specific CD8+ T cells to levels necessary for both diagnostic and therapeutic applications. This quantitative analysis and investigation to nanoparticle design properties was lacking within both the fields of cell-modulating/enriching particles and aAPC technology.

Chapter 5 is the manuscript Hickey, John W., et al. "Increasing the Throughput and Adaptability of Nanoparticle Tools to Isolate and Identify Many Antigen-specific T cells." In Preparation. The data and story center around engineering both magnetic particle properties and the methods of enriching and expanding rare antigen-specific T cells for detection. We build off our work in Chapters 3 and 4 to use larger, more effective 300 nm aAPCs to enrich and expand antigen-specific T cells in a higher-throughput 96-well plate. What's more, we create universal aAPC and detection beads to multiplex the system further. This work provides a platform to increase the throughput of enrichment and expansion and increase its adaptability and adoption by other laboratories.

Chapter 6 is the manuscript Hickey, John W., et al. "Engineering an Artificial T-Cell Stimulating Matrix for Immunotherapy." Advanced Materials. Resubmitted. The data and story center around the creation of a novel, artificial T cell stimulating Matrix (aTM) from extracellular matrix (ECM) hydrogels for immunotherapy applications. We use a clinically relevant model of adoptive T cell transfer, to test T cells stimulated by our new material and compare to traditional materials used to activate T cells. We show significant tumor burden delay in an established, aggressive, immunosuppressive murine

melanoma with endogenous, antigen-specific T cells stimulated on the aTM compared to traditional methods of T cell activation. We investigated important material properties key for the significant increase in tumor efficacy. We found both the stiffness of the aTM was critical due to the mechanically sensitive signaling through the TCR (T cell receptor) in both murine and human T cells. Furthermore, we explored the how the extracellular matrix (ECM) influences T cell stimulation and memory phenotype, which has not been previously explored in the context of T cell stimulation. It is the unique combination of both of these parameters that increases T cell activation and skew the phenotype polarization during T cell expansion producing more functional, phenotypically memory T cells. What's more, we utilized this new material with an optimized parameter set, to provide both antigen-specific and pan-T cell activation in both murine and human systems, which has important implications for both CAR T cell and adoptive T cell therapy, ACT.

Chapter 7 is a summary of my contributions to other projects not directly my own. This includes the work I have done in collaboration with Dr. Green's lab in creating and testing polymeric, biodegradable aAPCs for T cell activation and immunotherapy and my contribution to other student's projects within the lab. Here I will summarize major findings rather than in great detail and will not show data as these were not my primary thesis projects.

Chapter 8 is a general summary of my chapters and outlines potential future work that could be done along with some preliminary data that is not included in the previous chapters.

Chapter 2. Engineering Platforms for T Cell Modulation[1]

2.1 Introduction

The immune system is a complex organization of many different cell types that protect the human body from infection and disease. This cellular network is made up of innate and adaptive immune cells that can detect and eliminate pathogens with extreme precision. The ability of immune cells to provide constant surveillance and protection throughout the entire human body makes it a powerful shield against foreign material. However, deficiencies in this system can expose vulnerabilities or result in disease. In these cases, therapeutics have been developed to modulate the immune response for more favorable outcomes.

Within the adaptive compartment exist T cells, a subset of lymphocytes responsible for cell-mediated immunity. T cells can detect and destroy infected cells while leaving other nearby healthy cells unharmed. Their precision and cytotoxic ability make T cells a popular target for immunotherapies. Because of their complex activation pathways, interaction with other cell types, and biodistribution, many emerging therapeutics utilize engineering concepts to mimic or alter their normal response. Here, we will review these immunoengineering approaches for modulating the T cell response.

[1] This chapter is reprinted (adapted) with permission from "Hickey, John W., Alyssa K. Kosmides, and Jonathan P. Schneck. "Engineering Platforms for T Cell Modulation." International review of cell and molecular biology 341 (2018): 277-362." Copyright 2018 Elsevier.

2.1.1 The T cell response

Minimally, T cells require two signals for activation—signal 1, a specific peptide presented in the context of the major histocompatibility complex (MHC), and signal 2, a co-stimulatory signal such as B7/anti-CD28 monoclonal antibody (mAb).[1] The peptide-MHC complex presented by an antigen presenting cell interacts with the T cell via its T cell receptor (TCR) and is what confers the specificity of the T cell's activation. Signal 2 provides co-stimulation and is required for the activation of naïve T cells. B7 on an antigen presenting cell, which interacts with CD28 on the T cell, is thought of as the prototypical co-stimulatory molecule, although many different co-stimulatory molecules exist that modulate the T cell expansion, phenotype, and functionality.[2–11] T cells are also exposed to a third soluble signal, signal 3, that modulates their activity, including pro-inflammatory or anti-inflammatory cytokines, which are released in an autocrine and paracrine fashion.[12]

Before activation, TCR are pre-clustered in small 35-70 nm islands with 7-30 TCRs per island.[13] Upon recognition of cognate antigen, these nanoclusters begin to concatenate and form what is known as the immune synapse.[14] The lateral organization of the microscale immune synapse is defined by supramolecular activation clusters, or SMACs. TCR and CD28 co-localize within the central SMAC (cSMAC), with a TCR-rich core surrounded by a CD28-rich periphery.[15,16] Larger adhesion molecules, such as LFA-1, localize within the peripheral SMAC (pSMAC).[17] This nanoscale co-localization of TCR and CD28 is necessary for activation, as separating signal 1 and signal 2 activation by several microns inhibits T cell activation.[18]

There are two major subsets of T cells—CD4+ and CD8+ T cells, otherwise known as T helper cells and cytotoxic T cells, respectively. Upon activation, CD4+ T cells differentiate into different subtypes and can carry out multiple functions, from activating B lymphocytes to suppressing the immune reaction.[19,20] The major subtypes include Th1 and Th2, type 1 and 2 T helper cells,[19] Th17 cells that play roles in allergy and autoimmunity,[21] and Treg cells[22] that play important roles in immune response homeostasis. Cytotoxic CD8+ T cells secrete cytokines and kill target cells upon activation.[23] This subtype is responsible for selectively eliminating virally infected cells. Upon activation, T cells clonally divide, secrete cytokines, and most importantly, maintain a memory response that provides long-term protection.

In most cases, the immune system is a powerful defense against infection and disease. However, dysfunctions or deficiencies in any part of the system can reduce its effectiveness or even create disease itself. Cancer's ability to evade immune recognition, chronic infection, and autoimmune diseases provide opportunities to intercept and correct the immune response.

2.1.2 The Cancer-Immunity Cycle

Cancer arises from the culmination of a series of mutations that lead to a break in normal cell-regulating functions, including enhanced proliferation or a lack of normal apoptotic processes. This can lead to the expression of mutated neo-antigens,[24,25] differentiation antigens, viral antigens, or cancer-testis antigens that can be recognized as foreign by the immune system.[26] These antigens are presented on major histocompatibility class I molecules (MHC-I) by resident dendritic cells (DCs) and subsequently activate tumor antigen-specific T cells. While a T cell response can often be

mounted against these tumor-antigens, mechanisms of central and peripheral tolerance and immunosuppressive actions of the tumor micro-environment often hinder an effective immune response.[27]

The interplay between cancer and the immune system can be viewed as a potentially self-propagating cycle, termed the Cancer-Immunity Cycle, which has been elegantly reviewed by Chen and colleagues.[28] To achieve effective anti-tumor immunity, antigens released upon cancer cell death are processed and presented by antigen presenting cells to activate cognate T cells. These T cells may then recognize and kill the tumor cells, leading to a positive feedback loop for immune activation. Cancer occurs when there is a blockade in a step of this cycle that shields the tumor from immune recognition or attack.

In many cases, tumor antigens do not differ sufficiently from self antigens to be recognized as foreign by the immune system. This is evidenced by the fact that tumors with higher frequencies of neo-antigens, tumor-specific antigens derived from tumor mutations, correlate with better prognosis following immunotherapy.[24,29–31] Despite mutational load, the immunosuppressive tumor microenvironment also limits the immune response. There are three major pathways by which tumor cells evade immune attack—reduced MHC expression of tumor antigens, secretion of immunosuppressive factors, and the upregulation of negative costimulatory pathways within the tumor microenvironment.[32] Downregulation of MHC expression can protect tumor cell recognition by T cells and is often a method of tumor immune escape.[33] Tumor or stromal cells also can secrete soluble factors, including TGF-β, IL-10, and PGE_2, or express inhibitory molecules that suppress immune function. Tumor cells that upregulate

immunosuppressive TIM family proteins or programmed death ligand 1 (PD-L1) are correlated with poor prognosis.[34,35] Immunoengineering therapeutics thus often target these pathways to establish a more robust T cell response against the tumor.

2.1.3 Chronic Infection

Pathogens are usually rapidly eliminated by an adaptive immune response, to which effector T cells contribute in large numbers but then quickly contract to a smaller subset of memory T cells once the infection has been cleared. However, similar to cancer, chronic infection prolongs T cell exposure to antigen and inflammatory signals. This can cause 'exhaustion' of T cells, limiting their effectiveness.[36–38] Exhausted T cells have impaired effector function, lose the ability to secrete cytokines, and upregulate expression of immunoinhibitory molecules like PD-1 and CTLA-4.

Examples of chronic infection include viral infections like cytomegalovirus, HIV, and hepatitis C virus. T cell exhaustion prevents effective clearance of pathogenic infection.[39] However, this is not a permanent state as small molecule drugs or checkpoint molecules have been shown to reverse T cell functionality.[40,41] This provides inspiration and hope for engineering approaches to contribute to preventing and rescuing exhausted T cells for fighting chronic infection.

2.1.4 Autoimmunity

Auotimmunity arises when some level of self-tolerance is broken.[42–44] There are several mechanisms of generating immunological tolerance, which many times muddles the elucidation of direct causes of autoimmunity. Main mechanisms of controlling self-reactivity include central tolerance, antigen segregation, peripheral tolerance, regulatory T cells, and activation-induced cell death.

Central tolerance occurs as antigen-specific T cells first go through positive and negative selection in the thymus where T cells with strong-affinity TCRs for self-antigen are eliminated and those with intermediate binding are selected for. In some cases, strong affinity TCRs for self-antigen are selected for and are caused to differentiate into regulatory T cells. These cells can dampen the response of other self-reactive antigen-specific T cells that escape central tolerance. Additionally, self-reactive T cells that escape central tolerance can be eliminated by anergy or deletion by stimulation of the TCR without co-stimulatory signals.

Autoimmunity can be triggered by environmental factors, such as an infection, but also requires genetic factors. Examples of autoimmune disorders include type 1 diabetes, rheumatoid arthritis, Chron's disease, and multiple sclerosis. Severity can be manageable to life threatening, and, affecting nearly 8% of the population, it is a critical immunological problem to solve, at the root of which are T cells. Many therapies for autoimmune diseases are general immunosuppressants that globally downregulate the immune system. However, new therapies that utilize engineering approaches and can target specific activation receptors on T cells, activate Tregs for adoptive transfer, and engineer cytokine delivery and structure have the potential to work more specifically and eliminate off-target effects.[45]

2.2. T cell Modulation – Properties to consider when choosing and designing a T cell modulating platform

The dynamics of the immune synapse make T cell activation sensitive to many micro- and nano-scale properties.[46] The organization and composition of signaling molecules, as well as substrate size, shape, and stiffness, all play intricate roles in modulating T cell activation and resulting phenotype. Immunoengineering approaches allow for these factors to be individually varied and optimized. Here, we will review many of these properties to consider when engineering a platform to modulate T cell activity (Figure 2-1, Table 2-1).

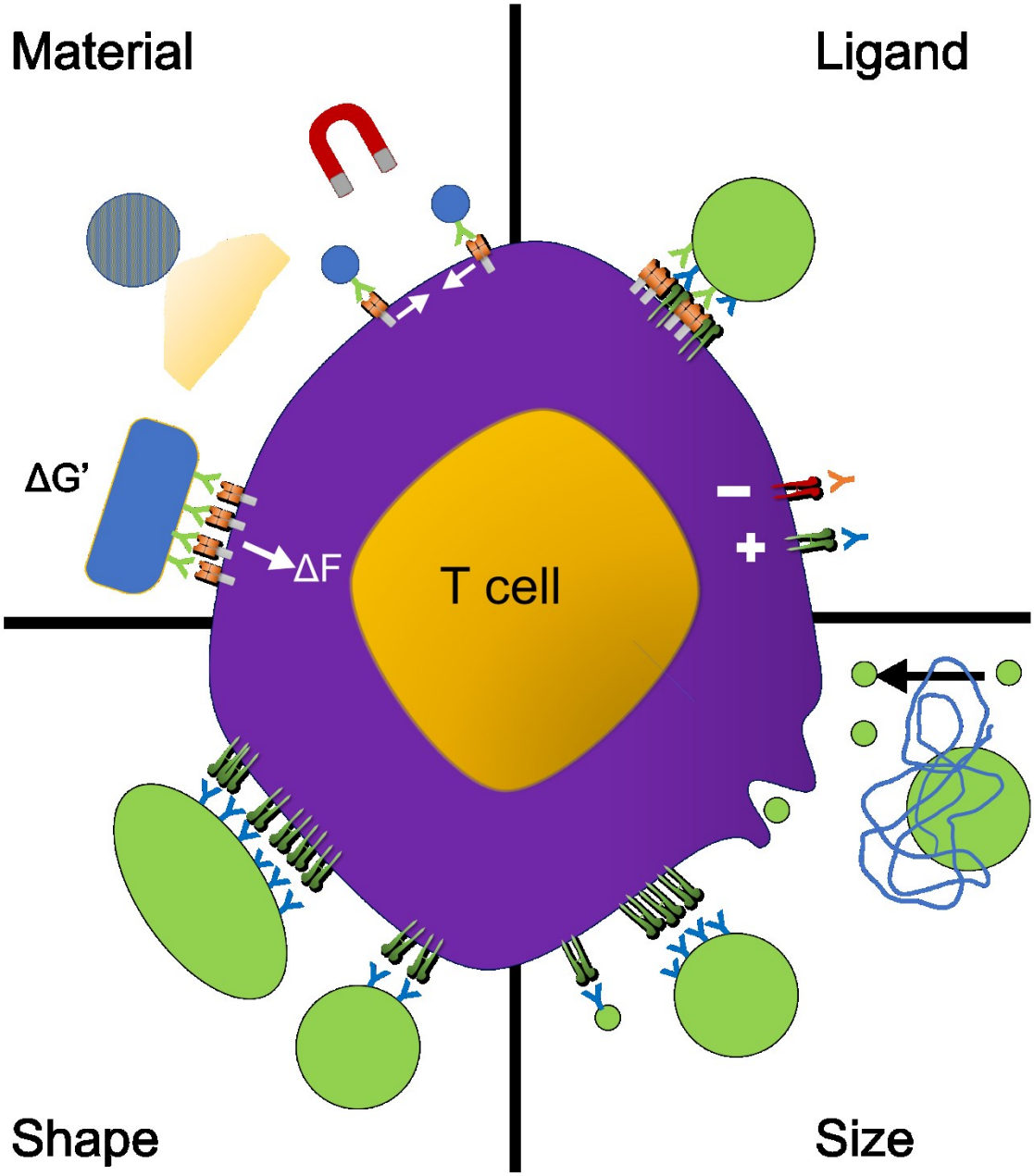

Figure 2-1: Properties to consider when choosing and designing a platform for modulating T cell activity. Ligand plays a role both in the endogenous density of localized receptors on the T cell surface and the type of receptor which could either inhibit or potentiate T cell responses. Size of the platform could influence its ability to i) navigate extracellular environment and reach T cells in vivo, ii) be taken up by T cells, or iii) enable multiple receptor interactions from the same particle. Shape of the platform could influence the number of ligand interactions with increased aspect ratios and limit uptake by non-specific cells. Material can a) influence the mechanical interactions with the T cell which can lead to beneficial mechanotraduction signaling, b) be utilized for controlled release of immunomodulatory molecules, or c) allow external control of materials such as clustering magnetic particles within a magnetic field.

Table 2-1: Summary of engineering design principles that can lead to control over T cell responses.

Engineering Design Parameter	Relationship to T cells	Engineering Example	Impact on T cells
	Engagement with nanometer sized T cell receptor clusters	Nanoparticle artificial antigen presenting cells	Increased avidity leading to sustained and more effective signalling above 300 nm
Size	Enhanced draining to lymph node of particles smaller than 150 nm	T cell vaccine particles	Increased response to antigen
	Enhanced tissue retention above 100 nm	Cytokine and co-stimulatory delivering particles	Decreased off-target effects with local tumor-immune cell activation
	Intracellular particle uptake below 1 μm	In vivo particle transfection of T cells for CAR T cell therapy	T cells were effectively transduced in vivo instead of needing to be removed
Ligand	Requirement of multiple co-stimulatory molecule engagement	Cell-based artificial antigen presenting cells	4-1BB limited apoptosis and surface bound IL-15 increased activation and memory phenotype
	Choice of co-stimulatory and co-inhibitory molecules affects T cell activation	Artificial antigen presenting cells; bispecific antibodies	Co-stimulatory molecule composition affects T cell proliferation, phenotype, and function
	Signal 1 choice dictates T cell subset to be activated	Bispecific T cell engagers	Targeting CD3 vs. peptide-MHC activates all T cells or certain subsets, respectively
	T cell activation is senstitive to signal density	Artificial antigen presenting cells	Nanoscale co-clustering of signaling molecules is required for robust T cell activation
Shape	Ellipsoidal particles reduce nonspecific RES phagocytosis	Drug delivery particles	Longer circulation times of particle-based therapeutics yield better outcomes
	Ellipsoidal particles increase T cell-particle contact area	Ellispoidal articifial antigen presenting cells	Increased contact area improves T cell stimulation by both nano- and micro-particles
Material	T cell receptor signalling is mechanotransductive	Varying antigen-presenting surfaces	Enhanced T cell activation occuring at stiffness around 100 kPa
	Enhanced circulation with "cloaking" materials	Adding CD47 to surface of nanoparticles	Decreased phagocytosis of particle artificial antigen presenting cells *in vivo*
	Ability to artificially cluster T cell receptors	Magnetic artificial antigen presenting cells	Clustering of receptors initiates effective T cell activation with small aAPCs at a lower dose
	T cells migrate and exist in 3D environments	artificial lymph nodes	3D collagen scaffolds with stromal cells creates lymph node like structures ex vivo and in vivo
	IL-2 necessary as 3rd signal	Biodegradable polymer scaffolds; drug carrier particles	Sustained local release of IL-2 and enables T cell infiltration

2.2.1 Ligand

Most fundamentally, T cell activation is modulated through different co-stimulatory and co-inhibitory pathways. When developing a therapeutic, one first has to

determine which specific signaling pathways to activate or inhibit. In addition to pathway choice, ligand nano- and micro-scale arrangement, density, strength, and duration can have a great impact on T cell activation.

T cells require a signal 1 for activation. This can be provided through stimulating the cognate TCR or CD3, which is constitutively associated with the TCR and is responsible for its intracellular signaling.[47] pMHC stimulation of TCR provides activation of only cognate antigen-specific T cells, whereas activation through CD3, with an anti-CD3 monoclonal antibody (mAb) for example, activates all T cells regardless of specificity.[1]

While signal 1 is required for activation to occur, the T cell response to that signal is modulated by dozens of types of co-stimulatory and co-inhibitory molecules.[48] In the absence of any co-stimulation, T cells develop an anergic, under-responsive state. CD28 is the prototypical co-stimulatory molecule, although several other co-stimulatory molecules exist that modify T cell proliferation and phenotype. For example, 4-1BB co-stimulation has been shown to preferentially activate CD8+ T cells over CD4+ T cells,[49] preferentially activate memory CD8+ T cell populations,[6] increase T cell maintenance of CD28 expression,[5] and increase CD8+ T cell secretion of IL-2.[7] Stimulation through the co-stimulatory molecules OX40 and CD27 expressed by T cells has also been shown to enhance activation.[3,4] Importantly, altering the combinations and ratios of different co-stimulatory molecules without varying total co-stimulation can have tremendous impacts on activation.[4,8]

Several co-inhibitory pathways exist that diminish T cell activation. Many of these pathways are involved with maintaining homeostasis and establishing a self-

regulated immune response following pathogen removal.[50] However, these inhibitory pathways can be utilized by cancer to cause immune evasion or be inhibitory or dysfunctional in autoimmune diseases and chronic infection and are thus often targets of immunotherapeutics. Programmed death 1 (PD-1) and CTLA-4 expressed by T cells are two commonly targeted checkpoint molecules.[51,52] Monoclonal antibodies blocking these checkpoint pathways as well as other immuno-inhibitory molecules such as IDO can rescue exhausted T cells.[53] Blocking inhibitory pathways along with activating co-stimulatory pathways can also further augment the T cell response in cancer[54,55] and in chronic infection.[56]

The nano- and micro-scale arrangement of signaling ligands plays an important role in modulating the T cell response by engineered platforms as would be speculated from the formation of an immune synapse during endogenous activation. At the microscale, a focal co-clustering of signal 1 and signal 2 molecules is necessary to initiate activation. When anti-CD3 mAb is patterned on a planar substrate in focal spots, T cells proliferate and secrete cytokines.[57] However, T cell activation is reduced when the same anti-CD3 mAb is tethered in an annular pattern that precludes centralized TCR clustering. Signal 2 must also be co-clustered with signal 1 during stimulation. Separating anti-CD3 and anti-CD28 by a distance of several microns inhibits IL-2 cytokine production.[18]

In addition to the microscale organization of stimulatory molecules, the TCR intermolecular distance must be sufficiently small to induce activation. When anti-CD3 is patterned on planar substrates at defined densities, only surfaces displaying anti-CD3 with intermolecular distances smaller than approximately 60 nm induce optimal activation.[58,59] Interestingly, the minimum intermolecular distance for CD4+ T cell-

specific activation with MHC II is close to 115 nm,[60] indicating that ligand organization may need to be modulated based on the T cell subset to be affected.

While TCR and CD28 organization have been more extensively studied, some data indicate that signaling through other co-stimulatory and co-inhibitory pathways may also be sensitive to nanoscale arrangement. T cell inhibition through PD-1 signaling has been shown to depend on the formation of microclusters within the immune synapse.[61,62] When the extracellular domain of PD-1 was extended to preclude its co-localization within the immune synapse, inhibition was reversed. 4-1BB has also been shown to localize within the immune synapse along with CD28 during co-stimulation.[63]

2.2.1.1 Density and Impacts on Signal Strength and Duration

The spatial arrangement of ligands on the surface of both naïve and activated T cells also affects the local density of ligands, which in turn has impacts on molecular and cellular interactions. TCRs are locally arranged on the surface of quiescent T cells in protein islands of about 35-70 nm in diameter and 300 nm in the longest dimension, with 7-20 TCRs found in one island.[13] Indeed, disruption of T cell lipid rafts by cholesterol depletion disrupts T cell activation further demonstrating the need for multivalent TCR clusters.[64] Upon TCR engagement and activation, these TCR nanoislands coalesce to form larger microclusters and eventually develop into the central supramolecular activation cluster (cSMAC) of the immune synapse.[13,65–67] Interestingly, the cognate ligand, MHC molecule, is organized similarly on endogenous APCs. As many as 25-125 MHCs are grouped in 70-600 nm protein patch.[68,69] Additionally, it has been shown that even specific protein-MHC complexes are clustered on the surface of APCs.[70,71]

This nanometer organization is important to modulating the sensitivity of T cell signaling. MHC and TCR binding is a low-affinity interaction with μM Kd as compared

to nM Kd for antibody-antigen interactions. Kd is a useful description of binding kinetics where it is the equilibrium concentration of ligand where half of the ligand is bound to its receptor, thus a lower concentration such as a nM Kd has much higher affinity for its receptor.[72] Consequently, the binding of several MHC and TCR complexes simultaneously is beneficial to initiate engagement of cognate APCs and T cells. Mathematical models of TCR and MHC binding events also show a need for multiple receptors in close proximity.[73] The models suggest that the reversible binding between MHC and TCR leads to activation when serial binding can occur.

In addition to initiating signaling between APCs and T cells, multivalent interactions would be important to providing sustained signaling.[74] Sustained signaling is essential for effective T cell activation and can influence the fate and function of resultant T cells.[75,76] *In vivo* experiments have shown that once T cells encounter antigen-specific APCs in the lymph node, they form stable connections for several hours.[77] These studies also demonstrated that this sustained connection is dependent on stable pMHC-TCR interactions.

In addition to these biological findings, researchers have corroborated these findings through directly modifying MHC density. First, researchers have artificially clustered the MHC on APCs and observed enhanced T cell activation with lower levels of MHC.[78] Second, the density of cognate MHC can be modulated by the dose of antigen given to APCs, and as density of surface cognate MHC decreased, so did the *in vivo* T cell response.[79] Third, MHC ligands were patterned on surfaces at varying densities, but the number presented to a T cell was controlled.[80] Here they found that the density was

more important than the number of presented ligands with at least four ligands in close proximity needed to activate a T cell.

In summary, TCRs and MHCs are naturally localized into dense regions, which allows increased cognate recognition and sustained signaling to occur because of serial engagement and multivalent interactions. Though we have focused our analysis how ligand density affects the MHC-TCR interaction, other ligands such as those in the immunological synapse also have distinct spatial locations and densities.[65,81] Therefore, T cell-modulating technologies should be designed with consideration given to the density and location of the ligand.

2.2.2 Size Considerations

In designing cell-modulating technologies, physical size is another important biological constraint. Like with considerations of ligand properties, size design considerations arise from features of T cells. This can arise from molecular size limitations like distances between ligands on the T cell as described in 2.1.3, or even due to the fact that T cells reside within the lymph node. Here we will review some of those interactions and how to design certain technologies based on these scales.

2.2.2.1 Molecular Interactions

When interacting in biological environments, both *ex vivo* and *in vivo*, the number of molecular species in a given environment can be astronomical. And with an equally large number of chemical reactions and molecular binding events occurring, it is hard to achieve the desired interaction and avoid unintended reactions. This poses unique challenges for maintaining the size of synthetic materials created to modulate T cells.

As these materials are usually designed on the micro- to nanometer scale, the decrease in size increases the free surface energy of the material. As a result of this small size, within minutes of being introduced to a biological media or *in vivo*, most engineered materials acquire a shell of adsorbed proteins known as a protein corona.[82] This protein shell can both determine the fate of the material and cause unintended consequences regardless of T cell targeting. For example, proteins can cause aggregation of the material, changing its size; increase cell-uptake; or even cause negative biological events, such as platelet activation.[83–85] Therefore, to control the size, engineers modulate the chemical and biological properties of the surfaces to be inert or covert materials, as described in 2.4.

2.2.2.2 Cellular Interactions

After encountering and interacting with proteins post-administration, therapeutic particles or materials will encounter cells. Cells take up volume around them as a form of communication and defense and often these materials become subject to this phenomenon. Antigen-presenting cells including macrophages phagocytose efficiently to clear antigen and also process antigen to elicit T cell responses. T cells on the other hand are less efficient at phagocytosis. Thus, careful design of particle properties can effect cellular and intracellular destinations of particle and cargo. A few notable principles have been able to be distilled from a number of particle size-related studies in cell uptake.[82,86,87]

First, particle size-dependent cell uptake differences are partially governed by required membrane wrapping energy. Larger particles on the scale of 3 μm and above require more energy to be taken up than smaller nanoparticles, which results in decreased cell uptake.[88] In the absence of surface coating, the uptake of small particles (<25 nm) is

lower than that of larger particles.[89] Here the surface exposed is insufficient to cause cell receptor-nanoparticle interactions necessary for endocytosis. This results in lower avidity between the cell membrane and particle and makes it more difficult not only for the particle to be "gripped" but also for the cell to initiate signaling for endocytosis machinery.[90]

Second, the cellular process for uptake also depends on particle size.[91,92] Phagocytosis is primarily seen with particles larger than 500 nm and pinocytosis with particles smaller than 500 nm.[93] Even within pinocytosis, cellular uptake processes can differ and have unique vesicle size limits, which then can provide differential intracellular delivery based on particle size. For example, micropinocytosis can engulf particles greater than 1 μm, whereas clathrin-mediated endocytosis can take up particles up to 120 nm, caveolin-mediated up to 60 nm, and clathrin and caveolin-independent endocytosis up to 90 nm.[94]

Third, cell-uptake parameters differ between different cell types. Cells of the mononuclear phagocytic system will exhibit greater cell uptake than endothelial or even T cells.[95] This could affect not only the volume of material that is taken up but also the size dependency trend.[96]

Understanding how size affects nanoparticle endocytosis will be especially important for the design not only of nanoparticles that can escape cellular uptake but also of effective NP therapeutics such as gene delivery vehicles where endocytosis is a critical component of the delivery process. To increase cell uptake for applications such as gene delivery, nanoparticles can be coated with cell-interacting ligands.[97,98] This can determine their intracellular destination by methods such as labeling the particle with a microtubule-

associated sequence (MTAS) and or nuclear localization signaling (NLS) sequence to target the nucleus.[99] Additionally, ligands can help to differentiate cell types, such as by coating the particles with antibodies to cell-specific proteins.[100,101]

Besides targeting cells with cell-specific antibodies, particles can be designed to directly provide signaling with ligands.[102] Here size also plays a role as the local density of ligand can be changed by changing the size of a particle. For example, the number of bioavailable ligands on a small 50 nm nanoparticle may only be 2, whereas the number may be closer to 200 on a larger 5 μm particle with equivalent density because the curvature of the particle decreases with increasing size.[103] This will affect the local ability to cluster receptors from a single particle and may impact T cell modulation as mentioned in 2.1.3, where the spatial relationship among cell surface receptors is critical for T cell signaling.

Finally, when engineering implantable materials (>100 μm) for *in vivo* applications, then the foreign-body response should be considered.[104] Here since cells cannot uptake the material, then the immune system will become activated based on adsorbed blood proteins. This will cause a cascade of events that may result in either 1) degradation of the material by reactive oxygen species, 2) segregation of the material by formation of scar tissue, or 3) integration of the material into the surrounding tissue. Recently, it has been suggested that the size of the implant can influence this response regardless of material choice, where implants above 1.5 mm in size led to reduced immune response and scarring.[105]

2.2.2.3 Tissue Interactions

In addition to the cellular destination of materials, material size also affects tissue distribution when injected *in vivo*.[82] T cells are a unique cell type in their mobility and

distribution throughout many different compartments.[106] They arise from within the bone marrow, develop in the thymus, travel from lymph node to lymph node via the lymphatic system and use the circulatory system to traffic to sources of infection within tissue and can reside there or in lymph nodes for years. Biodistribution will thus affect the ability to target specific T cells with engineered materials.

Broadly speaking, the impact of particle size on biodistribution can be classified by whether particles are introduced to the circulation or to tissues directly. Intravenous administration would be useful for targeting circulating T cells or for reaching T cells systemically. For intravenous administration, particles should be less than 4 μm to prevent occlusion of capillaries. Particles smaller than 6 nm will be cleared by the kidney, and larger particles will mostly be removed by the mononuclear phagocyte system in the liver and spleen. Most particles will end up being cleared from circulation within minutes, but a small percentage will enter different tissue compartments. For example, nanoparticles 20-200 nm in size have shown increased accumulation in tumor tissues based on the increased fenestration of the tumor capillaries—known as the enhanced permeability and retention effect.[107]

Tissue-based injection would be useful for targeting localized T cells in tissues or for reaching T cells in lymph nodes. Injected particles will diffuse or be convected through the extracellular matrix (ECM). Particles less than 50 nm can move efficiently through spaces in the ECM and be transported via the lymphatics to the lymph node, whereas larger particles are sequestered at the tissue injection site.[108,109] Upon reaching the lymph node, low molecular weight proteins (<70 kDa) will be shuttled to fibroblastic reticular cell-lined channels to B cell follicles, while larger proteins and particles will

need to be introduced into the lymph node by subcapsular sinus macrophages.[110] Similar properties govern particle transport in mucosal administration of particles, where particles smaller than 100 nm will have greater diffusion rates and penetration through mucus matrices.[111] Particles larger than 100 nm, may be limited to administration sites and undergo phagocytosis by macrophages or antigen presenting cells, which subsequently traffic to lymph nodes as mentioned in section 2.2.2. This property could be harnessed to mimic infection in design of biomaterial vaccines that lead to potent T cell responses.

In conclusion, particle size is a key design parameter that influences whether cell-modulating technologies will reach T cells. Additionally, it impacts how the particles interact with T cells and modulate T cell signaling.

2.2.3 Shape

When synthesizing synthetic platforms for T cell modulation, particle shape can have surprising impacts on their interaction with T cells and macrophages and their biodistribution. Spherical and ellipsoidal particles have differing interfacial geometries despite their similar length scales and can thus potentially be optimized for T cell interactions. By using shape to vary biodistribution, the half-life and cell and organ targets can also be modified.

Particle shape affects biodistribution in part by modifying phagocytosis by the reticuloendothelial system (RES). In contrast to spherical particles, ellipsoidal particles reduce nonspecific RES phagocytosis, an important consideration for extending the half-life of therapeutics injected *in vivo*.[88,112–114] In fact, phagocytosis is more dominantly affected by shape than by size in the range of approximately 1-10 μm.[112] However,

interestingly, receptor-mediated endocytosis of non-spherical particles is enhanced.[115] Thus, elongating particles for applications where targeted internalization is preferred, such as drug delivery, may also take advantage of longer circulation times.

In addition to affecting biodistribution and half-life, particle geometry plays an important role at the T cell-particle interface. While most T cell-interacting particles, such as artificial antigen presenting cells (aAPC), are spherical in nature, this shape does not recapitulate biological T cell-APC interactions. Spherical particles maximize the curvature and thus minimize the surface area of contact between the T cell and particle. This is especially detrimental at the nanoscale where ligand avidity decreases as particle size decreases, despite biocompatibility incentives to moving to smaller size scales. Ellipsoidal microparticle aAPC were shown to preferentially interact with T cells along their long axis and significantly increase T cell activation *in vitro* and *in vivo*.[116] Ellipsoidal nano-aAPC also result in a similar increase in T cell activation over spherical particles of similar size while also taking advantage of the increased biocompatibility and superior biodistribution due to small particle size.[117]

Particle shape can directly affect T cell activation by influencing avidity. For therapeutics meant to activate a T cell response, ellipsoidal geometries may be preferred due to increased interaction with the T cell surface and superior biodistribution. However, in addition to micro- and nano-particles, shape may be an important factor to consider in larger scaffolds that cannot be directly engulfed by macrophages. The degradation products of implantable T cell-stimulating devices, such as artificial lymph nodes, are often fibers or other non-spherical geometries and may be an important design parameter to limit an unwanted immune reaction.[118]

2.2.4 Material

The choice of material and control of material properties can impart unique functionalities on the T cell modulating technology. For example, *in vivo* applications need to consider biocompatible materials with low clearance, efficient targeting, low toxicity, and biodegradability. For *ex vivo* applications, a broader range of chemistries and materials can be employed to modulate and study T cell responses. Examples include using magnetic materials to cluster signaling components on the surface of the cell and modulating the stiffness of the material to enable study of mechanotransduction pathways.

2.2.4.1 Material Surfaces

As discussed in section 2.2, stability in biological fluids and the ability to evade the mononuclear phagocytic system enable therapeutics to reach and target T cells. To this end, reducing the formation of a protein corona on the material is a priority. Engineers have primarily utilized a hydrophilic polymer—polyethylene glycol (PEG)—to create a water-based shell to prevent protein adsorption and particle aggregation.[119–121] PEG has also been conjugated to protein-based therapeutics to increase solubility, stability, and circulation and reduce immunogenicity.[122]

Often, therapeutics are more than just a delivery vehicle and are coated with either targeting moieties or cell-modulating proteins. In these cases, a PEG layer can help improve stability, but it cannot shield attached protein components from initializing a protein corona or initiating uptake by the mononuclear phagocytic system. Another approach to shielding therapeutics is to use biology as inspiration. For example, liposomes are particles derived from biological lipids that form a bi-lipid membrane

similar to that of cells and can be used as a coating on particles to prevent aggregation and uptake.[123,124]

Similarly, particles have recently been coated with cell membranes, such as red blood cell membranes,[125] tumor cell membranes,[126] and leukocyte cell membranes.[127] Besides increasing stability and decreasing clearance, these membranes can confer additional advantages such as site-specific targeting for targeting inflammation. Lessons learned from these coatings and studying how red blood cells avoid uptake have revealed the importance of CD47 as a "don't eat me" signal.[128] Therefore, instead of coating the particle with entire membranes, researchers have also attached the CD47 protein to nanoparticles, leading to decreased cell uptake and increased circulation.[129]

As an alternative to coating materials with chemistries or biologics that prevent protein adsorption, these interactions can be taken advantage of intentionally. One example is the design of more efficient vaccines by Liu et al.[130] They designed their vaccine to have a hydrophobic tail so that it would bind to albumin and traffic to the lymph node. This approach resulted in a more efficient delivery of their vaccine to the lymph node, generating a more robust immune response.

2.2.4.2 Biointeractive Materials

Beyond avoiding the mononuclear phagocytic system, materials can also be designed to mimic biological properties to engage cells such as T cells. Biomolecules can be attached through adsorption, use of biologic interactions such as streptavidin-biotin, or direct chemical attachment. Already covered in section 2.1, coating of ligands on materials can mimic existing signals in the body enabling specific T cell modulation. Properties such as ligand choice, arrangement, and density are important factors to consider.

Beyond cell-surface ligands, biomolecules derived from the extracellular matrix or cytokines can be coated onto material surfaces. Utilizing such molecules can enable enhanced attachment of cells to synthetic scaffolds.[131] Additionally, these molecules such as growth factors can be used to polarize differentiation of cells including stem cells.[132]

The material stiffness also contributes to the signaling that occurs upon engagement by a cell. This is especially important in mechanotransduction-sensitive pathways. Mechanotransduction plays a role in cell-cell signaling, sensing aspects of the extracellular environment such as fluid flow, and enabling cell attachment and migration through the extracellular matrix.[133,134]

T cells are a very active and motile, and mechanotransduction plays a role in similar ways to other cells in areas of cell attachment and migration. More specifically mechanotransduction has also been implicated in TCR signaling.[135] As T cells scan the antigen presenting cell, the TCR can engage its cognate MHC, and the resulting force associated with recognition is necessary for T cell activation.[136] It has been hypothesized that this is due to a catch-bond-like behavior of the sensor due to conformational changes in the proteins that result from the force.[137,138]

Additionally, once initial TCR signaling has occurred, the immunological synapse develops, which contains integrins and F-actin on the periphery and enables strong adhesion between both cells.[139] Retrograde flow of actin drives engaged TCRs to the center of the immunological synapse, further exerting forces on the TCR-MHC. Additionally, APCs provide rigid surfaces by immobilizing intracellular cell adhesion molecule 1 (ICAM-1) on its surface, which is necessary for T cell activation.[140]

Therefore, mechanical properties are an important consideration for designing materials to directly interact with T cells.

Finally, the actual material can have immunomodulatory effects on immune cells. One noteworthy example is how the polymer poly(beta-amino ester) (PBAE) intrinsically activates the immune response as a vaccine particle. Researchers showed that maximal stimulation of the immune response was achieved with high molecular weight PBAEs, or short degradation time points even in the absence of traditional adjuvants.[141]

2.2.4.3 Bioresponsive Materials

A more recent development in material design is to engineer materials that react and respond to biological cues in the body.[142] The first example is to increase the biodegradation *in vivo* in targeted locations due to differences in the biological environment, such as changes in pH, redox potential, and enzyme content. Increased acidity in the stomach, tumor microenvironment, or lysosome can be used to cause protonation of the material and trigger to release its cargo.[143] Utilizing disulfide linkages, one can exploit the reductive environment of the cytosol or the nucleus as compared with the extracellular environment as another method of signaling release.[144] Finally, enzyme-reactive sequences can be designed into material to take advantage of the increased level of matrix metalloproteinases found in tumors to speed up degradation.[145]

Beyond biodegradation, bioresponsive materials can also be designed to respond to mechanical forces, heat, magnetic fields, radiation, and ultrasound to change size, shape, and chemical structure.[146] Mechanical forces, such as the shear stress induced by fluid flow in circulation, can be utilized to break up larger fragile materials into smaller pieces more amenable to circulation and tissue targeting.[147] Certain polymers have lower critical solution temperatures close to body temperature, such as N-isopropylacrylamide,

which decreases in size due to a phase change.[148] Magnetic materials can be controlled *ex vivo* by a magnetic field and caused to locally aggregate[149] or generate heat for therapy.[150] Similar control of size change and heat can be generated by gold and light-responsive polymers from activation by specific wavelengths of light.[151,152] Like magnetic materials, ultrasound-sensitive materials can be utilized both as imaging agents and to change the size of the material to release cargos locally.[153,154]

Bioresponsive material strategies can be leveraged to implement more effective modulation of T cells *in vivo* and *ex vivo*. First, these material properties could help to target T cells within specific compartments, such as the tumor microenvironment, or even specific T cell intracellular compartments. Second, control over T cell trafficking and response to cargo controlled by temporal external stimuli offers precise control over the timing and level of T cell responses.

2.2.4.4 Biocompatibility

Material biocompatibility is another important consideration for clinical translation.[155] Materials already used in FDA-approved devices or applications can make the clinical translation more straightforward, though this may limit the functionalities and engineering design in the therapy.[156] Translation becomes increasingly challenging when bioactive proteins and cellular components are added into the material intervention.[157]

2.3. Immunoengineering approaches

Engineering concepts have been applied to immunology to develop platforms that alter the T cell response. Scientists and engineers have developed biocompatible platforms that mimic antigen presentation, orchestrate the delivery of immune-modulatory drugs, or prompt a new type of immune interaction. These platforms have

been built upon a wide variety of biocompatible platforms, from engineered small molecules and cultured cell lines to biodegradable polymers. Many times, immunoengineering is used to attempt to more accurately mimic biological interactions, while other times, it is used to trigger a new type of interaction that may be more favorable to a patient. Here, we review previously engineered platforms, including protein engineering, synthetic particles, cell and genetic engineering, scaffolds and surfaces, and combination therapies.

2.3.1 Protein Engineering

At the smallest scale, proteins and small molecules can be engineered to target specific signals involved with T cell activation. This may involve developing a high affinity antibody to activate or block one or more immune-stimulatory or -inhibitory pathways, synthesizing modified cytokines that can more effectively bind their targets, or utilizing antibodies to target the delivery of a drug or cytokine to a specific anatomical site. In this section, we will review various molecular targeting approaches and how engineering principles have been applied to their design. We will focus on how these engineered molecules have been used as monotherapies, although many are used in combination therapies or encapsulated into synthetic particles or scaffolds to further modulate their delivery.

2.3.1.1 Engineered Cytokines

During T cell activation, T cells receive soluble pro-inflammatory or anti-inflammatory signals, often referred to as “signal 3.” These signals help to drive cell proliferation, differentiation, and chemotaxis, among other functions. Therapeutic administration of pro-inflammatory cytokines important for immune activation, most

commonly IL-2, can activate a robust anti-tumor immune response, but systemic injection is complicated by life-threatening toxicities.[158,159] The clinical use of cytokines is also hindered by their rapid clearance from the bloodstream, leading to a typical serum half-life on the order of minutes. Longer-acting engineered cytokines that can selectively activate immune subsets and antibodies that direct their localization are thus being developed.

In the field of cytokine engineering, scientists and engineers have developed cytokines with altered binding to immune cell subsets to create more clinically-favorable therapeutics. IL-2 signaling occurs through either a high affinity (K_D~10 pM) trimeric receptor complex, consisting of the IL-2Rα, IL-2Rβ, and IL-2Rγ (γ_c) chains or an intermediate affinity dimeric complex (K_D~1 nM) consisting of only the IL-2Rβ and γ_c chains. Different immune cell subsets modulate their sensitivity to IL-2 signaling by altering surface expression of the non-signaling IL-2Rα chain. Naïve effector T cells only express only the IL-2Rβ and γ_c subunits, whereas activated memory T cells and regulatory T cells also express the high affinity IL-2Rα and are thus more sensitive to IL-2 activation.[160] Importantly, pulmonary edema, a major toxicity upon systemic IL-2 administration, has been shown to be mainly IL-2Rα-dependent.[161] An engineered IL-2 "superkine" was evolved to have 200-fold increased affinity for the IL-2Rβ subunit and thus activated cells in an IL-2Rα-independent fashion. As a result, this IL-2 superkine significantly increased the expansion of $CD8^+$ T cells *in vivo* but did not alter regulatory T cell expansion compared to the wild type cytokine. By shifting the cellular response to favor immunostimulatory subsets, the IL-2 superkine significantly reduced pulmonary edema and increase anti-tumor efficacy.[162] Further modifications of this engineered IL-2

cytokine have demonstrated how modulating binding activity to the other subunits can result in development of agents that further manipulate the cellular response, such as IL-2 partial agonists or antagonists.[163]

Superagonists for other cytokine-receptor systems have also been developed. For example, IL-15 is a cytokine that contributes to T cell and NK cell development, proliferation, and activation.[164] Endogenously, IL-15 is bound to IL-15Rα and expressed on the cell surface of antigen presenting cells to T cells and NK cells displaying the intermediate affinity dimeric IL-2 receptor (IL-2Rβ/γ_c). Binding of IL-15 to the IL-15Rα subunit on the surface of APCs induces a conformational change that enhances its interaction with IL-2Rβ/γ_c; thus the administration of soluble IL-15 alone has only a moderate effect on T cell expansion. Administration of pre-formed complexes of IL-15 with recombinant IL-15Rα was shown to selectively induce robust expansion of memory CD8+ T cells and NK cells.[165] Building on this work, IL-15 superagonists were engineered by fusing the IL-15 cytokine to a truncated version the IL-15Rα subunit. These engineered fusions exhibited 4-5-fold more potent biological activity than the native IL-15 cytokine on IL-2Rβ/γ_c-expressing cells,[166] and later iterations of the superagonists were linked to Fc binding domains to prolong their effects through extension of serum half-life.[167]

While high-affinity superagonist cytokines may have increased potency compared to endogenous cytokines, they often do not solve the problem of systemic toxicities. To improve selective targeting, cytokines have been bound to tumor-targeting antibodies to increase their localization to the tumor microenvironment. Over a dozen types of

cytokine-antibody fusion proteins (immunocytokines) have been developed. In the simplest terms, cytokines can be linked via the N- or C- terminus of an antibody to leverage the spatial relationship between cytokine delivery and antibody binding.[168] Additional modifications of the antibody constant region can also affect how the fusion protein interacts with Fcγ receptors or initiates the complement cascade, or they can alter the molecular weight and biodistribution of the cytokine-antibody fusion.[169] In addition to targeting cytokines to the tumor microenvironment, the physical constraint of a tumor-targeting antibody with a T or other immune cell-targeting cytokine can be synergistic. For example, immunocytokines that target tumor-expressed antigens have been shown to increase interactions between tumor cells and T cells or natural killer cells much like a bispecific antibody that concurrently targets a tumor-associated antigen and an immune cell surface marker.[168] Other families of immunocytokines that link cytokines with tumor-associated extracellular matrix components are thought to mediate an anti-tumor effect primarily through localizing cytokine delivery.[170]

Immunocytokines have been developed that incorporate a wide variety of tumor-associated antigens, but the majority of these constructs utilize the same cytokines: IL-2, IL-12, IL-15, or TNF.[168] One example of a successful immunocytokine is a fusion between the anti-CD20 antibody rituximab and an IL-15 superagonist, which was shown to exhibit superior anti-tumor activity to rituximab alone.[171,172] By linking the superagonist cytokine with a tumor-targeting antibody, the fusion proteins were capable of taking advantages of three mechanisms: specific binding to CD20 on tumor cells; potent immune cell stimulation through the IL-2Rβ/γ_c receptor; and recruitment of antibody-dependent cellular cytotoxicity and phagocytosis through binding to Fcγ

receptors on macrophages and natural killer cells. Other immunocytokines that deliver anti-inflammatory cytokines for organ-specific autoimmune disease,[173] target cytokine delivery to necrotic areas of tumors through incorporation of anti-DNA antibodies,[174] or enact the blockade of tumor-expressed immune-inhibitory molecules[175] have also been developed.

2.3.1.2 Engineered Antibodies

In addition to the molecular engineering efforts on cytokines, there is great interest in engineering antibodies to block or stimulate cell targets, alter cell-mediated cytotoxicity and biodistribution, or selectively deliver drugs to the site of disease. Monoclonal antibodies can be evolved to selectively bind antigens that may be uniquely expressed or upregulated on tumor cells and also have the advantage of longer half-lives compared to small molecule drugs.[176] Their precision in targeting also mitigates off-target toxicities. However, beyond selecting a molecular target, applying engineering principles to their design can improve their biodistribution, alter their interaction with immune cells, turn them into a vehicle to specifically deliver a drug or nanoparticle to a disease site, or target them to multiple cell types simultaneously. The process of monoclonal antibody production[177,178] and the selection of target antigen[179,180] have been reviewed previously. Here, we explore how monoclonal antibodies have been engineered to customize their *in vivo* effects.

2.3.1.2.1 Monospecific Antibodies and Mechanisms of Action

Three common classes of therapeutic antibodies include: (1) antibodies whose major mechanism of action is through the blockade or stimulation of the targeted pathway; (2) antibodies that are used to deliver a drug payload; and (3) antibodies whose structure has been engineered to engage multiple different cell types simultaneously to

redirect functionality. Endogenously, antibodies often bind infected cells or foreign pathogens. The exposed constant region of these antibodies can then mediate antibody-dependent cellular cytotoxicity or complement-dependent cytotoxicity to destroy the targeted entity. Thus most fundamentally, antibody engineering often involves modification of the Fc region to modulate how the bound antibodies will interact with the immune system.[181] When antibody-mediated cell killing is desired, such as when antibodies target molecules on infected or tumor cells, isotypes such as human IgG1 are often incorporated that initiate these effects.[182,183] In other cases, an antibody may be developed to block or stimulate a certain pathway on a healthy cell-type, such as the programmed death 1 (PD-1) inhibitory molecule on T cells. For such cases in which cell death would be detrimental, the antibody is engineered to have an IgG2 or IgG4 isotype that has limited interaction with Fc receptors.[184] In all cases, antibodies are humanized by replacing the constant region and sometimes parts of the variable regions with the human sequence.[185]

The interplay between T cells and cancerous cells is multi-layered and complex. While cancerous cells may express mutated neo-antigens that are recognized by the immune system, they also often upregulate immunosuppressive molecules that inhibit efficient T cell stimulation and lack expression of co-stimulatory molecules.[48] Many monoclonal antibodies have been developed that block these inhibitory pathways on T cells or tumor cells or that directly stimulate signaling pathways on T cells to jumpstart the cancer immunity cycle. Clinical administration of soluble antagonist antibodies against the inhibitory checkpoint molecules PD-1[52,186] and its ligand, PD-L1,[187] and CTLA-4[51,188,189] have shown tremendous success in recent years. The success of these so-

called checkpoint blockade antibodies have been correlated with tumor mutation load—tumors with more mutations and more neoantigens are associated with improved clinical benefit from checkpoint molecule inhibitors.[190,191] Agonistic antibodies have also been developed that stimulate T cell signaling through co-stimulation, such as anti-CD28, anti-4-1BB, and anti-OX40 antibodies.[3,7,192,193] However, because of the structured arrangement of the signaling molecules during T cell activation, these synthetic co-stimulatory molecules are often delivered on particle platforms[4,8] that enable formation of the immune synapse.

The direct function of an antibody is often to affect a signaling pathway. However, antibodies have also been conjugated with various drugs and utilized as carriers to deliver payloads to specific T cells or tumor cells. In cancer immunotherapy, many of these so-called antibody-drug conjugates (ADCs) target tumor-expressed antigens, such as HER2, CD19, or CD22, and novel strategies have been introduced to increase tumor-specificity. For example, an ADC was developed that encodes an additional peptide sequence that shields the antibody's antigen binding site until it is cleaved within the tumor microenvironment.[194] This method can thus enhance tumor-specificity when the antigen target is not uniquely expressed by cancerous cells. This type of approach could also potentially be used to decrease off-target toxicities of checkpoint inhibitors and co-stimulatory antibodies as these are not limited to the cancerous tissue. Fusion proteins have also been developed that deliver multiple payloads simultaneously. For example, a tri-functional fusion protein linked an antibody against a tumor-associated antigen with both the co-stimulatory molecule 4-1BBL and the IL-15 cytokine.[195] The fusion protein was more efficient than corresponding bifunctional proteins in activating T

cells and inducing an anti-tumor response *in vivo*. The approach to treating lymphoid malignancies is slightly different; in this case, antibodies have been developed to deliver cytotoxic drugs to the malignant T cells themselves. An ADC targeting IL-7R, which is expressed on lymphatic cells, demonstrated how this method could be used to treat lymphoid malignancies or autoimmune disorders.[196]

2.3.1.2.2 Approaches Antibody Engineering

Many tools are being developed to speed up and diversify the discovery of novel antibody therapies or engineer of antibody variants. One such tool is the development of combinatorial antibody libraries.[197] There are nearly 10^{11} unique antibody sequences, and being able to screen or probe the unique antibody-antigen binding landscape may enable enhanced affinities or unique binding locations which may enable novel mechanisms of therapeutic action, ultimately allowing control over therapeutic antibody design. Nevertheless, the massive libraries would be unexploited if not for high throughput engineering techniques. One such technique is the development of yeast surface display affinity engineering.[198] Here antibody libraries can be cloned into yeast and fragments can be displayed and allowed to bind to a target protein. Antibodies to both the fragment and bound target protein identify high binders, which can be selected for and further mutated to increase affinity.

There are many variants in structural engineering of the antibody, with particular focus on Fc and Fab portions.[199,200] One example that targeted engineering of both ends, looked at eliminating non-specific thromboembolism events that occurred when the anti-CD40L antibody was administered to treat autoimmune diseases.[201] Specific targeting sequences of the antibody towards CD40L, termed a domain antibody, were fused to an Fc domain which was engineered to lack any Fc binding function. Eliminating the Fc,

eliminated platelet activation, thus reducing thromboembolism events, and allowing effective treatment of both models of transplantation and lupus.

2.3.1.2.3 Bi-specific Antibodies

One of the most powerful antibody-based approaches in cancer immunotherapy has been the development of bispecific antibodies. Bispecific antibodies are antibodies that have been engineered to comprise two different variable portions, each specific for a different antigen. Their specific structures encompass many formats, and each varies in terms of size, spatial relationship between antigen-binding sites, and synthesis protocol, which may affect their *in vivo* half-life and interactions with their respective ligands.[202] The physical constraint of the two antibody fragments is often central to their function, as bispecific antibodies are used to either physically link two different cell types or dimerize two different molecules on the surface of the same cell. Larger bispecific formats include the individual component antibodies linked by a chemical linker or the a Triomab, which maintains the full IgG shape by linking two half antibodies, each with one heavy and one light chain.[203] These families of bispecific antibodies can be easily synthesized by standard protocols to allow for high-throughput manufacturing, and they have extended half-lives compared to smaller proteins. However, they also maintain expression of the Fc region which may be recognized by Fc receptors and lead to unwanted off-target effects. At the opposite end of the spectrum are small bispecific platforms such as tandem single-chain variable fragments (scFvs), in which the heavy and light chains of two different variable domains are linked by a short serine-glycine linker.[204] These bispecific antibodies preclude Fc receptor recognition, but their small size (approximately 55 kDa) reduces half-life and necessitates constant intravenous infusion.[205]

Likely the most well-known type of bispecific antibodies in the field of cancer immunotherapy are bispecific T cell engagers (BiTEs). BiTEs link an anti-CD3 antibody fragment with an antibody fragment against a tumor-associated antigen, thus simultaneously activating T cells and physically linking them with tumor cells to induce lysis.[206] However, because BiTEs incorporate anti-CD3 rather than a pMHC, they non-specifically activate all T cells and thus are associated with dose-limiting toxicities including cytokine storms.[207] BiTEs have been developed linking T cell stimulation with various tumor-associated antigens such as CD19,[208,209] BCMA,[210] and EphA2.[211] However, like many targeted immunotherapies, they require engagement of a tumor-associated antigen and thus antigen escape is a concern. Interestingly, it was recently shown that BiTEs can mediate lysis of bystander tumor cells not expressing the targeted antigen.[212]

T cell-targeted bispecific antibodies have also been developed that cross-link two molecules on the surface of the same immune cell. A recent bispecific antibody, synthesized by chemically linking agonistic antibodies against the co-stimulatory receptors CD137 and CD134 on T cells, was more effective at activating an anti-tumor T cell response than either antibody individually.[213] In contrast with monotherapy, the platform uniquely induced preferential expansion of effector T cells. Thus, in addition to redirecting cells, bispecific antibodies can potentially impact T cell activation by physically clustering surface molecules. This approach may be particularly interesting for targeting other T cell signaling molecules since the activation process is highly sensitive to receptor clustering and spatial localization.

With the success of immune-activating bi-specifics, significant resources are being dedicated to increase the efficacy of current therapies while limiting toxicity. With nearly 60 preclinical drugs and 30 in clinical trials, knowledge gained from therapeutic efficacy will impact on our fundamental understanding of what constitutes ideal bi-specific properties, like pharmacokinetics.[214] Indeed techniques such as developing multiple-cancer epitopes for T-cell redirecting antibodies could increase the affinity and sensitivity of the therapy.[215] This would help to reduce non-specific toxicity such as cytokine storms that result from these immune-activating bi-specifics.

In addition to activating the immune system, development of bi-specifics is also expanding to other applications such as infectious and autoimmune diseases and diagnostic imaging. Besides T cell redirection, these bi-specifics have additional mechanisms of action: T cell recruitment, blockade of T-cell acting cytokines, inducing apoptosis, and inactivation of proteins. Indeed many autoimmune anti-cytokine therapies demonstrate additive effects when combined justifying the development of bi-specific for autoimmune diseases. Just one example includes a bi-specific developed towards TNF-α and IL-17 for the treatment of rheumatoid arthritis.[216] Here the bi-specific was engineered such that there were an additional two TNF-α and IL-17 Fab portions linked to Fc regions of the antibody, which induced significantly enhanced therapeutic reduction of arthritis potentially due to increased avidity. Similar results were found from a bi-specific targeting IL-17A and IL-6.[217]

HIV is an example of bi-specific design for infectious disease, where diversity and mutation lend for the need for combinatorial therapies. One example is a neutralizing antibody where one arm of the bi-specific is from antibodies towards either CD4 or

CCR5, which the HIV virus uses to enter the cell.[218] The other arm is composed of a Fab that is specific to viral envelope epitopes. These bi-specifics reduced viral load and provided complete protection upon viral challenge. Another example to broaden the diversity and increase the avidity of a neutralizing HIV antibody is the development of a tri-specific antibody which recognizes the CD4-binding site, V3 glycan patch, and the envelope membrane proximal external region.[219] The tri-specific antibody demonstrated enhanced and broad neutralization in comparison to mono-specific antibody therapies.

Another avenue for future bi-specific development is improving production and yield of the antibody. Here principles of directed evolution, cell engineering of hybridomas, and protein engineering of bi-specific structure will aim increase yield to decrease high cost associated with these therapies. Alternatively to *in vitro* production, bi-specifics could be produced *in vivo* through transfection of the bi-specific antibody construct. This was recently demonstrated in production of therapeutic levels of an anti-CD3/CD20 bi-specific in a mouse for effective anti-lymphoma therapeutic responses.[220]

2.3.2 Synthetic particles

In contrast to soluble antibodies and small molecules, nanoparticle-based therapies can be engineered to affect biodistribution and drug release profiles. Soluble or particle-conjugated signals can be conjugated to the surface or encapsulated within synthetic particles to directly affect T cell signaling or alter how other cell types interact with T cells. By altering the size, shape, material, or injection route of a particle, drugs can target specific immune subsets in defined timeframes. Here, we will review previous work in this field of immunoengineering and demonstrate how micro- and

nanotechnology can be used to deliver extracellular and intracellular signals to modulate T cell responses.

2.3.3.1 aAPC

Artificial antigen presenting cells (aAPC) are micro- or nano-sized platforms designed to mimic endogenous antigen presenting cells for T cell activation. aAPC are three dimensional cellular or synthetic platforms that minimally present the two necessary signals for T cell activation—peptide MHC, signal 1 (s1), and a co-stimulatory molecule, such as B7-1/B7-2 or αCD28 monoclonal antibody, signal 2 (s2).[221,222] aAPC have been explored in adoptive cell therapy (ACT), *ex vivo* activation of autologous lymphocytes with aAPC expressing tumor-specific peptide-MHC (pMHC), followed by re-infusion of the expanded cells into the patient.[223] Large numbers of expanded lymphocytes, up to 10^{11}, are needed to treat a single patient with ACT.[224] Additionally, research has shown the importance of not just quantity but, more importantly, quality of the resultant cells for a long-lived effector population post-transfer.[225]

Acellular aAPC have grown in importance for a variety of reasons. One reason is cost. Synthetic platforms can decrease costs by creating a more easily manufactured all-in-one off-the-shelf therapy. Another reason is that endogenous antigen-presenting cells (APCs) can become immunosuppressed and even immunosuppressive in cases such as cancer and chronic infection.[226–228] This poses problems for the achievement of effective innate anti-cancer responses, therapeutic vaccines and immunotherapies, and *ex vivo* activation of T cells for adoptive transfer. Thus, extensive work has been done to optimize acellular aAPC. Specifically, we will focus on engineering developments of the aAPC that has led to increased functionality: geometry, shape, signaling molecule choice, and material.

2.3.3.1.1 Size

aAPC size has implications to mimicking surface engagement of endogenous cells, biodistribution, and interaction with the nanoscale arrangement of receptors. Historically, micron-sized aAPC platforms were developed to mimic the endogenous APCs.[8,229–232] Large, micron-scale particles reduce the curvature at the T cell-aAPC interface and can thus interact with multiple TCRs and induce robust activation. However, spherical microparticles with low MHC signal 1 density cannot activate T cells to the same extent as particles with high density despite increasing particle dose.[230,233] Currently, this size is the preferred size for attaching the aCD3 and aC28 molecules used to expand polyclonal populations from tumor infiltrating lymphocyte populations for adoptive immunotherapy.[234]

Previously it was believed that nanoparticle aAPC could not induce robust T cell activation similar to large aAPC.[230,235] In one case, biodegradable aAPC of 150 nm and 8 μm were formed and showed that microparticles provided enhanced stimulation to antigen-specific T cells, although nanoparticles resulted in some minimal stimulation.[235] In another report, latex particles of 0.5 to 5 μm were engineered, and it was shown that larger particles generated greater responses.[230] It was hypothesized that the T cells needed to interact with a contiguous area of stimulatory ligands as opposed to the smaller areas provided by smaller particles.

However, this large size hinders the ability of aAPC to be used *in vivo.* Particles larger than 2 μm have a chance to cause embolization. Larger particles also have limited abilities to diffuse out into target organs where T cells reside and increases the rate of uptake by the mononuclear phagocytic system. To address this, researchers developed two versions of nanoparticle aAPC from iron oxide and quantum dot materials 30-100

nm in size.[236] Here, nanoparticles were shown to provide effective antigen-specific stimulation of both murine and human CD8+ T cells and provide tumor prevention. Furthermore, biodistribution studies were done to show that the smaller aAPC drained more efficiently to the lymph node that larger aAPC remained in the subcutaneous injection site.

In an effort to provide mechanistic insight into why these nanoparticles were functional, researchers varied both nanoparticle aAPC size and ligand density.[103] Here, particles of 50 nm, 300 nm, 600 nm, and the traditional 4.5 μm were compared head-to-head with controlled densities and quantities of signal. Interestingly, the smallest (50 nm) aAPC were again found to be less effective; however, aAPC 300 nm and above were just as effective as large 4.5 μm particles. Mechanistically this could be due to A) nearby clustering of signaling molecules was important and B) that particles larger than 300 nm aAPC are able to provide effective local engagement of multiple TCRs, while 50 nm aAPC only engage single receptors. This was confirmed by overcoming this limitation by both artificially clustering 50 nm aAPC with a magnetic field and adding saturating doses of 50 nm aAPC.

Ligand density can also be an important parameter, which should be considered in conjunction with size. Increasing the density of the ligand on smaller 50 nm aAPC did not overcome this effect, suggesting a larger particle footprint is needed to engage TCRs in protein nanoislands.[13,103,237] As the ligand spacing increased to greater than 100 nm, the ability to stimulate CD8+ T cells was abolished even for particles larger than 300 nm. This was consistent with the ligand requirements found from planar surface studies[60,238,239] and could explain why nano-aAPC were not stimulatory previously.

Therefore, both nano- and micro-sized aAPC can be effective with control of the ligand density, as both properties affect the area and number of ligands available to stimulate a CD8+ T cell effectively.

2.3.3.1.2 Shape

Despite their success in activating T cells at the cell-particle level, microscale particles have poor biodistribution and are thus suboptimal for *in vivo* applications. Microparticles cannot take advantage of the enhanced permeability and retention (EPR) effect to localize aAPC at the tumor site[240] and do not effectively drain to lymph nodes where immune stimulation occurs.[236,241] Thus, recent work has explored ways to optimize aAPC on more biocompatible, nano-scale platforms.

The spherical shape of aAPC is popular largely because of the ease of synthesis or fabrication procedures, such as emulsion techniques for PLGA.[242,243] However, spheres minimize the contact area at the T cell-aAPC interface despite the importance of multivalent pMHC-TCR interactions. Recent work has demonstrated how altering aAPC geometry can improve the stimulatory capabilities of both micro- and nano- aAPC. Importantly, modifications to aAPC shape have also helped to bring nano-aAPC into the playing field.

Ellipsoidal synthetic aAPC can be developed by physically stretching spherical PLGA particles made by standard emulsion techniques.[116] These oblong particles can be generated with aspect ratios over 6 and conjugated with equivalent protein densities, allowing for comparison between them and their spherical counterparts. Increasing the micro-aAPC aspect ratio (i.e., degree of stretching) positively correlates with CD8+ T cell proliferation and maximally induces a 20-fold stronger T cell response. Interestingly, proliferation did not increase linearly with increased particle stretching but rather resulted

in more significant gains at specific aspect ratios. This geometry-driven change in T cell proliferation was shown to be correlated with changes to the T cell-aAPC interface. Ellipsoidal aAPC bound to more T cells, and individual contact areas were larger than those in spherical interactions, thus suggesting that increased avidity and interactions with multiple TCR may drive their improved efficacy.

The geometry effect is also maintained on the nanoscale.[117] Ellipsoidal nano-aAPC with spherical diameters on the order of approximately 200 nm induce a five-fold stronger T cell response than their corresponding spherical nano-aAPC. As shown with other systems,[88,112,113] ellipsoidal aAPC resisted uptake by RES cells and thus had longer circulation times *in vivo*. This increased ability to stimulate T cells and longer circulation times led to significantly increased T cell proliferation *in vivo*.

In contrast to methods that manipulate the geometry of the base particle, magnetic fields have also been utilized to alter how nano-aAPC interact with T cells. Superparamagnetic spherical iron-dextran aAPC with a diameter of 100 nm do not normally activate a robust T cell response. However, when an external magnetic field is applied, the nano-aAPC cluster on the T cell surface, changing the perceived shape and size of the aAPC by the T cell, and likewise increase proliferation.[103,244] This method enables nano-aAPC to activate rare endogenous T cell populations for adoptive cell transfer.

2.3.3.1.3 Ligand Choice

Ligand choice is another critical parameter in the development of aAPC. Traditionally, aAPC are conjugated with the two necessary signals for T cell activation—anti-CD3 mAb or a specific pMHC, signal 1, and B7 or anti-CD28 mAb, signal 2. The choice of anti-CD3 mAb or pMHC dictates whether all T cells or only T cells

recognizing a specific target are activated. Often, a specific pMHC will be chosen to target antigen-specific T cell responses, although interesting work has demonstrated how phenotypic markers can be used post-nonspecific activation to select specific T cell subsets.[245] A great deal of work in antigen discovery and immunogenicity has been conducted and is ongoing in the selection of a specific pMHC targets for different applications.

Despite the fact that signaling through CD28 is the main co-stimulatory signal provided by synthetic aAPC, the composition of co-stimulatory signals greatly impacts T cell activation. There are dozens of different types of co-stimulatory signal 2 molecules, and altering the combinations and ratios of these signals can impact proliferation, phenotype, and survival *in vivo*. These T cell co-stimulatory molecules include pathways such as CD70-CD27, CD40-CD40L, 4-1BB-4-1BBL, OX40L-OX40, and others expressed on the antigen presenting cell and T cell, respectively.[48]

Studies have shown that co-stimulation through 4-1BB during the rapid expansion protocol for adoptive cell transfer improves the expansion and effector function of tumor-specific T cells.[246] 4-1BB co-stimulation has also been associated with the preferential expansion of memory T cells, which are often desired for *in vivo* transfer applications.[247] Combining multiple co-stimulatory signals on the same aAPC also can have significant effects on T cell functionality. A study combining CD28, 4-1BB, and CD27 signaling on K562 aAPC demonstrated that certain combinations of the co-stimulatory molecules can increase proliferation over 10-fold.[4] Even when the same total amount of co-stimulation is present, simply changing the ratio of signal 2 ligands can impact the resultant T cells. In one study, micron-sized polystyrene aAPC conjugated with different ratios of anti-

CD28 and anti-4-1BB mAb affected antigen-specific proliferation as much as five-fold.[8] Other co-stimulatory molecules, such as activation through OX40[192] and CD40L,[248,249] which have been shown to have stimulatory effects on T cells, could also be incorporated in next generation aAPC. A new type of aAPC activation platform where each type of signaling molecule is separated onto distinct, magnetically clustered nanoparticles allows for high throughput customization of signal 2 choice, ratio, and amount by enabling an infinite number of activation conditions from a finite number of functionalized nanoparticles.[250] Using this platform, combinations of anti-CD28, anti-4-1BB, and anti-CD27 signaling were shown to affect T cell proliferation and phenotype. This approach may serve as a useful mechanism to systematically study co-stimulatory composition.

In addition to the choice of signal 1 and signal 2, aAPC can be conjugated with other molecules to enhance their efficacy. CD47 is a molecule ubiquitously expressed by normal cells that protects self-cells against phagocytosis.[251] aAPC that also display CD47 have been shown to also be protected from phagocytosis and induce greater stimulation of T cells *in vivo*.[252]

2.3.3.1.4 Material

aAPC have been formed from materials that are inorganic, organic, biologically-derived, or a combination thereof. Each material choice enables unique functionality and imparts distinct aAPC properties. For example, functions include responsiveness to external stimuli, ligand mobility, biocompatibility, degradability, biodistribution, nanoscale arrangement of receptors, and encapsulation of additional modulators. Therefore, the desired function of the aAPC can drive selection of material.

Iron oxide based aAPC can be effectively used in adoptive immunotherapy expansion protocols as they can be easily removed through magnetic field separation,

prior to infusion.[221,253] Magnetic forces have been used additionally to induce aAPC clustering on the surface of CD8+ T cells and enrich antigen-specific cells.[244,254] First, clustering of nanoparticle iron oxide aAPC within a magnetic field lead to much greater stimulation of CD8+ T cells at a much lower dose of aAPC than without the magnetic field.[244] This increased TCR cluster size on the surface of the T cells has been shown to be important for T cell activation.[66] The enhanced *ex vivo* stimulation translated to increased *in vivo* efficacy of adoptively transferred cells in a tumor treatment model. More recently, magnetic fields have been used to home magnetic aAPC *in vivo* to tumor sites to mediate effective tumor killing.[255]

Beyond clustering, Perica et al. used these antigen-specific nano-aAPC to magnetically enrich for antigen-specific CD8+ T cells.[254] The approach is to first add the aAPC to bind rare antigen-specific CD8+ T cells, then enrich the antigen-specific cells, and because the aAPC are still bound to the enriched cells, simultaneously stimulate only the enriched cells to proliferate. Impressively, antigen-specific murine and human CD8+ T cells were expanded more than 1,000-10,000-fold over their precursor frequency. This was used to identify novel neoantigens predicted by tumor sequencing and also used in adoptive transfer model of murine melanomas.

Organic materials are used for improved biocompatibility, biodegradation properties, ability to form shapes other than spheres, and capacity to encapsulate material.[256] This is true as well for the aAPC. Particle aAPC have been made from poly(lactic-co-glycolic acid) (PLGA), which is a component of several FDA-approved devices and therapeutics and has high biocompatibility, allowing aAPC to be used for direct *in vivo* therapy.[257] Direct *in vivo* therapy with aAPC is desirable not only because it

would allow continued modulation and activation of CD8+ T cells *in vivo* but also because it would potentially eliminate the need for *ex vivo* stimulation. These biodegradable aAPC were effective at stimulating CD8+ T cells *ex vivo* and provided enhanced activation in response to a tumor when combined with checkpoint blockade molecule anti-PD1. This *in vitro* finding was confirmed *in vivo* as the combination of aAPC and anti-PD1 was able to delay tumor growth in an aggressive melanoma cancer treatment model more than either individual modality alone. Additionally, polymers like PLGA are plastic, so they can be formed into different shapes as discussed in section 3.3.1.2, which may enable enhanced biodistribution and T cell contact.[116,258]

Moreover, organic particles formed by emulsion techniques can be utilized for encapsulation of soluble signals. T cell stimulation often requires a third signal from cytokine IL-2 from CD4+ T cells to become fully activated and have the capacity to proliferate.[259–261] Steenblock et al. developed a PLGA aAPC with IL-2 encapsulated to mediate close paracrine delivery of the cytokine while the aAPC are bound to antigen-specific CD8+ T cells to mimic signal 3 delivery *in vivo*.[262] Having the IL-2 encapsulated improved the CD8+ to CD4+ T cell ratio and enhanced CD8+ T cell activation with upregulation of the IL-2 receptor, CD25. Encapsulation of IL-2 was 100 times more potent than the simple addition of soluble IL-2 to the culture medium, suggesting the advantage of cytokine encapsulation.

As an alternative to organic materials, biological materials are another biocompatible platform to which T cell stimulatory signals can be attached. Beyond biocompatibility, these materials may evade the mononuclear phagocytic system more effectively and thus provide a more effective *in vivo* therapeutic. Another advantage for

biological materials is the ability to have fluid membranes, which may impact the mobility of the signaling receptors and allow for the needed clustering of the receptors upon engagement.

Recently, red blood cells (RBCs) have been utilized as a bio-inspired method for cargo delivery or as a depot of imaging agents.[263] RBCs have 'don't-eat-me' signals on their surface, which enables long circulation times. Sun et al. recently attached signaling molecules, including IL-2, to the surface of red blood cells.[264] While there was no *in vivo* work demonstrated, these provided effective stimulation to antigen-specific cells that were able to mediate cancer-specific killing *in vitro*.

Liposomes are particles developed from lipids that form a lipid bilayer similar to that of the cell, but the size can be modulated from the nm to μm range. Liposome based aAPC were developed to utilize clustering technology derived from lipid rafts to show that having distinct, locally dense MHC rather than diffusely spread MHC improved T cell activation.[265] Additionally, because it has been shown that endogenous MHCs are clustered in lipid rafts on DCs, another group has taken natural MHCs from DCs and added the molecules to liposomes.[266] These RAFTsome aAPC showed effective activation *in vitro* and tumor protection in an immunization model. This could be potentially used to load patient-derived MHCs pre-loaded with cancer antigens to induce a polyclonal antigen-specific response without characterizing individual antigenic specificities.

Finally, as each material has unique functionalities, researchers have aimed to combine materials for more elaborate aAPC designs. One example, is an aAPC developed from carbon nanotubes, polymer (PLGA) nanoparticles, and magnetite.[267] The

carbon nanotubes were used to form the particle scaffold, which proves the high surface area needed for effective multivalent aAPC-T cell interactions. The PLGA nanoparticles were loaded with IL-2 to induce paracrine signaling of signal 3. Furthermore, magnetite was embedded in these particles to enable magnetic removal of particles following T cell stimulation for adoptive immunotherapy. These aAPC provided effective long-term stimulation of both murine and human CD8+ T cells and delayed tumor growth in a melanoma treatment model.

2.3.3.2. Particles with ligands for T cells

In addition to creating artificial antigen presenting cells for activating T cell responses, pMHC molecules have been attached to particles for limiting the immune response.[64,268,269] This approach aims to mimic peripheral tolerance where presentation of antigen in the absence of costimulatory molecules leads to anergy, apoptosis, or conversion to a regulatory phenotype. Indeed this has been done for both attaching pMHC class I and II molecules and inducing both antigen-specific regulatory CD4+ and CD8+ T cells with the effect of reducing autoimmunity in multiple models including diabetes, multiple sclerosis, and arthritis. To be able to administer these particle intravenously, particles less than 20 nm were utilized for engineering studies to identify key parameters necessary for both *in vivo* function and safety.[269] Indeed similar to artificial antigen-presenting cell studies, density of the pMHC was a key component of the efficacy of their particles, where less than 3-6 nm intermolecular spacing was most efficacious in eliciting antigen-specific T cell responses. This density may allow enhanced binding with TCR nanoclusters and clustered binding in macroclusters is observed experimentally and confirmed *in silico* through modeling.

In addition to particles that interact only with T cells (i.e., aAPC) and particles that interact only with antigen presenting cells (i.e., particle-based vaccines), particles can be engineered to bind multiple cell types simultaneously, inducing new interactions or changing existing ones. In these instances, a nanoparticle platform is used to increase avidity for the targeted antigens or alter biodistribution. In one study, 50 nm particles were used to redirect a T cell response against a specific tumor antigen, similar in approach to bispecific T cell engagers.[270] These nanoparticles, termed antigen-specific T cell redirectors (ATR), were conjugated with an antibody against the CD19 tumor antigen and non-tumor peptide-MHC. When MHC-bound ATR were loaded with a human flu peptide, human flu-specific T cells were redirected to kill CD19+ tumor cells.

In contrast to a tumor cell-T cell dual-binding nanoparticle that presents a specific peptide MHC complex, nanoparticles that bind to other non-specific cell surface molecules on the two cell types have shown similar efficacy. For example, an 80 nm particle, termed immunoswitch, links antibodies against the co-stimulatory 4-1BB molecule expressed by T cells with antibodies against the co-inhibitory molecule PD-L1 expressed by tumor cells and thus converts an inhibitory signal into a co-stimulatory signal within the tumor microenvironment.[271] These particles were shown to increase effector-target cell conjugation and induce a more robust CD8+ tumor-infiltrating lymphocyte response and delay or eliminate tumor growth in multiple murine tumor models.

2.3.2.2 Particle vaccines for T cell activation

Synthetic particles can also be engineered to affect which cell types T cells interact with, alter a cell interaction that is already present, or alter the phenotype and activity of other immune cells that modulate T cell activity. Dendritic cells (DCs) play a

central role in orchestrating both the innate and adaptive immune response.[272] In an optimal response, dendritic cells express peptide fragments of invading pathogens as well as express co-stimulatory molecules that enable their efficient activation of T cells. However, in the instance of cancer or chronic infection, this process does not always occur appropriately. One method to initiate a more robust T cell response is thus to enhance antigen presentation or co-stimulation by DCs which can then mediate the T cell response. Since our analysis is focused on T cells we will only provide a brief summary of particle properties for vaccines, where more detailed reviews analyzing the density of antigen, size of particle, and material chemistry have already been completed.[273]

Activation of DCs and other antigen presenting cells, like T cell activation, is sensitive to the environment. A stimulatory environment with appropriate stimulation kinetics is crucial to induce activation rather than tolerance. In order to control the stimulatory conditions, DCs can be extracted from a patient, and the signals for activation can be fully controlled *ex vivo*. Cell-based DC vaccines, such Sipuleucel-T,[274,275] involve this *ex vivo* activation of DCs against a tumor antigen followed by their re-infusion into the patient where they can circulate throughout the body and activate an anti-tumor immune response. However, this approach is time-consuming and expensive as it involves manipulating cells outside of the human body and often has to be completed at non-local sites. Nanoparticles have generated great interest in the field of vaccine delivery due to their ability to be engineered to manipulate *in vivo* biodistribution and kinetics of vaccine delivery.[276] Biomaterials can also potentially be used to target vaccination to specific DC subsets which has an effect on vaccine efficacy.[277]

Various studies have explored using nanoparticles to effectively delivery antigen to DCs directly *in vivo*. In the design of nanoparticle-based vaccination, particle size plays an important role in lymph node trafficking. Pluronic copolymer-coated nanoparticles (25 nm) injected intradermally were shown to travel to draining lymph nodes through interstitial flow and remain there for at least 120 hours where they could activate a humoral and cellular immune response against a model antigen.[109] In contrast, particles just four times larger—100 nm—were approximately 10% as efficient and were undetectable in draining lymph nodes within 24 hours. In another study using polystyrene particles ranging in size from 20 nm to 2 μm, 40 nm particles most efficiently trafficked to lymph nodes and activated resident DCs.[278] Similar to spherical nanoparticles, nanodiscs have been used for vaccine delivery. Small vaccine-carrying lipoprotein nanodiscs approximately 10 nm in diameter were shown to be more effective than soluble vaccines.[279] These nanodiscs were coupled with antigen peptides and adjuvant and were shown to elicit up to 47-fold greater frequency of tumor-specific T cells than soluble vaccines. Utilization of a nanodisc carrier allowed antigen and adjuvant to accumulate in lymph nodes, where there is a high density of dendritic cells, more than soluble injected vaccines. Most successful particle-based vaccines are engineered with sub-100 nm particles. Particles larger than approximately 200 nm require cellular transport by DCs in the skin to travel to the lymph node.[280]

Particle-antigen conjugates have also been used to generate tolerance in the setting of autoimmune diseases. These approaches focus on delivering auto-antigen similar to particle vaccines, but in the absence of danger signal to generate tolerance. One recent example utilized a quantum dot base particle to enable imaging of trafficked

particles within lymph nodes and cellular compartments.[281] Interestingly, the investigators found that higher numbers of low density auto-antigen on the particles were more effective than lower numbers of high density auto-antigen in reducing autoimmunity in a model of multiple sclerosis in mice by increasing regulatory T cells. Potentially the therapeutic effect could be similar to how peripheral tolerance is developed through high systemic levels of auto-antigen in the absence of danger signal.

In addition to controlling antigen density and dose, co-delivery of immunosuppressive agents has been key for mediating effective regulatory immune responses in autoimmune therapies. One example is the use of adjuvants for toll-like receptors (TLRs) such as GpG, which promotes tolerance through TLR9. Because it is electrostatic it has been complexed with self-antigen to form polyelectrolyte multi-layer particles and used to effectively eliminate disease in a mouse model of multiple sclerosis.[282] Another example, utilized different sized microparticles, where a smaller 0.5-2 μm microparticle could be phagocytosed with either vitamin D3 or insulin B peptide, and a larger 30 μm microparticle could be a depot of immune-regulatory signal such as TGF-β or GM-CSF.[283] The combination of all four particles enabled prevention of diabetes through controlling dendritic cell phenotype and antigen presentation. In addition to the many various strategies to deliver self-antigen with particles,[284] researchers are also conjugating self-antigen to the surface of red blood cells to utilize a natural pathway for tolerance through the clearing of apoptotic cells.[285] Using this approach, there were benefits in alleviating multiple sclerosis and diabetes in mice both as a preventative and therapeutic treatment.

Various other similar techniques have been utilized that take advantage of nanoparticle trafficking to secondary lymphoid organs by altering size or the biomaterial or by incorporating specific receptors. Nanoparticle "backpacks" have been developed that deliver vaccines to lymph node DCs by binding DC receptors, such as CD40 or DEC-205, or by binding endogenous albumin.[130,286–289] In addition to modulating the biodistribution of the vaccine, approaches have been developed to alter how the delivered peptide is presented by the DC. During normal activation, intracellular antigens are presented on MHC-I and activate a cell-mediated CD8+ T cell response, whereas endocytosed antigens are presented on MHC-II and activate a humoral CD4+ T cell mediated response. To induce presentation by DC on MHC-I, nanoparticle-based vaccines have been developed that are capable of escaping the endosome upon internalization.[290]

2.3.2.3 Drug carrier particles

Synthetic particles that allow for the engineering of shape, modulation of biodegradation properties, and conjugation with or encapsulation of drugs that affect these various pathways provide a mechanism to direct drug release kinetics with defined distribution throughout the body. In terms of extracellular T cell modulation, conjugating artificial antigen presenting cells with the necessary signals for T cell activation is the main approach. However, biodegradable particles can also be used to selectively deliver soluble signals that affect T cell activation.

During endogenous T cell stimulation, T cells receive soluble "signal 3" molecules that drive proliferation and cytotoxicity.[12] These soluble mediators are secreted in a localized paracrine or autocrine fashion that increases their local concentration and limits exposure to the desired cells. Because these signals are often broadly immune

activating, local delivery ensures that only the target cells are affected to avoid undesirable autoimmune responses. This important aspect of local immune stimulation cannot generally be achieved when immune-activating drugs are administered systemically. To more closely mimic the endogenous process and enable maximum T cell expansion, nanoparticles have been used to selectively deliver stimulatory signals in a paracrine manner to T cells of interest. Biodegradable polymers are often the material of choice because their degradation and intracellular delivery properties can be manipulated.

Local delivery can be crucial especially in the context of autoimmune and allergic disease, where current therapies are systemic immunosuppression, though majority of the disease is not. One example of particle delivery of immunomodulatory agents, was the delivery of IL-2, TGF-β1, and Rapamycin biodegradable particles to suppress allergic contact dermatitis.[291] This combination mimic and potentiate the signals given by DCs to expand regulatory T cells *in vivo*. Encapsulation of these agents into particle allows co-delivery to eliminate potential immune activating effects of IL-2, local delivery to target inflamed areas, and prevent future allergic responses. Another example is biodegradable particle delivery of CCL22, a chemokine that recruits regulatory T cells, to treat autoimmune mediated dry eye disease,[292] transplant rejection,[293] and periodontal disease.[294]

Various methods have been developed to target these drug-delivery particles to specific immune subsets. One approach is to combine drug delivery with an aAPC to take advantage of both aAPC-based extracellular stimulation as well as localized drug delivery, as is the case with IL-2-encapsulated aAPC.[235,262] Biodegradable particles

decorated with specific pMHC have also been used to selectively deliver cytotoxic drugs to cognate T cells for applications in autoimmunity.[295]

Similarly, nanoparticles conjugated with T cell signaling molecules have been used to simply target the nanoparticles to T cells with the goal of intracellular drug delivery. Gelatin nanoparticles approximately 200 nm in diameter conjugated with anti-CD3 mAb have been shown to be selectively internalized by T cells.[296] Over 80% of T cell leukemia cells were observed to take up the particles, demonstrating the potential for nanoparticles for the delivery of intracellular signals. More recently, this approach has demonstrated success in transfecting T cells with genetic material. Anti-CD3 mAb-coated biodegradable nanoparticles approximately 150 nm in diameter were engineered to encapsulate a DNA plasmid encoding for a specific chimeric antigen receptor (CAR).[101] The particles showed specific transfection of T cells with approximately only 5% of non-T cells showing uptake following intravenous administration. Remarkably, systemic administration of these nanoparticles resulted in the same degree of anti-leukemia activity when compared to adoptive cell transfer of *ex vivo* transfected CAR T cells, which will be discussed below in greater detail. Thus, the nanoparticle approach was able to significantly reduce the cost and time requirements of lymphodepletion and *ex vivo* T cell manipulation. More specific targeting of T cell subsets is also possible, as anti-CD4 mAb conjugated lipid nanoparticles have been shown to selectively target CD4+ T cells *in vitro* and *in vivo*.[297] These nanoparticles selectively delivered CD45 siRNA and induced gene silencing up to 20% in CD4+ T cells five days post intravenous administration.

Localized drug delivery to T cells can also be achieved through combination with adoptive cell therapy. For example, nanoparticles can be covalently linked to T cells

expanded *in vitro* prior to re-infusion. In one study, drug-releasing nanoparticles were covalently linked to the surface of tumor-targeting T cells prior to adoptive cell transfer.[298] Using nanoparticles that released an inhibitor of immune-inhibitory signals, nanoparticle-functionalized T cells achieved greater expansion at the tumor site compared to systemic administration of the drug, achieving a 14 day survival advantage. Importantly, this study also demonstrated that the nanoparticles were translocated into the immune synapse during T cell activation. To further modulate not just the cell-proximity of drug release but also its temporal profile, T cell-bound nanoparticles have been developed that release drug only upon T cell stimulation.[299] When CD8+ T cells become activated, they release lytic granules, and this property has recently been used to trigger nanoparticle degradation. These nanoparticles, when bound to HIV-specific CD8+ T cells, were shown to enable the delivery of an immunotherapeutic to a site of high viral replication.

Most T cell-targeting nanoparticles for local drug delivery to date have targeted CD4, CD3, or TCR expression. However, it is important to appropriately select the targeting molecule for the most effective response. Whether or not a targeting molecule is internalized can significantly affect the T cell response to nanoparticle-mediated drug delivery. A study that investigated targeting nanoparticles that released a TGF-β inhibitor to T cell internalizing versus non-internalizing receptors showed differing responses, and this effect changed if T cells were conjugated with nanoparticles prior to adoptive cell transfer or targeted directly by intravenously administered particles.[300]

When widespread circulation of a drug is important, smaller particles or molecules are often preferred due to their superior biodistribution. However, in some

cases, limiting the circulation of a drug may be desired, such as with non-specific immune activators meant to target T cells infiltrating a tumor. Systemic administration of stimulatory molecules such as IL-2 and anti-4-1BB mAb are associated with various off-target toxicities due to widespread immune activation.[301,302] Thus, a different approach to drug delivery is to anchor drugs to particles and inject them locally at the site of interest for the purpose of prolonging drug retention. Studies have shown that anchoring IL-2 and anti-4-1BB mAb to the surface of liposomes approximately 160 nm in diameter significantly reduces off-target toxicities when injected intratumorally.[303,304] Even when injected intratumorally, the soluble antibody and cytokine were detectable at high levels 18 hours post-injection and resulted in significant weight loss of treated mice. In contrast, the nanoparticle-anchored drugs limited drug exposure to the tumor site and were shown to treat murine melanoma. Similar results have been observed with locally administered nanoparticles functionalized with anti-4-1BB and anti-PD-L1 mAbs.[271]

2.3.3 Cellular and Genetic Engineering

The ability to directly engineer cellular function through genetic techniques has increased due to new molecular tools such as CRISPR system (Clustered Regularly Interspaced Short Palindromic Repeats). Additionally, the motivation to engineer cells has increased with the recent success and approvals of chimeric antigen receptor (CAR) T cell therapy. Again, this section will look at engineering principles that enable specificity, control, and enhancement of these cellular engineering approaches and therapies.

2.3.3.1 Cell-based Artificial Antigen Presenting Cells

In addition to synthetic substrates, cell lines have been used to develop artificial antigen-presenting cells (aAPC) with the aim of eliminating the burden of using endogenous APCs for stimulating T cells for adoptive immunotherapy.[305] This cellular approach enables greater biomimicry than synthetic aAPC; however, standardization and stability of the construct can be difficult to control. Additionally, cells used for aAPC are often not APCs and do not express important co-stimulatory molecules or cytokines needed for effective T cell activation. Therefore, cell-based aAPC will need to be efficiently transfected, stably express manipulated genes, and downregulate all other non-specific HLA molecules to avoid activation of allospecific T cells.

A popular choice of cell line to manipulate is the K562 erythromyeloid cell line by retroviral transfection. Researchers have transduced this cell line to stably express Fcγ receptors and 41BB ligand.[306] Anti-CD3 and Anti-CD28 were added to form the complete aAPC to provide polyclonal T cell expansion. The addition of 41BB ligand induced effective T cell proliferation and limited CD8+ T cell apoptosis. Another group also showed the incorporation of the 41BB ligand improved stimulation with other co-stimulatory ligands, including CD70 and CD80.[4] Co-stimulation including CD83 was able to stimulate T cells without the addition of exogenous cytokines.[307] Thus, the choice of co-stimulatory molecule(s) for cell-based aAPC impacts the ability to provide effective T cell stimulation.

Cytokines act as a third signal in T cell stimulation and are expensive to add to cultures. Therefore, work is being done to incorporate the expression of T cell stimulating cytokines into cell-based aAPC. IL-21, a cytokine that signals through the IL-2Rγ receptor, has been included into the membrane of aAPC and increased the number of

CAR T cells and improved tumor killing *in vivo*.[308] Similarly, IL-15 has been stably expressed on the membrane of cell-based aAPC.[309] Although soluble IL-15 enhanced T cell activation and cytotoxicity, membrane-bound IL-15 established greater levels of activation, proliferation, and maintenance of the central memory phenotype, as well as nearly three times the cytotoxicity.

Researchers have also used cell-based aAPC to stimulate CMV (cytomegalovirus)-specific T cell responses.[310] Here they transduced their aAPC to express HLA-A2, CMV peptide, co-stimulatory marker CD80, and adhesion ligands ICAM-1 and LFA-3. This aAPC produced similar levels of antigen-specific cells compared to endogenous APCs and transfected primary B cells used as APCs. Similarly, this antigen-specific activation has also been applied to CD4+ T cells for immunotherapy.[311]

Beyond polyclonal and virus-specific antigens, these aAPC are primarily designed for adoptive immunotherapy in cancer therapy. To this end, cells were engineered to activate cancer-specific T cells recognizing the MART-1 antigen found within melanoma.[312] Importantly, these cells were developed under Good Manufacturing Practices (GMP) guidelines, enabling the potential translation to the clinic. Another example of generating tumor-specific T cells is the manipulation of another popular cell line, fibroblast NIH 3T3 cells. Telomerase-specific CD8+ T cells were activated by engineered 3T3 fibroblasts in an effort to target tumors overexpressing the protein.[313] T cells stimulated by these aAPC were cytotoxic in a chromium release assay against human telomerase reverse transcriptase expressing tumor cell lines.

2.3.3.2 CAR T cells

Chimeric Antigen Receptor (CAR) T cells are T cells that have been genetically engineered to express a receptor with two major functions: 1) antigen recognition, typically through antibody binding, and 2) T cell activation through phosphorylation of canonical intracellular domains.[314] These CAR T cells have had tremendous clinical success in treating B cell tumors.[315–317] Recently, Tisagenlecleucel became the first FDA-approved CAR T cell therapy for pediatric patients with recurrent B cell acute lymphoblastic leukemia after failing two previous therapies.[318] This has spurred development of CAR T cell construct for applications other than cancer including regulatory CAR T cells for autoimmune disease and tissue transplantation.[319] Despite incredible clinical progress, major hurdles face the translation of this technology, including safety, specificity, and cost.[320,321] Here we will highlight some of the more recent engineering approaches used to address these issues.

One of the main toxicities associated with CAR T cell therapy is the severe cytokine release syndrome or cytokine storm, leading to complications and death.[322–324] Clinically, groups have managed the toxicities by using biomarkers, such as cytokine levels, as an indication for early intervention.[322] More recently, researchers have developed techniques to "turn off" CAR T cells to limit the toxicity. One example is the incorporation of the Caspase-9 gene into the CAR T cell construct.[325] When the small molecule AP1903 is administered, this dimerizes to cause apoptosis in CAR T cells.

Another method of decreasing the toxicity of CAR T cells is to increase the specificity of the construct. For current therapies, the construct identifies CD19, which is expressed on both healthy and malignant B cells. To target cancers specifically,

researchers are targeting antigens like HER2, NY-ESO-1, ROR-1, and MUC16 that are overexpressed within tumor tissues.[324,326–328]

An additional method to increase the specificity is to engineer the CAR construct to recognize tumor-specific antigens expressed in HLA molecules similar to how TCR molecules recognize antigens. The majority of CAR T cells are developed from single-chain variable fragments (scFvs). Early scFvs originated with tumor-specific monoclonal antibodies; however, utilizing scFvs have much higher affinity than TCRs which can cause issues in intracellular signaling and may not recognize intracellular antigens. Indeed scFvs have been made to recognize cancer antigens in the context of HLA, but the affinity of the construct limited efficacy as compared to a low affinity TCR construct recognizing the same HLA-antigen construct.[329] To accomplish scFv design, researchers employed antibody engineering techniques as mentioned in section 3.1.2 such as phage display to fine tune antibody specificity and affinity towards the desired peptide HLA complex. This limits discovery to affinity and specificity, but does not inform on cell activity upon ligation or even expression. Researchers have recently developed another screening technique which includes transduction of T cells with scFv libraries, such that structural design and specificity can be linked back to function and phenotype.[330,331]

Further specificity and control can be programmed by development of a "two signal" approach, similar to canonical T cell stimulation where co-stimulation is needed. However, in this case CAR T cell co-stimulatory constructs are designed to recognize a second antigen to enhance the specificity of tumor killing.[332,333] Similarly, instead of an AND-gate, a NOT-switch can be developed by adding a second signal that is present on normal cells to act as an inhibitory signal, similar to canonical PD-1 signaling.[334] An On-

switch has also been reported, where CAR T cells can only be activated in the presence of a small-molecule to crosslink signaling domains.[335] Indeed the repertoire engineering approaches to regulate CAR signaling through modifying the signal inputs or interpretation is a growing field.[314]

Density can also be used to regulate specificity, with the design of lower affinity CAR constructs. One group decreased the affinity of EGFR-targeting CAR T cells to demonstrate lower toxicity to in normal cells that express a lower density of EGFR than cancer cells.[336] Additionally, the TCR-MHC interaction is lower affinity than antibody-antigen interactions and is proposed to confer increased sensitivity to lower density of antigens through serially signaling.[73] This fact may also help in targeting lower density antigens where increased sensitivity is required and has been shown to result in increased efficacy of CAR T cells in comparison to higher affinity antibody-based CAR T cells.[329]

Ultimate specificity could be achieved by targeting neoantigens. Neoantigens are novel antigens that are produced by mutations in the tumor.[337,338] Adoptive transfer of endogenously activated neoantigen-specific T cells has also shown good clinical responses.[339,340] However, adopting this approach to CAR T cell therapy is difficult because each patient has unique mutations, identifying the reactivity to mutations is time-consuming, and development of a CAR-T cell with a TCR is less established.

While limiting toxicity is a primary aim of advancing CAR T cell therapy, there are developments being investigated in tandem to increase its efficacy. One main challenge facing all immunotherapies is the tumor immunosuppressive environment. To combat this, CAR T cells can be used in conjunction with checkpoint blockade molecules[341] or be programmed to decrease inhibitory markers like PD-1,[342] secrete pro-

inflammatory cytokines,[343] and create OR-switches to target multiple antigens independently.[344]

Exhaustion is a challenge that faces CAR T cells in addition to adoptively transferred cells. To overcome exhaustion and increase the functionality of their CAR T cells, researchers have adopted the more recent CRISPR/Cas9 genome editing technology.[345] CRISPR/Cas9 allowed the insertion of the CAR T-cell receptor α constant region of the genome to more accurately mimic T cell receptor expression. Indeed CAR constructs were downregulated following stimulation and then re-expressed similar to TCRs upon T cell activation, which led to a decrease in exhaustion markers. Doing so generated CAR T cells that were much more potent than conventionally retrovirally transduced CAR T cells in treating a mouse model of acute lymphoblastic leukemia.

Additionally, standardizing cell source and maintenance of cell phenotype *ex vivo* have been challenges for efficacy, particularly for regulatory CAR T cell development. In a recent study researchers isolated regulatory T cells that were CD25+CD45RA+, which show more stable maintenance of regulatory phenotype and confirmed the phenotype stability by examining epigenetic markers close to FOXP3.[346] These cells were effective at preventing graft-versus-host disease in a mouse model; however, development and expansion of these cells still required substantial time, multiple processes, and feeder cells.

Finally, cost and technical challenges are major hurdles to translating this therapy for widespread adoption. One reason is all the *ex vivo* manipulation of patient cells, limiting this therapy to specific certified locations. To eliminate the need for *ex vivo* handling of cells, Smith et al. developed nanoparticles that transfected immune cells *in*

vivo by targeting the CD3 receptor on T cells.[101] They demonstrated effective *in vivo* transfection and tumor treatment in model murine tumors.

2.3.3.3 Other Genetic Engineering Applications

Genetic engineering of T cells goes beyond CAR T cells in the fields of infectious disease and autoimmunity. The HIV virus targets CD4+ T cells through human chemokine receptor 5 gene (CCR5). To minimize HIV disease spreading and latency in patients, researchers knocked out the CCR5 gene in *ex vivo* manipulated CD4+ T cells and reintroduced into patients.[347] CD4+ T cells without CCR5 persisted longer than untreated cells and patients who received the therapy had increased levels of CD4+ T cells and lower levels of viremia.

Another example of knocking-down a gene takes inspiration from the success that checkpoint blockade therapy has experienced. Researchers used a CRISPR Cas9 approach to eliminate expression of PD-1 by CAR T cells.[342] Gene editing produced much more functional CAR T cells in completely eliminating established tumors that expressed PD-L1. Finally, engineering of cytokine and chemokine receptors has been used to study cytokine pathways and also to control activation of T cells *in vivo*.[348,349]

Genetic engineering has been used to convert and maintain T cell phenotype. CD4+ regulatory T cells are an example of this genetic manipulation because the stable expression of regulatory constructs play a crucial role at establishing and maintaining tolerance; however, when isolated and cultured *in vitro* often may lose their phenotype or effector T cells will dominate. To solve this, lentiviral transduction of CD4+ T cells with FOXP3 enabled sustained suppressor activity by naïve and memory T cells.[350] Transduced CD4+ T cells with FOXP3 or IL-10 have demonstrated tolerance induction in models of tissue transplantation.[351,352] In addition to FOXP3, CD4+ T cells have been

transduced to express class II MHC loaded with autoantigen and FOXP3 and enhanced suppression of autoimmune arthritis in mice.[353]

2.3.4 Scaffolds and Surfaces

Similar to particle-based technologies, scaffolds and surfaces are materials that can be engineered to directly modulate T cell responses. What makes scaffolds and surface technologies unique are the a) ability to directly pattern and coat with proteins in distinct geometric locations, b) ability to tune unique biophysical properties such as stiffness, c) size of the material enabling development of multicellular interactions, d) capacity to move to three dimensional interactions and potential to create artificial organs. Here we will focus on both 2D and 3D technologies that can be utilized both *in vitro* and *in vivo* to modulate T cell function.

2.3.4.1 2D

2.3.4.1.1 Patterning and Coatings

Modern lithographic techniques have enabled precise geometric patterning on the micron scale. This has been utilized by researchers in developing biocoatings and micron-sized structures to further probe T cell biology. Additionally, with the rise of tissue and stem cell engineering, biomaterial engineers have developed materials that can vary in stiffness to probe mechanotransduction pathways. Researchers have also employed these materials to study TCR signaling.

The geometric organization of stimulatory and non-stimulatory molecules during T cell activation is highly regulated as seen in the immune synapse needed for T cell activation.[65,66] By using multiple rounds of microcontact printing, researchers were able to control locations of signal 1 (anti-CD3) and signal 2 (anti-CD28) on planar surfaces.[354] T cells stimulated with the two signals segregated demonstrated enhanced signaling

rather than when they are co-clustered. The geometry was distinguished by signal 2 activation pathways such as PKC-θ and LcK.[18,354] Similar results were demonstrated with signal 1 and adhesion molecule ICAM-1.[57] If signal 1 (anti-CD3) was not clustered in a centralized format, T cells did not form efficient contacts or fully activate. Microcontact printing is a technology that has elucidated important microscale geometric arrangements of receptors.

Another technique is block copolymer micellar nanolithography. This technique allows nanometer resolution of biomolecule printing, where gold nanoparticles are hexagonally packed and coated with a distinct layer of polymer that can be removed, to which biological compounds can be attached.[355] A number of researchers have used this technique to probe the question of the influence of nanoscale signal 1 density on T cell activation. Interestingly, the reports found commonly that when using antigen-independent signal 1 with anti-CD3, efficient T cell activation required ligands to be spaced below 60-70 nm apart.[58,59] When using antigen-specific signal 1 (peptide-loaded MHC class II), the threshold was even higher at around 100 nm spacing.[60] Although these articles did not include co-stimulatory or adhesion molecules, they demonstrate the importance of ligand density in providing effective T cell stimulation.

In addition to confining biomolecules my micro or nanoprinting, biomolecules can be coated with lipid bilayers onto surfaces to mimic the fluidity of the cell membrane.[356] Researchers have used this technique to coat silica surfaces with a lipid bilayer with signal 1 (peptide loaded MHC) and adhesion molecule ICAM-1.[357] However, these molecules were constrained by microfabricating barriers of differing sizes and shapes to observe the effects of restricting ligand mobility. By observing how

signaling molecules formed, moved, and clustered helped elucidate processes of the immune synapse formation such as the process of TCR microclusters developing before transfer to the c-SMAC.

2.3.4.1.2 Mechanical Manipulation of Materials

Beyond microfabrication to enable ligand location, this technique can form structures to help probe additional biophysical properties such as creating elastomer micropillars for mechanical signaling processes. TCR signaling has been implicated to be a mechanosensitive process,[135] so researchers have attached signal 1 and signal 2 to micropillar arrays to observe the force generation of T cells in engagement with activation signals.[358] They found that nearly a 100 pN force was generated through the TCR, though CD28 signaling assisted to increase the forces generated. The localization of intracellular proteins regulating contractility suggested interaction of the TCR with intracellular cytoskeleton similar to focal adhesions.

Additionally, bulk material stiffness has been modified to study the mechanosensitive TCR signaling. T cell stimulating ligands have been attached to two different surfaces—polyacrylamide and poly(dimethylsiloxane)—were manufactured to have stiffness vary from 10 kPa-2 mPa.[359,360] In both studies optimal stiffness was found to be around 100 kPa. The stiffness additionally was found to impact T cell differentiation and functionality of the T cells, highlighting this important consideration for T cell-stimulating surfaces.

2.3.4.2 3D

2.3.4.2.1 3D Scaffolds for T Cell Immunotherapy

Increasing the porosity of materials can lead to cells sensing three dimensional environment. Dimension can be utilized to create environments which deliver protein or cell products in a more controlled fashion or promote additional cell-cell interactions

needed for functional T cell development. Three dimensional *in vitro* environments can also be used to more accurately mimic interactions that occur within the body. These organ mimics could be further developed to replace resected or dysfunctional immune organs.

Like their particle counterparts, scaffolds can be developed from biocompatible and biodegradable materials that have the potential to release cargo in a controlled fashion. However, when injected, scaffolds are not motile and rather act as a depot delivery system. This is effective in cases where localized delivery is needed.

A specific example is cytokine delivery, as it can be delivered locally to avoid the many off-target effects of systemic administration. IL-2, a cytokine that influences T cell responses and is an FDA-approved therapy but has significant toxicities and side effects.[361] To minimize off-target effects, researchers have encapsulated IL-2 into polymeric biodegradable scaffolds.[362] This product could be injected, sustained release of IL-2 over days, and enabled cell infiltration to the scaffold.

Besides loading scaffolds with cytokines, cells can be transferred as well. Early on, antigen presenting cells were the focus of adoptive transfers. DCs have been loaded or recruited to a variety of scaffolds loaded with chemokines, adjuvants, and antigen with the purpose of stimulating and recruiting antigen-specific T cells.[363,364] Beyond DCs T cells have recently been transferred *in vivo* in the form of scaffolds.[365–367] The first example demonstrated that loading regulatory T cells (Tregs) onto a PLGA scaffold with islets was effective at protecting grafts from autoimmune rejection in a type 1 diabetes model.[365] Co-localization and retention of the Tregs and islets was necessary to skew the local microenvironment to immunoinhibitory, thus enabled by the scaffold technology.

This further eliminated non-specific systemic immunosuppressive effects of Treg adoptive transfer.

Another example is the delivery effector T cells to destroy cancer cells.[366,367] T cells were loaded on an alginate hydrogel along with co-stimulatory aAPC loaded with IL-15 superagonist.[367] Here scaffolds were utilized to deliver and further activate T cells in the resection bed or in the tumor local microenvironment. Drastic differences were observed. T cells delivered locally and with additional stimulation were able to cure mice of established tumors, while adoptively transferred T cells did not eliminate tumors. In another study, CAR T cells were loaded into the scaffold and demonstrated similar efficacy in combination with a stimulator of IFN genes (STING agonist).[366] The controlled release of STING agonists created a vaccine-like environment which prevented the escape of heterogenous tumor cells not expressing antigens recognized by CAR T cells.

In addition to *in vivo* delivery and stimulation of T cells for adoptive therapy, 3D environments have been created *ex vivo* to enhance T cell stimulation.[368] High-aspect-ratio mesoporous silica micro-rods (MSRs) were coated with lipid bilayers, signal 1 and signal 2, and IL-2 to induce T cell stimulation. T cells migrated into the scaffolds and formed more dense clusters of cells than traditional microparticle aAPC and produced higher levels of proliferation and produce anti-tumor treatment.

2.3.4.2.2 Tissue Engineering Lymphoid Organs

Three dimensional scaffolds are utilized frequently to create *ex vivo* organoids which enable more complex analysis of multiple cell types in a more physiological manner.[369] However, 3D *ex vivo* culture is not without challenges including difficulty of working with multiple cell types, large requirements for nutrients, extended culture times,

and ability to analyze with current techniques. To tackle some of these issues in developing a human artificial lymph node, Giese et al. compared different bioreactors, source of immune cells, and material for scaffolds.[370] Based on T cell activation and lymphocyte swarming, they determined nonwoven polyamide fibers and collagen performed best as scaffolds inside disposable bioreactors. Similarly, researchers found that collagen infused scaffolds provided T cells with the best environment to migrate in 3D.[371] These scaffolds were used to study how T cell and DC migration differed in response to the chemokine CCL21.

Collagen based scaffolds have also been used to develop artificial lymph nodes *in vivo*.[372–374] Collagen sponge matrices were loaded with transfected thymus-derived stromal cells to express lymphotoxin α and activated DCs.[374] Implanted into the renal subcapsular space, these matrices recruited B cells, DCs, T cells, and endothelial cells to form tertiary lymphoid structures *in vivo*. Taken from these mice, these artificial lymph nodes could generate an immune response to a model OVA antigen when transferred into SCID mice. The responses were also shown to generate memory T and B cells that migrated to other secondary lymphoid organs such as the spleen.[373] Similar results were recently generated by implanting the scaffold with incorporating lymphotoxin-α1β2, CCL19, CCL21, CXCL12, CXCL13, and soluble RANK ligand (sRANKL) in place of the transfected cells.[372]

Collagen has also been employed in three dimensional scaffolds to generate human artificial lymphoid organs such as an artificial thymus.[375,376] The collagen coated a tantalum carbon coated matrix, to which a mixture of keratinocytes and fibroblasts were added *ex vivo*. Hematopoietic stem cells were added to the matrix, which initiated the

maturation of both CD4+ and CD8+ T cells with a diverse repertoire of TCRs similar to a natural thymus. The resultant T cells generated effector based responses when stimulated, yet were tolerant to self MHC. Development of artificial lymphoid organs can thus elucidate our understanding of how endogenous organs are formed, their function, provide models for testing immunotherapies, and potentially replace dysfunctional immune organs altogether.

2.3.5. Combination immunotherapies

Methods of both direct T cell activation and blockade of inhibitory checkpoint pathways have resulted in exciting results in preclinical studies and clinical trials. However, there remains a large population of patients who do not respond to monotherapies. Thus, it has become evident that targeting a single stage of the Cancer-Immunity Cycle is not sufficient and that combination therapies that target multiple complementary pathways will have a greater chance of capturing a large response pool. Because there is a diverse array of inhibitory and stimulatory pathways that affect T cell activation, monotherapies often allow for tumor escape through the upregulation of alternative pathways.

Combination therapies against multiple checkpoint molecules can de-activate multiple different T cell inhibitory pathways. Notably, anti-PD-1 mAbs have been co-administered with anti-CTLA-4 mAb in several clinical trials. Because these two pathways are non-redundant, blocking both can synergize T cell activation. The combination therapy significantly enhances the objective response rate to as high as 60%, but also increases the amount of adverse toxicities associated with widespread immune

activation.[51] Importantly, the efficacy of combination checkpoint blockade in comparison to monotherapy is stratified by biomarker expression, such as PD-L1, in a patient's tumor and indicates the importance of using biomarkers to guide therapeutic interventions to reduce costs due to unnecessary combinations.[188] Additional combinations of inhibitory molecule blockades have also demonstrated improved efficacy. Doublets of anti-CTLA-4, anti-PD-L1, and an IDO inhibitor all enhanced the re-activation of tumor infiltrating lymphocytes in a murine melanoma model. These studies demonstrated that the combination therapies were effective by re-activating tumor infiltrating lymphocytes rather than inducing new T cell migration.[53] Thus, in tumors lacking T cell infiltration, combination therapies that also induce migration into the tumor may be more effective.

Combination therapies that link T cell stimulation with checkpoint blockade aim to intervene at the two major ways by which T cell activation is modulated. T cell stimulation can be mediated directly through the administration of co-stimulatory antibodies, or indirectly through a DC-based vaccine. Even when an anti-tumor or anti-viral T cell population is present, however, activated T cells upregulate inhibitory molecules such as PD-1 and CTLA-4 in a homeostatic fashion. Tumor cells can also upregulate inhibitory ligands such as PD-L1, especially in response to T cell secretion of IFN-γ, which diminish the activity of these cells.

Checkpoint blockade has now been combined with almost every approach to T cell stimulation to maintain activation. In chronic viral infection, co-administration of antagonistic antibodies against PD-L1 and agonistic antibodies against 4-1BB were shown to enhance the expansion of viral-specific CD8+ T cells compared to monotherapy.[56] The combination therapy also impacted the kinetics of the T cell

response, indicating that combination therapies may be used to modulate how quickly T cells are expanded against a certain antigen. In cancer immunotherapy, anti-PD-1 mAb checkpoint blockade synergizes with *in vivo* aAPC administration to activate CD8+ T cells against a tumor-expressed antigen.[257] The combination therapy, but neither monotherapy, was able to inhibit the growth of palpable murine melanoma and was shown to be mediated by a decrease in PD-1 expression and increase in tumor-specific T cell expansion. Similarly, co-administration of anti-PD-1 and anti-4-1BB can enhance an anti-tumor response by modulating T cell phenotype and density of tumor infiltrating lymphocytes.[54,55] Checkpoint blockade has also been shown to increase the efficacy of peptide-pulsed DC vaccination, in this case blocking inhibitory molecules on DCs.[377]Various other approaches have shown synergy between the combination of anti-PD-1 checkpoint blockade and granulocyte macrophage colony-stimulating factor,[378] OX40 and CD27 co-stimulation with anti-PD-L1 checkpoint blockade,[3] and anti-OX40 co-stimulation and vaccination.[192]

Checkpoint blockade has also been combined with therapeutics that enhance tumor immunogenicity. Treatments that induce tumor cell death or increase mutational load, including oncolytic viruses, radiation, or chemotherapy, can enhance antigen presentation and activation to tumor-specific T cells.[379] However, the anti-tumor T cell response is often still limited by the expression of inhibitory molecules by both tumor and immune cells. Radiation has been shown to synergize with anti-CTLA-4 checkpoint blockade, with local radiation leading to the regression of even distant metastases.[380,381] However, resistance to this dual treatment was shown to be mediated at least partially by tumor upregulation of PD-L1. In response to this observation, combination therapy

comprised of radiation, anti-CTLA-4, and anti-PD-L1 was shown to increase the response rate and minimize tumor immune escape.[382] Checkpoint blockade also can increase the efficacy of oncolytic viruses that preferentially infect and lyses cancerous cells. A study with the oncolytic Newcastle Disease Virus demonstrated that its combination with anti-CTLA-4 could completely eliminate established murine melanoma and even lead to an improved abscopal effect.[383]

While combination therapies often involve the co-administration of multiple therapeutics, another approach to combination therapy is to develop a single therapeutic with multiple mechanisms of action. CD80, the ligand expressed by antigen presenting cells that induces T cell proliferation upon ligation with T cell expressed CD28, has additional binding partners. CD80 has also been shown to bind PD-L1 and plays a role in inducing apoptosis of activated CD8+ T cells.[384,385] This dual interaction has been taken advantage of in a soluble form of CD80 as a therapeutic.[386] This CD80-Fc fusion protein was shown to both neutralize the inhibitory PD-1/PD-L1 interaction while simultaneously stimulating T cells through CD28.

While combining stimulatory and inhibitory molecules in a single all-in-one therapeutic may be desirable from an engineering perspective, the immunological mechanisms behind their success may indicate that sequential delivery may be more effective. In one study, anti-PD-1 administration following anti-OX40 co-stimulation was effective at delaying tumor growth, but not vise-versa or co-injection—it was necessary for the co-stimulation to first boost the T cell response to a state where checkpoint molecules played a role in inhibiting the response.[387] Thus, sequential delivery or biodegradable particles that can mediate this type of release may be beneficial.

Most recently, a combination therapy clinical trial including the indoleamine 2,3-dioxygenase (IDO) inhibitor, epacadostat, with an anti-PD1 antibdoy, pembrolizumab, failed a phase III clinical trial.[388] This combination which targets to block both immunosuppressive metabolic signals and surface ligands from the tumor microenvironment that diminish T cell activity. However, there was no improvement in progression-free survival when compared with pembrolizumab alone. Consequently, while many combinations do have rational pairings, much is to be learned about how combinatorial pairings should be prioritized and tested as therapies to increase the success rate of costly clinical trials.

2.4. Summary and Next-Generation Therapies

Over the past two decades, we have seen a dynamic interaction between our interest in developing new immune-based therapeutics and our understanding of pathogenesis of disease such as cancer and chronic infection. As our understanding grows, so does our capacity to engineer desired T cell responses. This has also provided enthusiasm for developing novel therapies with T cells. Here we have reviewed general salient engineering principles to control T cells based on basic concepts of T cell biology. We have provided analysis and examples of researchers using these basic principles to control T cells with protein engineering, synthetic particles, cellular and genetic engineering, and scaffolds and surfaces.

Going forward, several areas will continue to be improved using engineering principles. Frequently unintended consequences like autoimmunity, cytotoxicity, or premature cell death result due to a number of unidentified variables activated by

engineered inputs. Control over T cell outputs will come from greater understanding of T cell signaling and increased precision in the therapeutic. For example, CAR T cell therapy will benefit from greater systems biology approaches to study complex T cell activation networks and also from development of more sophisticated CAR constructs such as AND, OR, and NOT switches or kill-switches.

On the other hand, many T cell-based therapies and modulators have extremely high price tags, and as we increase the precision or functionality, this caveat should be kept in mind. Engineered solutions which decrease cost of therapy will enable widespread translation of therapy that is still personalized. An example may be to engineer methods that successfully manipulate T cells *in vivo* instead of requiring prohibitively expensive procedures, equipment, personnel, and centers to handle cells *ex vivo*.

While we have spent time focusing on engineering T cells, progress in T cell therapy will come as other cell types are considered or even simultaneously targeted. T cells are a part of both a broader immune system, spend time traveling through several other organ systems, and require communication and activation from other cells. Additionally, other cell types contribute to the pathogenesis and cure of a disease. For example, the requirement necessary to eliminate large, aggressive, immunoinhibiting tumors required checkpoint blockade, recombinant IL-2, tumor antigen antibody, and a T cell vaccine enabling NK, DC, CD4+, and CD8+ T cell interactions and killing of tumor cells.[389]

Many current advancements have come through cross-disciplinary efforts to tackle important clinical problems. Success has generated clinical, academic, and

industrial interest with contributors from immunology and engineering fields. Continued improvements will come with similar engineering approaches as described here, but hinge on interdisciplinary collaborations and dissemination of progress. In conclusion, control over T cells will enable further control over disease and enhanced understanding of the immune response.

Chapter 3. Biologically Inspired Design of Nanoparticle Artificial Antigen-Presenting Cells for Immunomodulation[2]

3.1 Introduction

Engineering the body's immune system is an attractive approach to treating and preventing diseases. CD8+ T cells are good targets for implementing precision immunomodulation against pathogens and tumors with antigen-specificity. Furthermore, the memory response of these cells gives this approach potential long-term durability. As a consequence, controlling CD8+ T cell responses is one of the goals of adoptive cell therapy (ACT) for cancer immunotherapy.[390] However, the activation of CD8+ T cells for therapy is costly and technically challenging. One of the main hurdles of ACT is generating enough functional antigen presenting cells (APCs) to stimulate anti-tumor CD8+ T cells. Endogenous APCs from cancer patients are frequently dysfunctional due to immunosuppression from the tumor microenvironment. Additionally, ACT often requires multiple leukophoreses; and yet the outcomes vary significantly from patient to patient.[226–228]

[2] Sections of this chapter are reprinted (adapted) with permission from "Hickey, John W., et al. "Biologically inspired design of nanoparticle artificial antigen-presenting cells for immunomodulation." Nano letters 17.11 (2017): 7045-7054." Copyright 2017 American Chemical Society.

3.2 Results

3.2.1 Engineering different sized aAPCs with both similar and varying ligand densities

To bypass cell-based endogenous APCs, we have developed particle-based artificial antigen presenting cells (aAPCs).[28,231] These particles are coated with the two stimulatory signals needed for effective CD8+ T cell activation—peptide loaded major histocompatibility complex (pMHC) (Signal 1) and co-stimulatory anti-CD28 (Signal 2) (**Figure 3-1**a). Using a particle-based system offers a convenient off-the-shelf product and cellular replacement for ACT, ultimately leading to the control and standardization of CD8+ T cell activation.

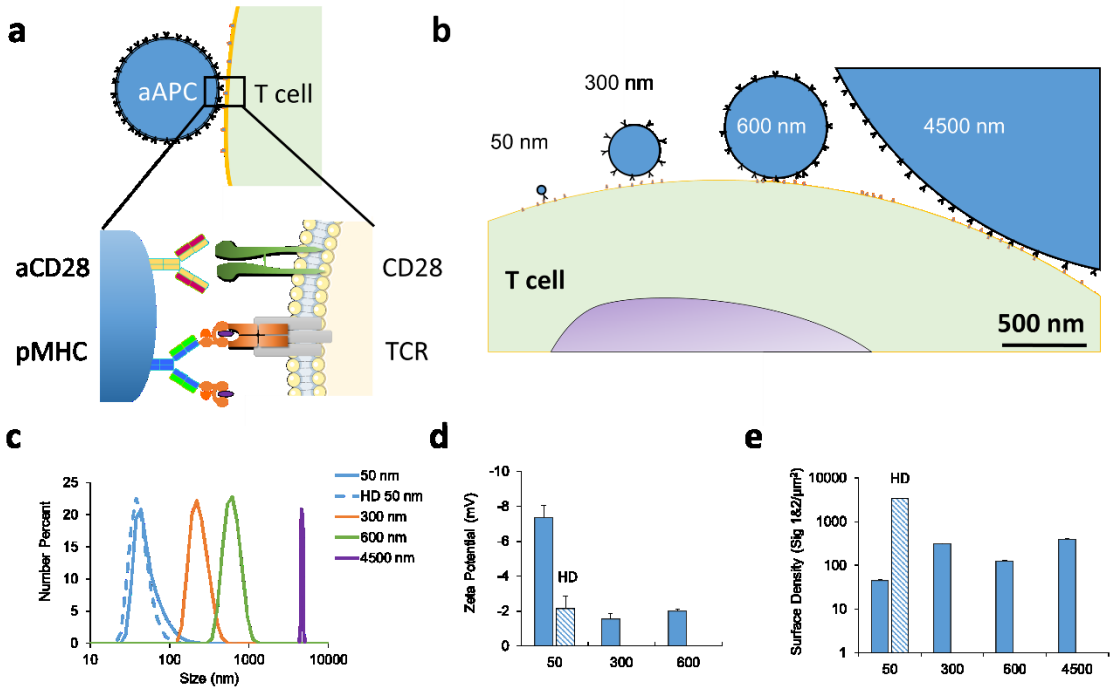

Figure 3-1: Particle aAPCs are made with different sizes and ligand surface densities. (a) Schematic showing interaction between particle-based aAPC and cognate antigen-specific T cell. Stimulation is mediated through two signals. Signal 1 is antigen-specific and is between peptide loaded MHC-Ig (pMHC) and cognate TCR. Signal 2 is a costimulatory signal mediated between the binding of anti-CD28 and CD28 ligand on the T cell. (b) Schematic depicting relative sizes and ligand densities of aAPCs to a T cell. Scale bar = 500 nm. (c) Dynamic light scattering (DLS) measurements showing size distributions of nanoparticle aAPCs. 4500-nm aAPC size was analyzed by light microscopy (d) Zeta potential measurements for different sized particles in PBS (error bars show s.e.m., n=3). (e) The surface density of ligand defined as the number of Signal 1 and 2 molecules per μm2 of the aAPC particle surface area, measured by fluorescent antibody detection (error bars show s.e.m., n=4).

Furthermore, particle-based aAPC properties can be engineered to more efficiently activate and modulate antigen-specific T cells.[222] For example, the shape of the particle can be changed to promote increased attachment with the T cells,[116,267] biodegradable particles can be used to modulate T cells *in vivo*,[258] particles can encapsulate and deliver other cell modulators such as cytokines,[262,267] and can be used in combination therapies such as with checkpoint blockade molecules.[257]

Particle size and stimulatory ligand surface density are important determinants that influence the interaction of particles and cells.[82] Our original designs of aAPCs were

based on particles of several microns in diameter—chosen to mimic the endogenous APCs.[231] However, using micron-sized particles presents a challenge for *in vivo* application due to the issue of potential embolization. Nanoparticles offer enhanced biodistribution to reach lymph nodes if injected subcutaneously,[109] or to reach tumors if injected intravenously.[391] More recently, we have demonstrated that nanoparticle (NP) aAPCs with an average size of 50 nm can provide therapeutic benefit in adoptive cell transfer models.[244,254] Also, others have recently employed nanoparticles with only pMHC conjugated (no co-stimulation) to induce a regulatory response instead of activating T cells for autoimmune applications.[64] Here the size was also explored, but in a limited size range between 4-20 nm.[269] Therefore, the detailed effect of particle size on T-cell activation efficiency has not yet been well defined.

Differences in particle dimensions could have implications due to nanometer-scale structures of signaling molecules at the surfaces of T cells and APCs. It has been shown, for example, that T cell receptors (TCRs) are pre-clustered into protein islands of around 35-70 nm in radius and 300 nm at the longest length scale with 7-30 TCRs per island.[13,392] Furthermore, pMHC patches have also been observed on APCs with radii from 70-600 nm and about 25-125 pMHC per patch.[69] Therefore, we hypothesized that nanoparticles with similar size dimensions to TCR islands and pMHC patches would result in more effective engagement and activation of T cells.

Another parameter important to T cell activation is stimulatory ligand density. CD4+ T cells are insensitive to activation when the density of Signal 1 (pMHC) is too low. Interestingly, for antigen-independent stimulation with anti-CD3, the activation threshold was a maximum linear distance of 60-70 nm;[59,238] however, the linear distance

was close to 115 nm for pMHC class II molecules.[60] Thus, nanometer scale distances and ligand densities have clear implications for nanoparticle aAPC design and may offer novel insights to how the influence of ligand density is impacted by being attached to a mobile platform.

In this study, we tailored size, stimulatory ligand density, and concentration of particle aAPCs to modulate T cell activation (**Figure 3-1**b). Our strategy is based from an effort to see whether design considerations of T cell biology, such as TCR organization, will improve the efficiency of nano-sized aAPCs. These findings will provide important guidance to control the efficiency of T cell stimulation using nanoparticle-based aAPCs for immunotherapeutic applications.

We prepared aAPCs from superparamagnetic iron oxide nanoparticles (SPIONs). SPIONs can be formulated to have a defined size range and can be manipulated in a magnetic field. We conjugated chimeric pMHC-Ig loaded with model antigen SIY (Signal 1) and anti-CD28 antibody (Signal 2) at a 1:1 molar ratio to particles of different average sizes—50 nm, 300 nm, 600 nm, and 4500 nm. All aAPC particles were stable post-conjugation and maintained distinct size populations (**Figure 3-1**c, **Figure 3-2**,**Table 3-1**). All nanoparticle aAPCs across sizes and densities had between -1 and -10 mV zeta potential when measured in PBS at a pH of 7.4 (**Figure 3-1**d). While the density of stimulatory signals between different sized aAPCs varied slightly, for the 50-nm aAPCs we were able to make a high (HD) and low density (LD) version where the ligand density differed by 100-fold (**Figure 3-1**e, **Figure 3-2**,**Table 3-1**).

Table 3-1: Tabular summary of aAPC particle properties and conditions used within experiments.

aAPC name	Average size (nm)	Ligand density signals/μm²	# effective ligand/aAPC	# aAPCs/T cell @ 2 pM	Chemistry and Particle Source	Figures particles were used in
50 nm	**55**	**44**	**0.05**	**34,582**	**EDC/NHS, Ocean Nanotech**	**1, 2a, 3, 4, 5, S1, S6-12**
HD 50 nm	44	3,440	4.2	411	Miltenyi	5, S9-12
300 nm	**299**	**309**	**5.1**	**138**	**EDC/NHS, Ocean Nanotech**	**1, 2a, 3, 4, 5, S1, S6-12**
600 nm	621	124	3.4	175	EDC/NHS, Ocean Nanotech	1, 2a, 3, 4, 5, S1, S6-12
4.5 μm	**4640**	**393**	**375.2**	**0.1**	**Epoxy, ThermoFisher**	**1, 2a, 3, 4, 5, S1, S6-12**
M 50 nm	31	127	0.1	12,044	Sulfo-SMCC, Micromod	2b-e, S2-5
M 300 nm	**402**	**184**	**3.0**	**232**	**Sulfo-SMCC, Micromod**	**2b-e, S2-5**
M 600 nm	578	164	7.6	65	Sulfo-SMCC, Micromod	2b-e, S2-5

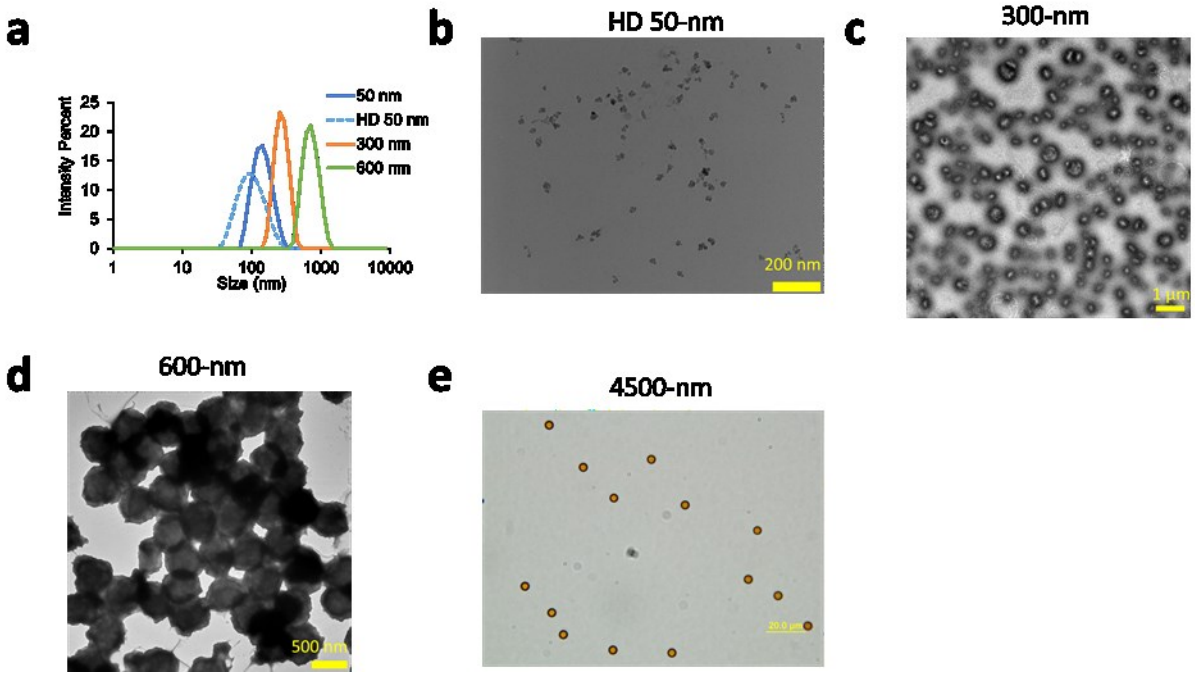

Figure 3-2: Further characterization of formed particle aAPCs. (a) Dynamic light scattering (DLS) measurements showing size distributions of nanoparticle aAPCs by Intensity Percent. (b-e) Representative images of functionalized aAPCs. (b-d) TEM images of (b) HD 50-nm (scale bar = 200 nm), (c) 300-nm (scale bar = 1 μm), (d) 600-nm (scale bar = 500 nm), and (e) of 4500-nm aAPCs with light microscopy (scale bar = 20 μm).

3.2.2 The influence of aAPC particle size on T cell activation

Using the panel of well-defined, nanoparticle-based aAPCs, we found a size-dependent association with T cell activation. At a concentration of 2 pM of particle-bound Signal 1, Kb-SIY, we observed a significant decrease in the ability for 50-nm aAPCs to stimulate their cognate 2C CD8+ T cells compared to particles larger than 300 nm (**Figure 3-3**a). We controlled for the total number of bound pMHCs in all experiments because this parameter has been a critical factor in T cell activation in past studies, and not the number of aAPCs.[236] Although we kept the surface ligand concentration constant in each condition, a greater number of smaller aAPCs were added than larger aAPCs because larger aAPCs had more surface-bound ligand per particle. At 2 pM, 50-nm aAPCs only produced a 5-fold CD8+ T cell expansion, which statistically differed from all larger particles. All particles larger than 300 nm produced around 12-fold T cell expansion—a value indicative of a robust stimulation of T cells for a 7-day culture period—and were not statistically different from one another. The differences between 50-nm and larger aAPCs to provide stimulation were consistent with the need to engage local islands of Signals 1 (pMHC) and 2 (aCD28) greater than 50 nm in diameter for effective CD8+ T cell stimulation.

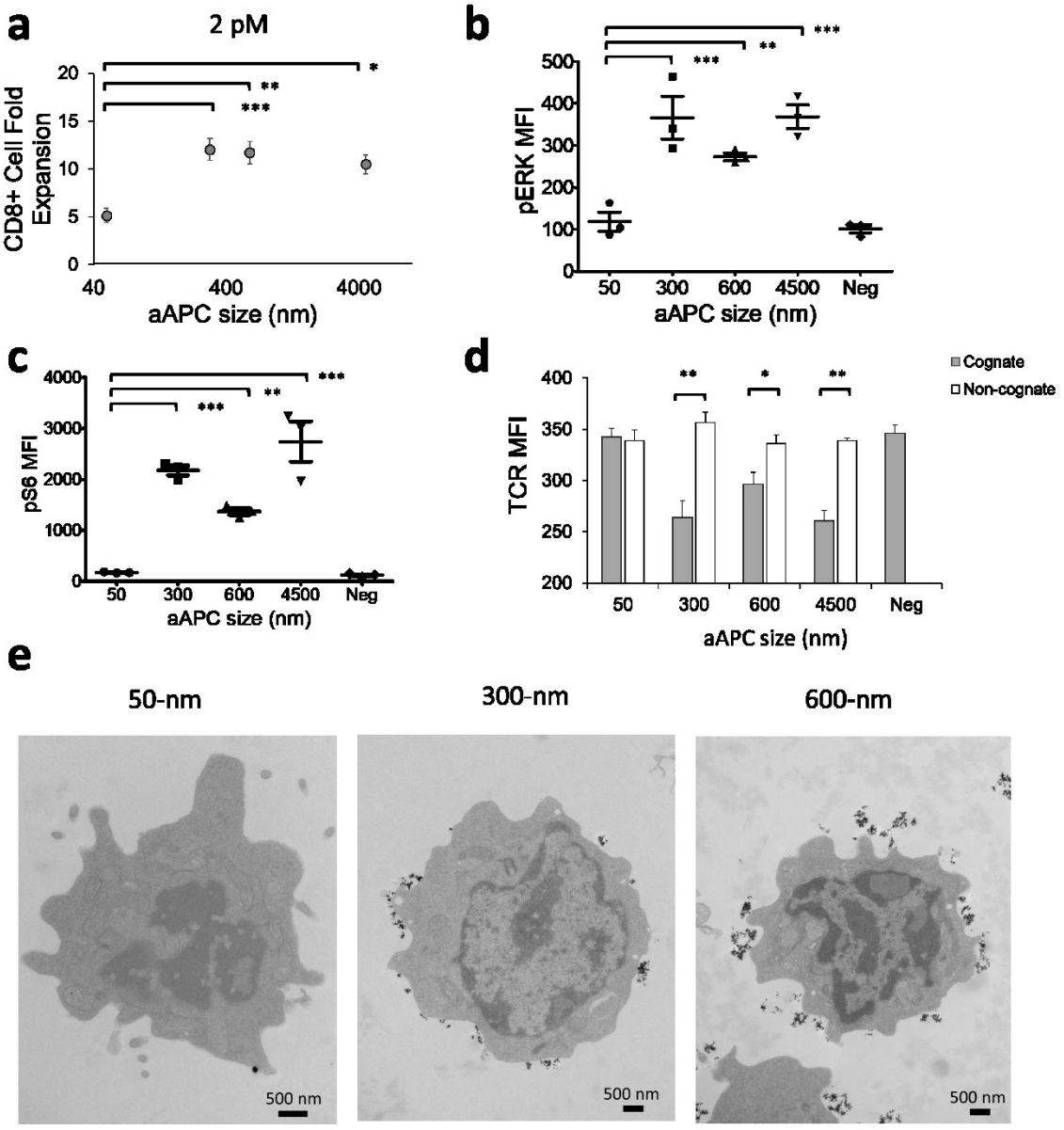

Figure 3-3: Particle aAPC size influences ability to activate CD8+ T cells. (a) Antigen-specific T cells are cultured with aAPCs at a controlled total dose of 2 pM conjugated pMHC and fold proliferation is measured 7 days later (error bars show s.e.m.; ***$p < 0.0005$, **$p < 0.005$, *$p < 0.05$, $n = 9$, one-way ANOVA with Tukey's post test). (b-c) Mean fluorescent intensity (MFI) for (b) phosphorylated ERK and (c) phosphorylated ribosomal protein S6 of CD8+ T cells cultured with aAPCs at 37 °C for 30 minutes (error bars show s.e.m.; ***$p < 0.0005$, **$p < 0.005$, *$p < 0.05$, $n = 3$, one-way ANOVA with Dunnett's post test). (d) MFI for TCRβ of CD8+ T cells cultured with aAPCs at 37 °C for 5 hours (error bars show s.e.m.; **$p < 0.005$, *$p < 0.05$, $n = 3$, Student's T test). (e) Transmission electron microscopy (TEM) of 2C CD8+ T cells incubated with 50-, 300-, 600-nm aAPCs for 1 hour at 4 °C (scale bar = 500 nm).

To show this size-dependent effect is independent of particle preparation, we formulated aAPCs from another set of iron-oxide particles of 50-, 300-, and 600-nm diameters (**Figure 3-4**, **Table 3-1**). We observed ineffective stimulation with the 50-nm aAPCs when compared to the larger aAPCs (**Figure 3-5**a). Importantly, we did not observe any activation by aAPCs with non-cognate pMHC (Kb-TRP2) and anti-CD28 of any size (**Figure 3-5**b). Repeating this experiment in another particle system substantiated the evidence of a size-dependent effect observed with nanoparticle aAPCs.

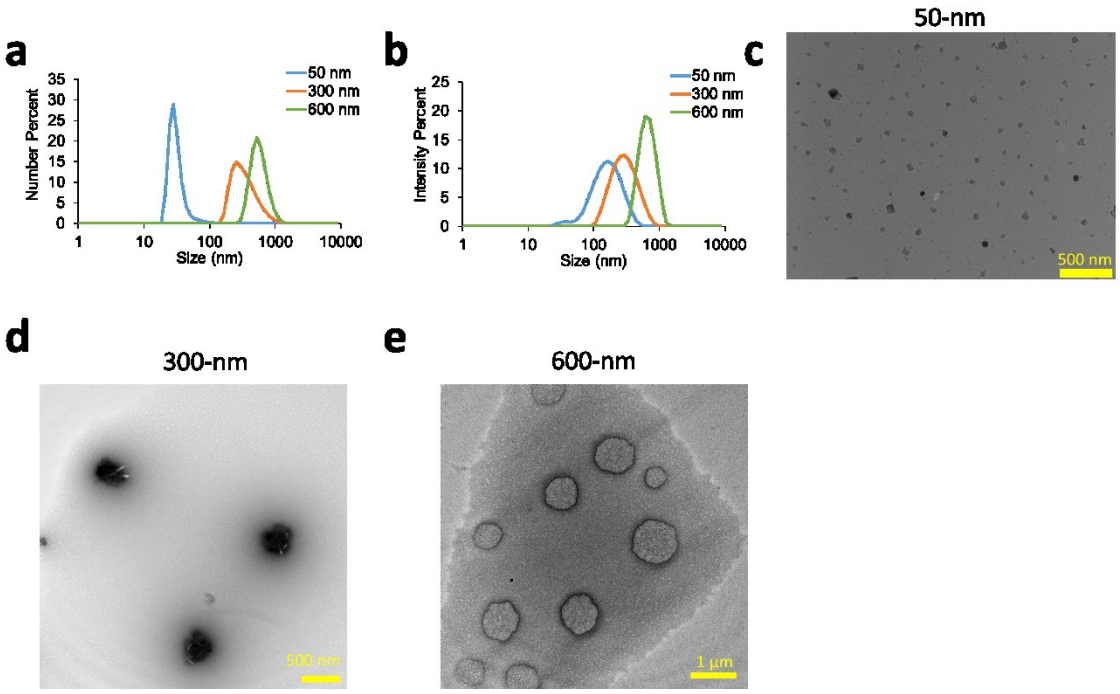

Figure 3-4: Particle characterization of formed aAPCs derived from another company (Micromod). (a-b) Dynamic light scattering (DLS) measurements showing size distributions of nanoparticle aAPCs by (a) Number Percent and (b) Intensity Percent. (c-e) Representative TEM images of functionalized aAPCs of 50-nm (scale bar = 500 nm), (d) 300-nm (scale bar = 500 nm), and (e) 600-nm (scale bar = 1 µm).

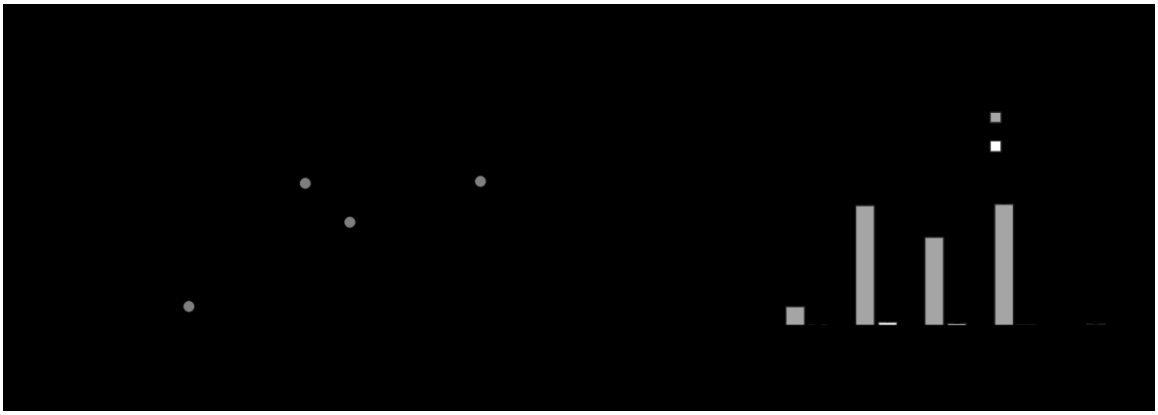

Figure 3-5: Size dependent effect is still observed when using another source of iron oxide particles, but not with non-cognate aAPCs. (a-b) Antigen-specific T cells are cultured with 2 pM of aAPC-bound pMHC and fold proliferation is measured 7 days later for (a) cognate (error bars show s.e.m.; ***$p < 0.0005$, **$p < 0.005$, *$p < 0.05$, $n = 3$, one-way ANOVA with Tukey's post test) and (b) non-cognate aAPCs.

These first two experiments examined proliferation as a functional readout for T cell activation; however, early signaling events may provide additional insight into the mechanism of the aAPC-T cell interaction. To do so we stimulated T cells for 30 minutes and examined MAPK signaling by staining for phosphorylated ERK1/2 (pERK). Similar to our proliferation results, we observed robust early signaling by 300-nm and larger aAPCs as indicated by the mean fluorescent intensity (MFI) of pERK, yet 50-nm aAPCs did not produce a detectable signal (**Figure 3-3**b, **Figure 3-6**a). Others have recently shown that local clusters of TCR-pMHC interactions are necessary both for T cell activation and for effective initial phosphorylation of ERK.[393] This result provided additional support to our hypothesis that 50-nm aAPCs are unable to cluster local TCRs to achieve robust T cell activation.

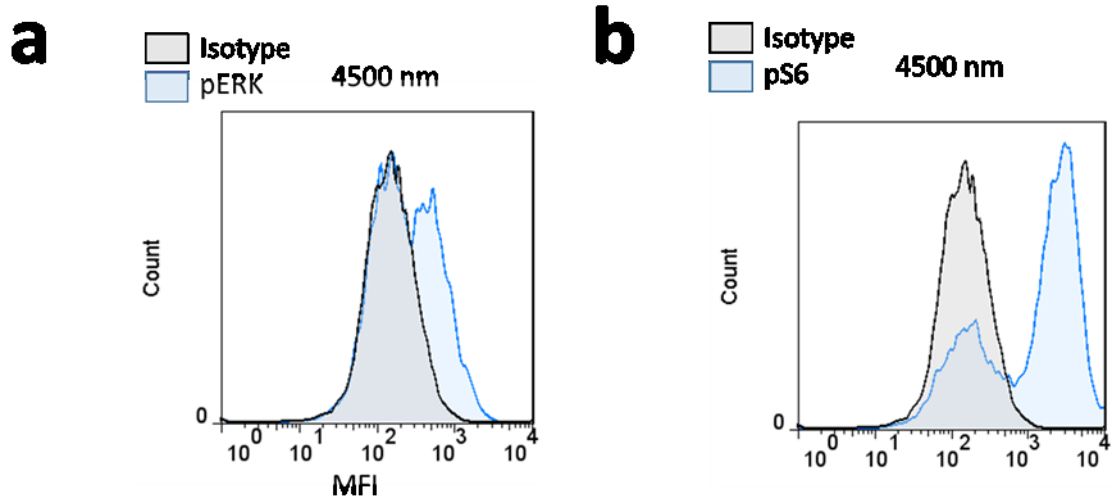

Figure 3-6: Isotype control staining for phosphorylation studies. (a-b) Example of isotype (grey) and phosphorylation (blue) staining for CD8+ T cells stimulated with 4500 nm aAPC at a 2 pM dose for (a) pERK and (b) pS6.

Another indicator of early, robust T cell activation is through effective mTOR signaling, where phosphorylated ribosomal protein S6 (pS6) is a downstream target of activated mTOR.[394,395] We stained for pS6 after activating the T cells for 30 minutes, and found consistent results between both proliferation and pERK data. Levels of pS6 for 300-nm and larger aAPCs were significantly higher than those produced by either 50-nm aAPCs or the non-stimulated negative control (**Figure 3-3**c, **Figure 3-6**b). Recently, it has been shown that effective pS6 staining is correlated to the duration of the APC-T cell contact.[396] Therefore, larger aAPCs may be able to contact CD8+ T cells longer because of greater multi-valent binding and thus provides another mechanism to the observed size-dependent effect.

Shorter signaling duration has been associated anergy in CD4+ T cells.[396] We did not expect the aAPCs to induce anergy because we have conjugated a Signal 2, co-stimulation (anti-CD28) in addition to pMHC, which has been shown to induce activation rather than anergy in T cells.[397,398] Nevertheless, we wanted to confirm whether the

reduced activity of CD8+ T cells from 50-nm aAPCs was due to suboptimal signaling or just ineffective engagement of the CD8+ T cell. We first examined TCR downregulation, which is associated with TCR engagement and T cell activation.[399,400] We stimulated T cells with 2 pM dose of the aAPCs and observed a significant decrease in TCR expression for cells stimulated with 300-, 600-, 4500-nm aAPCs, but not 50-nm aAPCs when compared to non-cognate aAPCs and no stimulation controls (**Figure 3-3**d). Additionally, we probed for a regulatory phenotype at day 7 as defined by other researchers who use pMHC-only (no co-stimulation) and have induced an immunoregulatory CD8+ T cell response, which are both CD122+ and CD44+.[64,269] After stimulating with aAPCs, we found no significant difference in the percentages between all aAPCs (**Figure 3-7**). Moreover, we formulated a 300-nm particle with only pMHC (which we term 300 S1), to replicate the type of particle used in previous studies. Importantly, here we found that there was a significant increase in the percent of a regulatory phenotype at day 7 (**Figure 3-7**)—further substantiating evidence for the importance of having both pMHC (Signal 1) and co-stimulatory anti-CD28 (Signal 2) on the particle for an immune activating response. These data point to ineffective engagement of the CD8+ T cell rather than suboptimal signaling leading to anergy by the 50-nm aAPCs.

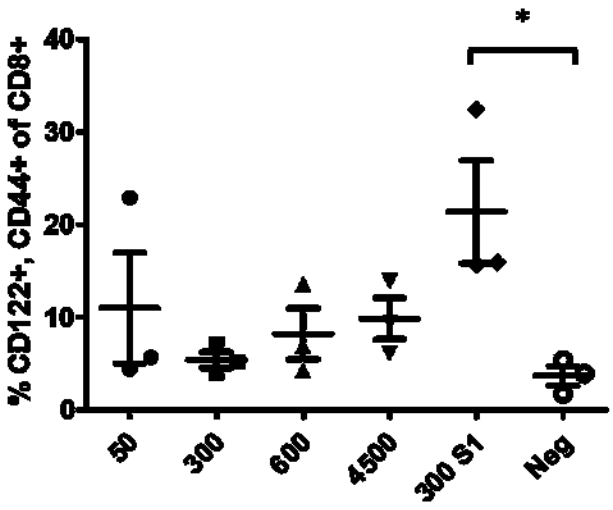

Figure 3-7: Only aAPCs with only pMHC KbSIY attached (no anti-CD28), 300 S1, showed a significant increase in the percent of CD122+, CD44+, CD8+ T cells after 7 days of culture with aAPCs at a 2 pM dose of aAPCs (error bars show s.e.m.; *$p < 0.05$, $n = 3$, One way ANOVA with Dunnett's post test).

To better understand the interaction of different sized particle aAPCs and T cells we imaged the aAPCs and T cells using transmission electron microscopy (TEM). Interestingly, very few 50-nm aAPCs attached to the T cells, where on average only about one particle attached to a T cell in the 70-nm slice, whereas many more 300- and 600-nm aAPCs attached to the surface of the T cells (**Figure 3-3**e). Additionally, the 300- and 600-nm aAPCs were distributed over the surface of the T cell, yet there seemed to be areas where multiple particles attached near each other. These images support both of our proposed mechanisms for why we observe the size dependent effect—size of TCR clusters and duration of attachment via increased avidity. More specifically, we observed that the 50-nm aAPCs were not clustered, nor attached well to the T cell compared to the larger 300- and 600-nm aAPCs.

3.2.3 Minimum aAPC dose for T cell expansion reveals size-dependent properties

To further probe the size-dependent phenomenon we asked if we could overcome the restriction with increasing the dose of pMHC and thus total particle numbers. Schematically we are testing if by adding excess aAPCs, then multiple 50-nm aAPCs could diffuse and engage a single TCR cluster and achieve similar T cell activation, or if clusters need to be ligated by a single larger nanoparticle (**Figure 3-8**a). Furthermore, by adding more aAPCs, this may increase the number of aAPCs bound at one time and increase the signaling duration. Indeed, at surface saturating concentrations of 50-nm aAPCs (18 pM of particle-bound Kb-SIY), 50-nm aAPCs were able to stimulate the CD8+ T cells just as well as the larger particles (**Figure 3-8**b). All aAPCs produced around 12-fold CD8+ T cell expansion with no statistical difference between any of the groups. We confirmed that this saturating dose of nanoparticle-based aAPC stimulation resulted in similar final CD8+ T cell phenotype (surface markers) and functionality (cytokine analysis), further supporting that TCR clusters may be activated by multiple smaller particles, but not necessarily by a single particle 50-nm or less (**Figure 3-9**).

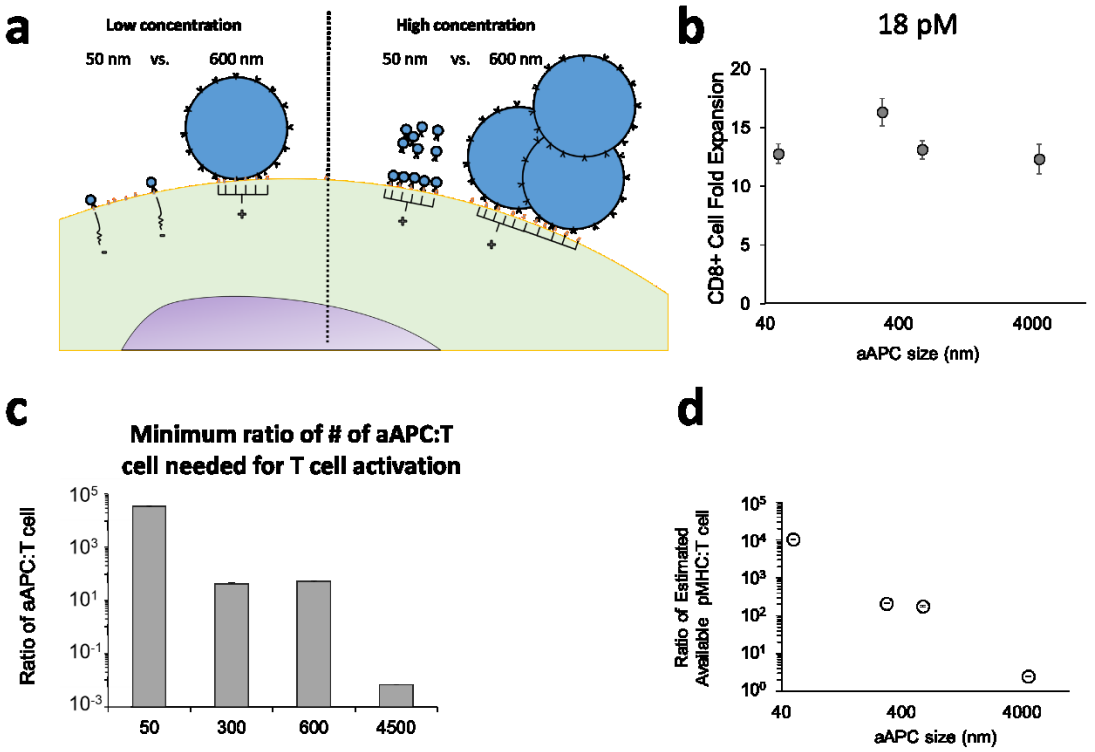

Figure 3-8: Particle aAPC concentration reveals saturating concentration of 50-nm aAPCs needed to activate CD8+ T cells. (a) Schematic depicting hypothesis that saturating the T cell with 50-nm aAPCs is needed for the same nanoisland cluster-based activation as lower concentration larger 300 nm particles (600-nm aAPCs are depicted). (b) 18 pM dose of particle-conjugated pMHC is used to stimulate CD8+ T cells for 7 days and fold expansion is measured (no significant differences between aAPCs, one-way ANOVA, n=13). (c-d) Dose-titrating amounts of particle aAPCs to activate T cells for 7 days determined lowest dose or (c) ratio of number of aAPCs to T cells or (d) estimated pMHC per T cell needed for activation (error bars show s.e.m., n=4).

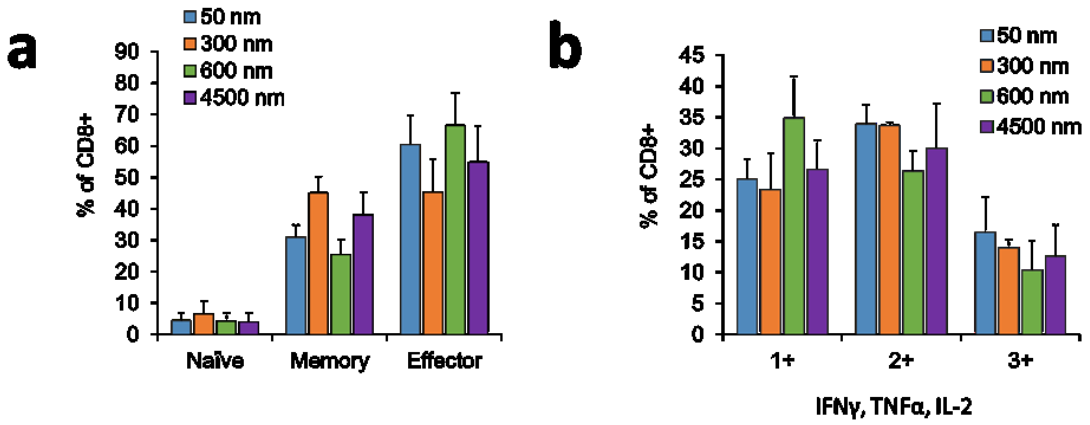

Figure 3-9: CD8+ T cells stimulated with particle aAPCs of different sizes result in similar CD8+ T cell phenotype and functionality. (a, b) CD8+ T cells were stimulated by particles of different sizes for 7 days at a concentration of 18 pM of particle-bound Kb-SIY and (a) phenotypic cell surface markers (CD62L, CD44) and (b) intracellular cytokine production as measured by triple, double, and single positive cells (IFNγ, TNFα, IL-2) were measured as a percent of CD8+ (n=3).

We extended this finding by quantitating the minimum number of aAPCs required for activation at each aAPC size. Interestingly, this revealed three separate patterns in the number of aAPCs needed to provide effective T cell signaling (**Figure 3-8**c). First, the minimum number of 50-nm aAPCs needed to activate T cells is similar to the number of TCRs per T cell, which is reported to be around $0.5 – 1 \times 10^5$ per T cell.[401] Second, larger aAPCs, 300- and 600-nm, require many fewer aAPCs than the number of TCR per T cell, and much lower than the estimated number of nano-islands per T cell — ca. 15,000, assuming about 30 TCR per island. Third, the 4500-nm aAPCs required even fewer aAPCs — less than one per T cell.

The high number of 50-nm aAPCs required for activation further confirms that there is a need for a surface saturating amount of aAPCs, since nanoparticle aAPCs diffuse through solution, their binding with TCRs will be stochastically distributed over the surface of the CD8+ T cell. Estimating the T cell to have around 50,000 TCRs, to achieve complete nano-island ligation, all or most TCRs should be bound by 50-nm aAPCs (**Figure 3-10**a). Furthermore, the need for many fewer 300- and 600-nm aAPCs supports the idea that individual particle aAPCs can bind multiple TCRs in TCR nano-islands to achieve local stimulation with only one particle per island. Finally, the low numbers of 4500-nm aAPCs points to a different signaling mechanism where multiple TCR clusters are bound by a single particle; and multiple T cells can be stimulated by the same particle. The need for a surface saturating amount of 50-nm aAPCs can also be examined by plotting the ratio of particle aAPC surface area to cell surface area (**Figure**

3-10b). Consequently, this shows that 50-nm nanoparticles need nearly a 1:1 ratio of particle surface area to T cell area to activate T cells, whereas aAPCs larger than 50 nm need less than a 1:5 ratio of particle to T cell surface area.

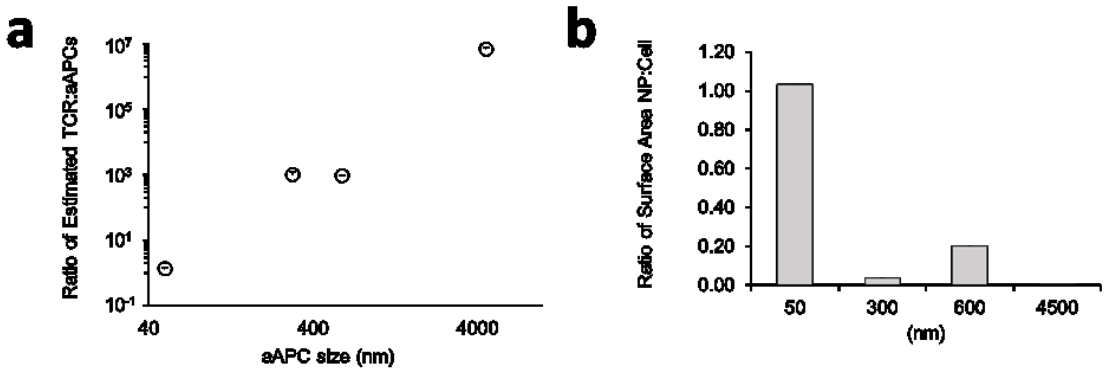

Figure 3-10: 50-nm aAPC require saturating dose of particles to provide T cell activation. (a-b) Dose-titrating amounts of particle aAPCs to activate T cells for 7 days determined lowest dose (number of aAPCs) and therefore (a) number of estimated TCRs per particle aAPC needed. The number of TCRs per T cell was estimated to be 50,000 based on literature values, and (b) surface area ratio of particle aAPC to T cell needed. The size of the T cell was simulated to be 10 μm (error bars show s.e.m., n=4).

To connect our findings involving synthetic aAPCs to studies with endogenous APCs, we calculated the average number of available pMHCs per T cell (**Figure 3-8**d). Previous studies have reported between 1-400 pMHCs are needed to activate a CD8+ T cell.[402–409] While for aAPCs the pMHC is conjugated to a solid scaffold and not within a mobile lipid bilayer with additional signaling molecules, the results seen are consistent with previous reports. We found that the "cell-sized" 4500-nm aAPCs required about 3 pMHCs per T cell. These averages were also similar to numbers found through direct observation of cell-based APCs, where 10 pMHCs were needed to activate a CD8+ T cell and only 3 pMHCs were needed to activate for killing.[407] The 300- and 600-nm aAPCs both required close to 200 pMHCs per T cell, which also falls within the range that has been calculated by indirect averages of endogenous APCs. In contrast, 50-nm aAPCs

required more than 10,000 pMHCs per T cell—pointing to the spatial relation or on-rate of the pMHCs when engaged may be important parameters for activation rather than total pMHCs available to a T cell.

3.2.4 Magnetic clustering of 50-nm aAPCs reveals need for receptor clustering

Cells are able to dynamically rearrange and cluster receptors on their surface for enhanced function and signaling.[78,410,411] We sought to mimic receptor clustering of the diffusely bound 50-nm magnetic particles on the surface of the T cell by applying a magnetic field (**Figure 3-11**a). Thus, if individually bound TCRs by 50-nm aAPCs can be physically made to cluster using magnetic force, and effective signaling is generated, then this would strengthen our hypothesis of the importance of spatially activating TCRs in clusters.

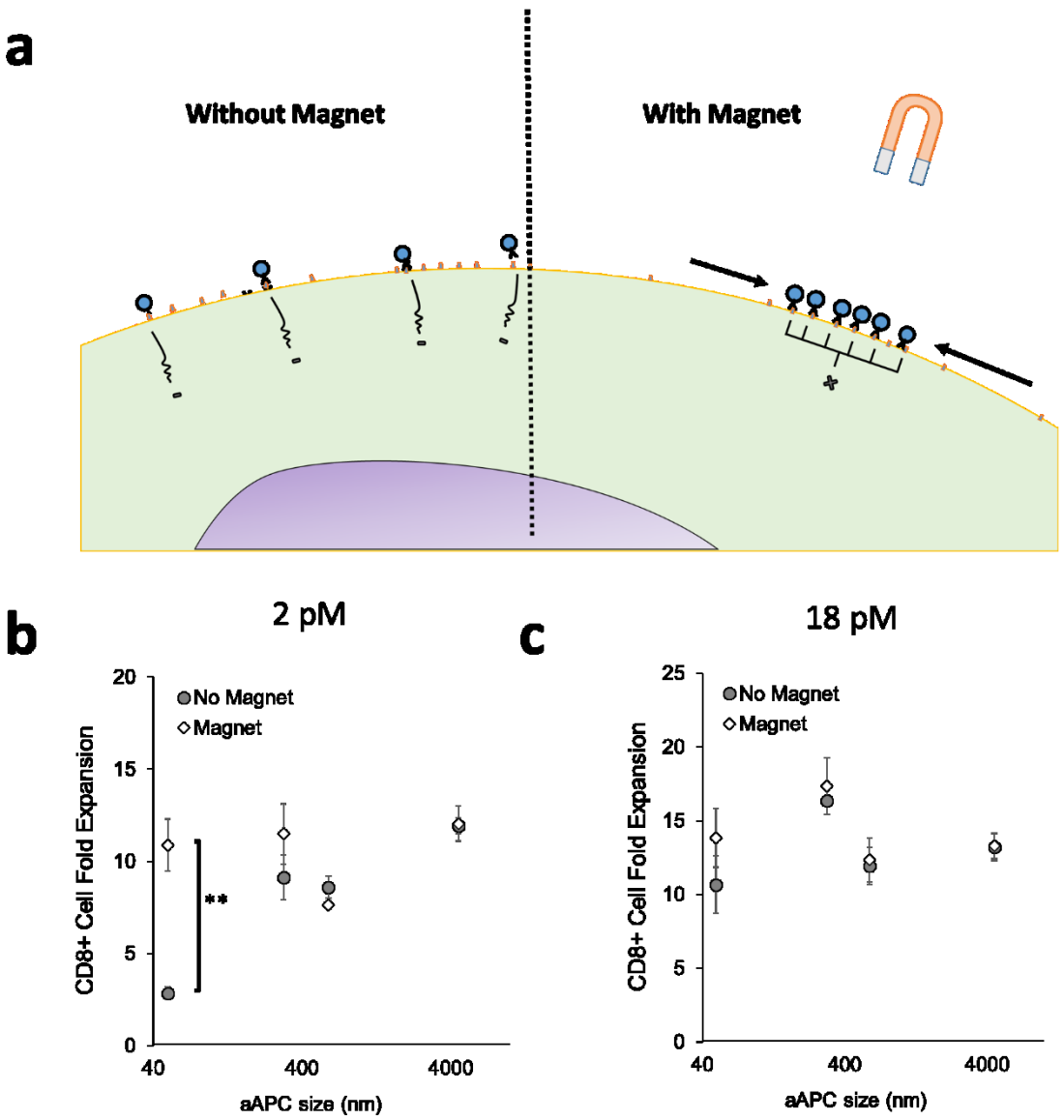

Figure 3-11: Particle aAPC can be artificially magnetically clustered at sub-saturating concentrations. (a) Schematic demonstrating the effect of magnetic fields on the 50-nm particle aAPCs to achieve artificial clustering. (b, c) CD8+ T cells and particle aAPCs were cultured for 7 days with or without the presence of a magnetic field and counted for fold expansion at either (b) 2 pM or (c) 18 pM dose of particle-conjugated pMHC (error bars show s.e.m.; **p < 0.005, n = 5-7, Student's T test).

To artificially cluster TCRs, we placed T cells with 50-nm SPION aAPCs within a static magnetic field.[244] Indeed, artificially clustering 50-nm aAPCs at sub-surface saturating amounts stimulates CD8+ T cells to the same level as surface saturating conditions (**Figure 3-8**b, **Figure 3-11**b). Within a magnetic field 50-nm aAPCs produce

approximately a 12-fold, statistically different CD8+ T cell expansion in contrast to the 3-fold expansion without a magnetic field. Artificial clustering of 50-nm aAPCs were comparable to larger aAPCs without artificial clustering. Magnetic clustering of larger aAPCs and surface saturating amounts of 50-nm aAPCs did not further increase CD8+ T cell stimulation, suggesting there is no added benefit to the magnetic field other than providing artificial clustering of diffuse 50-nm particles (**Figure 3-11**c).

3.2.5 The influence of ligand density and size on T cell activation

This result demonstrated that artificial clustering of Signals 1 (pMHC) and 2 (anti-CD28) improved signal activation, suggesting a particle size-dependent signaling effect that is linked with stimulatory signaling molecule clusters. However, taking a reductionist approach and modeling the surfaces of the particle and the T cells as spheres we determined that a confounding variable is the number of ligands available from particle aAPCs to interact with T cells (**Error! Reference source not found.**a, **Figure 3-13**, **Table 3-1**). Even if there are similar densities of ligands for particles of different sizes, differences in geometry can lead to differences in number of ligands actually available to engage T cells. We calculated the number of available ligands for each spherical particle at the initial contact (**Figure 3-12**a). As the particle size decreases, there is an increase in particle curvature and a decrease in ligands available to interact with T cells.

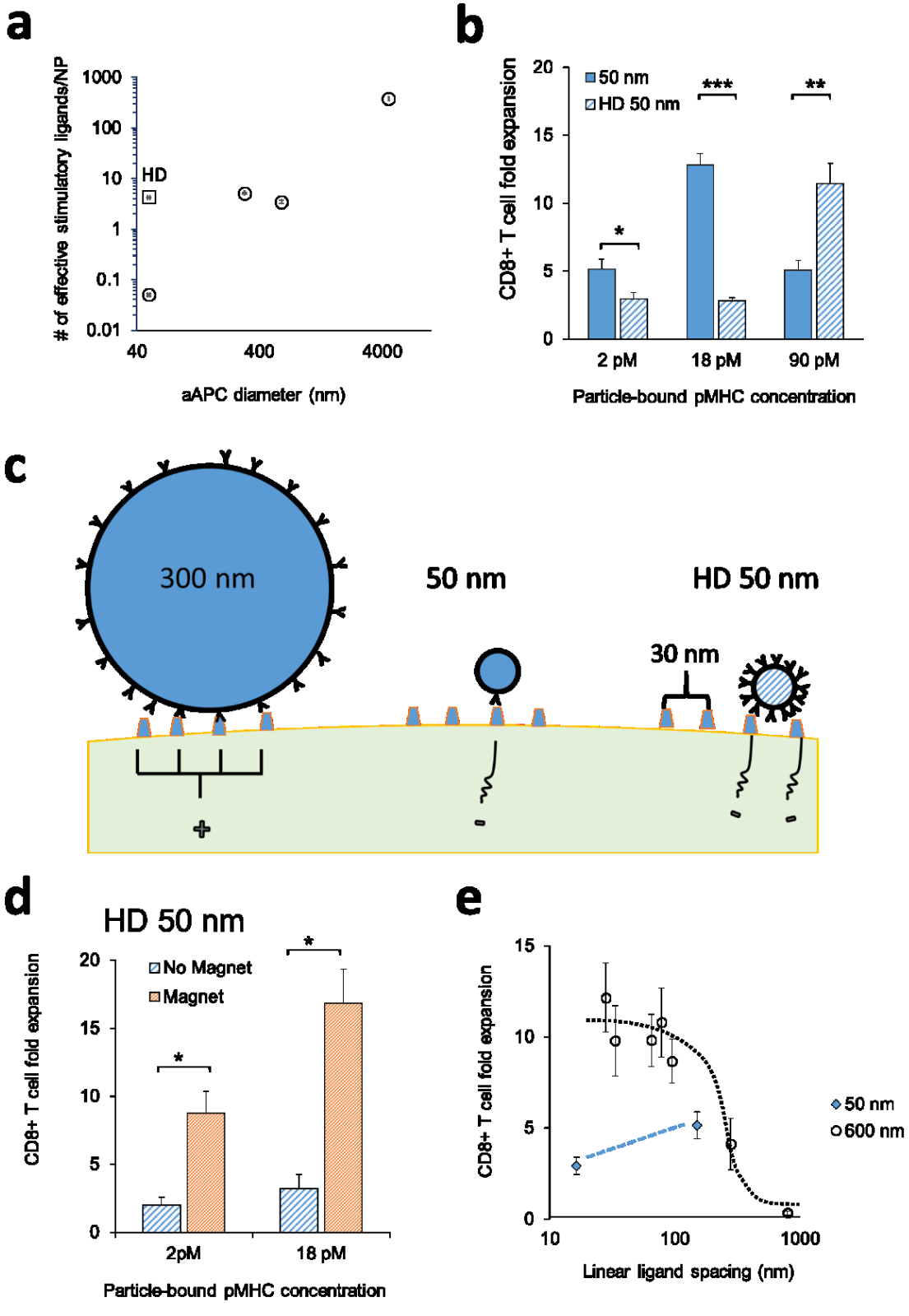
a
# of effective stimulatory ligands/NP
1000
100
10
1
0.1
0.01
HD
40
400
4000
aAPC diameter (nm)
b
CD8+ T cell fold expansion
50 nm
HD 50 nm
***
**
*
20
15
10
5
0
2 pM
18 pM
90 pM
Particle-bound pMHC concentration
c
300 nm
50 nm
HD 50 nm
30 nm
d
HD 50 nm
CD8+ T cell fold expansion
No Magnet
Magnet
*
*
20
15
10
5
0
2pM
18 pM
Particle-bound pMHC concentration
e
CD8+ T cell fold expansion
15
10
5
0
10
100
1000
Linear ligand spacing (nm)
50 nm
600 nm

Figure 3-12: Normalizing the effective available activating ligands does not overcome size-dependent stimulation capacity of aAPCs. (a) Calculated values of number of effective stimulatory ligands per particle. The square represents the HD 50 nm aAPCs made. (b) CD8+ T cells were incubated with equivalent doses aAPC-bound pMHC of either 50 nm or HD 50 nm aAPCs for 7 days and fold expansion was measured (error bars show s.e.m.; ***p < 0.0005, **p < 0.005, *p < 0.05, n = 10-13, Student's t test). (c) Schematic showing how aAPC size influences ligand-TCR interaction (spaced at ~30 nm) in TCR islands, where larger particles facilitate more effective TCR ligand interactions, thus promoting T cell activation. (d) The effect of a magnetic field for either aAPC amounts at 2 pM or 18 pM of particle-bound pMHC (error bars show s.e.m.; *p < 0.05, n = 5, Student's t test). (e) 600-nm aAPCs with different ligand densities were incubated with T cells at 2 pM of particle-bound pMHC and fold expansion of CD8+ T cells was measured on day 7; 50 nm data replotted for comparison (error bars show s.e.m.; n = 5).

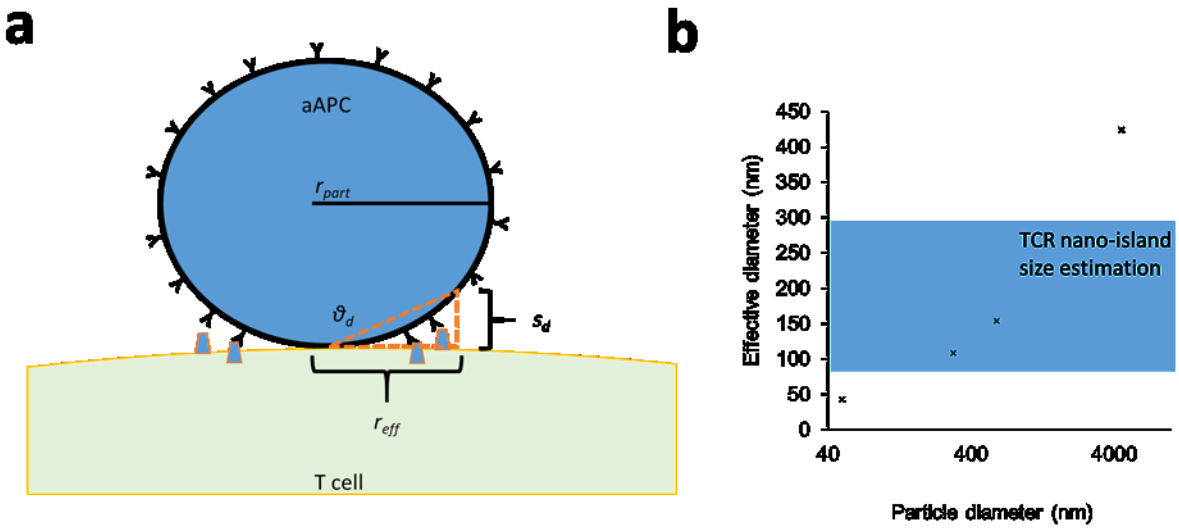

(1) $$r_{eff} = \sqrt{r_{part}^2 - (r_{part} - s_d)^2}$$

(2) $$\theta_d = \tan^{-1}\frac{s_d}{r_{eff}}$$

(3) $$SA_{eff} = \frac{\theta}{\pi/2} \cdot \pi \cdot r_{part}^2$$

(4) $$\#\ ligand_{eff} = lig.dens./NP \cdot SA_{eff}$$

Figure 3-13: Spherical geometry of particle aAPC limits the actual size and number of ligands interacting with the T cell. (a) Schematic showing the defined effective radius (reff) of the particle aAPC. This is governed by the separation distance (sd) between the pMHC on the surface of the aAPC. This is the distance that prevents attached pMHC from engaging TCR on the surface of the T cell due to distance. We find the reff using Equation 1, which is defined from the geometry of a circle. In order to define effective surface area as a percent of surface area we used Equations 2 and 3. Equation 2 finds the angle of the effective surface by using the sides of the defined triangle reff and sd. We then use the effective surface area and nanoparticle ligand density to find the effective number of stimulatory ligands/particle from Equation 4. (b) Calculated effective diameters are plotted versus actual diameters to show estimated size of interaction for aAPCs. Lightly shaded blue region indicates estimated T cell receptor nano-island estimations previously described.

To decouple the effect of multiple-ligands per TCR nanocluster and stimulation signal cluster size, we prepared 50-nm aAPCs with a higher density of Signals 1 and 2 (HD 50-nm). HD 50-nm aAPCs have the same effective radius (r_{eff}) as their 50-nm counterparts (**Figure 3-13**a) but a shorter distance between ligands—thus, presenting comparable numbers of effective stimulatory molecules as larger aAPCs (**Figure 3-12**a). Using these HD 50-nm aAPCs, we confirmed the size-dependent constraints of 50-nm aAPCs as they are also unable to stimulate T cells effectively at 2 pM of particle-bound pMHC in terms of cellular proliferation (**Figure 3-12**b) and in early activation events like ERK phosphorylation, mTOR signaling, and TCR downregulation (**Figure 3-14**). HD 50-nm aAPCs were even less efficient in activating T cells than the regular density 50-nm aAPCs at the 18 pM dose, and required a total dose of 90 pM of particle-bound pMHC to produce a similar maximal T cell expansion. This is to be expected as a large number of HD 50-nm aAPCs is still needed to achieve saturation binding of nanoparticles to T cells. Interestingly at the higher dose of 90 pM, HD 50-nm aAPCs produced a greater apparent expansion of T cells than their regular density 50-nm counterpart. This could be due to particle toxicity or to activation-induced T cell death evoked by adding so many regular density 50-nm aAPCs. Non-cognate 50-nm particle aAPCs at the same dose did not cause any additional toxicities as compared to a traditional 4500-nm aAPC stimulation (**Figure 3-15**a), ruling out toxicity due to particle numbers. Proliferation analysis by CFSE dilution at the 90 pM dose demonstrated effective cell stimulation and division with the 50-nm aAPCs at an earlier time point than that observed with HD 50-nm aAPCs, consequently pointing to activation-induced T cell death (**Figure 3-15**b-c).

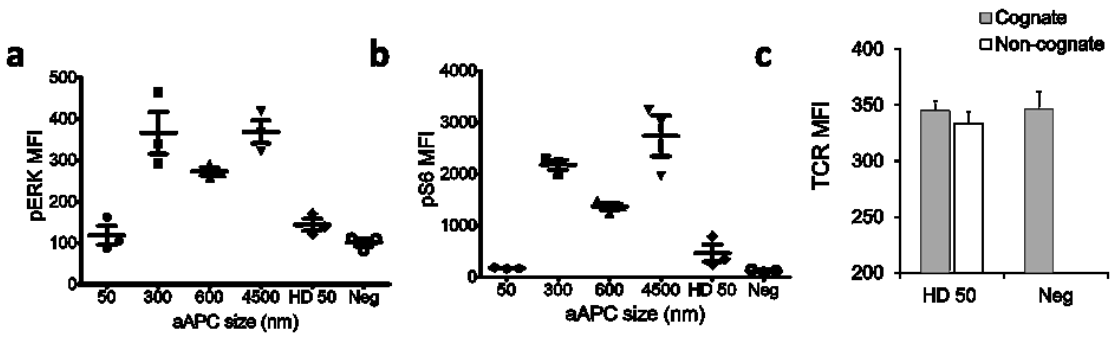

Figure 3-14: Ineffective activation of CD8+ T cells also observed for HD 50 nm aAPCs at a 2 pM dose with early activation events. (a-b) MFI of phosphorylation of (a) ERK and (b) ribosomal protein S6 for HD 50 nm aAPCs. Other groups were replotted for comparison purposes. (c) MFI for TCRβ of CD8+ T cells cultured with aAPCs at 37 °C for 5 hours for cognate and non-cognate aAPCs. Negative control was replotted for comparison purposes.

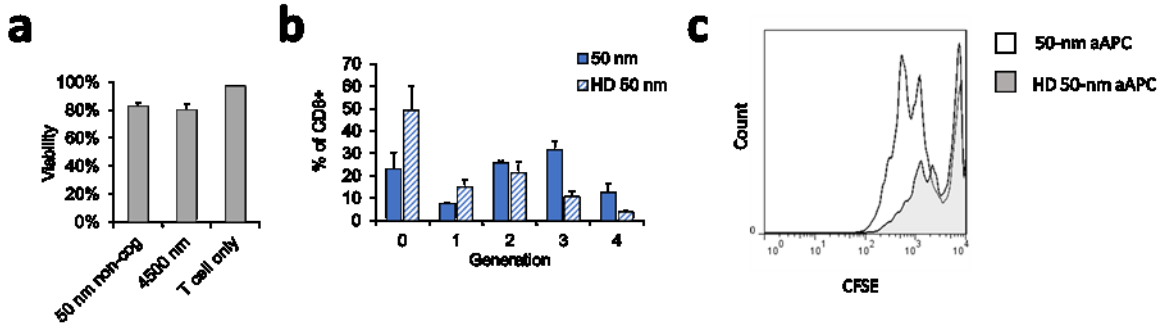

Figure 3-15: High concentrations of 50-nm aAPCs are not toxic due to particle doses, but to overactivation-induced cell death. (a) CD8+ T cells were incubated with 90 pM controlled non-cognate pMHC aAPCs for 7 days and viability was measured. T cells without aAPCs and T cells stimulated with traditional 4500 nm aAPCs are shown for comparison purposes for a normal antigen-specific stimulation (n=3). (b) CD8+ T cells were stimulated for three days and proliferation is characterized by CFSE dilution and characterization of percent of cells in each generation (n=3). (c) Representative flow cytometry plot of CFSE dilution experiment.

Thus, even with normalized ligand availability, 50-nm aAPCs were less effective than larger aAPCs at stimulating T cells under sub-saturating conditions. These findings support the notion that the size of the aAPCs is particularly important in achieving T cell activation rather than differences in ligand availability. This could be explained by TCR

density, as it has been reported to be on the order of 1,200 TCR/μm^2.[13] Linearly, this translates to about 30 nm spacing between TCRs, which means that even if small particles have a high density of ligand, all available ligands may not be beneficially engaged over the entire surface of the TCR island. Consequently, small particles result in fewer TCR-MHC interactions, and fail to result in sustained activation of the TCR island by an individual particle (**Figure 3-12**c). In contrast, larger particles can have multivalent binding with nanoclusters leading to a rapid on-rate of local TCRs.[412–414]

To further investigate the relationship between the observed size-dependent effect and potential mechanism of TCR cluster activation we again used a magnetic field to artificially cluster the HD 50-nm aAPCs at sub-saturating concentrations. We observed effective CD8+ T cell stimulation at both the 2 pM and 18 pM concentrations only when the particles were artificially clustered in a magnetic field (**Figure 3-12**d). These results further indicate that activation of TCRs in clusters is important for effective T cell activation and agrees with previous studies that demonstrate the importance of pMHC clustering on endogenous APCs for T cell activation.[78]

This study shows that in addition to ligand spacing (**Figure 3-16**a), size of the stimulatory island (particle size) is also important for T cell activation. Previous studies with T cells involving TCR nano-arrays have shown a stimulatory molecule spacing requirement for T cell activation of around 70-120 nm.[59,60,238] We observe differences from this reported trend with 50-nm aAPCs. Even when using 16 nm linear spacing between ligands we did not observe as effective stimulation as with larger particles with even larger linear distances between ligands (**Figure 3-16**a).

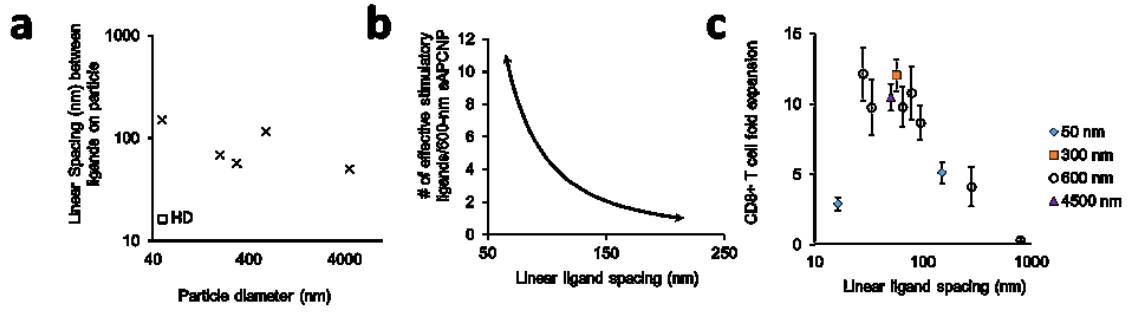

Figure 3-16: Linear ligand density and size of nanoparticle aAPCs are important for T cell stimulation. (a) Linear spacing between stimulatory molecules on the surface of the aAPC for different sized aAPCs. (b) Graph representing the relationship between the linear ligand density and the number of effective ligands presented from a 600-nm aAPC. (c) 600-nm aAPCs with different ligand densities were incubated with T cells at 2 pM concentration and fold expansion of CD8+ T cells was measured on day 7 and 50 nm, 300 nm, and 4500 nm data replotted for comparison (error bars show s.e.m.; n = 5).

Since the size of the particle appears to be a driving factor in our findings, we probed how ligand density influenced T cell stimulation with 600-nm aAPCs. Theoretically, 600-nm aAPCs are able to engage multiple receptors with a linear ligand spacing up to about 150 nm (**Figure 3-16**b). Since this is close to the values reported from TCR nanoarrays, we hypothesized that we would notice a drop-off in T cell activation with ligand densities in this regime. To test this hypothesis, we formulated 600-nm aAPCs with seven different ligand densities (distance between ligands), ranging from 27 nm to 800 nm and added these at a 2 pM concentration to CD8+ T cells (**Table 3-2**).

Table 3-2: Tabular summary of 50- and 600-nm aAPC particle properties and conditions used to examine the impacts of ligand density and spacing.

Nanoparticle size	Ligand density signals/μm^2	# effective ligand/aAPC	Linear Ligand Spacing (nm)	# aAPCs/T cell @ 2 pM
50	**44**	**0.05**	**150**	**34582**
50	3438	4.2	16	411
600	**942**	**38.74**	**33**	**15**
600	237	11.0	65	54
600	**164**	**7.6**	**78**	**79**
600	112	5.2	95	115
600	**13**	**0.6**	**279**	**1003**
600	2	0.07	795	8129

We observe that for 600-nm aAPCs, expansion of CD8+ T cells began to decrease substantially at spacing of about 100 nm (**Figure 3-12**e, **Figure 3-16**c), which is similar to values reported for TCR nano-arrays. Therefore, this shows the importance of engineering ligand spacing as well as size of aAPCs for effective T cell activation.

3.3 Discussion

Our ability to provide a mobile stimulatory unit by conjugating the stimulatory ligands to a particle instead of a nano-array allowed us to probe unique mechanisms of T cell activation. This particle-based aAPC system enables simultaneous control of both the number of stimulatory molecules and the density of these molecules, something that is difficult to achieve with substrate-conjugated signals. Additionally, whereas substrate-conjugated signals allow the study of how T cells might adapt to a fixed stimulation, particle-conjugated signals allow the study of native T cell biology where stimulation

signals are also mobile. Another distinction between this and previous studies is that here we study CD8+ T cells, where previous studies have investigated the effect of ligand spacing and density on CD4+ T cells.

This study provides a systematic understanding of how particle aAPC parameters such as particle size, surface ligand density, and concentration collectively influence T cell activation. We demonstrate that aAPCs larger than 300 nm were more effective at activating CD8+ T cells, presumably due to their ability to initiate clustering of pMHC-TCR and costimulatory interactions due to their size. Mechanistically, once particles bind to TCR nanoclusters, larger particles have an enhanced ability to bind other TCRs with pMHCs and CD28 with anti-CD28 leading to multivalent binding of receptors and sustained signaling necessary for T cell activation.[412–414] This is consistent with recent data from 1) immunoregulatory pMHC-only nanoparticles, 2) DNA chimeric antigen receptors, and 3) endogenous antigen presenting cells. For immunoregulatory pMHC-only nanoparticles, higher ligand densities led to increased activity of the particles and clustered attachment to T cells.[20] Indirectly, we also observed this as non-cognate aAPCs (with anti-CD28) prevented full activation of CD8+ T cells co-cultured with cognate aAPCs—presumably because they compete for CD28 binding and decrease the ability for multivalent binding (Supplemental Fig. 12). For DNA chimeric antigen receptor T cells, it was necessary that a small group of the receptors be clustered by the counterpart DNA (pMHC) for effective activation.[393] For endogenous APCs, pMHC molecules containing identical peptide sequences are found clustered on the surface of APCs and lead to effective T cell activation.[68,70,71] Furthermore, effective nanocluster signaling has been

shown to be necessary for T cell activation prior to the formation of supramolecular activation centers.[415]

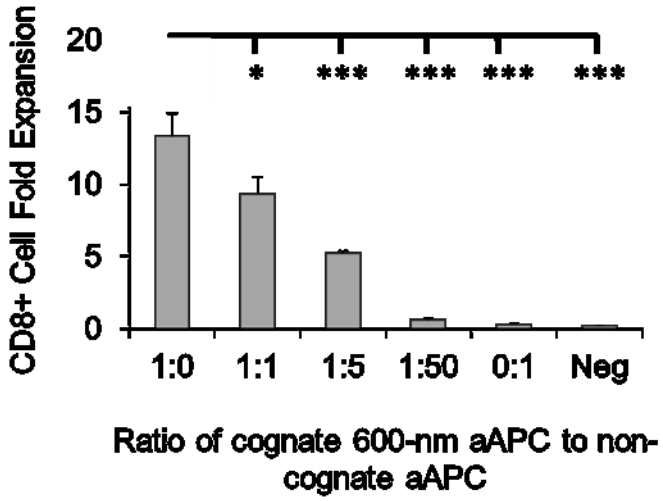

Figure 3-17: Addition of non-cognate aAPCs decreases the activation of antigen-specific T cells in a dose dependent manner. 600-nm cognate (Kb-SIY/anti-CD28) and 600-nm non-cognate (Kb-TRP2/anti-CD28) were mixed at the indicated ratios respectively and cultured for 7 days (error bars show s.e.m.; ***$p < 0.0005$, **$p < 0.005$, *$p < 0.05$, $n = 3$, one-way ANOVA with Dunnett's post test).

In this systematic and quantitative analysis of aAPC particle size, we revealed the importance of designing cell-modulating nanoparticles with biology in mind. Here we considered both APC and T cell biology where primarily the field has been focusing on mimicking APCs. Furthermore, these mechanistic studies have implications for aAPC design for optimal therapeutic applications. One application is in utilizing the magnetic properties of the SPION aAPCs for magnetic enrichment of antigen-specific cells. Antigen-specific T cells occur at very low frequencies—at about 1 in every 10^5 to 10^6 T cells—and are therefore difficult to detect.[416] As immunotherapies have continued to develop, techniques surrounding identification and isolation of rare antigen-specific T cell have grown in importance. Additionally, previous work has indicated that an

enriched cell population can be activated to have therapeutic potential.[254] Therefore, aAPCs that are able to bind multiple TCRs may result in greater specificity and avidity and in greater enrichment of antigen-specific T cells. Our studies lay a foundation of quantitative analysis of particle aAPC size that pave the way for similar studies in the development of optimal aAPCs for magnetic enrichment.

Furthermore, these findings can provide aAPC design guidance in the *in vivo* activation of antigen-specific T cells. Using aAPCs to stimulate CD8+ T cells *in vivo* overcomes several challenges of the cancer immunity cycle and adoptive T cell transfer (ACT).[417] Endogenous APCs, such as dendritic cells (DCs), are immunosuppressed, and can even be skewed to be immunosuppressive themselves.[418–420] This results in either deficient activation or immunosuppression of CD8+ T cells. Using aAPCs would bypass the need for DCs and allow effective and precise stimulation of antigen-specific CD8+ T cells. Additionally, in ACT, T cells are taken from a patient and cultured *ex vivo* then injected back into the body.[390] This process of *ex vivo* culture is time-consuming, technically challenging, and costly.[421–423] Therefore, *in vivo* activation of antigen-specific T cells is a primary goal of the field. Yet, achieving saturating conditions of 50-nm aAPCs *in vivo* may be impractical due to both poor nanoparticle-based biodistribution and retention, and low frequency of antigen-specific T cells.[82,416] Thus, the goal is to engineer a particle that could achieve optimal biodistribution yet not require saturating amounts of aAPCs to activate a T cell. Our studies provide the basis for development of different sized biocompatible aAPCs to achieve robust *in vivo* immunotherapies.

3.4 Conclusion

In conclusion, we demonstrated how biologically inspired design of nanoparticle aAPCs to mimic a cell can lead to increased functionality of the particle and reveal aspects of cellular function. We utilized a reductionist approach to isolate the important properties of particle size and ligand density. Though we studied this in a model system with CD8+ T cells for immunotherapeutic applications, our findings and quantitative approach can impact and be implemented in other areas of cell modulation and mimicry.[82,424]

3.5 Experimental Methods

Mice and Reagents. 2C TCR transgenic mice were kept as heterozygotes by breeding on a C57/BL6 background. C57BL/6j mice were purchased from Jackson Laboratories (Bar Harbor, ME). All mice were maintained per guidelines approved by the Johns Hopkins University's Institutional Review Board.

Particle Fabrication. Soluble MHC-Ig dimers, Kb-Ig, was produced in-house and loaded with peptides as described[1] and anti-CD28 antibody was purchased from Biolegend (37.51; BioLegend, San Diego, CA, USA). NHS (NHS) labeled super paramagnetic iron-oxide particles (SPIONs) were purchased from OceanNanotech (Springdale, AR, USA). Conjugation of MHC-Ig dimer and anti-CD28 proteins to the particles was carried out per manufacturer's recommendations (**Figure 3-18**). Briefly, SPIONs were washed while on a STEM-cell magnetic column (Vancouver, Canada) with PBS three times and then incubated with equimolar amounts of MHC-Ig and anti-CD28 at ratios of 0.1 mg of total protein to 1 mg of SPIONs. SPIONs and protein were allowed to react for 24 hours at 4°C.

Tris-HCl buffer was added to the SPIONs to quench any unreacted functional groups and SPIONs were subsequently magnetically washed three times with PBS with 2% bovine serum albumin (BSA). 4500 nm particles—Dynal Particles—were purchased from ThermoFisher (Halethorpe, MD). MHC-Ig and anti-CD28 were conjugated to the surface as established previously[2].

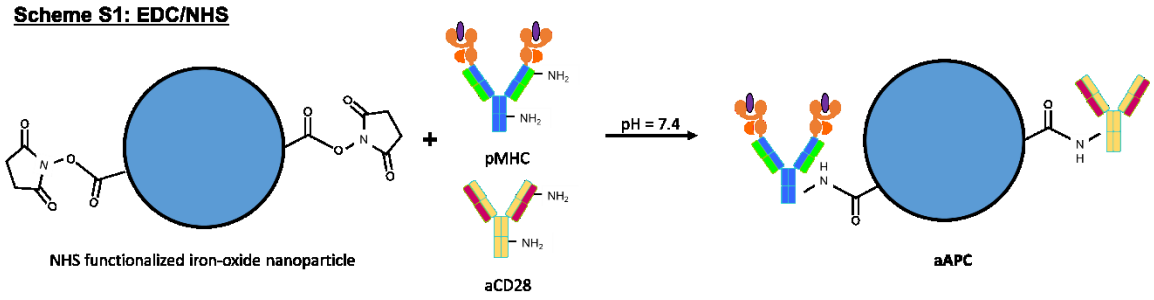

Figure 3-18: Scheme 1

Using NHS labeled magnetic nanoparticles worked effectively for a facile conjugation with our pMHC-Ig and anti-CD28; however, we were not able to substantially increase the density of the ligand by adding additional ligand to the reaction. To control the density and increase the ligand density on the particles we aimed to functionalize amine-coated iron oxide particles with a higher density of reactive groups. SPIONS were purchased from Micromod (Rostock, Germany) and functionalized according to manufacturer's recommendations (see https://www.micromod.de/daten/File/Technotes/Technote_202_1.pdf and https://www.micromod.de/daten/File/Technotes/Technote_201_2.pdf) (**Figure 3-19**). Briefly, amines were then reacted with Sulfo-SMCC (Proteochem, Hurricane, UT) and then magnetically washed. MHC-Ig and anti-CD28 were modified with 2-iminothiolane (Traut's reagent) purchased from Sigma Aldrich (St. Louis, MO). Excess 2-iminothiolane

was washed away from protein solution by using a Vivaspin 20 50kDa MWCO concentrator (GE Healthcare, Little Chalfont, United Kingdom). Traut's reagent targets the same free amines that would be targeted in the conjugation of the antibodies to NHS-labeled particles. Therefore, the orientation of the antibodies or Signals does not change between chemistries, only the linkers. Washed and activated particles and MHC-Ig and anti-CD28 were then mixed and reacted. The resultant product was washed and stored at 4°C. HD 50 nm aAPCs were conjugated by Miltenyi Biotec (Cologne, Germany).

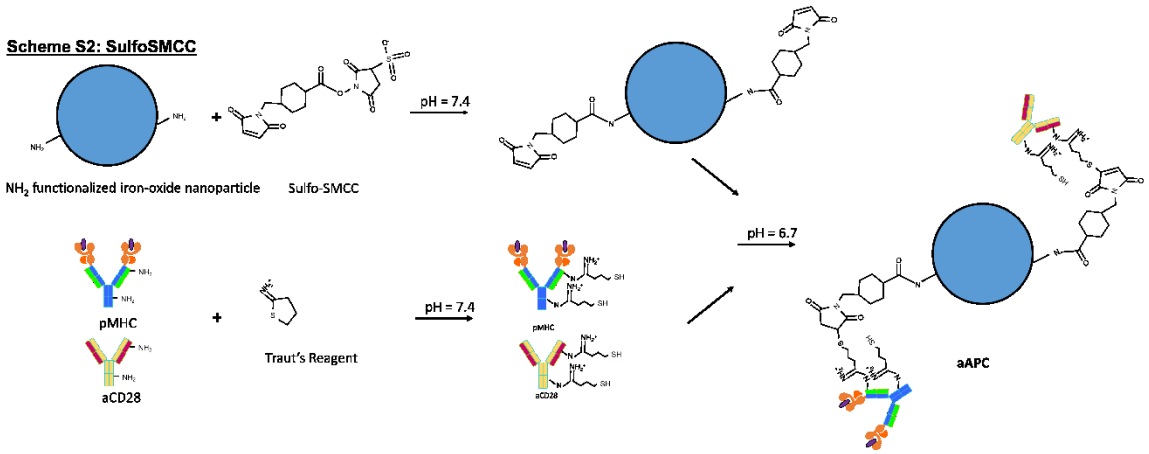

Figure 3-19: Scheme 2

Particle Characterization. NP size and zeta potential was measured using a Zetasizer DLS. Protein surface density was measured through a fluorescent detection assay. Briefly, particles were either stained with FITC-conjugated rat anti-mouse Ig λ1, λ2, λ3 light chain, clone R26-46, or FITC-conjugated mouse anti-armenian/syrian hamster IgG, clone G192-1 (BD Pharmingen, Franklin Lakes, New Jersey) for 1 hour at 4°C. Particles were washed three times with 1x PBS. Particles were then collected in 1x PBS and subsequently the fluorescence was quantified using a Synergy HTX Multi-mode florescent plate reader (BioTek, Winooski, VT, USA). Particle concentration was measured using a

spectrophotometer at a 405 nm reference. Imaging of particle aAPCs by Transmission Electron Microscopy (TEM), was done on a FEI Tecnai 12 and Philips EM 420 electron microscopes. Samples were allowed to adhere to discharged nickel grid covered with carbon film for 30 minutes. Solution was removed with a Kim wipe and then the samples were stained with 2% uranyl acetate for 45 seconds. The grids were then washed three times and allowed to dry at room temperature.

***In Vitro* T Cell Activation.** Lymphocyte isolations were completed as previously described[3]. Briefly, CD8+ T cells were isolated from the spleen and lymph node from a 2C transgenic mouse by using a mouse CD8+ T cell negative isolation kit from Miltenyi Biotec (Cologne, Germany) and following manufacturer's instructions. 2C transgenic mice have CD8+ T cells with identical TCRs, which recognize the SIY peptide loaded into the mouse pMHC Kb. All aAPCs had pMHC Kb loaded with SIY and co-stimulatory molecule anti-CD28, except for non-cognate aAPCs which had an irrelevant peptide, TRP2, loaded into pMHC Kb and co-stimulatory molecule anti-CD28, and 300 s1 particles which only contained pMHC (no costimulatory molecules). CD8+ T cells were activated by NPs at indicated doses as previously described.[254] Briefly CD8+ T cells were plated with nano-aAPCs at 100,000 cells/mL in complete RPMI-1640 medium supplemented with 10% fetal bovine serum and T cell growth factor, a cytokine cocktail derived from condition media produced from stimulated human PBMC as previously described.[425] T cells were fed with media with double concentration of T cell growth factor on day 3. Fold expansion and viability was determined by harvesting and counting cells by Trypan Blue staining and hemocytometry. For magnetic stimulations, T cells were isolated and plated as described

above, but tissue culture plates were set between two neodymium N52 disk magnets (K&J Magnetics, Jamison, PA, USA) as described previously.[244]

For experiments determining the minimum surface area ratio of NP aAPC to CD8+ T cells, T cells were incubated with decreasing ratios of NP aAPCs. The activation cut-off was defined as CD8+ proliferation above 1-fold the initial number of CD8+ T cells as measured on day 7. The graphs were generated by a custom-MATLAB script, with the grid size showing the representative surface area of a NP aAPC and the shading demonstrating NP aAPC needed for activation.

Cell proliferation was also characterized by dilution of CellTrace™ CFSE Cell Dye per manufacturer's recommendations (ThermoFisher). Briefly, isolated CD8+ T cells were suspended in 1 mL of PBS, and 1 μL of CellTrace™ CFSE Cell Dye suspended at 5 mM was added to the solution and placed in a cell incubator for 20 minutes at 37°C. Then 5 mL of complete RPMI-1640 medium supplemented with 10% fetal bovine serum was added and allowed to incubate in a cell incubator for 5 minutes at 37°C. Cells were then washed twice in complete RPMI-1640 medium supplemented with 10% fetal bovine serum and counted. Cells were then stimulated for three days. On day 3, cells were counted and 200,000 cells were taken and stained with a solution of 1:100 APC-conjugated rat anti-mouse CD8a, clone 53-6.7 (BD Pharmingen) for 15 minutes at 4°C. Cells were then washed with FACS was buffer and read on a BD FACSCalibur.

T Cell Phosphorylation Analysis. 2C CD8+ T cells were isolated as described above and particle aAPCs were incubated with T cells for 30 minutes at 4°C and then activated for 30 minutes at 37°C. Samples were then washed in a 96 well plate with PBS and fixed with pre-warmed (37°C) BD Phosflow 1x Lyse/Fix Buffer (BD Biosciences, San

Jose, CA) for 10 minutes at 37°C. Fixative was washed twice from the samples with PBS and pre-chilled (-20 °C) BD Phosflow Perm Buffer III was added dropwise to each sample and gently mixed and incubated at -20 °C for 30 minutes. This mixture was spun down and the supernatant was removed and then washed three times with FACS wash buffer. Samples were then stained with a solution of FACS wash buffer with 1:50 PE-conjugated rat anti-mouse CD8a, clone 53-6.7 (BD Pharmingen) and either a 1:100 Rabbit anti-Phospho-S6 Ribosomal Protein (Ser235/236), clone D57.2.2E, or Rabbit anti-Phospho-p44/42 MAPK (Erk1/2) (Thr202/Tyr204), clone 9101, or Rabbit IgG Isotype Control, clone DA1E (Cell Signaling Technology, Danvers, Massachusetts) for 45 minutes at room temperature. Samples were then washed with FACS wash buffer and then stained with a solution of FACS wash buffer with 1:250 of Alexa Fluor 647-conjugated Goat anti-Rabbit IgG, polyclonal (ThermoFisher) for 45 minutes at room temperature. Samples were washed and resuspended with FACS wash buffer and read on a BD FACSCalibur.

T Cell Receptor Downregulation. 2C CD8+ T cells were isolated as described above and particle aAPCs were incubated with T cells for 30 minutes at 4°C and then activated for 5 hours at 37°C. Cells were washed with FACS wash buffer in a 96 well plate and then stained with a solution of FACS wash buffer with 1:100 PE-conjugated rat anti-mouse CD8a, clone 53-6.7 (BD Pharmingen) and 1:100 Alexa Fluor 647-conjugated anti-mouse TCR β chain, clone H57-597 (Biolegend) for 30 minutes at 4°C. Samples were then washed and resuspended with FACS wash buffer and read on a BD FACSCalibur.

T Cell Phenotype Characterization. After 7 days of culture, T cells were counted using a hemocytometer. 200,000 T cells were taken to stain for phenotypic markers. Cells were stained with a 1:100 solution of PE-conjugated rat anti-mouse CD62L, clone MEL-

14 (BD Pharmingen), APC-conjugated rat anti-mouse CD8a, clone 53-6.7 (BD Pharmingen), PerCP-conjugated rat anti-mouse CD44, clone IM7 (Biolegend), and 1:1000 of LIVE/DEAD® Fixable Green Dead Cell Stain (ThermoFisher) for 15 minutes at 4°C. Cells were then washed with FACS wash buffer and read on a BD FACSCalibur. For CD122+, CD44+, CD8+ T cell experiments, the same protocol was followed, but a 1:100 solution of PE-conjugated Rat Anti-Mouse CD122, clone TM-Beta 1 (BD Pharmingen) was used instead of the PE-conjugated anti-mouse CD62L.

T Cell Cytokine Functionality Characterization. After 7 days of culture, T cells were counted using a hemocytometer. 500,000 T cells were taken per condition and separated into restimulation or no-stimulation groups. A solution of 1:350 BD GolgiStop Protein Transport Inhibitor (BD Biosciences) and 1:350 BD GolgiPlug Protein Transport Inhibitor (BD Biosciences) was added to the cells in RPMI-1640 medium supplemented with 10% fetal bovine serum. Microparticle Dyanl-based aAPCs were added to cells to be restimulated at a 1:1 ratio. Cells were then allowed to incubate in a cell incubator for 6 hours at 37°C. Following the incubation, cells were washed and then stained with 50 μL of a 1:100 solution of PerCP-conjugated rat anti-mouse CD8a, clone 53-6.7 (Biolegend) and 1:1000 LIVE/DEAD® Fixable Aqua Dead Cell Stain (ThermoFisher) for 30 minutes at 4°C. Cells were then washed with PBS and 100 μL of BD Cytofix/Cytoperm Fixation and Permeabilization Solution was added to the cells and allowed to sit overnight at 4°C. Following the fixation step, 100 μL of 1x BD Perm/Wash Buffer (10x solution diluted to 1x in a solution of 2% bovine serum albumin in PBS) was added to the cells and washed. Cells were again washed with 200 μL 1x BD Perm/Wash Buffer. Cells were then stained with a solution of 1:100 solution of PE-conjugated rat anti-mouse IFNγ, clone XMG1.2

(BD Pharmingen), APC-conjugated rat anti-mouse IL2, clone JES6-5H4 (BD Pharmingen), and PE-Cy7-conjugated rat anti-mouse TNFα, clone MP6-XT22 (Biolegend) for 1 hour at 4°C. Cells were washed with FACS wash buffer and then read on a BD LSR II flow cytometer. Background cytokine staining was accounted for by subtracting cytokine positive cells in non-stimulated conditions from the re-stimulated cells.

Transmission Electron Microscopy (TEM) of T cells and Particles. Thin sections, 60 to 90 nm, were cut with a diamond knife on the Reichert-Jung Ultracut E ultramicrotome and picked up with Formvar coated 2x1 mm copper slot grids. Grids were stained with 2% uranyl acetate (in 50% methanol) followed by lead citrate, and observed with a Philips CM120 at 80 kV. Images were captured with an AMT XR80 high-resolution (16-bit) 8 Mpixel camera.

Effective Particle Diameter and Ligands Available Calculations. To calculate the average number of available ligands it is assumed the particles and the CD8+ T cells are spherical. The separation distance from the particle and cell is assumed to be 5 nm to be the limit where a productive interaction to occur. This distance is used to calculate the effective radius of a particle's interaction with the CD8+ T cell with Equation 1, where r_{eff} is the effective radius, r_{part} is the radius of the particle and s_d the separation distance.

1) $$r_{eff} = \sqrt{{r_{part}}^2 - (r_{part} - s_d)^2}$$

The effective radius is used to find the angle of interaction between the particle and the CD8+ T cells using Equation 2, where θ_d is the angle between the particle and the CD8+ T cell to where s_d, and r_{eff} is the effective radius.

2) $$\theta_d = tan^{-1}\frac{s_d}{r_{eff}}$$

The angle of interaction between the particle and CD8+ T cell can be used to calculate the effective surface area engaged between the particle and the CD8+ T cell using Equation 3, where SA_{eff} is the effective surface area engaged, θ is the angle of interaction, and r_{part} is the radius of the particle.

3) $$SA_{eff} = \frac{\theta}{\pi/2} \cdot \pi \cdot r_{part}^2$$

The effective number of ligands presented by each particle can then be calculated with the effective engaged surface area of each particle with Equation 4, where $lig.\ dens./NP$ is the ligand density of each NP aAPC, and SA_{eff} is the effective surface area of each particle.

4) $$\#\ ligand_{eff} = lig.\ dens./NP \cdot SA_{eff}$$

Chapter 4. Efficient magnetic enrichment of antigen-specific T cells by engineering particle properties[3]

4.1. Introduction

The clinical success of recent advances in immunotherapies such as checkpoint blockade, chimeric antigen receptor T cell therapy, and adoptive cell transfer (ACT) shows the critical importance of using the immune system to fight disease. Particularly, finding and eliciting antigen-specific responses has gained significance as this minimizes off-target side-effects including autoimmunity while creating durable memory.[340,390,426] However, understanding, diagnosing, and predicting antigen-specific immune cell responses has been limited due to the exceptionally low frequency of these cells. For example, antigen-specific CD8+ T cells are between 1-in-10^4 to 1-in-10^6 CD8+ T cells.[416,427] Thus, there is a need for techniques to isolate and characterize antigen-specific immune responses for cancer, autoimmune, and pathogen responses.

We have previously developed an approach to magnetically enrich and expand these rare antigen-specific CD8+ T cells to detectable levels for immunotherapy.[254] We created artificial antigen-presenting cells (aAPCs) by chemically attaching dimeric major

[3] Sections of this chapter are reprinted (adapted) with permission from "Hickey, John W., et al. "Efficient magnetic enrichment of antigen-specific T cells by engineering particle properties." Biomaterials 187 (2018): 105-116." Copyright 2018 Elsevier.

histocompatibility complex (MHC-Ig), that can be loaded with antigenic peptide sequences, and anti-CD28 monoclonal antibody to the surface of a magnetic nanoparticle (**Figure 4-1A**). The peptide-MHC complex (pMHC) confers antigen-specificity and binds the T cell receptor (TCR) while the anti-CD28 promotes stimulation through the co-stimulatory receptor CD28 on the surface of the T cell.

The initial design was based on a 50 nm particle to mimic other current antibody cell-based particle isolations. However, this "one size fits all" approach may not be optimal for antigen-specific T cell enrichment which depend on lower affinity pMHC-TCR interactions. Recently, we and others have studied how aAPC nanoparticle size and ligand density affect the stimulation and expansion of antigen-specific T cells,[103,428] and have found that T cells are sensitive to both size and ligand density due to the necessity for local TCR clustering and sustained signaling. Particles larger than 300 nm were able to efficiently cluster multiple TCRs presumably through multivalent interaction with TCR-rich nano-islands.[13,392] Consequently, we hypothesized that aAPC nanoparticle size and ligand density would also affect the enrichment of antigen-specific T cells due to differential particle-T cell interactions such as multivalent binding.

Here we systematically studied particle properties, which provide the most effective enrichment of antigen-specific target cells, with outputs of both cell recovery and fold enrichment. We compared different aAPC particle sizes and their abilities to enrich antigen-specific T cells and correlated this back to their binding activity. We varied the ligand choice and density to determine optimal configurations and examined how the concentration of particles affects the recovery and purity of antigen-specific cells. With multiple engineering inputs and outputs we revealed that there are competing optima,

where enhancing one property may increase one output but decrease another. Study of the parameter landscape allowed us to optimize to balance these competing optima to achieve higher percentages and numbers of antigen-specific T cells for both detection and therapeutic applications.

4.2. Materials and Methods

Mice. Mice were maintained per guidelines approved by the Johns Hopkins University's Institutional Review Board. C57BL/6J mice were purchased from Jackson Laboratories (Bar Harbor, ME). 2C T cell receptor transgenic mice were kept as heterozygotes by breeding on a C57BL/6 background. Mice were used between 8–10 weeks of age.

Peptide-MHC Dimer Production. Dimeric peptide-loaded MHC-Ig was produced as previously described[250]. Briefly, Kb-Ig was produced using hybridoma cell lines in serum free media and captured on a NP sepharose column. Kb-Ig was loaded with the SIYRYYGL peptide (GenScript, Piscataway, NJ) using active protein folding via buffer exchange and washed using membrane ultrafiltration with a Vivaspin 20 50 kDa MWCO (GE Healthcare). Non-cognate TRP2 peptide (SVYDFFVWL), (GenScript), was loaded in the same way. Fluorescent KbSIY was produced by labeling with Fluorescein-5-Isothiocyanate (FITC 'Isomer I') (Sigma Aldrich, St. Louis, MO) per manufacturer's recommendations. Briefly, a 1 M carbonate-bicarbonate buffer at a pH of 9.0 was added at a 1:10 ratio to the KbSIY. FITC-isothiocyanate was dissolved in DMSO (Sigma Aldrich) at a concentration of 1 mg/mL and added to the KbSIY at a 5:1 molar ratio and allowed to react for 2 hours at room temperature. FITC-KbSIY was washed using membrane

ultrafiltration at a 50 kDa MWCO (GE Healthcare). To make staining MHC-Ig, loaded dimeric MHC-Ig was biotinylated by reacting a 20-molar excess of EZ-Link™ Sulfo-NHS-Biotin (ThermoFisher) for 30 minutes at room temperature and then washing the protein using membrane ultrafiltration.

Artificial Antigen Presenting Cell Production. Artificial antigen-presenting cells were produced as previously described.[103] Briefly, magnetic particles functionalized with NHS surface groups of various sizes were purchased from OceanNanotech (Springdale, AR, USA). Loaded antigen-specific dimeric MHC-Ig KbSIY and equimolar anti-CD28, clone 37.51 (purchased from BioXCell (West Lebanon, NH)) were conjugated to the surface of the particles per manufacturer's recommendations.

For higher density aAPCs, magnetic particles with amine surface groups of various sizes were purchased from Micromod (Rostock, Germany). Particles were functionalized with Sulfo-SMCC (Proteochem, Hurricane, UT) and antigen-specific dimeric MHC-Ig KbSIY and equimolar anti-CD28 were thiolated with Traut's reagent (2-iminothiolane) (Sigma Aldrich) and then mixed with the functionalized particles per manufacturer's recommendations. Signal-1 only particles were produced accordingly; however, no anti-CD28 was included in the reaction with the magnetic particles. Similarly fluorescent particle aAPCs were produced by a similar process except that the MHC-Ig KbSIY attached was labeled with FITC. 4500 nm Dynal Particles were purchased from ThermoFisher (Halethorpe, MD) and dimeric MHC-Ig KbSIY and equimolar anti-CD28 were conjugated to the epoxy-coated surface as established previously.[231]

To achieve closely equivalent densities of dimeric MHC-Ig and anti-CD28 on the surface of different sized particles, the ratio of protein added to the total particle surface

area was kept constant. For example, 0.5 mg of 50 nm particles have the same total surface area as 4.6 mg of the 300 nm particles. Thus, 0.5 mg of total protein was added to react with each of these particle batches respectively. For co-conjugation of Signals 1 and 2, 0.5 mg of Signals 1 or 2 represents a supersaturating amount for both proteins, *i.e.* it is 10-fold higher than the theoretical maximum amount of protein needed for conjugating to the particle surface. The amount of protein to add was determined by increasing the total protein added to the conjugation reaction, and choosing the value where the final protein density on the particle plateaued.

Particle Characterization. The amount of protein conjugated successfully to the surface of the particles was quantified through fluorescent staining. The amount of MHC-Ig was quantified by staining with FITC-conjugated rat anti-mouse Ig λ1, λ2, λ3 light chain, clone R26-46, and the amount of anti-CD28 was quantified by staining with FITC-conjugated mouse anti-Armenian/Syrian hamster IgG, clone G192-1 (BD Pharmingen, Franklin Lakes, New Jersey). Particles were stained with 1 μL of the antibody for 1 hour at 4 °C, then washed three times, and fluorescence was read on Synergy HTX Multi-mode florescent plate reader (BioTek, Winooski, VT, USA). Protein was quantified by comparison to fluorescent standard curve of staining antibodies, and particle number was quantified by absorbance using a spectrophotometer at a 405 nm reference.

Doped Enrichment. 2C or C57BL/6J CD8+ T cells were obtained by using a mouse CD8+ T cell negative isolation kit from Miltenyi Biotec (Cologne, Germany) and following manufacturer's instructions. 2C transgenic mice have CD8+ T cells with the same T cell receptor that recognizes the mouse MHC Kb loaded with the SIY peptide. These 2C CD8+ T cells were labeled with CellTrace™ CFSE Cell Dye per manufacturer's

recommendations (ThermoFisher). Briefly, CD8+ T cells were suspended in 1 mL of PBS and 1 μL of CFSE to make a final concentration of 5 μM. This was incubated at 37 °C for 20 minutes and then incubated for 5 more minutes with 5 mL of complete RPMI-1640 medium (ThermoFisher) supplemented with 10% fetal bovine serum (Atlanta Biologicals, Flowery Branch, GA). Labeled cells were then washed twice more in RPMI-1640 medium supplemented with 10% fetal bovine serum.

These CFSE-labeled 2C CD8+ T cells were then counted with a hemocytometer and added at a 1:1000 ratio to C57BL/6J CD8+ T cells and mixed thoroughly in a PBS buffer with 2 mM EDTA and 0.5% Bovine Serum Albumin (Gemini, Sacramento, CA). Particle aAPCs were then added to this mixture at the indicated amounts per $1x10^6$ total CD8+ T cells and allowed to bind at 4 °C for 1 hour. Binding was done at 4 °C to minimize cell uptake of the aAPCs. This particle cell-mixture was then washed magnetically. For smaller 50 nm particle aAPCs, the cell-particle mixture was washed three times with PBS using a Miltenyi MS column which amplifies the magnetic field needed for smaller particles. The larger particles larger than 50 nm were washed using a STEM-cell magnetic column (Vancouver, Canada) with PBS three times. All particle-cell mixtures were eluted in 500 μL of PBS and counted via a hemocytometer. This eluted product was then stained with the APC-conjugated rat anti-mouse CD8a, clone 53-6.7, antibody (BD Pharmingen) for 15 minutes at 4 °C, washed, and read on a BD FACSCalibur.

Fold enrichment was determined by dividing the percent of 2C positive cells in the eluted particle-cell mixture by the percent of 2C positive the native 1:1000 doped mixture. Percent cell recovery was calculated by dividing the number of 2C positive cells in the eluted particle-cell mixture by the number of 2C positive the native 1:1000 doped mixture.

The 2C cell counts were calculated by multiplying the number of cells in each mixture by the measured percentages from flow cytometry.

Particle Binding. Particle aAPCs were allowed to bind with 2C CD8+ T cells at 4 °C for 1 hour at various ratios of particle aAPCs to T cells. This mixture was washed and then stained with a 1:350 ratio of PE labeled rat-anti-mouse IgG for 15 minutes at 4 °C. PE labeled polyclonal goat-anti-mouse IgG1 (ThermoFisher) recognizes the mouse IgG of the dimeric Kb-Ig on the particles to discriminate and quantitate particles on the surface. Excess antibody was washed away from the particle-cell mixture and then the cells were read on a BD FACSCalibur to determine the percent of cells bound with respect to the non-particle-bound 2C CD8+ T cells of background staining.

Particle Off-rate. Fluorescent aAPCs were allowed to bind with 2C CD8+ T cells in FACS wash buffer at 4 °C for 1 hour at a saturating dose particle aAPCs to T cells as determined by particle binding experiments. Samples were washed with FACS wash buffer and a 0 time point was read on a BD FACSCalibur. Then a super-saturating amount (greater than 50 molar excess) of 1B2 anticlonotypic mAb was added to the T cell-particle mixture. The 1B2 antibody recognizes the 2C TCR and competes for binding with particle KbSIY. Samples of the mixture were taken periodically and read via flow cytometry to quantify the number of particles still attached.

Particle Endocytosis. Fluorescent aAPCs were allowed to bind with 2C CD8+ T cells at 4 °C for 1 hour at a saturating dose of particle aAPCs to T cells as determined by particle binding experiments. A third of cell-aAPC mixture was taken and stained with a 1:350 ratio of APC-labeled polyclonal goat-anti-mouse IgG1 for 15 minutes. Stained cells were then washed and stained with a 1:100 ratio of PerCP-conjugated rat anti-mouse CD8a,

clone 53-6.7, antibody (BD Pharmingen) for 15 minutes at 4 °C, washed, and read on a BD FACSCalibur. The other two-thirds of the cell-aAPC mixture was added to a 96 U-bottomed plate in complete RPMI media supplemented with 10% FBS. The cell-aAPC mixture was then incubated for either 3 or 18 hours at 37 °C in a cell incubator. At the indicated time points, another third of the cell-aAPC mixture was harvested and stained as indicated above and read on a BD FACSCalibur.

Confocal Microscopy of aAPCs and 2C CD8+ T Cells. The same experimental set-up was utilized for confocal microscopy as described in the particle endocytosis experiments. However, following incubation cells were stained with a 1:100 ratio of APC-conjugated rat anti-mouse CD8a, clone 53-6.7, antibody (BD Pharmingen) for 15 minutes at 4 °C. Then cells were fixed with a solution of 4% paraformaldehyde in PBS for 20 minutes at room temperature. Cells were then washed and stained with DAPI (ThermoFisher) according to manufacturer's instructions for 10 minutes at room temperature. Cells were washed and then imaged on a Zeiss LSM780-FCS confocal microscope.

Development of Particle Binding Model. We attempted to model aAPC-T cell binding with a multivalent kinetic model, as described by Stone and group [429]. In their paper, they developed a kinetic model for a multivalent pMHC complex dissociating from T cells. We expanded this model for nanoparticles with given numbers of TCR-pMHC contacts, n:

$$L_nT \underset{\mu}{\overset{nk_{off}}{\rightleftharpoons}} L_{n-1}T \underset{2\mu}{\overset{(n-1)k_{off}}{\rightleftharpoons}} \cdots L_jT \underset{(n-j+1)\mu}{\overset{jk_{off}}{\rightleftharpoons}} \cdots L_2T \underset{(n-1)\mu}{\overset{2k_{off}}{\rightleftharpoons}} LT \xrightarrow{k_{off}} L_{sol}$$

We follow their assumption that the off-rates of TCR-pMHCs ($\boldsymbol{k_{off}}$) and multivalent on-rates ($\boldsymbol{\mu}$) are independent of the binding of neighboring MHC with TCR,

allowing use of stoichiometric coefficients alone to account for avidity effects. These assumptions lead to the following differential equations:

$$\frac{d[LT]}{dt} = -k_{off}[LT] + 2k_{off}[L_2T] - (n-1)\mu[LT]$$

$$\frac{d[L_2T]}{dt} = -2k_{off}[L_2T] - (n-2)\mu[L_2T] + (n-1)\mu[LT] + 3k_{off}[L_3T]$$

...

$$\frac{d[L_jT]}{dt} = -jk_{off}[L_jT] - (n-j)\mu[L_jT] + (n-j+1)\mu[L_{j-1}T] + (j+1)k_{off}[L_{j+1}T]$$

...

$$\frac{d[L_nT]}{dt} = -nk_{off}[L_nT] + \mu[L_{n-1}T]$$

Utilizing this model we derived the equation that was used within this manuscript to model T cell-aAPC binding, based on the following assumptions:

The concentration of nanoparticles bound to TCRs equals:

$$L_B = \sum_{j=1}^{n}[L_jT] \quad \textbf{(1)}$$

Also, particle unbinding occurs when singly bound particles fall off:

$$\frac{d[L_B]}{dt} = -k_{eff}^{off}L_B = -k_{off}[LT] \quad \textbf{(2)}$$

Finally, to determine what [LT] equals, we assume mass equilibrium of bound forms, based on the exponential decay behavior of our particles and μ being at least ten times larger than k_{off} to get:

$$[L_2T] = \frac{(n-1)\mu}{2k_{off}}[LT]$$

$$[L_3T] = \frac{(n-2)\mu}{3k_{off}}[L_2T] = \frac{(n-2)(n-1)\mu^2}{6k_{off}^2}[LT]$$

...

$$[L_jT] = \frac{k_{off}}{n\mu}\binom{n}{j}\left(\frac{\mu}{k_{off}}\right)^j[LT] \quad (3)$$

Substituting equation (3) into equation (1):

$$[L_B] = \frac{k_{off}[LT]}{n\mu}\sum_{j=1}^{n}\binom{n}{j}\left(\frac{\mu}{k_{off}}\right)^j$$

$$= \frac{k_{off}[LT]}{n\mu}\left[\sum_{j=0}^{n}\binom{n}{j}\left(\frac{\mu}{k_{off}}\right)^j - 1\right]$$

$$= \frac{k_{off}[LT]}{n\mu}\left[\left(1+\frac{\mu}{k_{off}}\right)^n - 1\right] \quad (4)$$

Solving for $[L_B(t)]$ in equation (2) and substituting in equation (4) for $[L_B]$ in terms of $[LT]$:

$$\frac{L_{bound,t}}{L_{bound,0}} = exp\left[-k_{off}^{eff}t\right] = exp\left[\frac{-n\mu}{\left(1+\frac{\mu}{k_{off}}\right)^n - 1}\right] \quad (5)$$

Enrichment and Expansion of Endogenous Antigen-specific T cells. CD8+ T cells from C57BL/6J mice were obtained with a mouse CD8+ T cell negative isolation kit from

Miltenyi Biotec (Cologne, Germany) following manufacturer's instructions. aAPCs were then added to the CD8+ T cells to incubate at 4 °C for 1 hour with mixing. The ratio of aAPCs to T cells was controlled based on the total T cell signaling molecules conjugated to the surface of the particles—230 fmol of signaling molecules (or 115 fmol of peptide-loaded MHC) per every $1x10^6$ CD8+ T cells. This ratio was determined from early experiments by comparing different sized aAPCs in doped enrichment studies (Fig. 6A), and from our previous experience using 50 nm aAPCs for enrichment and expansion of rare endogenous antigen-specific T cells [254].

After incubation with the particles, the mixture was magnetically washed three times. For smaller 50 nm particle aAPCs, the cell-particle mixture was washed using a Miltenyi MS column, while the 300 nm aAPCs mixtures were washed using a STEM-cell magnetic column. The first wash was with a PBS buffer with 2 mM EDTA and 0.5% Bovine Serum Albumin. The second wash was with complete RPMI-1640 medium supplemented with 10% fetal bovine serum. The third was with complete RPMI-1640 medium supplemented with 10% fetal bovine serum and T cell growth factor, a cytokine cocktail derived from condition media produced from stimulated human PBMC as previously described [425]. The resulting washed cells were eluted in 0.5 mL of RPMI-1640 medium supplemented with 10% fetal bovine serum and T cell growth factor. The cells were then counted on a hemocytometer, resuspended at a concentration of 250,000 cells/mL, and plated in 96 u-bottomed plates. On day 3, cells were refed using media (50% of the initial plating volume) with a doubled concentration of T cell growth factor.

On day 7 cells were harvested and stained with Trypan Blue, and viable cells were counted via hemocytometry. Samples were divided and stained for antigen-specific CD8+

T cells. The first portion of cells was stained with 1 μg of biotinylated-cognate KbSIY and a 1:100 ratio of APC-conjugated rat anti-mouse CD8a, clone 53-6.7 (BD Pharmingen) in FACS wash buffer for 1 hour at 4 °C. The second subset of the sample was stained with 1 μg of biotinylated-noncognate KbTRP2 and a 1:100 ratio of APC-conjugated rat anti-mouse CD8a, clone 53-6.7 (BD Pharmingen) in FACS wash buffer for 1 hour at 4 °C. All samples were then washed with PBS and then stained with a 1:350 ratio of PE-labeled streptavidin (BD Pharmingen) and a 1:1000 ratio of LIVE/DEAD™ Fixable Green Dead Cell Stain (ThermoFisher) in PBS for 15 minutes at 4 °C. Cells were then washed and read on a BD FACSCalibur. Percent antigen-specific cells were calculated by subtracting the percent gated in cognate stained CD8+ T cells from non-cognate stained CD8+ T cells. Number of antigen-specific cells was determined from multiplying the percent of antigen-specific cells by the number counted following cell harvest. For the experiment comparing high density (HD) 50 nm and 300 nm expansion of endogenous CD8+ T cells without enrichment, the same protocol was followed just excluding the magnetic washing at day 0.

Functional Analysis of Antigen-specific CD8+ T Cells. On Day 7 of culture, approximately 100,000 CD8+ T cells were isolated and stained with either 1 μg of biotinylated-cognate KbSIY or 1 μg of biotinylated-non-cognate KbTRP2 in sterile PBS for 1 hour at 4 °C. All samples were then washed with PBS and stained with a 1:350 ratio of PE-labeled streptavidin (BD Pharmingen) in PBS for 15 minutes at 4 °C. Cells were subsequently washed in complete RPMI-1640 medium supplemented with 10% fetal bovine serum and resuspended in 100 μL of media. To inhibit protein transport and probe for degranulation, 10 μL solution of 1:50 FITC anti-CD107a, 1:350 BD GolgiStop Protein Transport Inhibitor (BD Biosciences), and 1:350 BD GolgiPlug Protein Transport Inhibitor

(BD Biosciences) in PBS was added to the samples. Cells were incubated at 37 °C for 6 hours. After incubation, cells were washed and stained with 1:100 PBS solution of PerCP-conjugated anti-mouse CD8a, clone 53-6.7 (Biolegend) and 1:1000 of LIVE/DEAD® AmCyan Fixable Aqua Dead Cell Stain (ThermoFisher) at 4 °C for 30 minutes. Cells were subsequently fixed and permeabilized with 100 μL BD Cytofix/Cytoperm Fixation and Permeabilization Solution (BD Biosciences) overnight. Cells were washed with 1x BD PERM/Wash buffer with 2% BSA the following day and stained with 1:100 solution of APC-conjugated rat anti-mouse IFN-γ, clone XMG1.2 (BD Pharmingen) in PERM/Wash buffer with 2% BSA at 4 °C for 1 hour. Stained cells were read on BD LSR II flow cytometer.

4.3. Results

4.3.1 aAPC size impacts antigen-specific T cell enrichment efficiency

To study how engineering nanoparticle aAPC properties affect the ability to enrich antigen-specific T cells, we doped in fluorescently-labeled antigen-specific CD8+ T cells at a 1:1000 ratio to CD8+ T cells from a B6 mouse. The antigen-specific cells were isolated from a 2C transgenic mouse that recognizes the SIY peptide loaded into the MHC K^b (**Figure 4-1B**). Using a magnetic field, we enriched antigen-specific cells with our different sized magnetic aAPCs. We detected the percent antigen-specific T cells by flow cytometry and calculated the fold enrichment (**Figure 4-1C**).

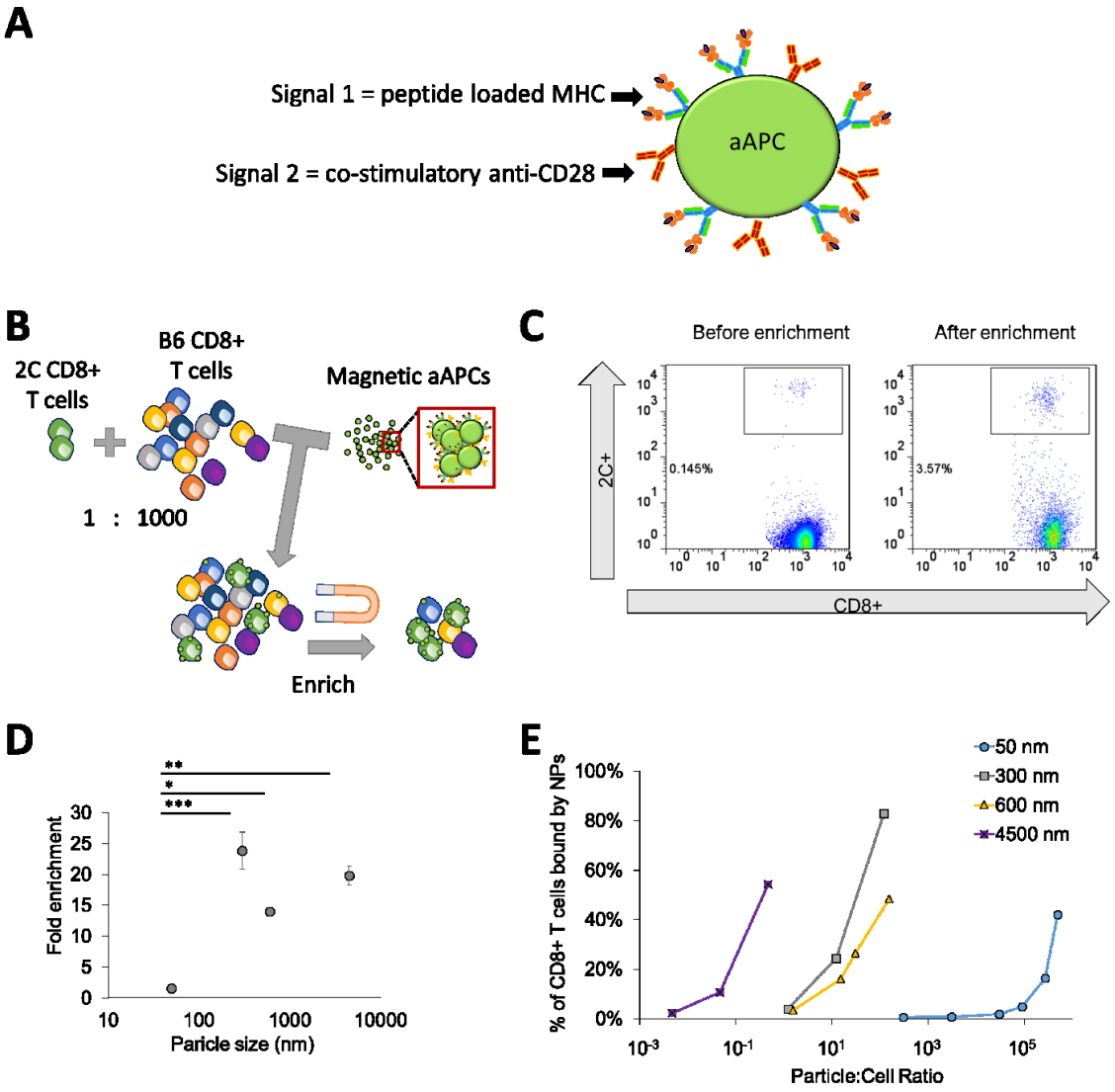

Figure 4-1: Particle aAPC size influences antigen-specific cell enrichment. (A) Artificial antigen-presenting cells (aAPCs) are formed by conjugating Signal 1, which is antigen-loaded dimeric MHC-Ig, and Signal 2, which is co-stimulatory antibody towards CD28. Together they provide antigen-specific recognition and signaling to activate antigen-specific T cells and proliferate. (B) Experimental set up to identify key particle parameters influencing antigen-specific T cell enrichment. Fluorescently labeled transgenic 2C T cells were doped in at a 1 to 1000 ratio with wildtype non-specific B6 T cells. Schematic not drawn to scale in order to visualize aAPC binding to cells. (C) An example flow plot of fold enrichment that is characterized by analyzing pre-enrichment and post-enrichment populations by flow cytometry. (D) Fold enrichment is significantly lower in 50 nm aAPCs compared to other sized aAPCs at an amount of particles controlled for 115 fmol of pMHC-conjugated to the surface per 106 CD8+ T cells (error bars show s.e.m.; ***$p < 0.001$, **$p < 0.001$, *$p < 0.05$, $n = 3$, one-way ANOVA with Tukey's post test). (E) Binding avidity changes based on particle size, where aAPC dose was varied and the percent of transgenic CD8+ T cells bound by particles was quantified by flow cytometry.

We evaluated the effect of nanoparticle size on the ability to enrich by developing particle aAPCs of 50-, 300-, 600-nm, and 4.5-µm diameters with similar ligand densities of pMHC and anti-CD28 monoclonal antibody (44, 300, 124, and 392 molecules of Signal 1 and 2 per μm^2 of particle respectively—data originally published in[103]) (**Figure 4-2)**. Smaller aAPC sizes were chosen with distinct size distributions and at the nanometer resolution to enable capability with *in vivo* administration of aAPCs and enriched antigen-specific T cells as a therapy, whereas larger 4.5 µm aAPCs were included for comparison, as they are the standard anti-CD3/anti-CD28 aAPC used to activate polyclonal T cells in ACT [231]. We controlled the amount of SIY-loaded MHC and anti-CD28 on the particle surface across various particle sizes. This theoretically normalizes the number of binding events each TCR should encounter. Particles 300 nm and larger, were effective in enriching antigen-specific cells about 20-fold, whereas 50 nm aAPCs were significantly less effective, only providing a 1.5-fold enrichment (**Figure 4-1D**).

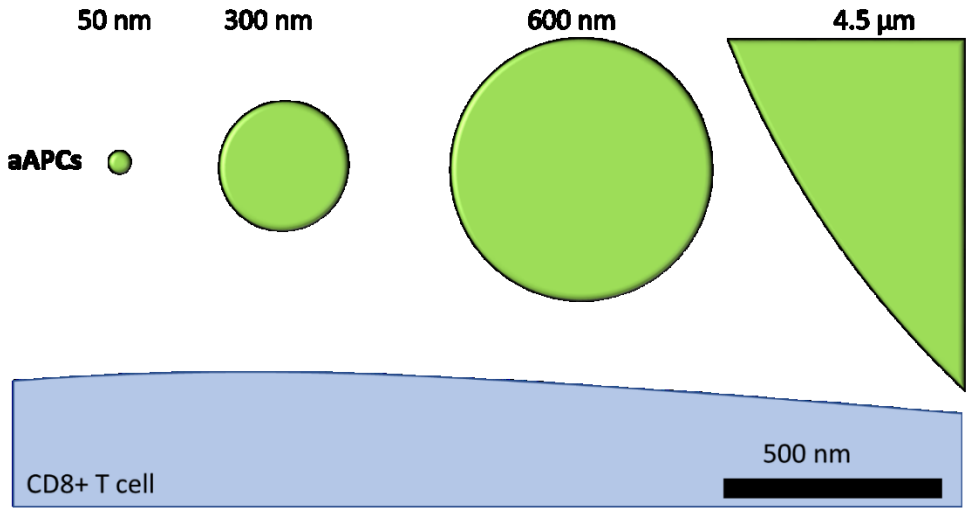

Figure 4-2: Schematic demonstrating relative size of particle aAPCs sizes used in the studies to a CD8+ T cell. Scale bar = 500 nm.

We hypothesized that aAPCs larger than 300 nm have multivalent interactions with the TCRs and lead to greater binding with the T cell thereby enhancing enrichment. To test this hypothesis, we incubated our different sized aAPCs with cognate 2C CD8+ T cells at varying doses to examine their equilibrium binding. Interestingly, we observed a size-dependent trend with the aAPCs ability to bind to the T cells (**Figure 4-1E, Figure 4-3**). As aAPC size increases, fewer aAPCs are needed to effectively bind to the CD8+ T cell indicating a higher avidity of the aAPC for the cognate T cell. For example, to achieve greater than 40 percent of the T cells bound to particles, the ratio of particles to T cells for 4.5 μm, 600 nm, 300 nm, and 50 nm are around 1, 10, 10, and 10^5 respectively. The increase in avidity further substantiates our hypothesis that aAPCs engage clusters of TCR and co-stimulatory molecules.

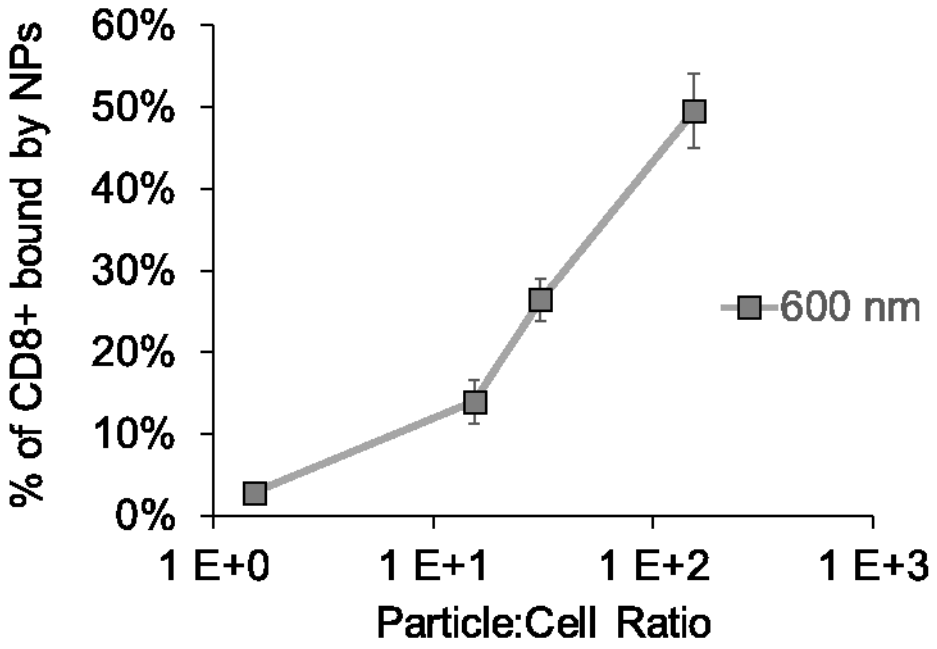

Figure 4-3: The ratio of 500 nm aAPCs to CD8+ T cells was varied and particles and T cells were incubated for 1 hour at 4 °C and percent of CD8+ T cells bound by NPs was determined by flow cytometry by staining for both the CD8+ T cells and particles (n=4 and error bars representing s.e.m.).

4.3.2 Decreasing aAPC concentration improves T cell enrichment but decreases cell recovery

Based on the more efficient binding of larger aAPCs, we hypothesized that decreasing the total number of aAPCs could reduce enrichment of non-cognate CD8+ T cells. We postulated that by eliminating excess particle aAPCs would decrease the number of lower affinity non-specific interactions. By decreasing the concentration of the 300 nm aAPCs about 20-fold, we were able to increase enrichment from 20-fold to 60-fold (**Figure 4-4A**). However, when evaluating enrichment, we recovered much fewer cells in general. We thus counted the number of cells that went into each enrichment and also the number after enrichment to determine the percent cell recovery of our doped antigen-specific cells. While we achieved much greater levels of antigen-specific enrichment, the percent recovery of these cells decreased substantially to nearly 5% (**Figure 4-4B**).

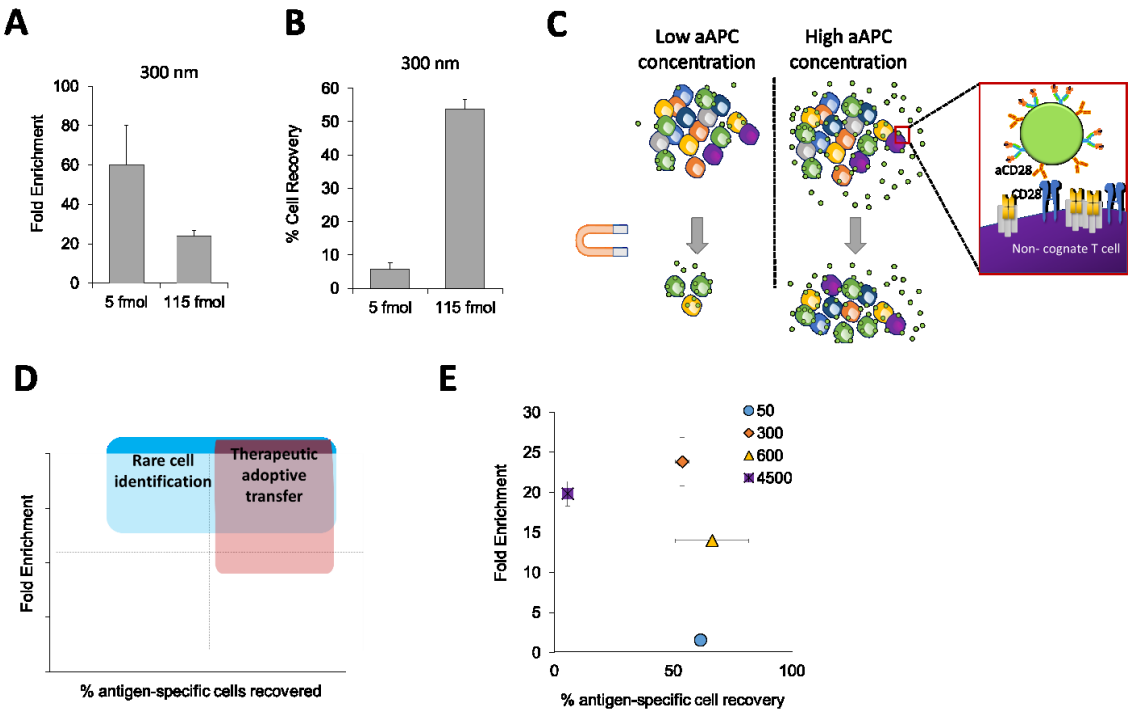

Figure 4-4: Particle aAPC concentration affects fold enrichment and percent antigen-specific cell recovery. (A) Increased enrichment when decreasing concentration of 300 nm particle aAPCs (n=3). (B) Decreased cell recovery when decreasing concentration of particle aAPCs as measured by hemocytometry and flow cytometry (error bars show s.e.m.; n = 3). (C) At high concentrations of aAPC particles increase cell recovery but also have increased non-specific interactions potentially due to the reason they have both antigen-specific signals and non-specific co-stimulatory signals. (D) High cell recovery and high cell enrichment are needed for adoptive immunotherapy applications and high cell enrichment is wanted for diagnostic applications. (E) Size dependent differences in fold enrichment and antigen-specific cell recovery at a concentration of 115 fmol aAPC-bound pMHC (error bars show s.e.m.; n = 3).

From these results we observed competing optima, where reducing aAPCs leads to greater enrichment, but decreases binding and recovery of total antigen-specific cells (**Figure 4-4C**). Selecting conditions for enrichment depends on the application for antigen-specific T cell enrichment. For cell therapy applications, high cell recoveries are desired as the effectiveness of cell-based therapies increases with increasing number of effector cells.[417] In contrast, fold enrichment is more important for detection purposes, but still requires a threshold of total cell recovery to achieve accurate readouts. When plotting our enrichment results on a graph that indicates both antigen-specific cell recovery and

enrichment (**Figure 4-4D**), it is apparent that there is a trade-off between non-specific T cell binding and low antigen-specific T cell recovery rates, pointing to the fact that the concentration of aAPCs in the enriching solution is an important parameter to optimize (**Figure 4-5**).

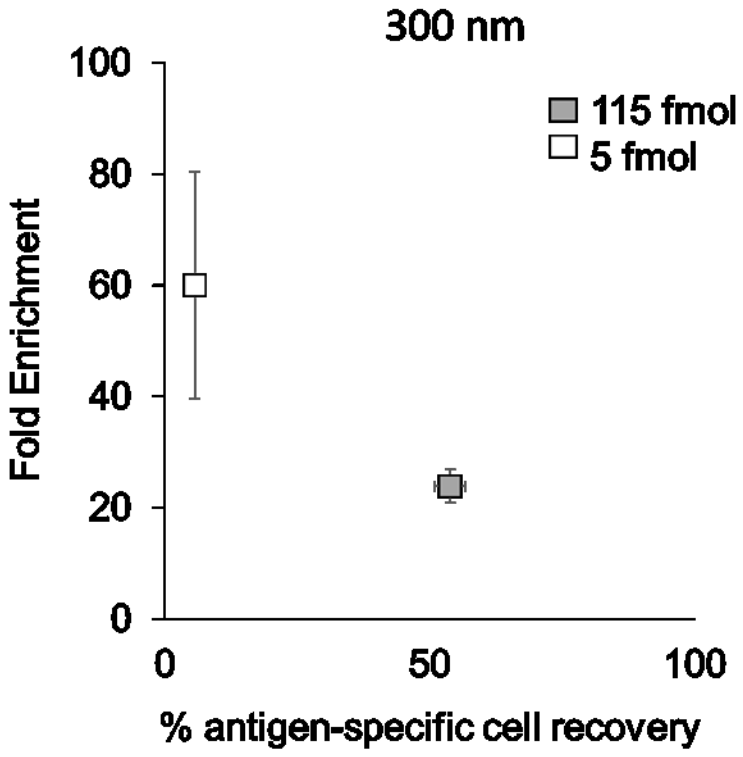

Figure 4-5: Tradeoff between fold enrichment and percent antigen-specific T cell recovery in altering the concentration of magnetic particle aAPCs. Data from panels Figure 2B and 2C replotted together (error bars show s.e.m.; n = 3)

Based on these results, we quantified the percent of antigen-specific cells recovered in enrichment experiments with different-sized aAPCs. Although there were minimal differences in fold-enrichment of particles larger than 300 nm (**Figure 4-1C**), we can observe drastic effects of the size of the particle on enrichment and cell recovery (**Figure 4-4E**). It appears that there is also a balance between size in both achieving high enrichment and high percent cell recovery, with an optimal size of 300 nm aAPCs achieving both the highest fold enrichment and highest percent cell recovery.

This phenomenon could be due to a balance between collective magnetic strength of the particles attached to a T cell and individual magnetic strength of a particle. The first requirement to successfully enrich a cell is an adequate magnetic force. Thus, there is a need to maximize the aggregate magnetic strength of the particles to successfully magnetically isolate the tagged cell. However, there is also a requirement to minimize individual particle magnetic strength to prevent particle disassociation from the cell.[430,431]

The magnetic strength of an individual particle is related to total iron oxide and thus related to volume or diameter cubed. However, the collective magnetic strength of particles bound to a given T cell, assuming spherical square-packing, is proportionally related to the diameter (**Figure 4-6**). A square-packing estimate is more conservative biologically, where there is less packing per surface area than hexagonal-packing; however, the proportion is equivalent, with just a constant difference. Thus, mathematically we also see the competing optima between decreasing the diameter to the third power and increasing it proportionally to achieve both high percent recovery and high fold enrichment. This could explain why we observe an optimal 300-nm size, which achieves both the greatest antigen-specific CD8+ T cell enrichment and cell recovery (**Figure 4-4E**).

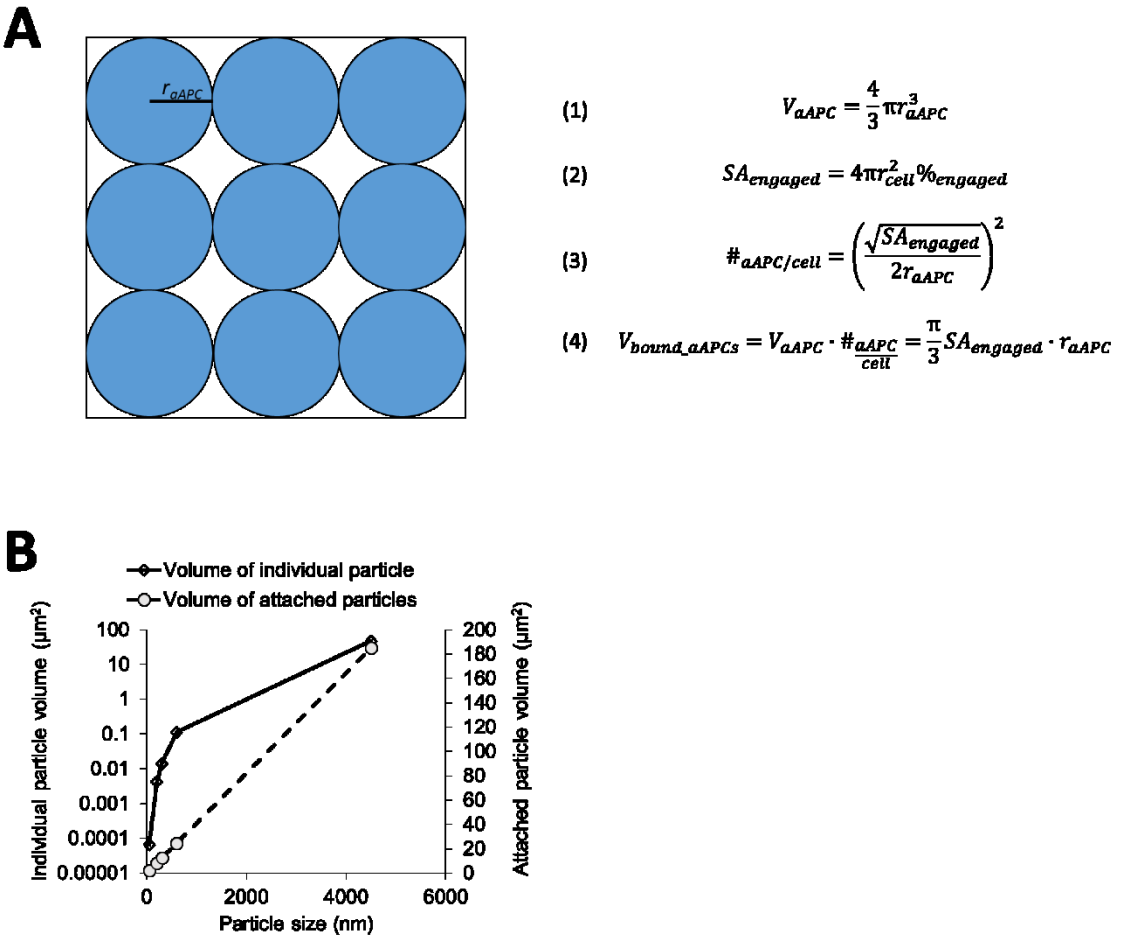

Figure 4-6: Magnetic strength depends on particle volume; too high of individual particle volume (∝ r3) can lead to disassociation with target cell and too low of collective attached particle volume (∝ r) can lead to inefficient isolation. (A) Schematic of sphere-packing diagram illustrating maximum packing of aAPC on a surface from a 2D slice at the location of 50% of the volume of the sphere. Equation 1 indicates volume for an aAPC used with raAPC representing the radius of the particle. Equation 2 indicates the equation for surface area of the cell that is engaged where rcell represents the radius of the cell and %engaged represents the amount of the surface of the T cell available for binding. Equation 3 indicates the maximum number of aAPC per T cell given a certain surface area of the T cell that can be engaged. Equation 4 represents the collective volume of the bound aAPCs to a given T cell. (B) Using analysis and equations from A we plot the volume of an individual particle (primary y axis) or the volume of attached particles assuming a given engaged surface area (secondary y axis) based on particle diameter.

4.3.3 Increasing ligand density increases aAPC avidity and improves antigen-specific CD8+ T cell isolation for small 50 nm-sized aAPCs

Besides particle size, another important design parameter of aAPCs is the density of the stimulatory ligand on the surface of the particle (**Figure 4-7A**). This has been shown to influence the ability to activate T cells presumably due to both clustering of nearby TCRs and co-stimulatory signals and also increased signal duration due to a more avid interaction.[60,103,239,432] We similarly hypothesized that increasing the particle avidity would increase enrichment of antigen-specific CD8+ T cells.

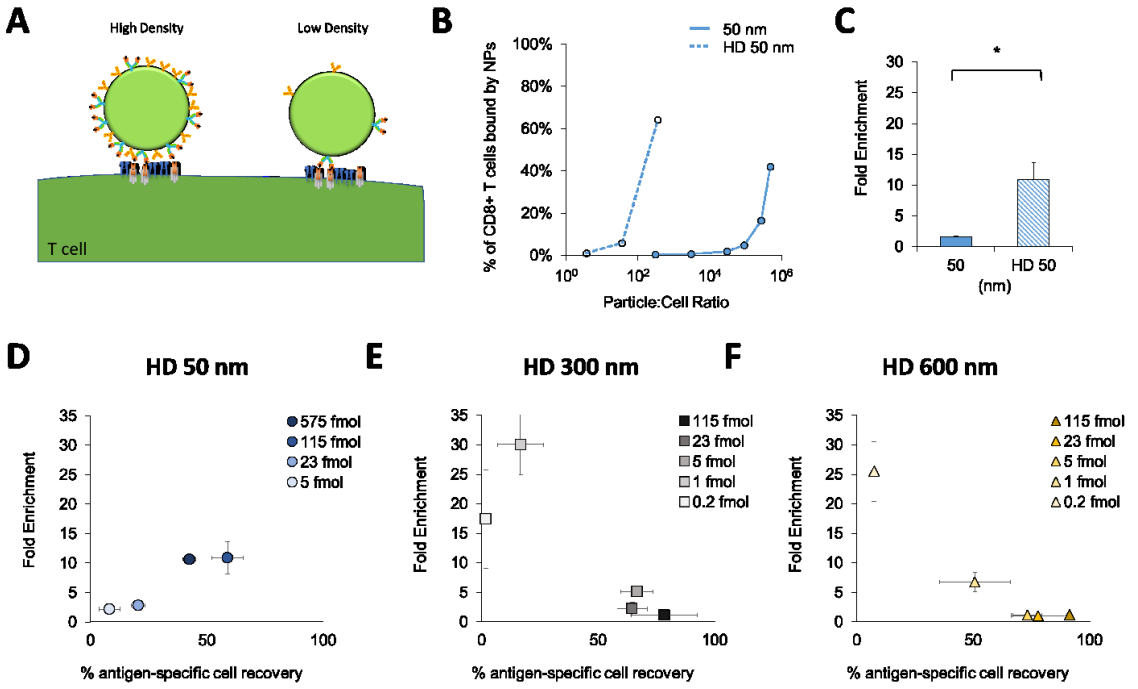

Figure 4-7: Particle ligand density influences target cell enrichment. (A) Ligand density of aAPC affects local density and thus avidity with T cell. (B) Binding avidity increases for 50 nm particles with increased density of ligand. (C) Increasing ligand density improves fold enrichment of 50 nm aAPCs at a concentration of 115 fmol aAPC-bound pMHC (error bars show s.e.m.; *$p < 0.05$, n = 3, Student's T test). (D–F) Increasing the surface ligand density increases the fold enrichment of 50 nm aAPCs (D), but leads to greater non-specific enrichment by (E) 300 nm and (F) 600 nm aAPCs (error bars show s.e.m.; n = 3).

To study this, we developed aAPCs with nearly a 100-fold increase in ligand density termed high-density (HD) 50 nm. These HD 50 nm aAPCs bound to cognate CD8+

T cells much more effectively than their lower density counterparts (**Figure 4-7B**). For example, to achieve above 40% of T cells bound to particles, 10^5 of 50 nm particles per cell were required, while only 10^2 of HD 50 nm particles per cell were needed. We hypothesized that this several log difference in binding would lead to greater enrichment. Indeed, the HD 50 nm aAPCs enriched more effectively than the 50 nm aAPCs (**Figure 4-7C**). However, the 10-fold enrichment was still lower than the 300 nm aAPCs, and even by changing the concentration of these HD 50 nm aAPCs we were unable to increase the enrichment or percent of antigen-specific recovery (**Figure 4-7D**). This inability to further increase enrichment could be due to either the low magnetic strength of the smaller particles, or an increase in non-specific interactions leading to lower enrichments.

To further explore the effects of ligand density, we made higher density versions of the 300 and 600 nm aAPCs (**Figure 4-8A**). These higher density versions also exhibited enhanced binding compared to normal density aAPCs (**Figure 4-8B**). However, when compared at the same concentration (controlled by total particle-bound protein), the HD 300 and 600 nm aAPCs provided little to no enrichment (**Figure 4-8C**). We hypothesized that the increase in ligand density also led to an increase in non-specific binding, and that by decreasing the concentration we could achieve higher values of enrichment. While decreasing the concentration helped improve the enrichment, it also decreased valued of cell recovery below 50% (**Figure 4-7E, F**). This demonstrates the importance of ligand density and also in the context of particle size to both achieve effective enrichment and cell recovery. This is another illustration of competing optima, where increasing ligand density may lead to increased binding with cognate T cells, which will increase cell recovery.

However, increasing ligand density may also lead to increased non-specific interactions such as binding with CD28 on non-cognate T cells, thus decreasing enrichment.

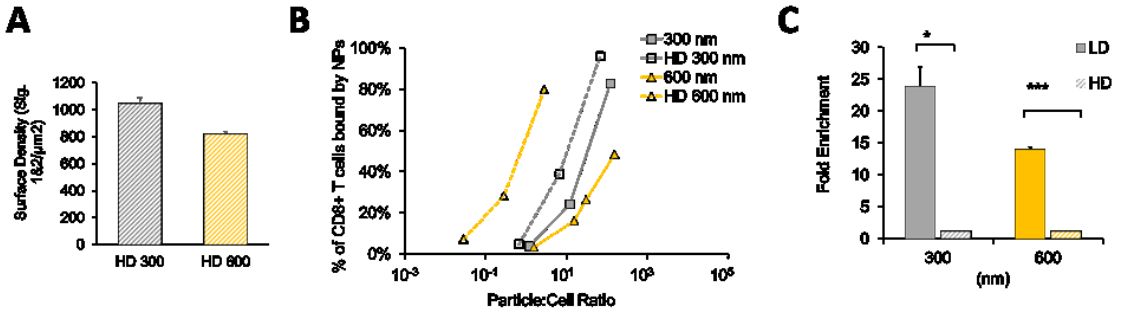

Figure 4-8: Increasing the ligand density increases avidity of larger aAPCs. (A) Density of Signals 1 and 2 per μm2 of particle surface area for HD 300 and HD 600 particles (n=2, error bars show s.e.m.). (B) Binding avidity increases for increasing the ligand density on 300 nm and 600 nm particles. (C) Fold enrichment significantly decreases with high density 300 nm and 600 nm aAPCs compared to regular density aAPCs at the same concentration (error bars show s.e.m.; ***$p < 0.0005$, *$p < 0.05$, $n = 3$, Student T test).

4.3.4 Eliminating signal 2 significantly improves antigen-specific CD8+ T cell enrichment

Based on all of our previous results where we saw significant non-specific binding and lower enrichment values with particles presenting both pMHC and anti-CD28, we hypothesized that if we eliminated non-specific anti-CD28 from our particles, we would increase specificity as CD28 is expressed by all T cells (**Figure 4-9A**). Decoupling the co-stimulatory molecule from T cell stimulation has been shown to lead to anergy and even inhibitory phenotypes.[269,433,434] However, recently we have shown that the co-stimulatory molecule can be separated from the aAPC on the nanoscale and added after enrichment if these two particles are co-clustered in a magnetic field.[250] Encouraged by these recent results we developed particles with only pMHC (Signal 1 or S1 only aAPCs) attached at high ligand densities for sizes of 50, 300, and 600 nm.

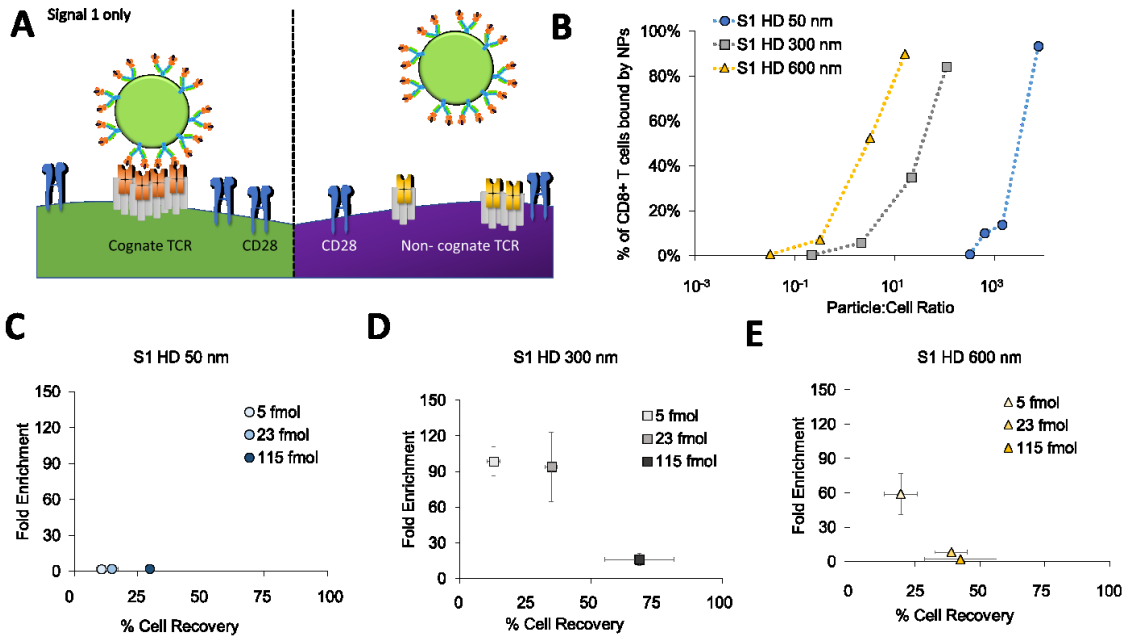

Figure 4-9: Eliminating non-specific co-stimulatory ligand from particle aAPCs to improve enrichment. (A) Signal-1 only aAPCs only have antigen-specific MHC which should eliminate many non-specific interactions. (B) Binding avidity is dependent on size of the aAPC and decreases for each size when anti-CD28 antibody is eliminated. (C–E) Eliminating non-specific co-stimulatory decreases fold enrichment for (C) 50 nm aAPCs but increases fold enrichment for (D) 300 nm and (E) 600 nm aAPCs (error bars show s.e.m.; n = 3).

The S1 only particles exhibited the same particle size-dependent increase in binding to cognate CD8+ T cells as with the canonical aAPCs (**Figure 4-9B**). However, eliminating anti-CD28 from the particle decreased the particle binding compared to their canonical HD S1/S2 aAPC counterparts (**Supplemental Fig. 6A–C**). This is not surprising as the antibody anti-CD28/CD28 interaction is a higher affinity interaction (nanomolar K_D) than the pMHC-TCR interaction (micromolar K_D).[400]

We next probed the ability for the 50, 300, and 600 nm S1 only particles to enrich antigen-specific cells. S1 50 nm aAPCs did not provide effective enrichment, where even at their highest concentration of particles there was only 2-fold enrichment (**Figure 4-9C**).

However, eliminating signal 2 from 300 nm aAPCs significantly improved specificity, where up to 90-fold enrichment was achieved with 40% recovery (**Figure 4-9D**). This was also true for S1 600 nm aAPCs but exhibited lower cell recovery percentages (**Figure 4-9E**). In general, cell recovery percentages were lower for S1 only particles at the same aAPC concentration than observed for the HD particles with anti-CD28 (**Figure 4-9D–F**). This agrees with our observation that HD S1 particles bind less effectively at the same dose than the HD S1 and S2 particles (**Figure 4-10**). Thus, we would expect increasing cell-recovery percentages with increased doses of S1-only particles.

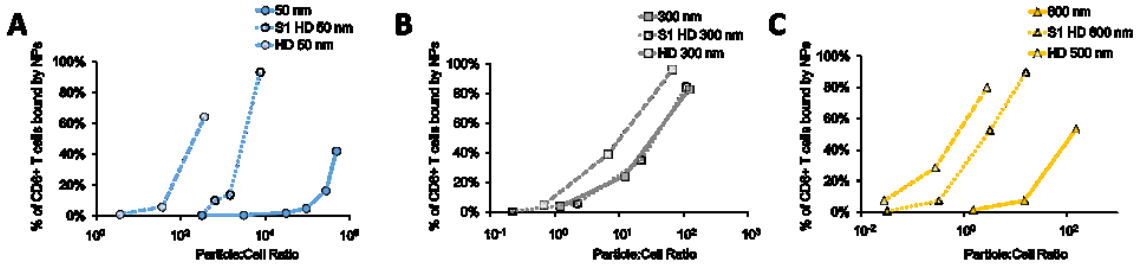

Figure 4-10: Eliminating non-specific co-stimulatory signal anti-CD28 from particle aAPCs decreases binding affinity even with a high density of ligand for (A) 50 nm, (B) 300 nm, and (C) 600 nm. Data presented is replotted for comparison purposes.

Achieving 90-fold enrichment is significantly better than enrichments we had previously achieved, where at most we were able to enrich up to 10-fold.[250,254] This increase in cell enrichment efficacy could be utilized to identify rare antigen-specific T cells earlier and more accurately.

4.3.5 Multiavidity interactions of larger aAPCs with T cells are seen by both experimental and modeling analysis

Since even S1-only aAPCs showed a size-dependent enrichment, we hypothesized that smaller aAPCs have fewer chances for multi-receptor binding leading to faster off-

rates for our S1 50 nm particles. We also hypothesized that larger particles would dissociate more slowly than smaller ones because they have more contact area with the T cell and thus more available ligands, schematically illustrated in **Figure 4-11**. This should be even more pronounced for S1 50 nm particles as the spacing of TCRs is estimated around 30 nm.[13,392]

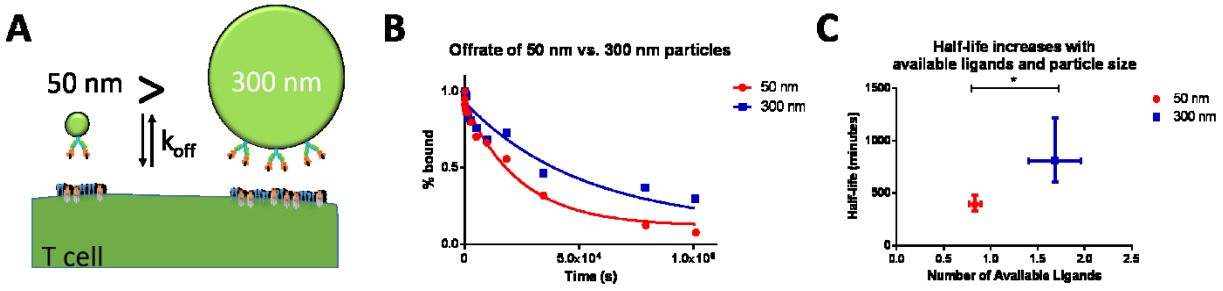

Figure 4-11: Nanoparticle size affects avidity and effective off-rate from T cell surface. (A) Schematic of how size of particles affects number of ligands available to interact with T cell receptors. (B) HD S1-only 50 nm particles dissociate more rapidly than S1-only 300 nm particles, as determined by an off-rate experiment. (C) Larger particles have increased numbers of available ligands and longer half-lives (error bars show s.e.m., * $p<0.05$, Student's t test).

To quantitatively assess this hypothesis, we conducted off-rate experiments by incubating 2C CD8+ T cells with saturating amounts of fluorescently labelled 50 and 300 nm Signal 1 KbSIY particles and then competing them off with 1B2, an anticlonotypic antibody for the 2C CD8+ TCR. We then fit the off-rate data for the S1 50 nm and S1 300 nm particles with an exponential decay function (**Figure 4-11B**, $R^2 = 0.98$ and 0.89, respectively) and found that the effective off rate of 50 nm particles was significantly faster than 300 nm particles ($p=0.001$, unpaired t test).

To associate these off-rates with multi-ligand binding, we estimated available ligands from the aAPCs to the CD8+ T cell based on particle size and total conjugated protein as quantified through fluorescent staining (**Figure 4-12**). S1 300 nm particles had a total of 100 ± 29 dimer proteins, while S1 50 nm particles had 8.3 ± 1.5 dimer proteins

per particle. The number of available ligands was estimated by assuming as we have done previously[7] that the ratio of available to total ligands is equal to the ratio of the area of a spherical cap of height *h* to the total surface area of a particle with diameter *D*, as described in Equation [1] and that the distance of interaction between particles and the T cell is within 5 nm.

$$\frac{N_{available}}{N_{total}} = \frac{\pi Dh}{\pi D^2} = \frac{h}{D} \quad (1)$$

Based on this conservative, static ratio we determined that S1 50 nm and S1 300 nm particles had 0.8±0.1 and 1.7±0.3 available ligands, respectively, leading us to attribute this difference in effective off-rate and half-life to the 300 nm particle having more available ligands despite a slightly lower density (**Figure 4-11C**).

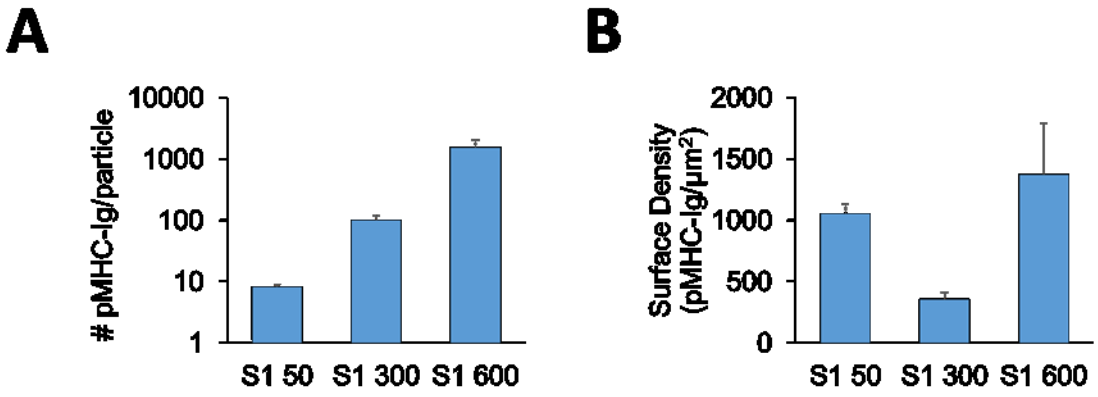

Figure 4-12: Surface ligand density of pMHC-Ig on S1 only particles. (A) Number and (B) surface density of pMHC-Ig on particles (error bars show s.e.m. n = 3–6).

To explore the design space of aAPC-T cell binding, we decided to mathematically model the effect of multi-ligand binding on particle off-rate. This will clarify how effective off-rate would change as the number of available ligands increases for other particle configurations and ligand densities. To do so we extended a kinetic model developed for oligomers with three available binding sites to particles with any

given number of available binding sites.[429] The model, as shown in Equation [2] below relates the effective off rate (k_{off}^{eff}) to the number of binding sites (n), the monomeric off rate (k_{off}) and the multivalent on-rate (μ) by assuming mass equilibrium between all states of binding and that k_{off} and μ are independent of binding of neighboring MHC with TCR.

$$\frac{L_{bound,t}}{L_{bound,0}} = exp\left[-k_{off}^{eff}t\right] = exp\left[\frac{-n\mu}{\left(1+\frac{\mu}{k_{off}}\right)^{n}-1}\right] \quad (2)$$

While the first assumption is difficult to validate, the latter assumption about rapid interconvertibility and mass-equilibrium is corroborated by the exponential decay behavior of our particles from the cell surfaces and that μ is at least 10 times larger than k_{off}. By fitting our values for k_{off}^{eff} according to equation [2], we were able to estimate the parameters k_{off} and μ and determine the behavior of k_{off}^{eff} as the number of available ligands increases (**Figure 4-13**). We found that k_{off}^{eff} decreases very rapidly, as was expected based on the significantly different off-rates of our S1 50 and S1 300 nm particles. Thus, both experimental and modeling approaches demonstrated that both the ligand density and the size of the nanoparticles are crucial to determining the local number of ligands affecting the avidity of the T cell and aAPC interaction. These results could help explain why there is so much more non-specific binding with our high density 300 and 600 nm particles that include anti-CD28 on the surface, which has a much higher affinity for non-specific CD28.

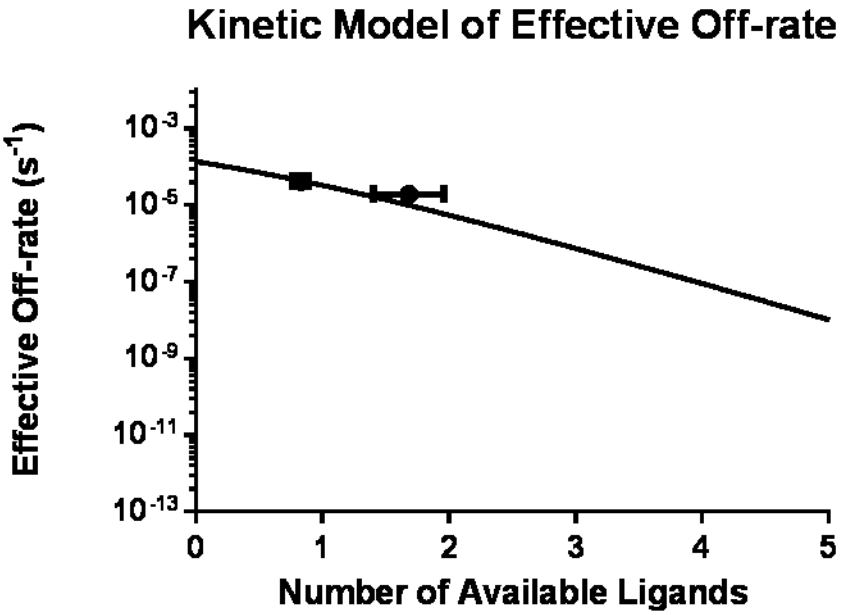

Figure 4-13: Kinetic model (see Supplementary Text) shows rapid decrease in effective off-rate of nanoparticles as the number of available ligands increases (error bars show s.e.m, R2 =0.65).

4.3.6 The effects of aAPC size and ligand density on endogenous antigen-specific enrichment and expansion

Beyond antigen-specific T cell identification, enriching antigen-specific CD8+ T cells can be applied in ACT applications. Magnetic enrichment can benefit ACT by eliminating non-specific and regulatory cells in culture, which will also limit off-target immune responses *in vivo*. Therefore, the goal is to achieve the highest percentage and number of antigen-specific cells. For this purpose, aAPCs with both Signals 1 and 2 can be used to enrich and expand antigen-specific cells taken from patients to large numbers, decreasing the time, cost, and technical difficulty to achieve this therapy.[254]

Synthesizing what we have learned about particle properties in model systems, we aimed to study further how these studies translate to isolating endogenous rare antigen-

specific T cells. To test how particle size and ligand density affected cell enrichment and activation, we chose aAPCs with different fold enrichments, yet similar percent cell recoveries. Therefore, we selected 50 nm aAPCs with low enrichment, HD 50 nm aAPCs with intermediate enrichment, and 300 nm aAPCs with high enrichment capabilities—all with around 50-60% cell recovery (**Figure 4-14A**).

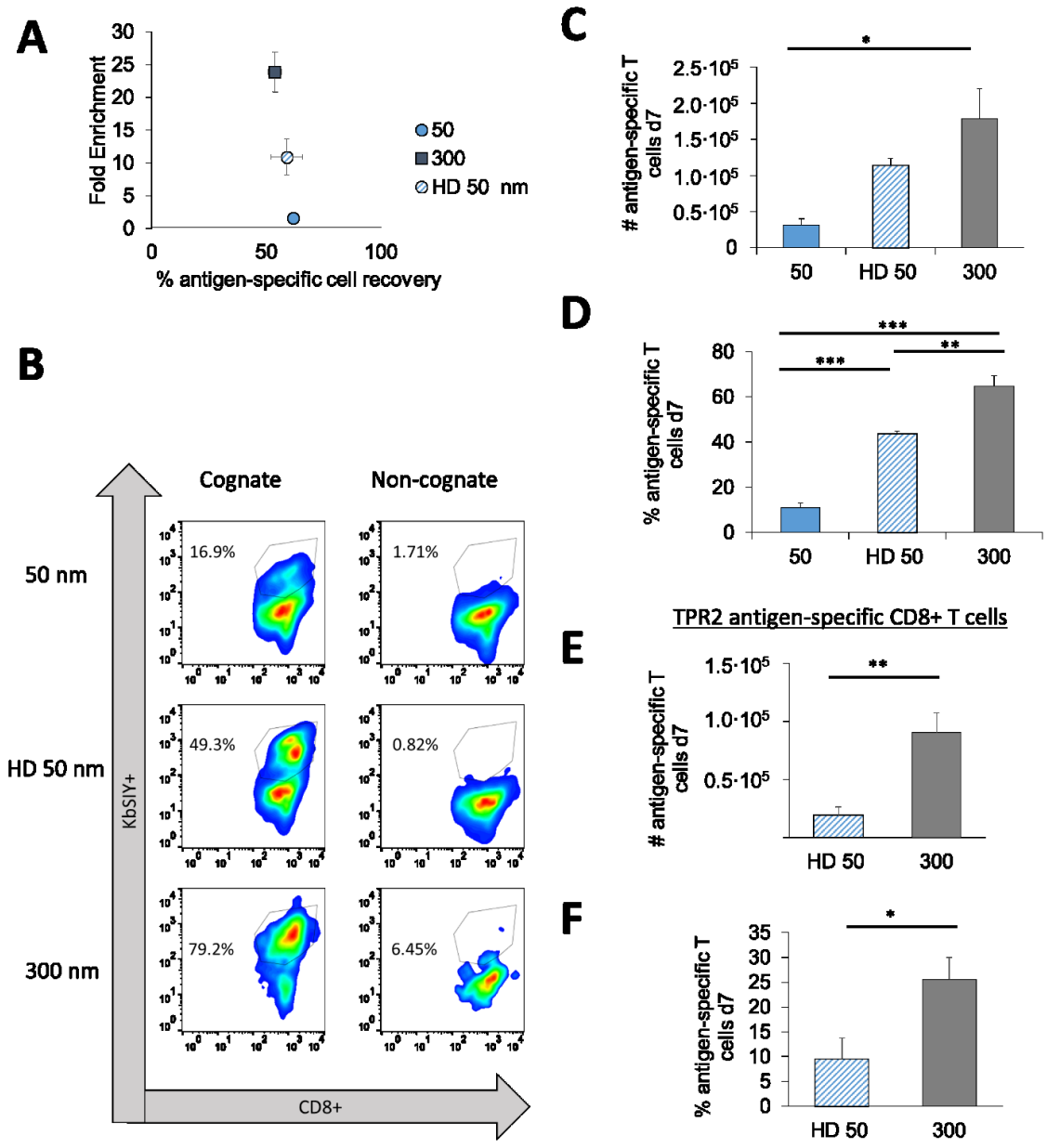

Figure 4-14: Particle aAPC size and ligand density influence the isolation and expansion antigen-specific CD8+ T cells from wildtype B6 mice. (A) Data replotted from Figures 2E and 3D to demonstrate three levels of fold enrichment over similar percentage antigen-specific recovery at an amount of particles controlled for 115 fmol of pMHC-conjugated to the surface per 106 CD8+ T cells (no statistical difference, error bars show s.e.m, n = 3, one-way ANOVA). (B) After 7 days of culture, cells were stained with a viability dye, anti-CD8+, and pMHC KbSIY (cognate) or pMHC KbSINF (non-cognate) to determine total percent and number of antigen-specific CD8+ T cells. (C) Number of SIY-specific T cells after enrichment and 7 days of culture differed (error bars show s.e.m.; *$p < 0.05$, n = 3–6, one-way ANOVA with Tukey's post test). (D) Percent SIY-specific T cells after enrichment and 7 days of culture differed (error bars show s.e.m.; ***$p < 0.001$, **$p < 0.01$, n = 3–6, one-way ANOVA with Tukey's post test). (E–F) After 7 days of culture, cells were stained with a viability dye, anti-CD8+, and pMHC KbTRP2 (cognate) or pMHC KbSIY (non-cognate) to

determine total (E) number and (F) of antigen-specific CD8+ T cells (error bars show s.e.m.; *p < 0.05, **p < 0.01, n = 4, Student's t test).

For these studies we enriched antigen-specific CD8+ T cells from the endogenous population representative of how one would approach clinical ACT. First, we expect our cell recoveries post-enrichment for high enriching aAPCs to be lower when starting with the same total number of CD8+ T cells pre-enrichment. Indeed, the overall number of recovered CD8+ T cells was consistent with previous enrichment experiments. The least amount of recovered cells was from the 300 nm aAPCs and the most from the 50 nm aAPCs (**Figure 4-15**).

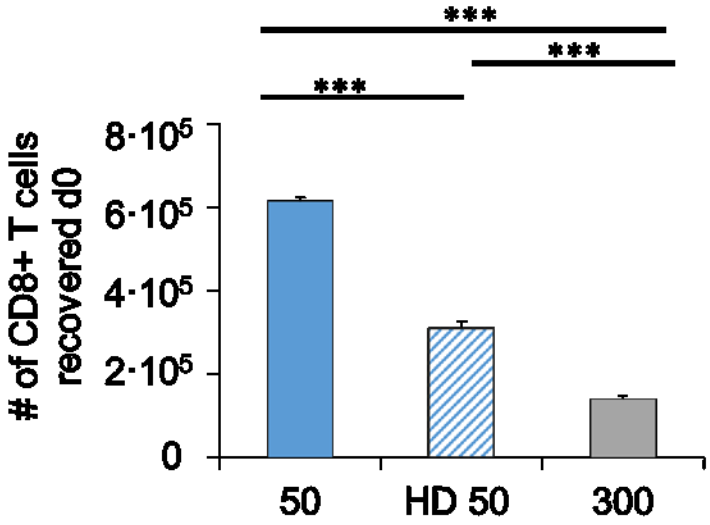

Figure 4-15: Day 0 cell counts from enrichment of endogenous CD8+ T cells mirrors enrichment trends from transgenic doped experiments. Particle aAPCs were incubated with CD8+ T cells (each beginning with 3x10^6 CD8+ T cells) and the enriched fraction was counted to determine the number of antigen-specific T cells (error bars show s.e.m.; ***p < 0.001, n = 3, one-way ANOVA with Tukey's post test).

We then cultured these enriched fractions for seven days to allow for stimulation and expansion. The process of enriching antigen-specific T cells should increase nutrient supply, stimulus to cell ratio, and room to expand *ex vivo*. Therefore, we expected that

increasing enrichment would also lead to an increase in total antigen-specific cell number on day 7.

On day 7, we stained the cells with anti-CD8 and pMHC KbSIY (cognate) and control KbSINF (noncognate) complexes (**Figure 4-14B**). The 300 nm aAPCs had significantly more antigen-specific cells than 50 nm aAPCs as expected, and more than the HD 50 nm while not statistically significant (**Figure 4-14C**). We also investigated whether antigen-specific CD8+ T cells generated from the enrichment and expansion process were functional by investigating cytokine and degranulation markers associated with enhanced killing.[39,41,435,436] We first investigated CD107a expression where this is a degranulation marker of lytic ability. Both 300 and HD 50 nm produced high percentages functional antigen-specific CD8+ T cells, where this resulted in 70% and 88% positive for CD107a (**Figure 4-16A**). Furthermore, upwards of 20% of antigen-specific CD8+ T cells were also positive for effector cytokine IFNγ—a marker of the functionality of killer cells (**Figure 4-16B**). Both readouts indicate robust expansion of functional antigen-specific CD8+ T cells. Frequencies of antigen-specific cells vary from 1-in-10^4 to 1-in-10^6; therefore, assuming the frequency to be between 0.0001–0.01%, the number of original antigen-specific cells was between 3 and 300. With the resultant number totaling close to $1.5x10^5$, this represents between a 450–45,000-fold expansion.

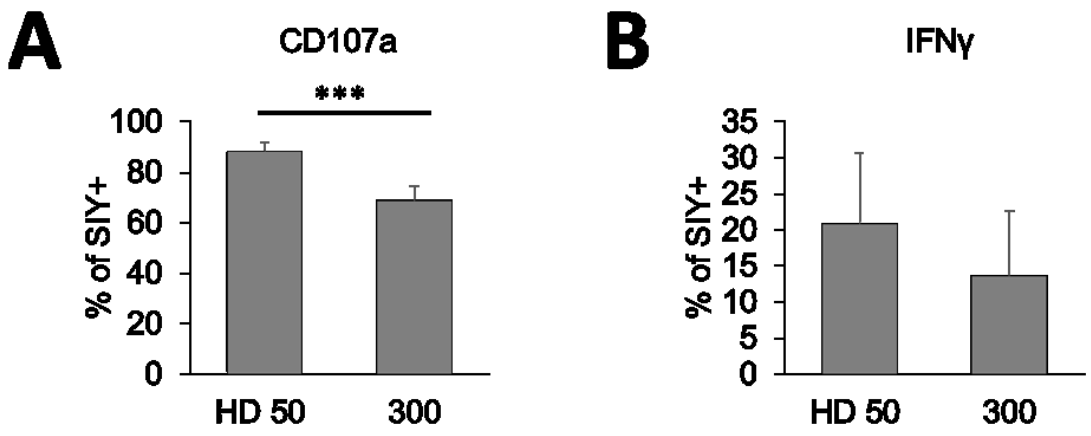

Figure 4-16: Antigen-specific CD8+ T cell resulting from 300 nm and HD 50 nm enrichment and expansions are functional. (A) Percent of antigen-specific SIY+ CD8+ T cells that are also positive for CD107a (B) IFNγ (error bars show s.d.; ***$p < 0.001$, $n = 6$, Student's T test).

To decouple how variables affect either enrichment or activation of rare-antigen specific cells we eliminated enrichment but still stimulated endogenous CD8+ T cells with HD 50 and 300 nm aAPCs. We see significant decreases in total cells generated by both the HD 50 nm and 300 nm aAPCs, indicating again the important role of enrichment (**Figure 4-17A–B**). HD 50 nm aAPCs demonstrated a greater reduction in antigen-specific cells, nearly 8-fold compared to only 5-fold reduction for the 300 nm aAPCs. This agrees with previous studies that demonstrated particles smaller than 300 nm are less effective at stimulating T cells, unless artificially clustered in a magnetic field.[7] Indeed, clustering HD 50 nm aAPCs in a magnetic field without enrichment increased the number of antigen-specific CD8+ T cells to be similar to activating with 300 nm aAPCs without any magnetic field (**Figure 4-17C–D**). Thus, during the enrichment process, the magnetic field may artificially cluster HD 50 nm aAPCs, allowing efficient activation closer to the 300 nm aAPCs.

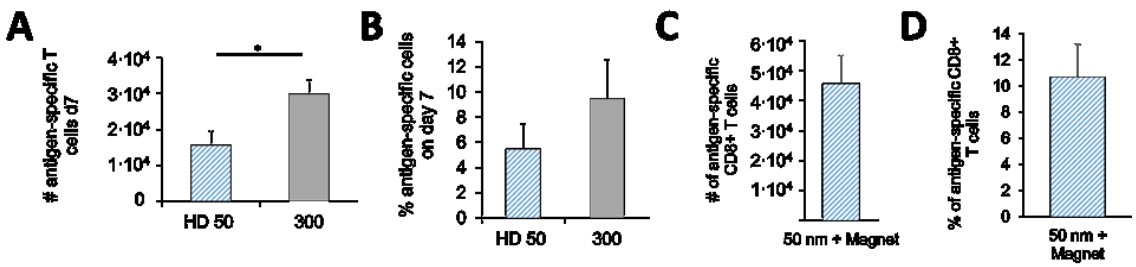

Figure 4-17: The importance of enrichment on antigen-specific T cell number and purity and understanding the impacts of magnetic clustering without enriching. (A) Number and (B) Percent of antigen-specific T cells for endogenous expansions without enrichment after 7 days of culture. Differences were significant from HD50 and 300 (error bars show s.e.m.; *$p < 0.05$, $n = 6–9$, Student's T test). (C–D) Culturing endogenous CD8+ T cells with HD 50 nm aAPCs in a magnetic field raises the antigen-specific T cells to similar levels of (C) number and (D) percent of 300 nm aAPCs cultured without a magnetic field (error bars show s.e.m. $n = 3$).

We also investigated if differences in particle endocytosis correlate with greater proliferation seen with 300 nm aAPCs. We studied this at saturating doses of aAPCs with cognate 2C CD8+ T cells across nanoparticle aAPC sizes. After 1 hour of cell incubation at 4 °C, particles were not internalized, but bound to the surface (**Figure 4-18**), which agreed with temperature-dependent receptor mediated endocytosis and our own previous studies.[103,244,250,437,438] After 3 and 18 hours of incubation at 37 °C, most particles dissociated from the cells (**Figure 4-19A**). More specifically, the percent of cognate CD8+ T cells bound to aAPCs decreased to below 20% for all conditions (**Figure 4-19B**). Of these aAPC-bound T cells, almost no uptake was observed with HD 50 nm aAPCs (**Figure 4-19C–E**). Greater uptake was observed in the 300 and 600 nm aAPCs, where the increased avidity of larger particles potentially enabled activation induced TCR-mediated endocytosis of particles,[439,440] albeit in only 5–10% of total antigen-specific cells (**Figure 4-19C–E**). Therefore, endocytosis likely contributes to further signaling in a subset of antigen-specific cells[441] and needs to be studied further for 300 nm aAPCs, but early cell-binding events appear to influence a greater proportion of antigen-specific cells.

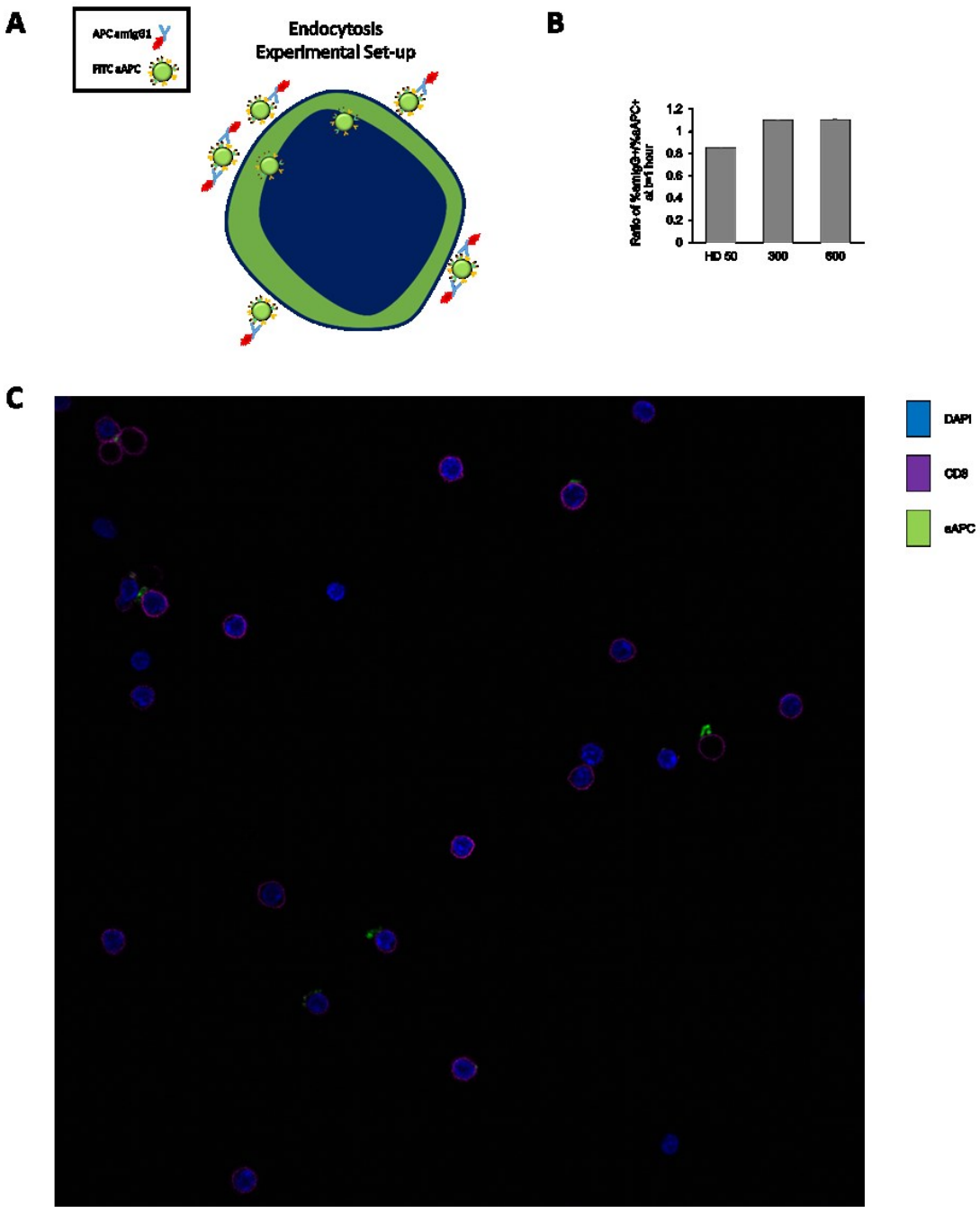

Figure 4-18: aAPCs primarily bind to the surface of cognate 2C CD8+ T cells after 1 hour binding at 4 °C. (A) Schematic of experimental set-up. aAPCs are fluorescently labeled with FITC, and then also stained with an anti-mouse IgG1 antibody to detect and discriminate extracellular aAPCs from intracellular aAPCs. (B) Ratio of percent of amIgG1+ CD8+ T cells over aAPC+ CD8+ T cells that have been incubate for 1 hour at 4 °C (error bars show s.e.m.; n=3). (C) Confocal microscopy image of 2C (CD8+ = magenta) T cells (DAPI=Blue) that have been incubated with HD 50 nm aAPCs (green) for 1 hour at 4 °C.

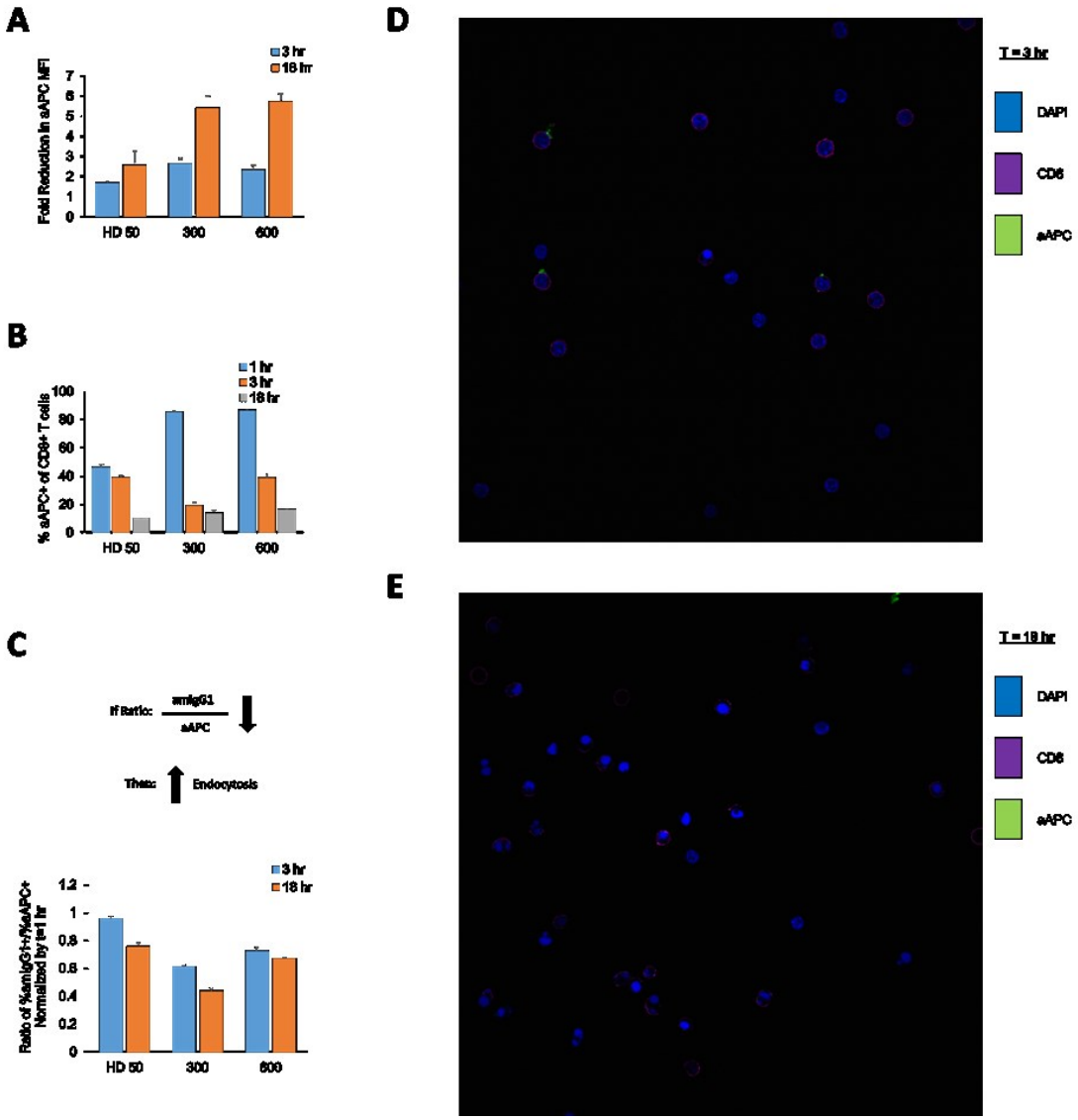

Figure 4-19: aAPCs dissociate from cognate aAPCs following incubation at 37 °C, with greater uptake observed for 300 nm and 600 nm aAPCs than HD 50 nm aAPCs. (A) Fold reduction of aAPC mean fluorescent intensity (MFI) associated with 2C CD8+ T cells after subsequent incubation for either 3 or 18 hours at 37 °C, normalized by MFI after 1 hour incubation at 4 °C (error bars show s.e.m.; n=3). (B) Percent of 2C CD8+ T cells bound to aAPCs after 1 hour incubation at 4 °C and subsequent incubations for either 3 or 18 hours at 37 °C (error bars show s.e.m.; n=3). (C) Ratio of percent of amIgG1+ CD8+ T cells over aAPC+ CD8+ T cells that have been incubate for 1 hour at 4 °C and subsequent incubations for either 3 or 18 hours at 37 °C normalized to initial ratios to account for any bead staining bias (error bars show s.e.m.; n=3). Values less than 1 indicate endocytosis with decreasing values indicating more endocytosis. (D–E) Confocal microscopy image of 2C (CD8+ = magenta) T cells (DAPI=Blue) that have been incubated with HD 50 nm aAPCs (green) for (D) 1 hour at 4 °C, then 3 hours at 37 °C and (E) 1 hour at 4 °C, then 18 hours at 37 °C indicate aAPC binding is restricted to the surface of the membrane and decreases association over time.

Finally, the degree of purity of antigen-specific CD8+ T cells is consistent with previous enrichment experiments with 300 nm aAPCs providing the highest percentage of

antigen-specific T cells (~65%) and the 50 nm aAPCs with the lowest (~15%) (**Figure 4-14D**). An increase in antigen-specific purity to nearly 65% is a major advancement for two major reasons. First, antigen-specific purity enables tumor-specific CD8+ T cells to propagate and fill the immunological space in a lymphodepleted patient, rather than non-specific CD8+ T cells. Second, the antigen-specific purity of a therapeutic product will limit off-target effects such as autoimmunity, where *ex vivo* stimulation could activate self-reactive T cells.

Even more dramatic increases in percentage (3-fold) and number (5-fold) of antigen-specific T cells were observed when targeting a shared tumor antigen TRP2 when 300 nm aAPCs were used and compared to HD 50 nm aAPCs (**Figure 4-14E–F**). Testing these sizes at another antigenic boundary condition validates our size and ligand-dependent findings that 300 nm aAPCs enrich and expand antigen-specific CD8+ T cells more effectively than smaller 50 nm aAPCs even with increased ligand density.

4.4. DISCUSSION

This acellular particle platform is an attractive approach because of its ability to be modular yet standardized across different patients. First, we do not need to produce and maintain variable and costly feeder cells for T cell expansions needed.[421,442] Second, this can be an off-the-shelf reagent that can be customized with any peptide sequence needed for patient specific responses. Third, the ability to use a magnetic field greatly enriches for antigen-specific cells and decreases nutrient competition and potential regulatory cells in culture. Fourth, with co-stimulation we can activate these cells to divide to create thousands of copies of themselves within short periods of time. Fifth, enrichment can increase the

purity of antigen-specific T cells in the final cell transfer product limiting the off-target side effects.

Beyond these benefits, the results described herein provide a path towards development of a higher throughput version of antigen identification and *in vivo* activation studies. Previously the enrichment and expansion process was developed with the 50 nm particle and required Miltenyi columns to enhance the magnetic field for enrichment.[254] However, with 300 nm particles, this enables the use of plate-based magnets, thus eliminating costly columns and enabling multiple enrichments to occur at the same time if done on 96-well plate magnets. The 300 nm particles are also still small enough to be injected *in vivo* as a therapy post enrichment or enrichment and expansion.[82] Since there is no commercially available aAPC, these benefits may enable transfer to other labs and adoption of these aAPCs both as a tool to isolate and study antigen-specific CD8+ T cells and as a therapy. Finally, we have previously observed enhanced stimulation from particles larger than 300 nm *in vitro,*[103] which could lead to enhanced *in vivo* activation of antigen-specific cells—potentially eliminating the *ex vivo* activation step after enrichment.

Cell modulation with particle platforms is becoming a more widely used tool to both study biological properties of cells and manipulate cell fate for cell therapy.[82,424] These studies continue to reveal the importance of heterogeneity in cell types and should drive particle design. Here we investigated how important particle parameters such as size, concentration, surface ligand density, and surface ligand choice affected enrichment of cells in a model system with CD8+ T cells for immunotherapeutic applications.

To achieve optimal magnetic enrichment of antigen-specific cells, particle parameters need to be balanced based on T cell biology. For particle size, the relationship

between the potential number of close-packed particles, individual and collective magnetic strength of particles, and local T cell ligand clustering need to be considered with an experimentally observed maximum for 300 nm sized particles. We further demonstrated that increasing ligand density can improve magnetic cellular enrichment, but this avidity also increases any non-specific existing interactions. These unwanted interactions can be limited by decreasing particle concentration or eliminating non-specific ligand on the surface of the particle. Finally, in combining enrichment with stimulation, we were able to achieve nearly 65% antigen-specific purity from an endogenous population of less than 0.01%, and nearly 5 times the number of antigen-specific cells from a shared tumor antigen.

For immunotherapeutic applications, many current forms of antigen-specific T cell identification are either costly or do not allow subsequent culture or manipulation of the cells.[443] On the other hand enriching antigen-specific T cells with superparamagnetic aAPCs could be more affordable, multiplexed, and allow subsequent culture—creating a new diagnostic tool and improving expansions of antigen-specific CD8+ T cells potentially to be used in antigen-specific therapies.

4.5. CONCLUSION

In conclusion, we have investigated unexplored biomaterial parameters of nanoparticle size, ligand density, particle concentration, and ligand choice in the enrichment of rare antigen-specific CD8+ T cells. Previous enrichment with aAPCs have been limited to 50 nm with a single ligand density. Quantitative control of parameters revealed that 300 nm aAPCs were most effective at both enriching and activating antigen-specific CD8+ T cells, shedding light on how particle design can be influenced and inspired

from T cell biology. This resulted in generating nearly 3-fold increase in the percentage and 5-fold in the number of antigen-specific CD8+ T cells for a shared tumor antigen. Ultimately, advancing the utility as a tool for identifying, characterizing, and utilizing antigen-specific immune responses, and offers a general case study in biomaterial nanoparticle property design to isolate rare cells.

Chapter 5. Increasing the Throughput and Adaptability of Nanoparticle Tools to Isolate and Identify Many Antigen-specific T cells

5.1 Introduction

T cells are critical immune cells which play roles in carrying out and bolstering immune responses against pathogens, self, allergens, and cancer[444]. They do so through recognizing target-specific peptide sequences presented in major histocompatibility complexes (MHC) with their unique T cell receptors (TCRs). Identifying and understanding which T cells are involved in immune responses can lead to targeted therapies. For example, once antigen-specific T cells are identifies in type 1 diabetes they could be targeted and eliminated[268,269,445]. Also, antigen-specific T cells are involved in recognizing and killing tumor and are at the forefront of many anti-cancer immunotherapies[444]. T cells can recognize over-expressed shared tumor antigens, or neoantigens which are the result of tumor-generated mutated proteins. Thus, once a target neoantigen can be identified a tumor vaccine, adoptive T cell transfer, or genetically modified T cells could be given for therapy[24,338,446].

Thus, there is great utility in identifying antigen-specific T cells to understand immune responses, disease, and potential therapies; however, identification is not so straightforward. Unique TCRs are generated through VDJ recombination with a possible 10^{14} unique TCRs [447], and the frequency of any one specific T cell is between 1 in 10^4 to 10^6 of T cells[416,427].

This diversity and frequency require conventional methods of cellular identification like flow or mass cytometry to be adapted[443]. Approaches to increase the sensitivity of staining reagents include multermerizing MHC onto platforms to increase avidity and sensitivity of staining reagents[448] and co-evaluation with staining intracellular cytokine production or phenotypic proteins[449–452]. Other techniques decrease background cells through magnetic enrichment by magnetic particles attached to peptide-loaded MHC (pMHC)[254,453,454]. However, these techniques also suffer from low throughput of the number of antigen-specific responses that can be identified at any given time. To improve throughput researchers have developed UV-cleavable peptides for more efficient peptide loading onto MHC tetramers[455] and combinatorial fluorescent labeling[456,457]. More recently, pMHC yeast displays have been developed but require downstream TCR sequencing for identification of reactive clones[458]. In summary, current techniques to identify antigen-specific T cells lack either sensitivity, throughput, or ease of use.

Here we build on previous techniques to enrich and expand rare antigen-specific T cells with peptide-loaded MHC (pMHC) and co-stimulatory molecules (such as anti-CD28)[250,254,459]. We increase the usability of this platform by eliminating costly cell isolation kits and show support from additional immune cells in antigen-specific T cell expansion. We adapt this technology platform to be higher throughput with capability to evaluate many antigen-specific T cells at once. To increase the sensitivity we also create a new detection magnetic particle which enables antigen-specific detection without expansion. Our work enables facile adoption of the technology by non-specialists and provides a high-throughput method for identification and analysis of antigen-specific T cell responses.

5.2 Results and Discussion

5.2.1 Enrichment and Expansion from Splenocytes

While the initial E+E protocol required a CD8+ isolation before incubating aAPCs with T cells[254], we wanted to attempt to increase the throughput and lower the cost of isolating and expanding antigen-specific T cells by enriching antigen-specific CD8+ T cells directly from splenocytes, bypassing a CD8+ isolation preparatory step (**Figure 5-1**a). We began by dividing harvested splenocytes in two, one population of which that went through a CD8+ isolation and the other that did not. We then enriched for KbSIY specific cells from both splenocytes and CD8+ T cells over a magnetic column, using the same number of particles for both conditions, and found that the E+E from splenocytes not only still worked but also dramatically improved the purity of the expanded population post-expansion (**Figure 5-1**b). Specifically, the percent and number of SIY-specific CD8+ T cells were doubled (**Figure 5-1**c) and tripled (**Figure 5-1**d), respectively, after seven days of expansion. We found similar results when expanding for self-antigen TRP2 (**Figure 5-2**). We then compared both the phenotype and function of antigen-specific cells from E+Es of the two different starting populations, finding that both populations post-expansion were predominantly effector memory (**Figure 5-1**e) and antigen-specific cells were similarly functional by intracellular cytokine stain in terms of degranulation marker CD107a and IL2 and TNFα production (**Figure 5-1**f).

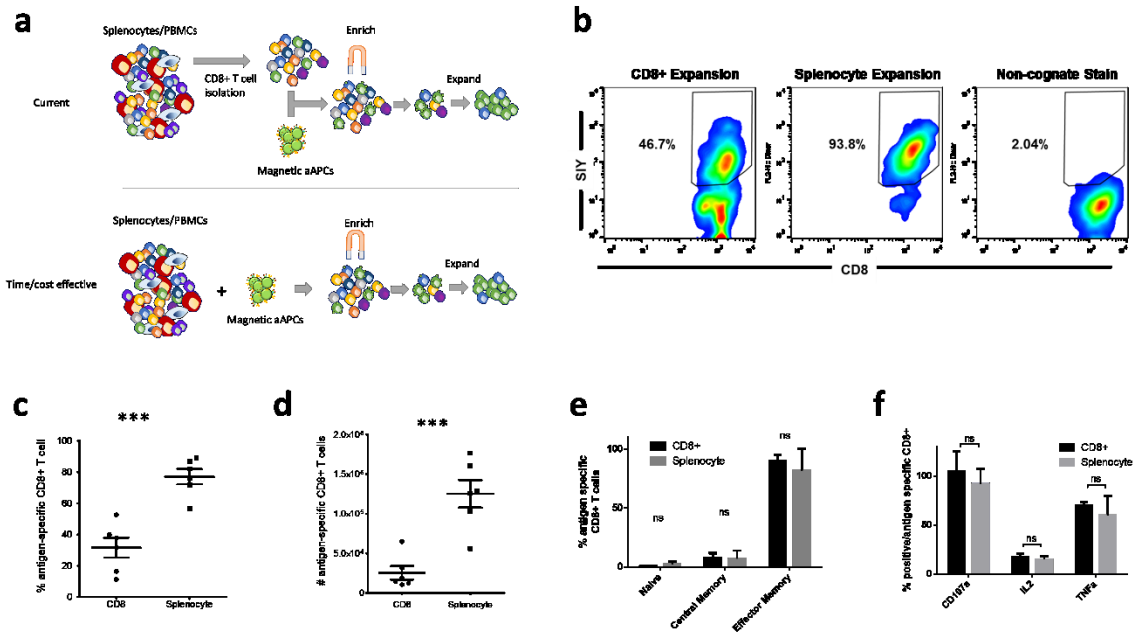

Figure 5-1: Decreasing the cost, time, and technical skill needed to isolate rare antigen-specific T cells and boosting activation with co-culture of non-CD8+ T cells. (a) Schematic of eliminating CD8+ T cell isolation from protocol for using aAPCs (artificial antigen-presenting cells) for enrichment and expansion of antigen-specific T cells. (b) Representative flow plot of CD8+ T cells 7 days post enrichment and expansion from CD8+ T cells vs. Splenocytes (c) Percent and (d) number of antigen-specific T cells resulting from aAPC enrichment and expansion two different starting populations of cells (CD8+ T cell purified, splenocytes) at day 7 (error bars show s.e.m.; $^{**}p < 0.01$, n = 6, Student's t-test, two-tailed). Enriching from splenocytes does not alter antigen-specific (e) phenotype or (f) cytokine production at day 7 (error bars show s.e.m.; ns $p>0.05$, n =3, one-way ANOVA with Tukey's post-test).

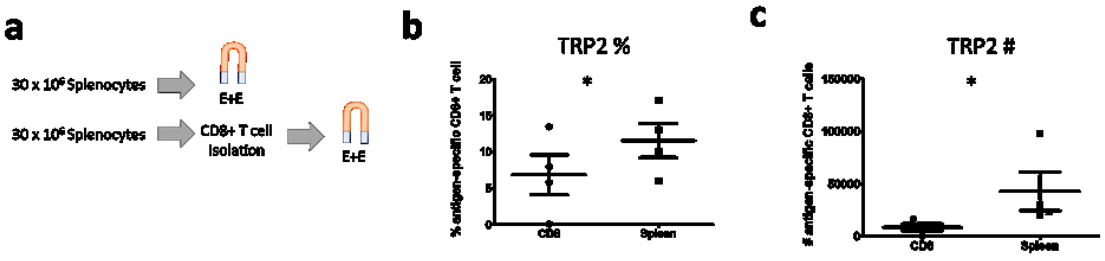

Figure 5-2: Enriching and expanding rare antigen-specific T cell populations directly from splenocytes and comparing to starting from purified CD8+ T cell populations. (a) Schematic of experimental set up for comparing different starting populations (splenocyte vs. purified CD8+ T cells). (b) Percent and (c) number of antigen-specific T cells (TRP2+) resulting from aAPC enrichment and expansion two different starting populations of cells (CD8+ T cell purified, splenocytes) at day 7 (error bars show s.e.m.; $^{*}p < 0.05$, n = 4, Student's t-test, two-tailed).

5.2.2 Understanding the Mechanism of Enhanced Output from Splenocyte 'E+E

After confirming that enrichment from splenocytes was not functionally altering the final cell population but was simply leading to a larger, purer antigen-specific population, we next began to probe how this occurred mechanistically. First we compared the efficiency of enrichment from both starting populations by doping CFSE labelled transgenic 2C or pmel CD8+ T cells into endogenous splenocytes, finding that there was no difference in terms of fold enrichment (**Figure 5-3**a) or percent cell recovery (**Figure 5-3**b) compared to CD8+ enrichments.

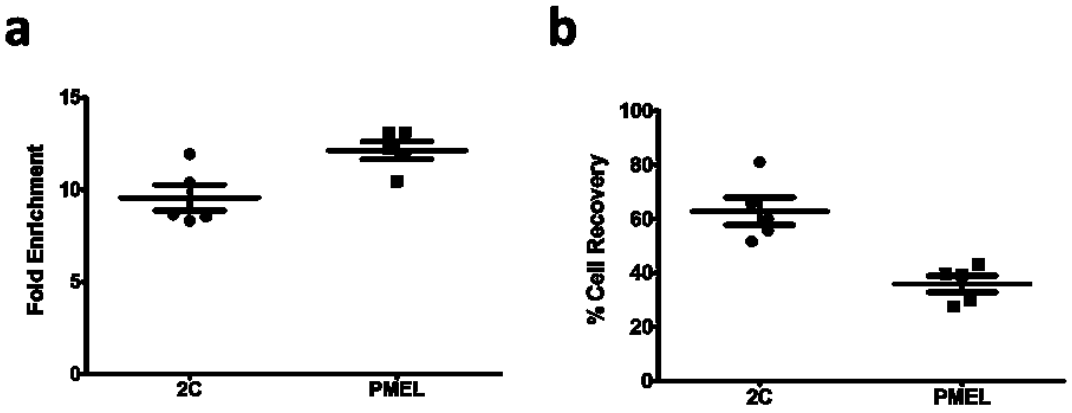

Figure 5-3: Enhancements in enrichment and expansion of antigen-specific CD8+ T cells from splenocyte starting populations do not come from increases in levels of fold enrichment or percent cell recovery of antigen-specific T cells on day 0. (a-b) Doping antigen-specific CD8+ T cells at (1:104) in endogenous splenocytes allow comparison of (a) fold enrichment and (b) percent cell recovery of 50 nm aAPCs that are not different from fold enrichment and cell recovery in CD8+ T cell populatinos (error bars show s.e.m., n=5).

We then investigated if splenocyte E+Es nonspecifically enriched non-CD8+ cell populations that could contribute to this enhanced expansion. First, we confirmed that our CD8+ isolation truly removed all other lymphocytes, macrophages, dendritic cells, and NK cells (**Figure 5-4**). Next, we compared cell composition-post enrichment on day

0 between splenocyte vs. CD8+ groups, finding that while enrichment from both populations was predominantly skewed towards CD8+ T cells, the splenocyte E+E starting population also included B cells (CD19+), NK cells (NK1.1+), CD4+ T cells, dendritic cells (CD11c+), and macrophages (F4/80+) (**Figure 5-5**a). Despite this relatively heterogeneous cell population on day 0, the splenocyte E+E converged to a relatively homogenous CD8+ population by day 7 (**Figure 5-5**b).

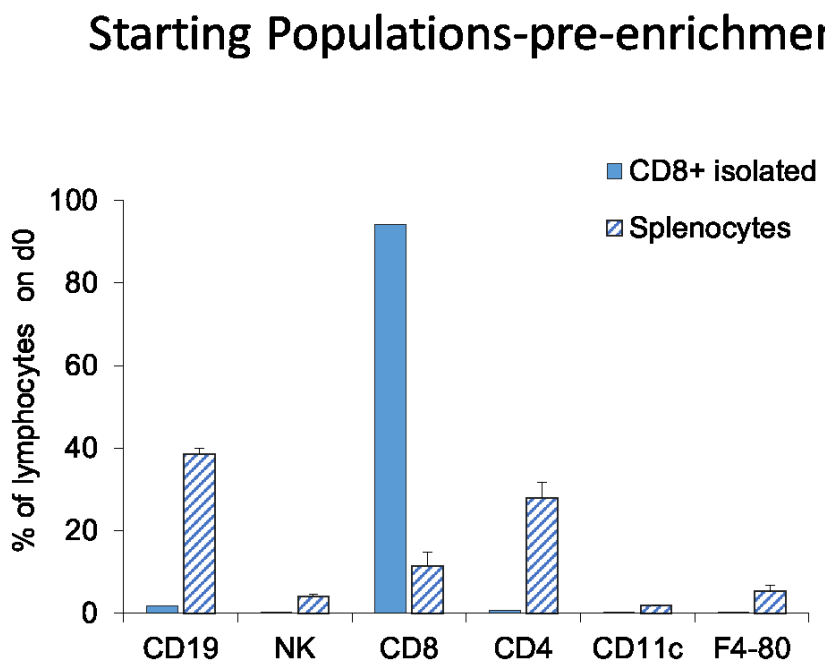

Figure 5-4: Percentage of different cell types from splenocytes and from CD8+ T cells purified with a no-touch CD8+ T cell isolation kit (n=1-2).

To confirm that these other cell populations were contributing to an enhanced output from our splenocyte E+E, we compared the percent (**Figure 5-6**a) and number (**Figure 5-5**c) of antigen-specific cells on day 7 if we added splenocytes to CD8+ T cells post-enrichment to dilute them back to their initial frequency, finding that doing so

significantly increased the number of antigen-specific cells. We then depleted various cell types pre-enrichment from splenocytes to determine which ones significantly impacted the output from the E+E, finding that depletion of dendritic cells (**Figure 5-7**a) and CD4+ T cells (**Figure 5-7**b) both significantly decreased the number of antigen-specific cells on day 7 (**Figure 5-5**d). As a potential mechanism of how non-CD8+ T cells were being enriched, we conducted enrichments from splenocytes using signal 1 only (s1) particles and co-clustering with signal 2 (s2) particles for expansion as previously described[250]. We found this approach did not significantly reduce the number of antigen-specific CD8+ T cells post-expansion compared to s12 particles (**Figure 5-5**e), although it did significantly reduce their frequency (**Figure 5-6**c) on day 7. Moreover, when examining the enriched populations from splenocytes using s12 vs. s1 particles, there were no significant differences between the two (**Figure 5-6**d), suggesting that the majority of nonspecific enrichment was occurring through other means.

Figure 5-5: Splenocyte E+E improves output through presence of specific subsets of non-CD8+ T cells (a) Cellular composition of post-enrichment fractions on (a) day 0 and (b) after 7 days of culture (error bars show s.e.m, n = 3). (c) Number of antigen-specific T cells resulting from aAPC enrichment and expansion of CD8+ T cells, splenocytes, or CD8+ T cells diluted to 10% post-enrichment with splenocytes (error bars show s.e.m.; **p<0.01, ***p<0.001)(d) Number of antigen-specific T cells resulting from aAPC enrichment and expansion from depletion experiments of splenocytes compared to CD8+ T cell purified (error bars show s.e.m.;*p< 0.05, ***p<0.001, n = 3–4, one-way ANOVA with Tukey's post test). (e) Number of antigen-specific T cells resulting from enrichment and expansion of splenocytes using S12 particles or from enrichment with S1 particles and expansion through co-clustering with S2 particles (f) Number of antigen-specific T cells resulting from aAPC enrichment and expansion of CD8+ T cells or CD8+ T cells mixed 1:1 with CD4+ T cells at day 7 (error bars show s.e.m.; ns p > 0.05, n = 4, Student's t-test, two-tailed). (g) Number of antigen-specific T cells resulting from aAPC enrichment and expansion from two different starting populations of cells (CD8+ T cell purified, Pan T cell purified) at day 7 (error bars show s.e.m.; **p < 0.01, n = 6, Student's t-test, two-tailed (h) Number of antigen-specific T cells from aAPC enrichment and expansion from CD8+ T cells or splenocytes with washed vs. unwashed particles (error bars show s.e.m.;**p< 0.01, n = 3, one-way ANOVA with Tukey's post test).

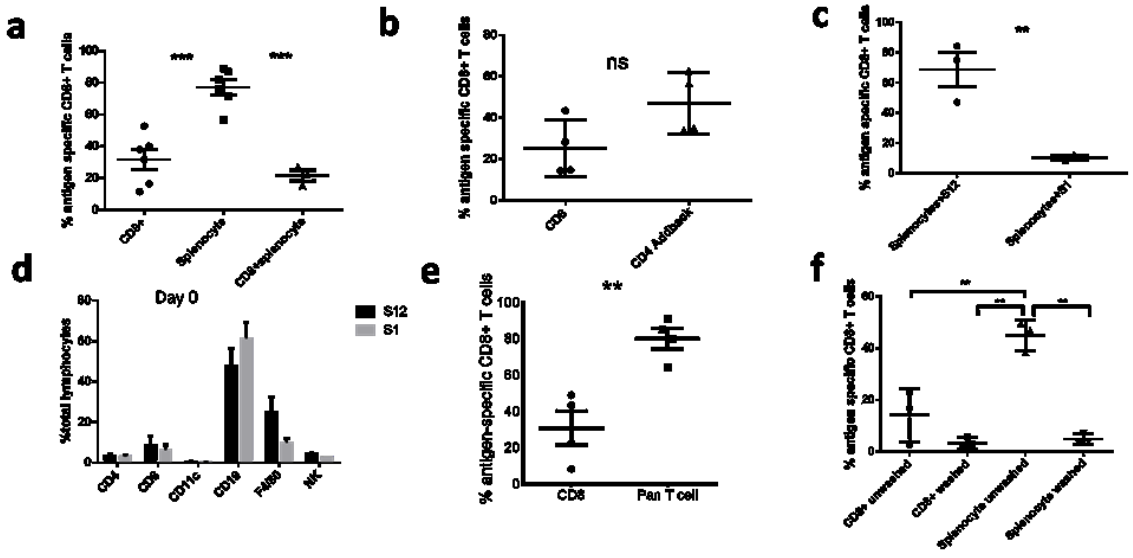

Figure 5-6: Splenocyte E+E improves output through presence of specific subsets of non-CD8+ T cells. (a) Percent of antigen-specific T cells resulting from aAPC enrichment and expansion of CD8+ T cells, splenocytes, or CD8+ T cells diluted to 10% post-enrichment with splenocytes (error bars show s.e.m.; ***p<0.001 Student's t test) (b) Percentage of antigen-specific T cells resulting from aAPC enrichment and expansion of CD8+ T cells or CD8+ T cells mixed 1:1 with CD4+ T cells at day 7 (error bars show s.e.m.; ns $p > 0.05$, $n = 4$, Student's t-test, two-tailed). (c) Percent of antigen-specific T cells resulting from enrichment and expansion of splenocytes using S12 particles or from enrichment with S1 particles and expansion through co-clustering with S2 particles (error bars show s.e.m.; **p<0.01, n= 3 Student's t-test) (a) Cellular composition of post-enrichment fractions on day 0 of S1 vs. S12 E+E (error bars show s.e.m, n = 2). (e) Percent of antigen-specific T cells resulting from aAPC enrichment and expansion from two different starting populations of cells (CD8+ T cell purified, Pan T cell purified) at day 7 (error bars show s.e.m.; **$p < 0.01$, $n = 6$, Student's t-test, two-tailed). (f) Percent of antigen-specific T cells from aAPC enrichment and expansion from CD8+ T cells or splenocytes with washed vs. unwashed particles (error bars show s.e.m.;**$p< 0.01$, $n = 3$, one-way ANOVA with Tukey's post test).

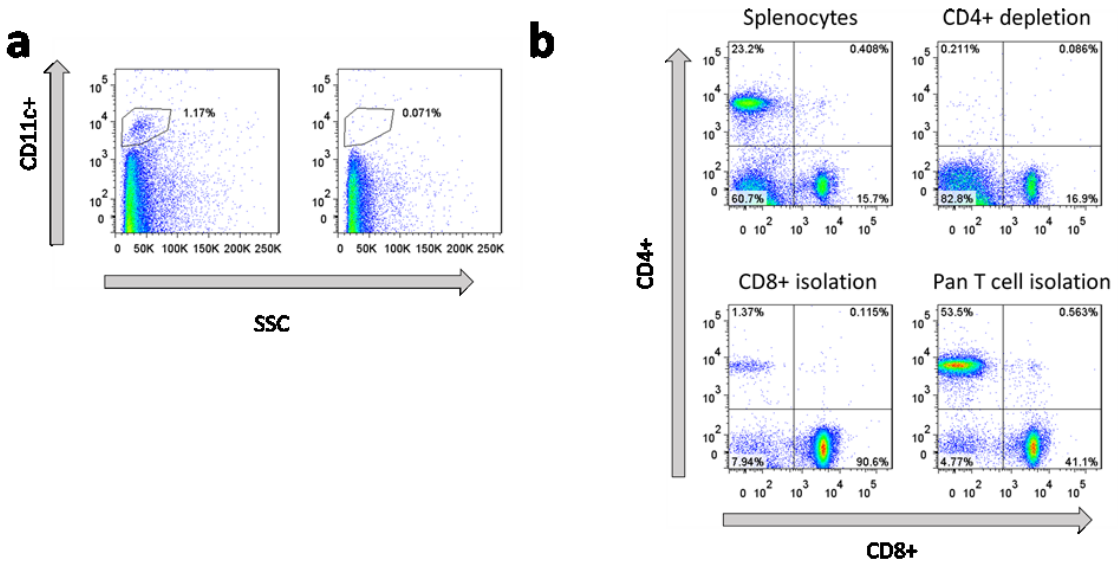

Figure 5-7: Understanding the contribution of other non-CD8+ T cells in enhancing antigen-specific CD8+ T cell activation through depleting populations pre-enrichment with aAPCs (a-b) Depletion of (a) CD11c+ cells and (b) comparison to splenocytes, Pan T cells, CD8+ isolation, and CD4+ depletion.

We then examined if CD4+ T cells alone were sufficient to improve the output from CD8+ E+Es, finding that mixing CD4+ T cells with CD8+ T cells 1:1 pre-enrichment slightly but not significantly improved the percentage (**Figure 5-6**b) and number (**Figure 5-5**f) of antigen specific T cells compared to CD8+ T cells alone, and along similar lines, beginning with the cell population that results from a Pan T cell isolation (**Figure 5-8** and **Figure 5-7**b) significantly boosts the number (**Figure 5-5**g) and frequency (**Figure 5-6**e) of antigen-specific T cells after a week. Finally, to further investigate the role of dendritic cells in the improved output, we tested the hypothesis that they could present peptide from aAPCs that had accumulated in solution over time by testing CD8+ and Splenocyte E+Es with the same number of aAPCs pre vs. post washing them over a magnetic column. We found that while washing aAPCs did not significantly alter the number (**Figure 5-5**h) or frequency (**Figure 5-6**f) of cells that resulted from CD8+ E+Es, they did dramatically reduce the output from splenocyte E+Es. Combined,

these mechanistic studies suggest that the enhanced output from splenocyte E+E can be attributed to both additional CD4+ help and other sources of antigen presentation beyond aAPCs alone.

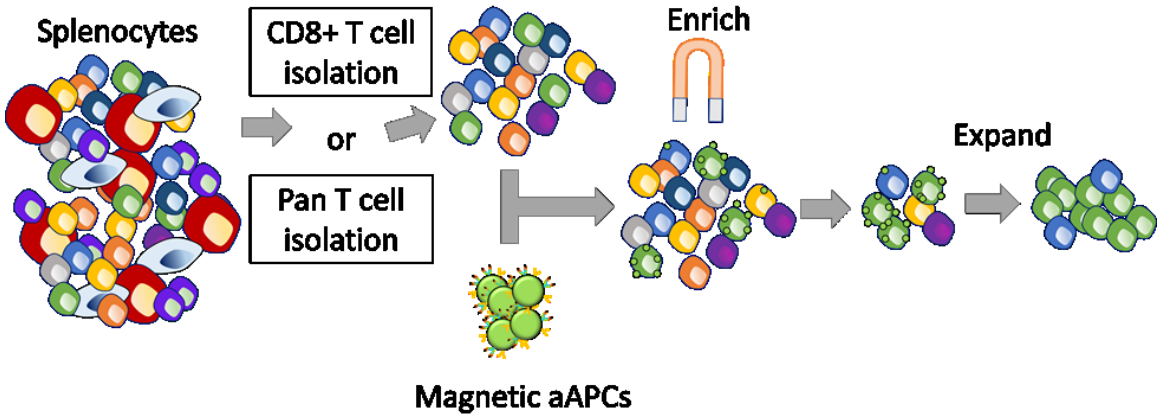

Figure 5-8: Schematic for comparing CD8+ T cell isolations and Pan T cell isolations in enriching and expanding antigen-specific T cells.

5.2.3 Increasing the Throughput of Enrichment and Expansion

Previous efforts for enrichment and expansion of antigen-specific T cells have included the use of 50-nm aAPCs[254], at which size require additional specially produced magnetic bead columns to produce magnetic fields strong enough to retain labeled cells. Here this limits the throughput and adaptability of the protocol. Previously, we have studied how the size of the aAPC impacts both T cell activation[103] and enrichment[459] and found that particles close to 300 nm were most efficient at activating and enriching antigen-specific T cells. These 300 nm aAPCs can be magnetically isolated with weaker magnetic fields and thus can be pulled by conventional neodymium magnets and thus adapted to a 96-well high-throughput set up (**Figure 5-9**a).

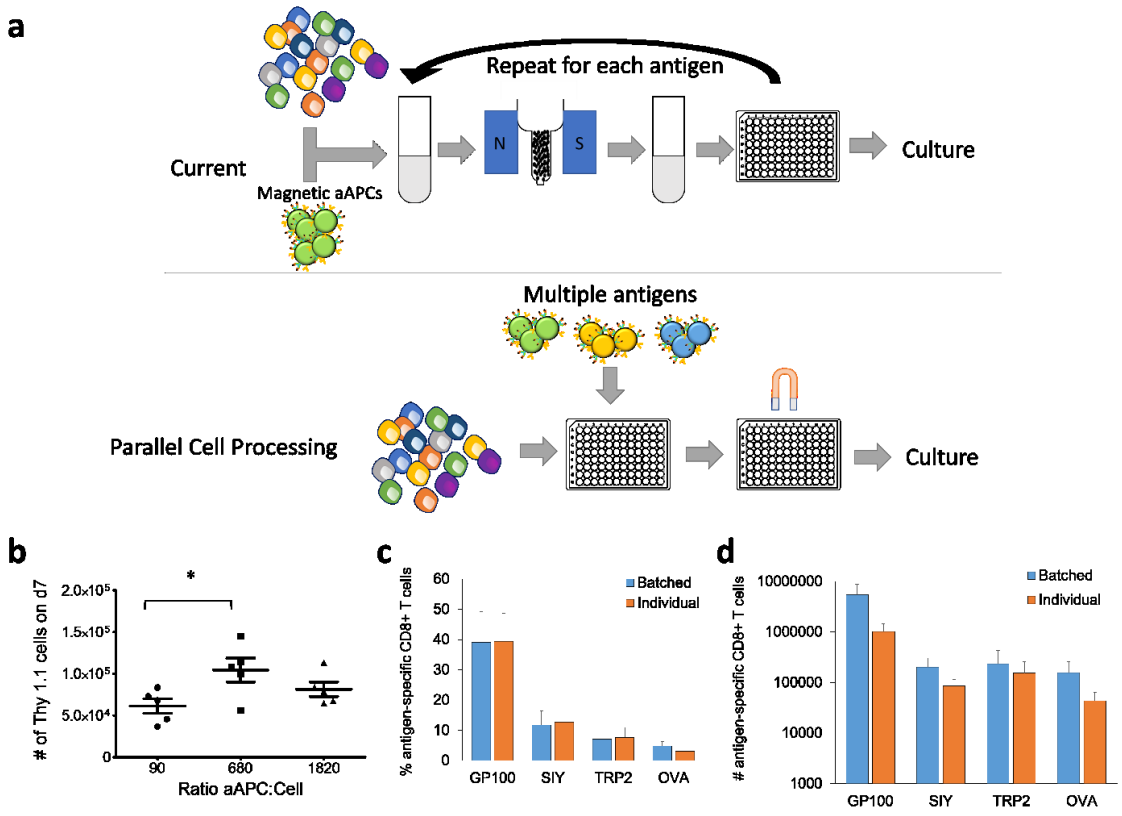

Figure 5-9: Increasing the throughput of enrichment and expansion of antigen-specific CD8+ T cells by increasing simultaneous parallel processing. (a) Schematic illustrating limitations of current approach to enrich rare cells by magnetic columns with 50-100 nm magnetic particles and increasing throughput by adapting a 96-well plate magnet approach with larger 300 nm magnetic particles. (b) By doping in Thy1.1+, transgenic PMEL CD8+ T cells into Thy1.2+ mice at a 1:1000 ratio, we determine effective aAPC:Cell ratios needed for the new enrichment and expansion protocol (error bars show s.e.m.;*$p< 0.05$, n = 5, one-way ANOVA with Tukey's post test). (c-d) Comparison of (c) percentages and (d) numbers of four different antigen-specific T cell populations and comparing having the aAPCs batched versus processing individually in parallel (error bars show s.e.m.; n = 7-14).

We have also found that particle concentration is a key factor affecting optimal enrichment and expansion of antigen-specific T cells[459]. Therefore, to screen particle concentrations in this 96 well format we doped transgenic pmel CD8+ T cells which recognize the gp100 peptide at a 1:10,000 ratio to background splenocytes. Though the 1820 aAPCs per cell ratio led to the highest fold enrichment and cell recovery on day 0 (**Figure 5-10**a,b), expansion after 7 days lessened differences between 680 and 1820

conditions with similar total antigen-specific T cells in culture (**Figure 5-9**b, **Figure 5-10**c). Additionally, using a magnet which pulled particle aAPCs into a ring around the outside (Ring magnet) instead of the bottom (Bottom magnet) substantially increased cellular enrichment and percent cell recovery in doped experiments (**Figure 5-11**). Thus, all other experiments were done with the 1820 aAPC to cell dose on the Ring magnet.

Figure 5-10: Establishing the proper dose of 300 nm aAPCs to use to enrich antigen-specific T cells. (a-b) Doping antigen-specific CD8+ T cells at (1:104) in endogenous splenocytes allow comparison of (a) fold enrichment and (b) percent cell recovery of 300 nm aAPCs at different ratios of aAPCs to cells (error bars show s.e.m.; *p < 0.05, **p<0.01, ***p<0.001, n = 5, one-way ANOVA with Tukey's post test). (c) Fold expansion of doped Thy1.1+ CD8+ T cells by day 7 after enrichment (day 0) and expansion (error bars show s.e.m.; n=5).

Figure 5-11: Comparing antigen-specific T cell enrichment from a 96-well plate magnet that either focuses magnetic particles to the bottom of the well (Bottom Magnet) or in a ring above the bottom of the well (Ring Magnet). (a-b) There is no difference in particle retention between bottom and ring magnets. Absorbance of particles that have been washed with a magnetic column three times (+) and compared to the original concentration of particles that have not been washed (-) at different stock concentrations of particles for both 96-well plate (a) bottom and (b) ring magnets. (c-d) Doping antigen-specific CD8+ T cells at (1:104) in endogenous splenocytes allow comparison of (c) fold enrichment and (d) percent cell recovery of 300 nm aAPCs on either bottom or ring magnets (error bars show s.e.m.; *$p < 0.05$, **$p<0.0001$, $n = 5$, Student's t-test, two-tailed).

Next we produced four individual, differentially antigen-loaded aAPCs (gp100, SIY, TRP2, OVA) and performed the enrichment and expansion process on an endogenous repertoire of T cells. We evaluated whether batching particle aAPCs or separating the cell sample into individual isolations would affect ability to enrich and expand antigen-specific T cells (**Figure 5-12**). Interestingly, both conditions produced similar percentages (**Figure 5-9**c) and slightly higher numbers of antigen-specific T cells (**Figure 5-9**d) suggesting that

either configuration could be used to identify antigen-specific T cells depending on the availability of sample or number of combinatorial staining reagents.

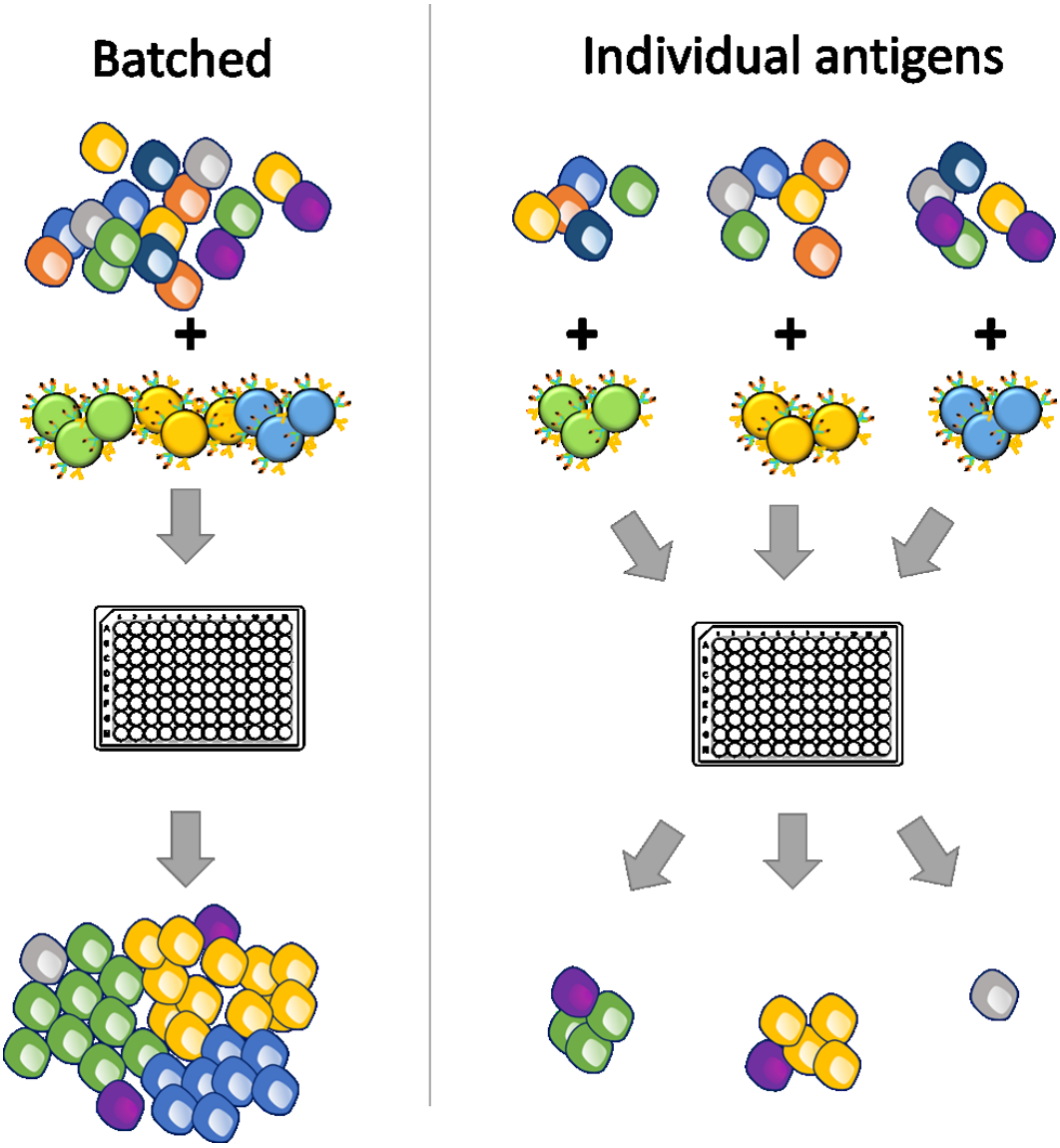

Figure 5-12: Schematic for comparing experimental set-up for comparing batched to individual antigen-specific CD8+ T cell enrichment and expansions.

5.2.4 Multiplexed Particle aAPC Production through Passive Loading

While the 96-well plate format provides a convenient, high-throughput approach to enrich antigen-specific T cells, creating individual, antigen-specific aAPCs is labor and reagent intensive. Previously, dimeric MHCs were loaded individually and then coupled to magnetic nanoparticles (Active Loading). Instead, now empty dimeric MHCs are conjugated directly to the magnetic nanoparticles creating a universal reagent, requiring only one particle synthesis and standardization amongst reagents (**Figure 5-13**a). These peptide-less aAPCs can be aliquoted into individual wells on 96 well-plates and be loaded efficiently through incubation with peptide (Passive Loading) for easily multiplexing the number of antigens that can be probed at once.

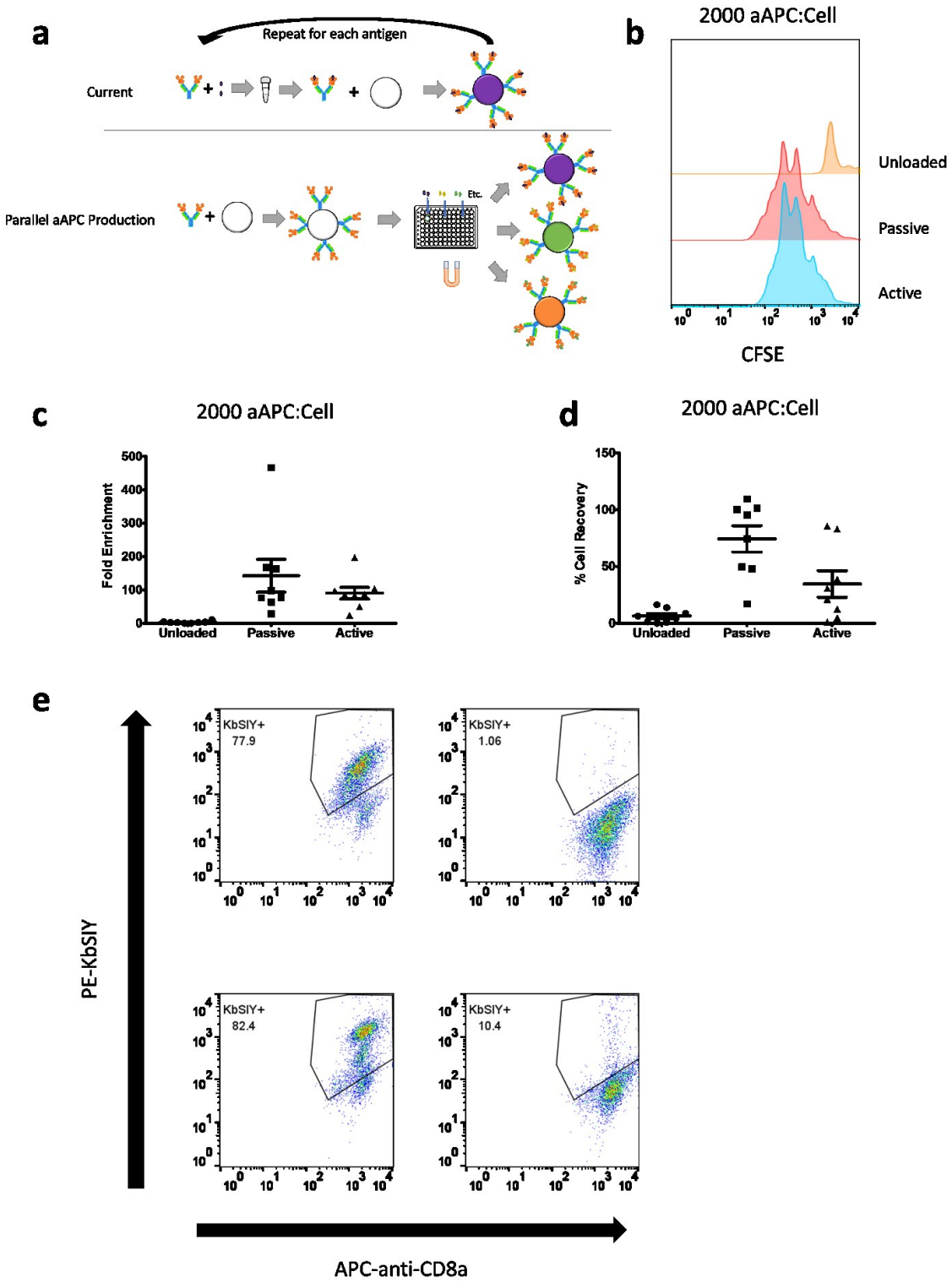

Figure 5-13: Increasing the throughput of enrichment and expansion of antigen-specific CD8+ T cells by parallel production of different particle aAPCs. (a) Schematic illustrating limitations of current approach to create individualized antigen-specific aAPCs and increasing throughput by creating universal aAPCs and then loading antigens post-conguation passively and using magnetic field to parallel processing. (b) CFSE

dye dilution demonstrates effective antigen-specific activation of passively loaded aAPCs as compared to actively loaded aAPCs. (c-d) Comparing the (c) fold enrichment and (d) percent cell recovery from unloaded, passive-loaded, and active loaded aAPCs in a doped Thy1.1+ system (error bars show s.e.m, n = 8). (e) Cognate and non-cognate staining of antigen-specific cells enriched and expanded for 7 days by passively-loaded aAPCs (two replicates shown).

To confirm that this universal stock approach to aAPC production produces similarly functional aAPCs we evaluated how well they stimulate antigen-specific T cells by incubating with pmel CD8+ T cells. Passive loaded aAPCs stimulated T cells just as well as active loaded aAPCs by CFSE analysis after 3 days of culture (**Figure 5-13**b, **Figure 5-14**a). In contrast, aAPCs that were not loaded (Unloaded) did not result in any background activation of the cells demonstrating both the specificity and efficiency of the peptide loading process. We used this assay to also determine appropriate amounts of peptide and incubation duration with aAPCs, where stimulation potential plateaued around 1 μg of peptide per 1.5 x 10^{10} aAPCs, and optimal time to incubate at this concentration was 1 hour (**Figure 5-14**b,c).

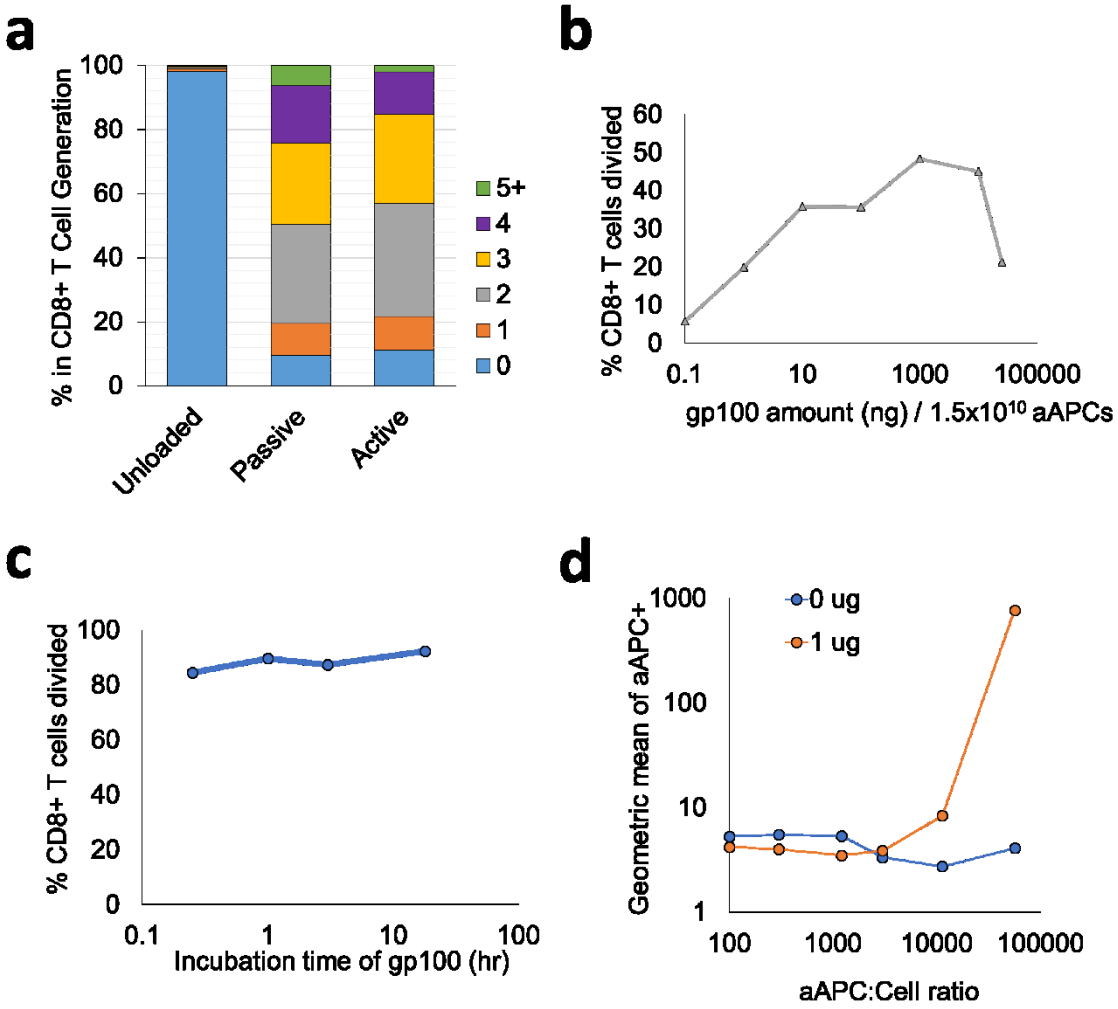

Figure 5-14: Passively loading 300 nm aAPCs with peptide post-conjugation result in antigen-specific binding and activation with similar efficacy to actively loaded aAPCs. (a-c) Quantification of CFSE dye dilution demonstrates (a) effective antigen-specific activation of passively loaded aAPCs as compared to actively loaded aAPCs, (b) amount of peptide and (d) time for incubation to be loaded for effective activation of antigen-specific T cells. (d) Mean fluorescent intensity of secondary antibody staining aAPCs that have attached to antigen-specific T cells comparing to unloaded (0 μg) aAPCs at various aAPC:T cell ratios.

In addition to how well the cells expand we tested the ability to bind and enrich antigen-specific T cells. Passively loaded aAPCs bound in a dose dependent manner to cognate T cells whereas there was little binding of similar doses of unloaded aAPCs (**Figure 5-14**d). In a doped enrichment experiment we observed similar to higher levels of

both fold enrichment (**Figure 5-13**c) and recovery (**Figure 5-13**d) of target cells with the passive loaded aAPCs compared to traditionally produced aAPCs, where unloaded aAPCs produced no antigen-specific enrichment. These results held true at both lower and higher aAPC to cell ratios (**Figure 5-15**). Thus, we tested the passive particles for enrichment and expansion of endogenous antigen-specific T cells and resulted in nearly 70-80% antigen-specific T cells by day 7 (**Figure 5-13**e). These results demonstrate effective enrichment and expansion by these universal particles and will provide a facile method for parallel production of many aAPCs simultaneously.

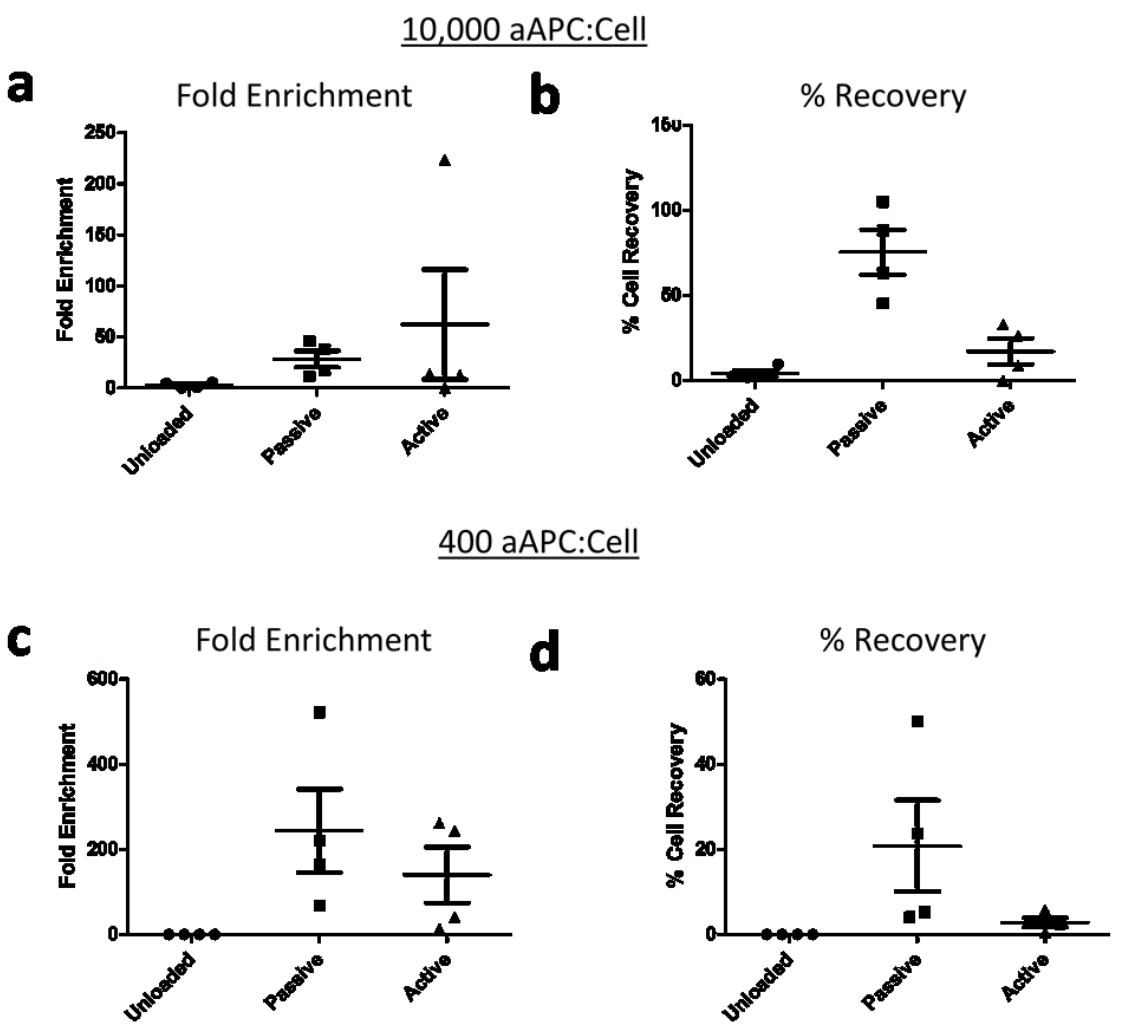

Figure 5-15: Passively loading 300 nm aAPCs with peptide post-conjugation result in effective antigen-specific enrichment with similar efficacy to actively loaded aAPCs at other doses. (a-d) Comparing the (a,c) fold enrichment and (b,d) percent cell recovery from unloaded, passive-loaded, and active loaded aAPCs in a doped Thy1.1+ system for (a-b) 10,000 and (c-d) 400 aAPC:Cell ratio (error bars show s.e.m, n = 4).

5.2.5 Development of Fluorescent Magnetic Beads for High-throughput Detection

With a multiplexed process for evaluating many antigen-specific T cells on the front-end, it is necessary to be able to also increase the throughput at the back-end of detection. The current method to produce detection pMHC complexes requires first

biotynylation of dimeric MHC and then loading with each individual antigen that must be washed away, which is labor intensive, costly, and results in losses of expensive MHC protein. Alternatively, we now produce another universal magnetic bead which we can attach the MHC to and then load efficiently with whatever peptide; however, this time the bead is also fluorescent (**Figure 5-16**a). This enables use of our previously established work from Figure 4 that passively loading peptides works well for antigen-specific binding and also that multivalent pMHC from a particle surface results in higher affinity interactions[459].

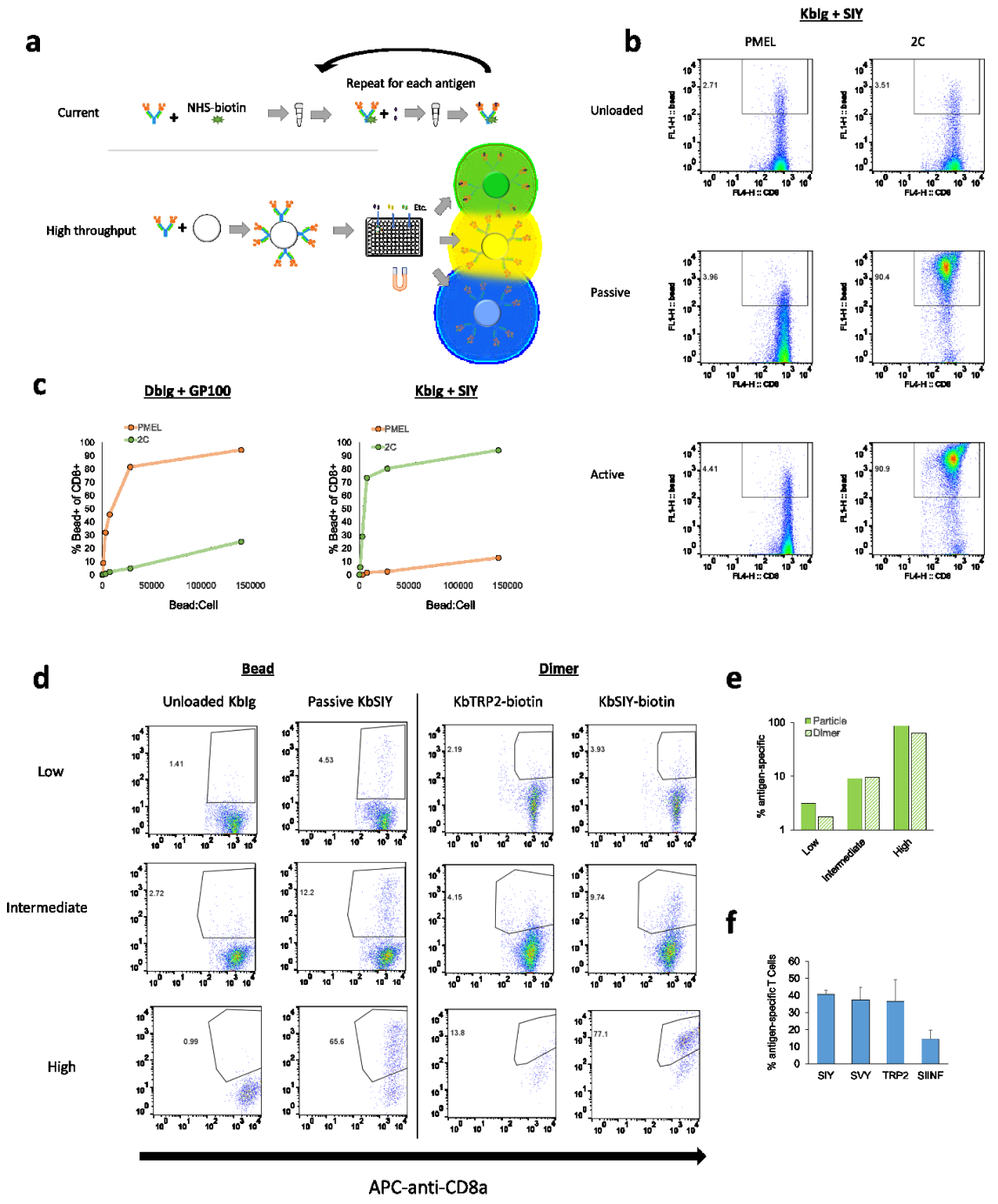

Figure 5-16: Increasing the throughput of enrichment and expansion of antigen-specific CD8+ T cells by parallel production of different particle detection particles. (a) Schematic illustrating limitations of current approach to create individualized detection dimers/tetramers and increasing throughput by creating universal detection fluorescent particles and then loading antigens post-conjugation passively and using magnetic field to parallel processing. (b) Both passive and active loaded fluorescent beads (KbIg loaded with SIY peptide) stain cognate antigen-specific transgenic 2C CD8+ T cells but not unloaded fluorescent detection beads (KbIg) with little background of non-cognate transgenic PMEL CD8+ T cells. (c) Level of background staining can be decreased by decreasing fluorescent bead dose for both DbIg and KbIg particles. (d,e) Fluorescent detection beads are at least as sensitive as current detection technology for antigen-specific T

cells at low, intermediate, and high frequencies at day 7 of the enrichment and expansion protocol. (f) Percent of antigen-specific CD8+ T cells enriched and expanded by passively-loaded aAPCs and detected on day 7 by fluorescent detection particles (n=4).

To create a fluorescent detection bead, we conjugated both unloaded and previously loaded dimeric-MHC to the surface of magnetic beads from several different bead types (Micromod, Spherotech, and Bangs). To test whether these magnetic fluorescent detection beads would work to stain antigen-specific T cells, we began by testing transgenic staining of either pmel CD8+ T cells (Dbgp100) or 2C CD8+ T cells (KbSIY). All conjugated beads stained antigen-specific T cells efficiently with low background binding to non-cognate cells and little to no binding of unloaded beads (**Figure 5-17**). Comparing across bead groups, Micromod most efficiently stained the highest percentage above background (~90%) and also the highest mean fluorescent intensity (MFI~1200) compared to Spherotech (70%, 600) and Bangs (60%, 400). For these reasons we moved forward with optimizing the Micromod magnetic fluorescent bead for detection. As both active and passive loaded fluorescent beads bound antigen-specific CD8+ T cells very efficiently with little background binding of unloaded fluorescent beads (**Figure 5-16**b), we further reduced the background by decreasing the bead to cell ratio (**Figure 5-16**c, **Figure 5-18**a). These results were also replicated when starting from a mixed population of immune cells and stained antigen-specific CD8+ T cells but not CD8- cells, demonstrating their specificity (**Figure 5-18**b,c).

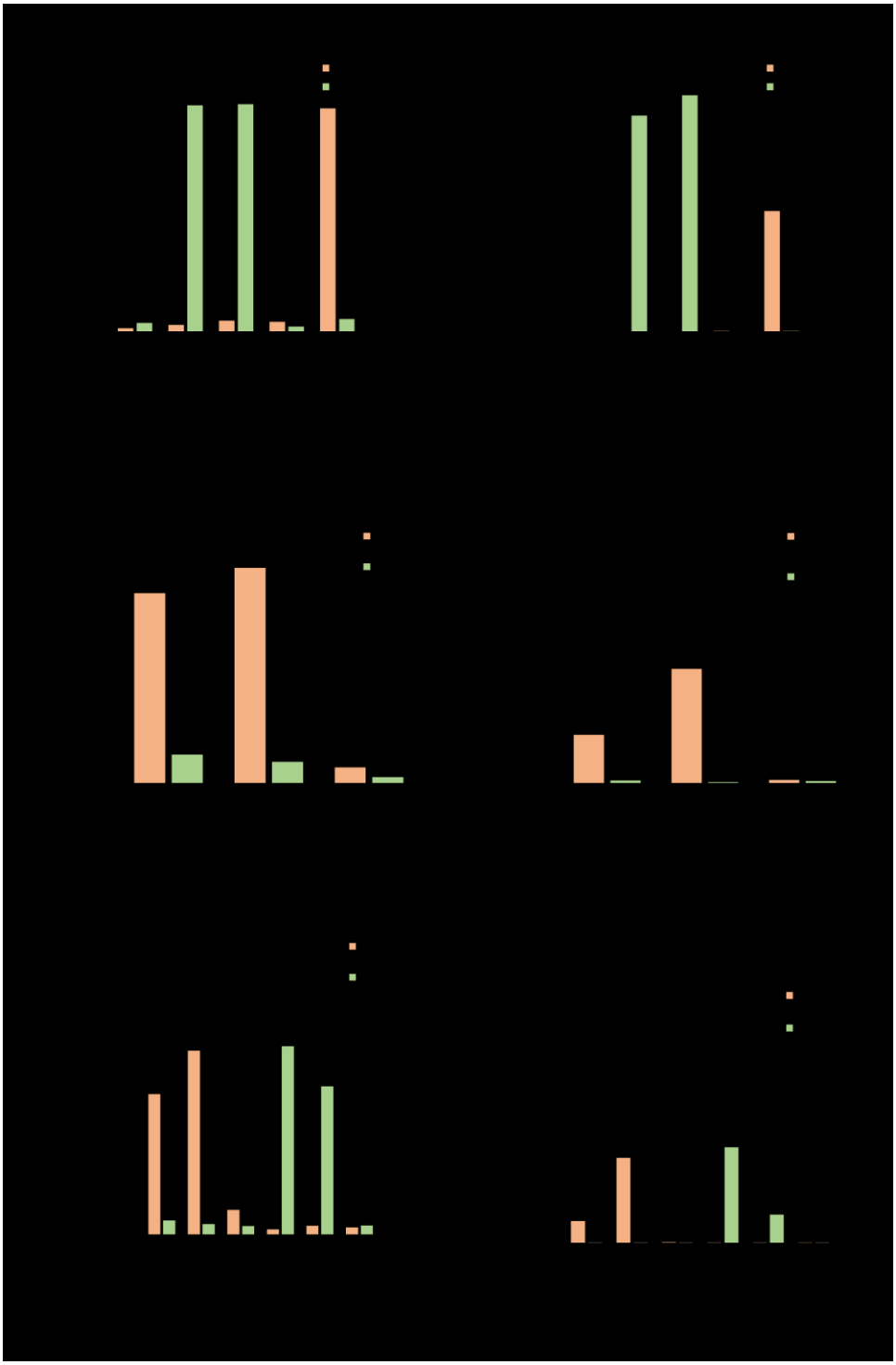

Figure 5-17: Fluorescent detection particles are specific to antigen-specific CD8+ T cells with low background binding. (a-f) quantification of (a,c,e) percent and (b,d,f) MFI of CD8+ T cells positive for fluorescent detection particles (unloaded, passive-loaded, and active loaded) for (a,b) Micrmod particles, (c,d) Spherotech particles, and (e,f) Bangs Labratories particles.

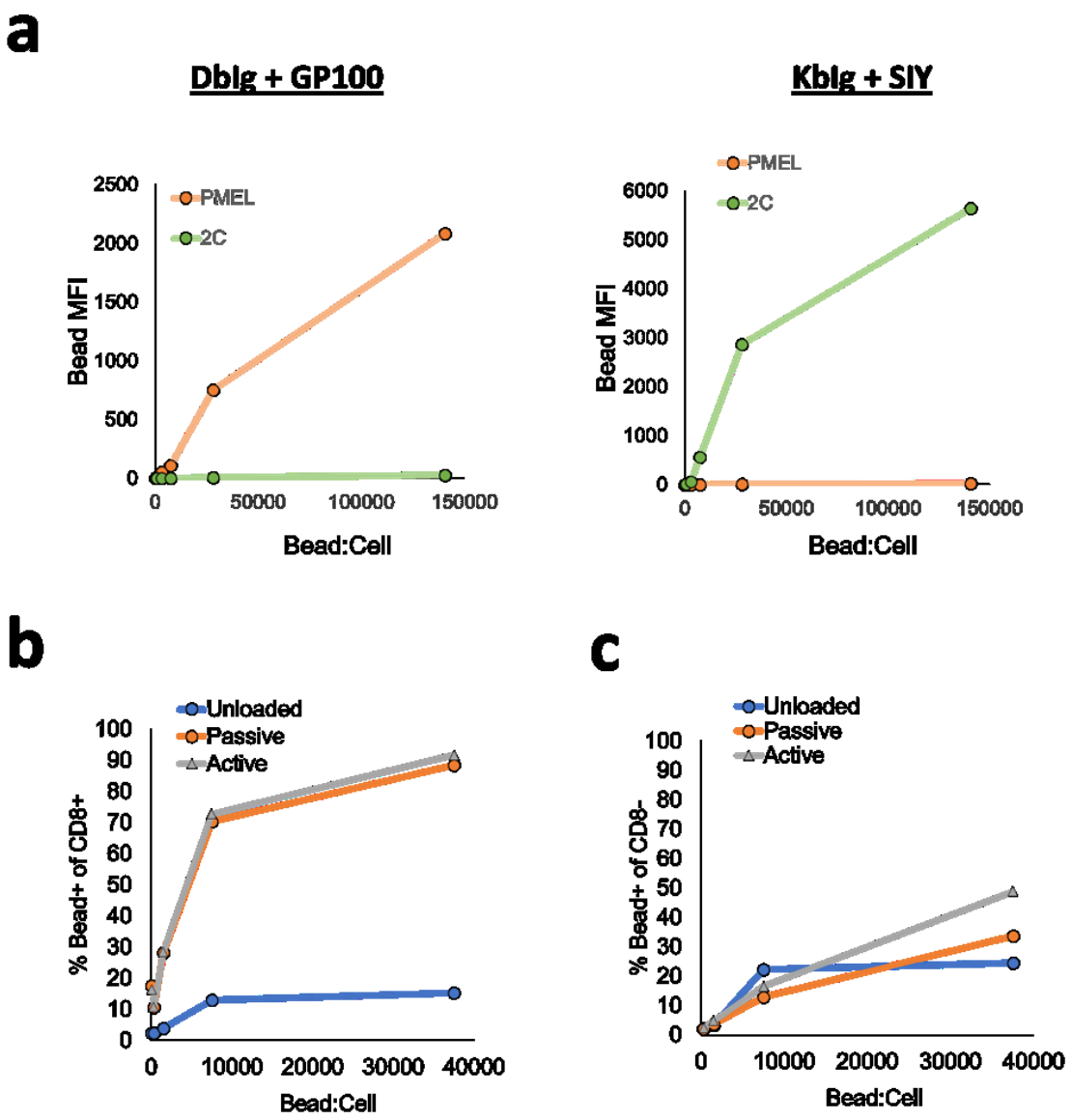

Figure 5-18: Fluorescent detection particles are specific to antigen-specific CD8+ T cells with decreasing background binding at lower concentrations of particles. (a) MFI of antigen-specific staining with particles where level of background staining can be decreased by decreasing fluorescent particle dose for both DbIg and KbIg particles. (b-c) Similar staining with fluorescent particles is observed for staining antigen-specific CD8+ T cells from a starting population of splenocytes. (b) Gated on CD8+. (c) Gated on CD8- of the same samples.

We then used these fluorescent detection beads at the back-end of our process to detect antigen-specific T cells at low, intermediate, and high antigen-specific frequencies. Comparing to our traditional biotinylated dimeric pMHC (Dimer), the fluorescent

detection beads are very efficient at detecting antigen-specific T cells with relatively low background (**Figure 5-16**d,e). Optimal fluorescent bead dose was found to be 3,000 bead to cell ratio for each of the end antigen-specific frequencies (**Figure 5-19**, **Figure 5-20**, **Figure 5-21**). With the established staining protocol we coupled our front-end optimized, high-throughput aAPC for enrichment and expansion and then detected on day 7 with our magnetic, fluorescent detection beads to successfully detect four antigens simultaneously and to percentages between 10 and 40% (**Figure 5-16**f, **Figure 5-22**).

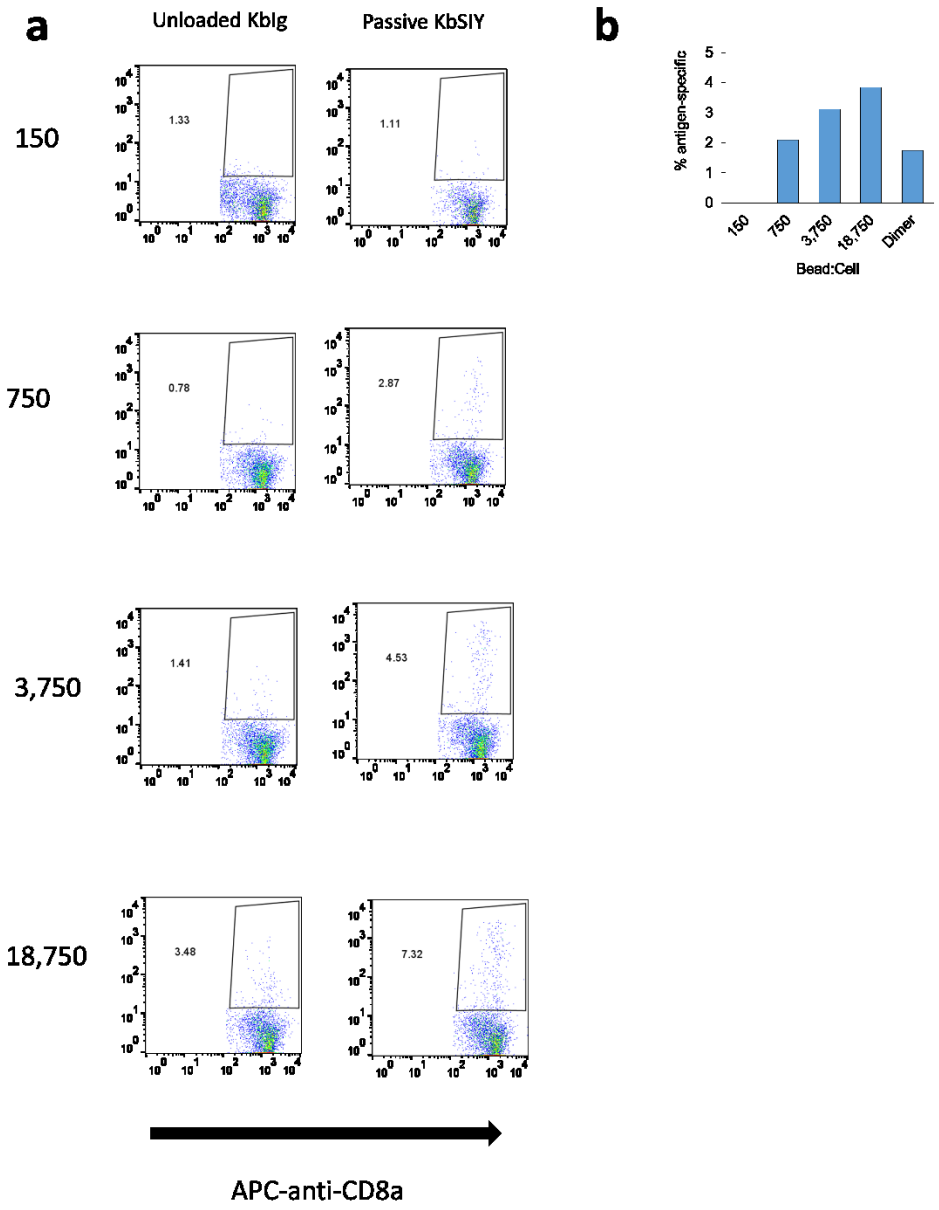

Figure 5-19: Titration of detection bead:cell ratios to evaluate optimal staining concentration for staining antigen-specific T cells on day 7 of the enrichment and expansion protocol with a low final percentage of antigen-specific T cells. (a) Flow cytometry plots of both passively loaded detection particles and unloaded detection particles. (b) Percentage of control staining (unloaded/non-cognate) were subtracted to evaluate final percentage of antigen-specific T cells on day 7 and compare to traditional biotynlated dimer staining reagents.

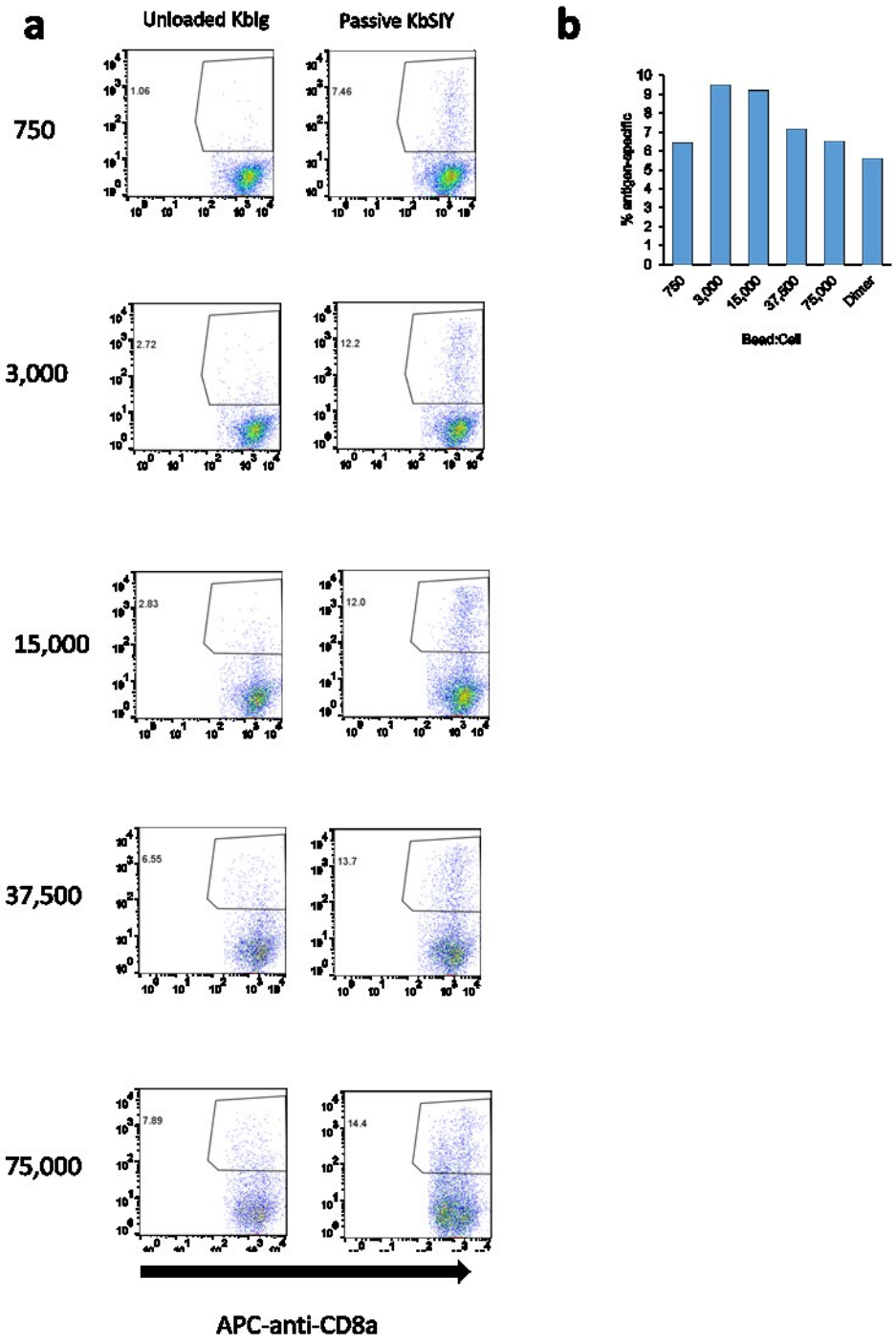

Figure 5-20: Titration of detection bead:cell ratios to evaluate optimal staining concentration for staining antigen-specific T cells on day 7 of the enrichment and expansion protocol with a intermediate final percentage of antigen-specific T cells. (a) Flow cytometry plots of both passively loaded detection particles and unloaded detection particles. (b) Percentage of control staining (unloaded/non-cognate) were subtracted to evaluate final percentage of antigen-specific T cells on day 7 and compare to traditional biotynlated dimer staining reagents.

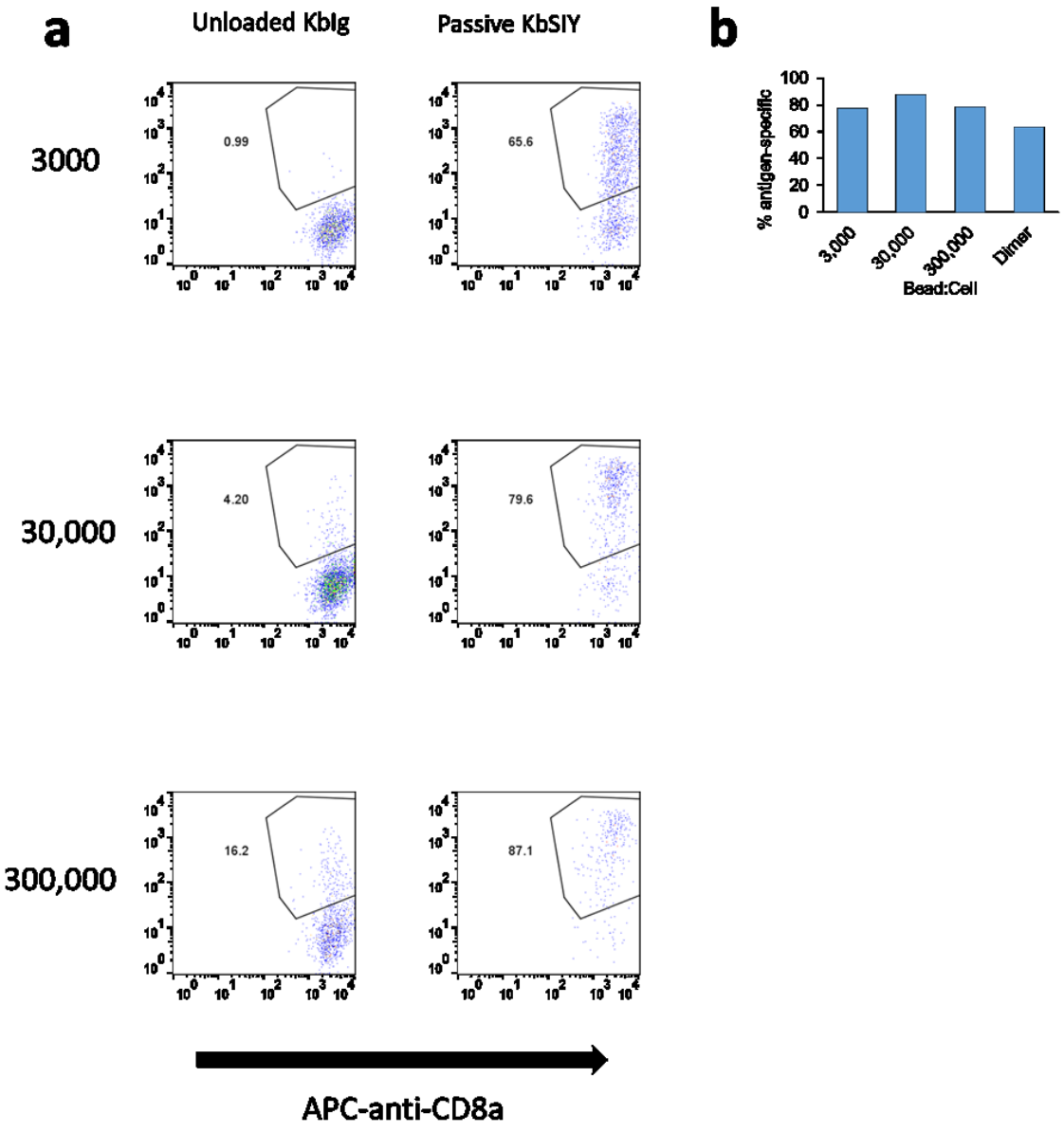

Figure 5-21: Titration of detection bead:cell ratios to evaluate optimal staining concentration for staining antigen-specific T cells on day 7 of the enrichment and expansion protocol with a high final percentage of antigen-specific T cells. (a) Flow cytometry plots of both passively loaded detection particles and unloaded detection particles. (b) Percentage of control staining (unloaded/non-cognate) were subtracted to evaluate final percentage of antigen-specific T cells on day 7 and compare to traditional biotynlated dimer staining reagents.

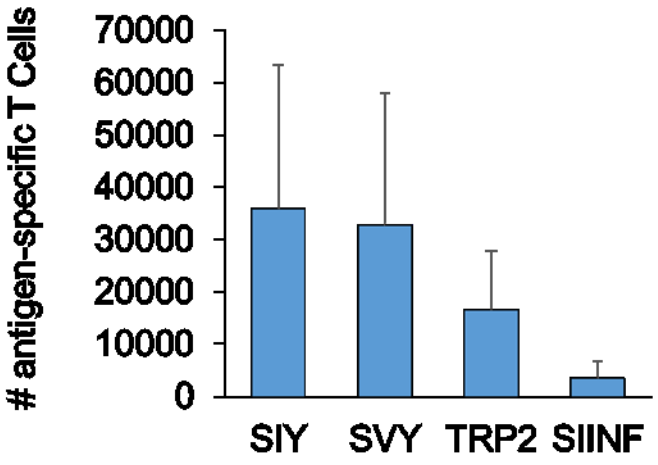

Figure 5-22: Average numbers of antigen-specific T cells after enrichment and expansion by passively-loaded aAPCs and detected on day 7 by fluorescent detection particles (n=4).

5.2.6 Day 0 Enrichment and Application of High-throughput Platform and Process to Human Antigen-specific T cells

Because these beads are also magnetic we hypothesized that we should be able to both enrich and detect at day 0 and potentially eliminate the need for the seven day culture period to expand the antigen-specific T cells to higher percentages. Starting from a 0.1% antigen-specific frequency (transgenic pmel cells), we significantly enriched populations nearly 70-fold at optimal bead to cell ratios, increasing to nearly 7% antigen-specific T cells (**Figure 5-23**, **Figure 5-24**a,b). Examining the doped antigen-specific T cells, nearly all (98%) of the cells stained positive with the fluorescent detection beads (**Figure 5-24**c); however, there was significant background binding as well where only close to 30% of the bead positive cells were antigen-specific.

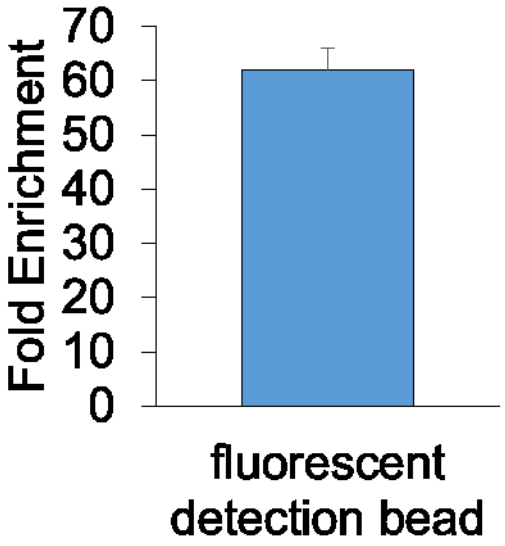

Figure 5-23: Fold enrichment of antigen-specific T cells with fluorescent magnetic beads.

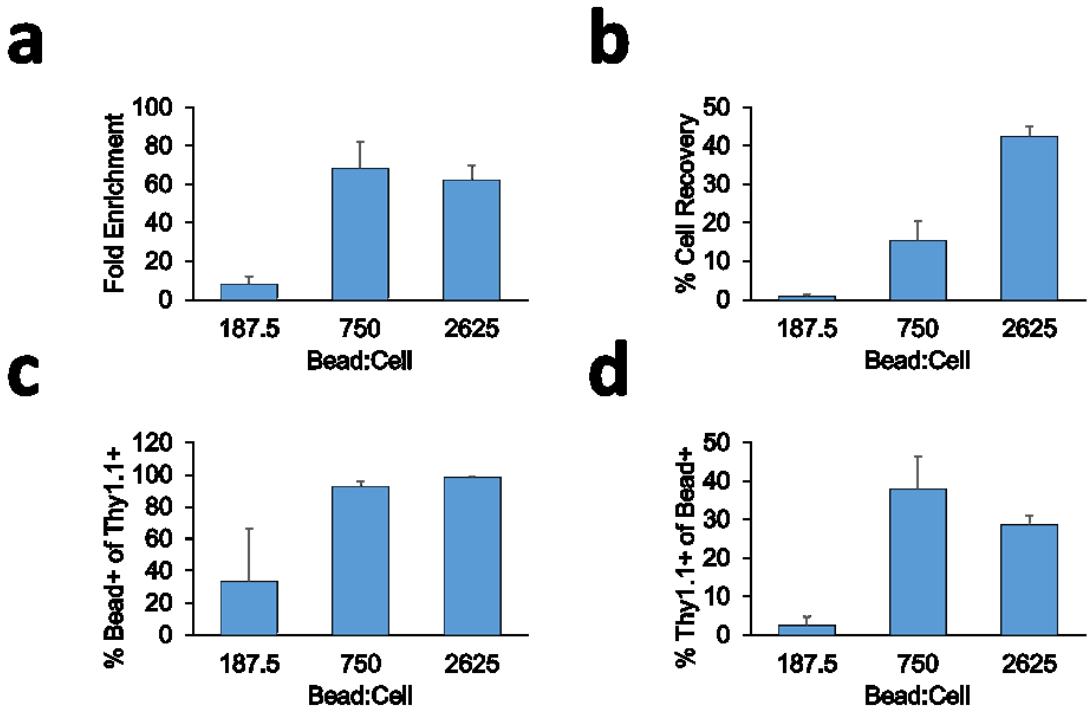

Figure 5-24: Titration of magnetic, fluorescent detection bead:cell ratios to evaluate optimal enrichment and expansion of doped pmel CD8+ T cells. (a) Fold enrichment and (b) percent cell recovery of antigen specific T cells post enrichment as analyzed by flow cytometry. (c) Percent of Thy1.1+ (pmel CD8+) that also stained positive with fluorescent detection beads. (d) Percent of bead+ that also stained positive with Thy1.1+ (pmel CD8+) (n=3, error bars denote s.e.m.).

5.3 Conclusion

Herein we have engineered a system and a magnetic nanoparticle technology to substantially improve detection of antigen-specific T cells and extend the throughput and adaptability of the process. First, we eliminated the need to enrich and expand antigen-specific T cells from purified CD8+ T cell populations. This decreased total cost and time to perform the assay, and also resulted in drastic increases in both numbers and percentages of antigen-specific CD8+ T cells resulting from beneficial interactions with CD4+ T cells increasing the sensitivity of the assay. Second, we modified the size of the particle aAPC to 300 nm based on previous work where we showed this was most effective in both enriching and expanding antigen-specific T cells[103,454]. Because of the increase in particle size we were able to use a conventional neodymium magnet and adapt the process of enrichment and expansion to a 96-well plate where multiple antigen-specific T cell responses can be processed in parallel. Third, to further increase multiplexing we created a universal aAPC where the MHC-Ig is conjugated to the surface of the particle and subsequently can be divided and loaded with any desired peptide sequence. Fourth, with an increased throughput and capability to multiplex, we also multiplexed our detection of antigen-specific T cell responses through creation of a universal fluorescent magnetic bead that can be loaded with any peptide to facilitate efficient and easy antigen-specific staining.

These engineered technologies and streamlined process for enrichment and expansion of antigen-specific T cells overcome critical difficulties in processing and identifying antigen-specific T cells. This enables researchers to easily adopt both the technology and process to study unprecedented number of antigen-specific T cell responses in infectious

disease, autoimmunity, allergy, and cancer. In particular, the ability to investigate multiple candidate antigen-specific T cells will be beneficial to cancer immunotherapy for neoantigen targeted therapy. Neoantigens are a result of mutated proteins from the tumor that the immune system has not been tolerized to; thus, represent unique and specific immune cell targets to the tumor[24,338]. Previous efforts to target neoantigens in therapy has led to dramatic clinical results in both adoptive immunotherapy and tumor vaccines[460,461]. However, neoantigen-specific therapies have been limited because of challenges in identifying antigen-specific T cell responses. With 100's to 1,000's of potential antigen candidates for each patient, current techniques can only examine a few antigen-specific responses at once and thus rely heavily on prediction algorithms and are labor intensive. Our technique overcomes many of these challenges and thus is poised to be used to identify neoantigen-specific cells and understand these responses to better use as a therapy. In conclusion, our method for identifying antigen-specific T cells will extend our ability to enrich, expand, and detect rare antigen-specific T cells enabling further understanding of the adaptive immune response.

Chapter 6. Engineering an Artificial T-Cell Stimulating Matrix for Immunotherapy

6.1 Introduction

T lymphocytes are increasingly targeted and utilized in immunotherapies with the success of checkpoint blockade, adoptive cell transfer (ACT), and chimeric antigen receptor (CAR) T-cell therapy[444]. For both ACT and CAR T cell therapies, T cells must be removed from patients, cultured and stimulated *ex vivo,* and then reinjected into patients for cancer immunotherapy[390]. This presents two major challenges. First, the number of T cells needed is very large, so they are cultured for 6-8 weeks at a time, by which time the cells' functionality and phenotype to mediate effective killing and long-term memory may have been lost or altered[37,442,462,463]. By improving the quality or phenotype and functionality *ex vivo*, therapeutic outcomes can also be improved significantly[234]. Second, antigen-specific stimulations utilize antigen-presenting cells that may be immunosuppressed and are often dysfunctional, or non-specific stimulation from synthetic surfaces through CD3 can result in expansion of irrelevant and potentially harmful clones[226–228].

There are several approaches to address these challenges including altering composition of cytokine cocktails, signaling pathway inhibitors, and feeder cells[224]. Additionally, the two signals necessary to stimulate the T cell receptor and costimulatory molecules have been conjugated to synthetic materials: inorganic or polymeric

particles[102,103,257,267] and surfaces[359,360,368]. While current synthetic T cell stimulation platforms are helpful in efficiently enriching and activating antigen-specific T cells[250,254,454], providing cell membrane-mimetic materials[368], and acting as *in vitro* or *in vivo* stimulators[257], however, none provide environmental cues similar to what T cells encounter in the lymphoid organs, such as the spleen or lymph node.

The extracellular matrix (ECM) is an important regulator of cellular function, including gene expression, differentiation, migration, proliferation, and morphology[464–467]. T lymphocytes primarily reside in the lymphoid organs. These unique microenvironments enable rapid communication, cell differentiation, and allow antigen-specific cells to expand thousands-fold in response to infection[468–471]. Even though it is well demonstrated that cells are influenced by ECM properties such as composition, stiffness, and bioactive cues that create unique microenvironments suited to the function of each cell and tissue[472], the role of ECM on T cell activation has not been investigated. Furthermore, bioengineering approaches have developed *ex vivo* culture environments with control over matrix properties for cell and tissue engineering applications[134,473–479]. We hypothesize that a biomimetic, engineered artificial T cell stimulating matrix (aTM) can improve the functionality and phenotype of *ex vivo* stimulation of T cells for therapeutic applications.

Here we generated aTM hydrogels from ECM-based materials with tunable stiffness and two types of key signaling molecules for T-cell stimulation of murine or human cells. This approach also provides ligands from the hydrogel matrix to ECM receptors on the T cell—contributing a potential additional signaling component[480]—in contrast to other T-cell stimulating materials. Additionally, the stiffness of the hydrogel matrix can be tuned allowing effective mechanotransduction required for effective T cell receptor (TCR)

signaling. We examine these unique biophysical properties and study them mechanistically for producing more functional antigen-specific T cells and assess their efficacy in preclinical models of tumor immunotherapy.

6.2 Results and Discussion

6.2.1 Engineering an Artificial T Cell Stimulating Matrix (aTM)

We formed ECM hydrogels by crosslinking thiolated hyaluronic acid (HA) with polyethylene glycol diacrylate (PEGDA) (**Figure 6-1**). HA is a linear polysaccharide and is the only non-sulfated glycosaminoglycan found distributed throughout the ECM, including lymphoid tissues[481] that impacts cell motility and adhesion, differentiation, gene expression, and proliferation[482–484]. Furthermore, we chose HA as an ECM mimic because it can be easily modified through tunable chemistry—which enables the addition of adhesive ligands[485,486], conjugation of drugs or growth factors[487], and control of the elastic modulus and porosity of the hydrogel[488,489].

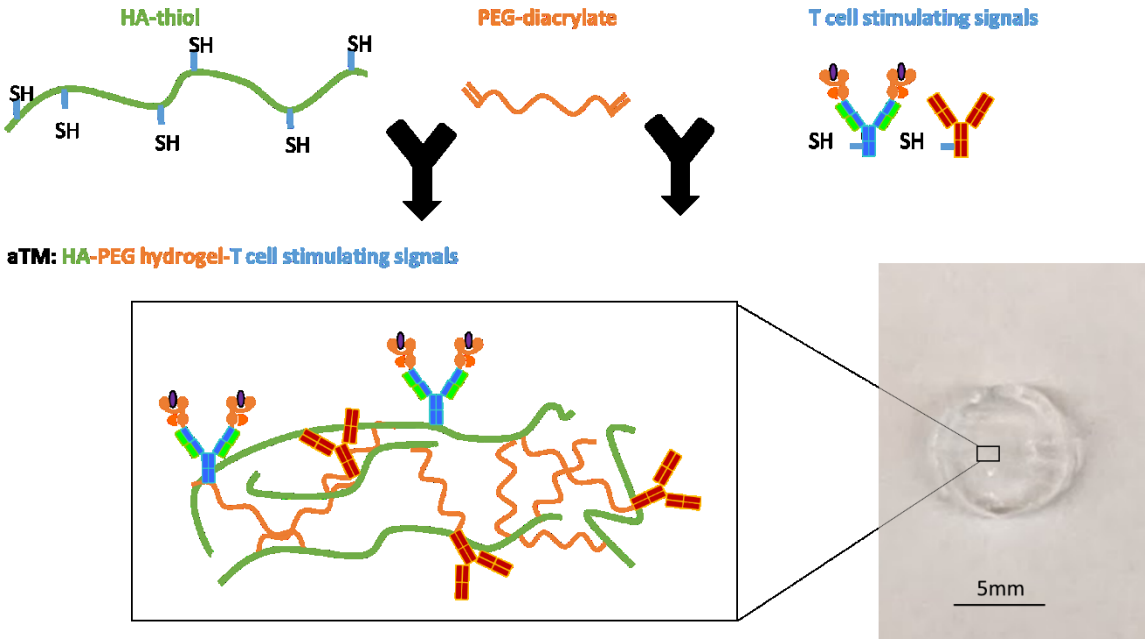

Figure 6-1: Schematic showing the three main components and conjugation chemistry of the hyaluronic acid hydrogels to form the artificial T cell stimulating matrix (aTM). Scale bar of photo is 5 mm.

We engineered this material into an antigen-presenting material by conjugating the signals (Signal 1 and Signal 2) needed for T cell activation directly to the scaffold (**Figure 6-2**A). We first used anti-CD3 and anti-CD28 antibodies for polyclonal wildtype B6 murine CD8+ T cell expansion. This presents a unique approach to use the biophysical properties of hydrogels to influence the potency of a stimulatory environment, which we term an artificial T cell stimulating matrix (aTM).

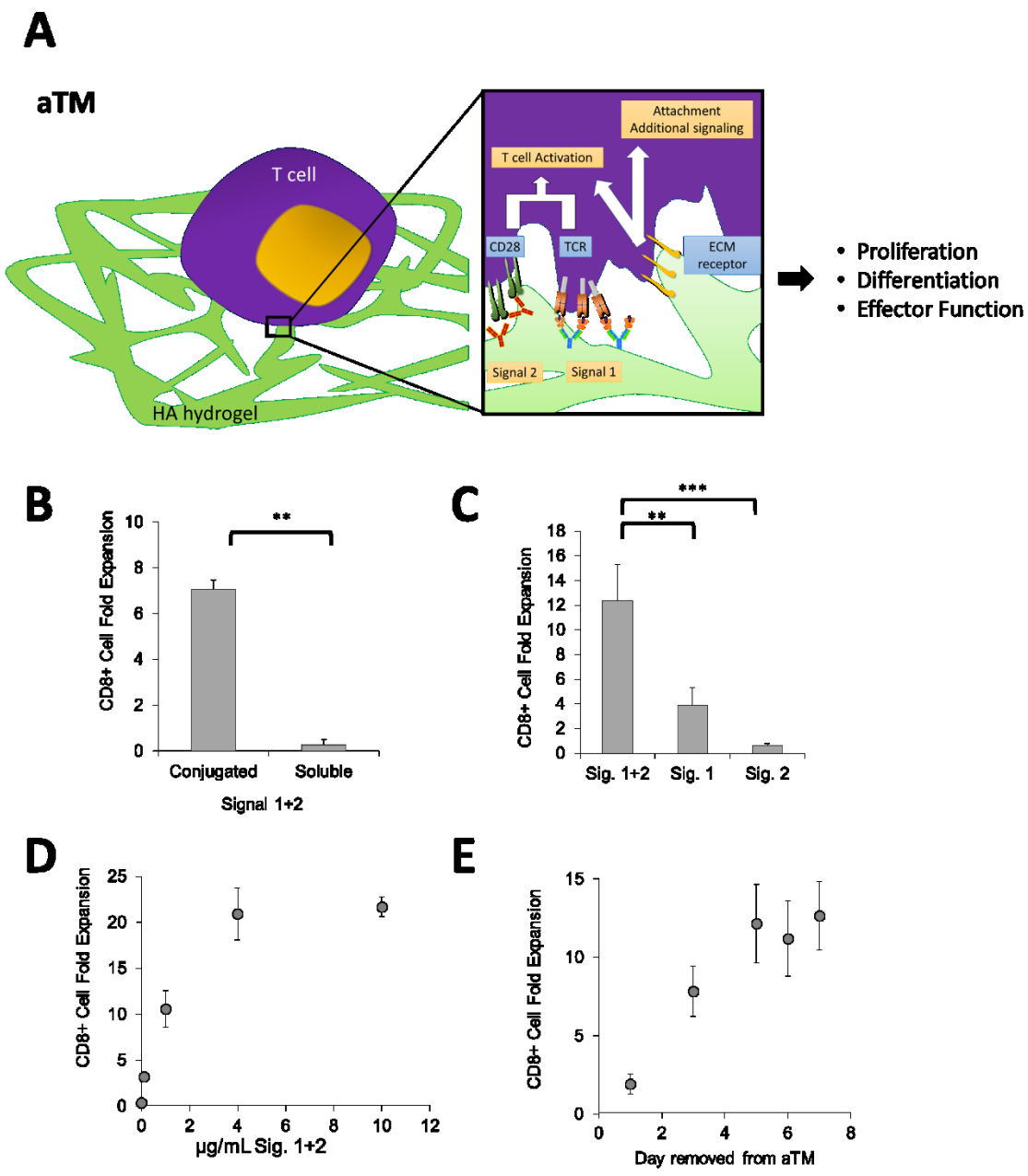

Figure 6-2: An artificial T cell stimulating matrix (aTM) is engineered by conjugating T cell stimulating signals to a hydrogel. (A) Schematic of aTM made from conjugating Signals 1 and 2 to a hyaluronic acid hydrogel. Attachment of Signal 1 and 2 enable effective T cell stimulation which leads to T cell proliferation, differentiation, and effector function. Receptors bind to ECM hydrogel and also contribute to attachment and T cell signaling. (B-D) B6 CD8+ T cell fold expansion measured after seven days of stimulation of the antigen-specific T cells on the hydrogels with (B) Signals 1+2 conjugated or soluble (error bars show s.e.m.; $^{**}p < 0.005$, n = 4, Student's t-test, two-tailed), (C) conjugated together or alone (error bars show s.e.m.; $^{**}p < 0.005$, $^{***}p < 0.0005$, n = 5–7, one-way ANOVA with Tukey's post test), and (D) at varying amounts of Signals 1+2, n = 5. (E) Day 7 CD8+ T cell fold expansion measured after seven days of stimulation of the antigen-specific T cells on the aTM. T cells were removed from aTM on the day noted and cultured on TCP until day 7.

Post-conjugation, nearly all (at least 85%) of the stimulatory signals conjugated remained attached to the scaffold post-gelation (**Figure 6-3**A). Direct conjugation of Signals 1 and 2 at 1 μg/mL (*i.e.* aTM) mediated about 7-fold polyclonal T cell proliferation, whereas the same hydrogel substrate with soluble Signals 1 and 2 showed little proliferation (**Figure 6-2**B). Substrates with only Signal 1 or 2 conjugated resulted in much lower T cell activation and proliferation (**Figure 6-2**C). Investigating different ratios of Signal 1 to Signal 2 at 1 μg/mL revealed that Signal 1 concentration was most critical, and that optimal T cell expansion occurred at a 1:1 ratio, which is used in all subsequent studies (**Figure 6-3**B, C). There are a number of different co-stimulatory molecules which may also provide T cell co-stimulation. Incorporation of a different co-stimulatory molecule anti-41BB at various ratios to anti-CD28 did not further enhance CD8+ T cell activation on the aTM, and also demonstrated the necessity of inclusion of anti-CD28 as a co-stimulatory signal for early activation of CD8+ T cells (**Figure 6-3**D).

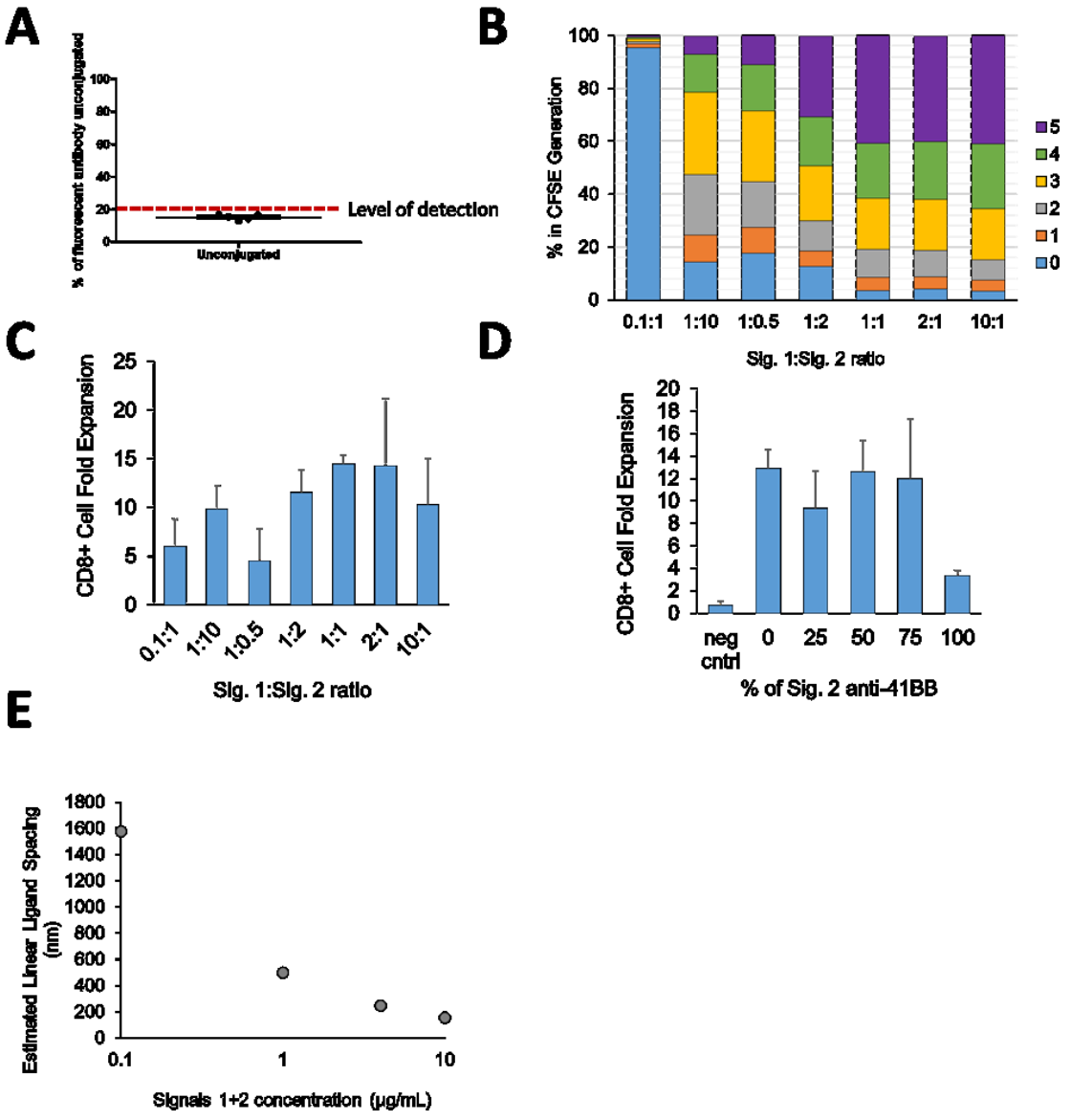

Figure 6-3: Conjugation efficiency and linear estimated ligand spacing on aTM hydrogels (A) Fluorescent antibody levels in the hydrogel washes were below level of detection, and show efficient conjugation efficiency (error bars show s.e.m., n=5). (B) Quantitation of percentage of T cells in each divisional generation based on CFSE proliferation dye dilution for different ratios of Signal 1 to Signal 2. (C) CD8+ T cell fold expansion after 7 days of culture with different ratios of Signal 1 to Signal 2, n=2-3. (D) CD8+ T cell fold expansion after 7 days of culture with various percentages of anti-41BB as co-stimulatory molecule percentage, n=4.(E) Estimated ligand spacing based on the Signal 1 and 2 concentration in the aTM solution.

The density of T cell stimulating signals is an important parameter to control and optimize. We and others have shown previously on particle and planar surfaces that effective T cell stimulation is observed when the inter-ligand spacing is maintained below

75-150 nm[60,103,239]. As we increased the concentration of stimulatory ligands on the aTM, the amount of CD8+ T cell proliferation increased, though it plateaued at around 20-fold expansion when 4 μg/mL of Signals 1 and 2 was used (**Figure 6-2**D). We estimated the surface density of the signals attached to the surface of the aTM for each concentration (**Figure 6-3**E). Our findings estimate that the spacing for ligands need to only be at least 500 nm apart (corresponding to 1 μg/mL), which is larger than previously reported values, potentially due to the fact that signals may not be evenly distributed across hydrogel surface and could be clustered on ECM polymers, or that compliant surfaces require less dense arrays of signal. Additionally, the viability of T cells decreased beyond 4 μg/mL of Signals 1 and 2 (**Figure 6-4**A), and thus less than 4 μg/mL or less were used for subsequent studies with a cell concentration of 0.1 x 10^6 cells/mL (**Figure 6-4**B). aTM also effectively stimulated CD8+ T cells from splenocyte starting populations at similar densities of Signals 1 and 2 (**Figure 6-4**C). Finally, CD8+ T cells required at least five days to be fully stimulated on the aTM surface, where suboptimal activation was observed when cells were removed from the hydrogels on days 1 and 3 (**Figure 6-2**E), indicating a need for dynamic engagement of conjugated stimulatory molecules.

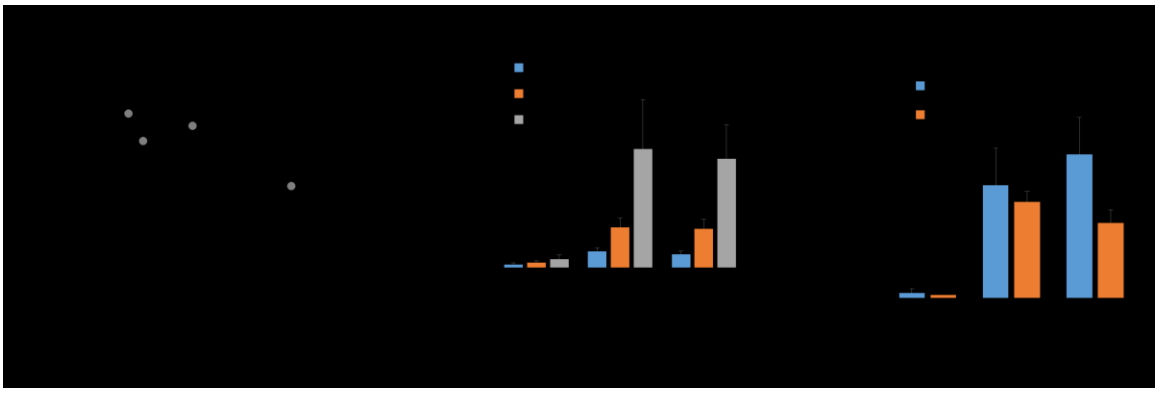

Figure 6-4: Density and ratio of stimulatory signals impacts on T cell activation on the aTM. (A) Viability of stimulated T cells measured on day 7 by trypan blue staining and hemocytometry for varying amounts of Signals 1+2 conjugated to hydrogels, n=4-5. (B-C) CD8+ T cell fold expansion after 7 days of culture with

(B) both varying Signals 1+2 conjugated and cell seeding densities, n=3 and (C) either purified CD8+ T cells or whole splenocyte populations, n=2.

6.2.2 Stiffness Matters: Soft aTM Favors T Cell Stimulation

In stem cells, matrix stiffness modulates cell function through mechanotransduction signaling mechanisms[133,134]. Secondary lymphoid tissue is a soft tissue and the stiffness has been reported to be between 0.1 to 2 kPa[490,491]. To control the mechanical stiffness of our hydrogel within this range, we altered the amount of crosslinker, varying the elastic modulus from 0.2 to 3 kPa and verified overall structures by scanning electron microscopy (SEM) (**Figure 6-5**A, B, **Figure 6-6**). A softer aTM (0.5 kPa) stimulated CD8+ T cell proliferation more effectively than the stiffer aTM (3 kPa) as determined by the dilution of the proliferation dye, carboxyfluorescein succinimidyl ester (CFSE) (**Figure 6-5**C). Greater than 80% of the CD8+ T cells divided past the first and second generation when stimulated on the 0.5-kPa aTM, while the majority of T cells on 3-kPa aTM did not divide at all (**Figure 6-7**). We further probed the spectrum of substrate stiffness to determine the optimal range for T cell stimulation. aTMs with a stiffness below 1 kPa were more effective at stimulating CD8+ T cell expansion, where we observed a dramatic decrease in T cell expansion occurs with aTM greater than 1 kPa (**Figure 6-5**D). We verified the integrity of gel stiffness after 7 days of incubation with minor changes in stiffness of both the 3 kPa and 0.5 kPa gels (**Figure 6-8**).

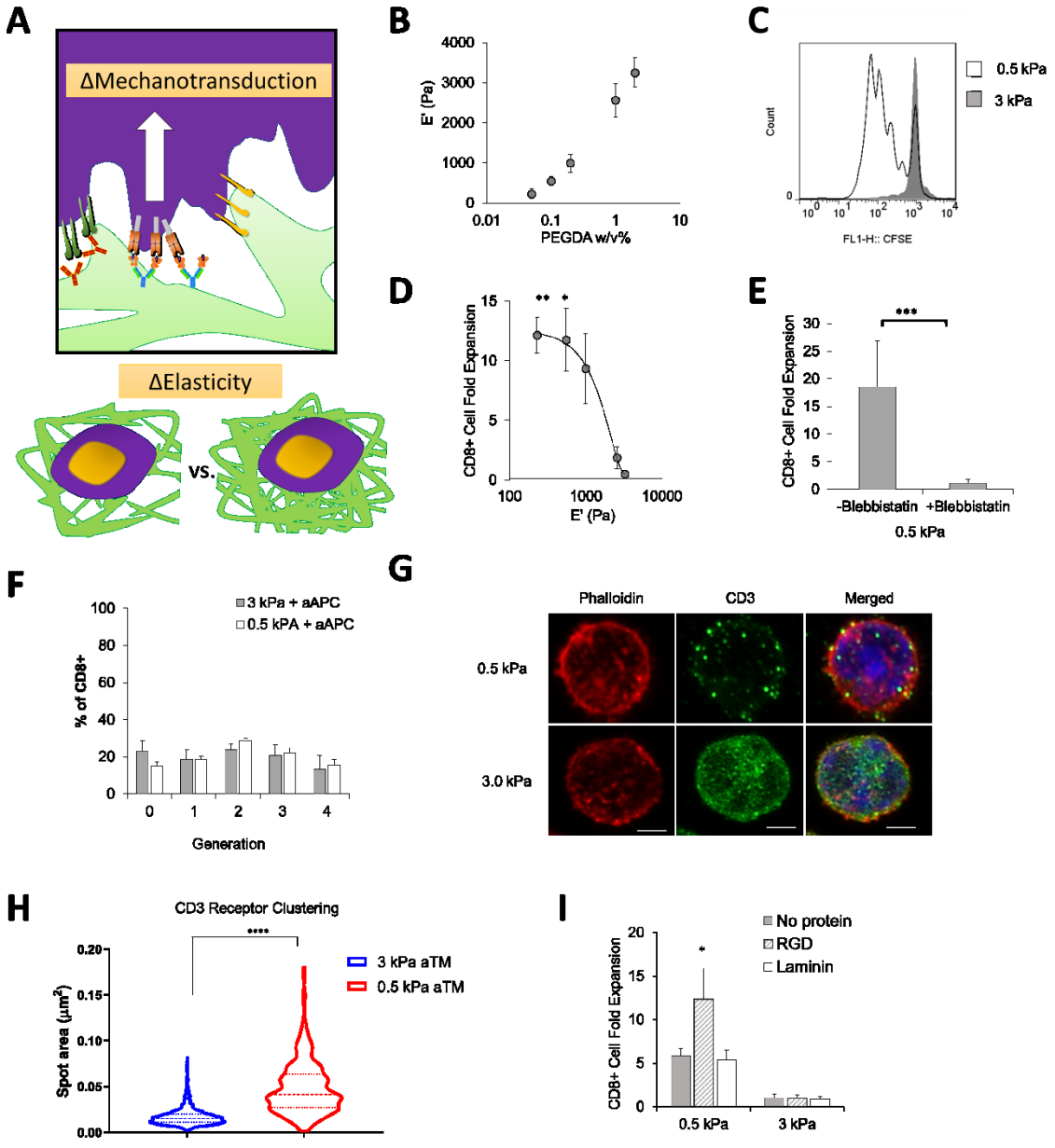

Figure 6-5: Tuning the stiffness of the aTM impacts T cell stimulation. (A) Schematic illustrating hypothesis that tuning stiffness of aTM may change the ability for cell mechanotransduction. (B) Elastic modulus measured by rheometry with varying PEGDA crosslinker weight percent (error bars show s.e.m., n = 3). (C) CFSE proliferation dye dilution measured after 3 days of stimulation of T cells comparing a stiff (3 kPa) and soft (0.5 kPa) aTM. (D) CD8+ T cell fold expansion measured after seven days of stimulation of the T cells on aTMs with varying stiffness (error bars show s.e.m.; *p < 0.05, **p < 0.005, n = 4-12, one-way ANOVA with Tukey's post test). (E) CD8+ T cell fold expansion measured for T cells stimulated on soft aTMs (0.5 kPa) with or without blebbistatin (error bars show s.e.m.; ***p < 0.0005, n = 4, Student's t-test, two-tailed). (F) Quantitation of percentage of T cells in each divisional generation based on CFSE proliferation dye dilution with T cells stimulated on HA hydrogels of different stiffness with aAPC (error bars show s.e.m, n = 4-8). (G) Airyscan super-resolution imaging of phalloidin and CD3 of CD8+ T cells cultured on either soft or stiff aTM (scale bar=2 μm.), (H) where a total of 515 spots were analyzed from 16 cells in the 0.5 kPa condition and 1580 spots were analyzed from 13 cells in the 3kPa condition. (Error bars show s.e.m.; ****p

< 0.0001, Student's t-test, two-tailed). (I) CD8+ T cell fold expansion measured after seven days of stimulation of T cells on the aTMs with either laminin and RGD attached (error bars show s.e.m.; *p < 0.05, n = 3-6, one-way ANOVA with Tukey's post test).

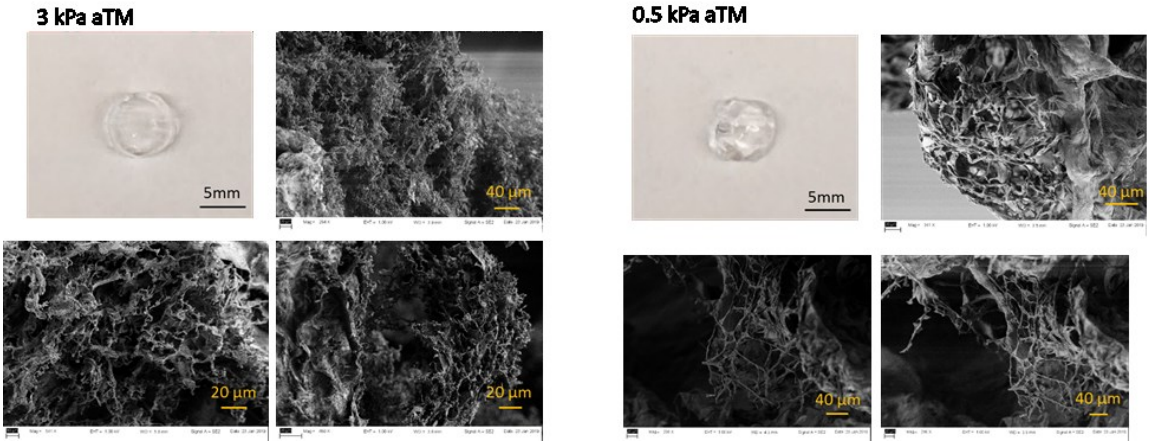

Figure 6-6: Structure of both soft and stiff aTM hydrogels as evaluated by macroscale imaging and scanning electron microscopy (SEM) of aTM hydrogels for both 3 kPa and 0.5 kPa hydrogels. Scale bars indicated in images.

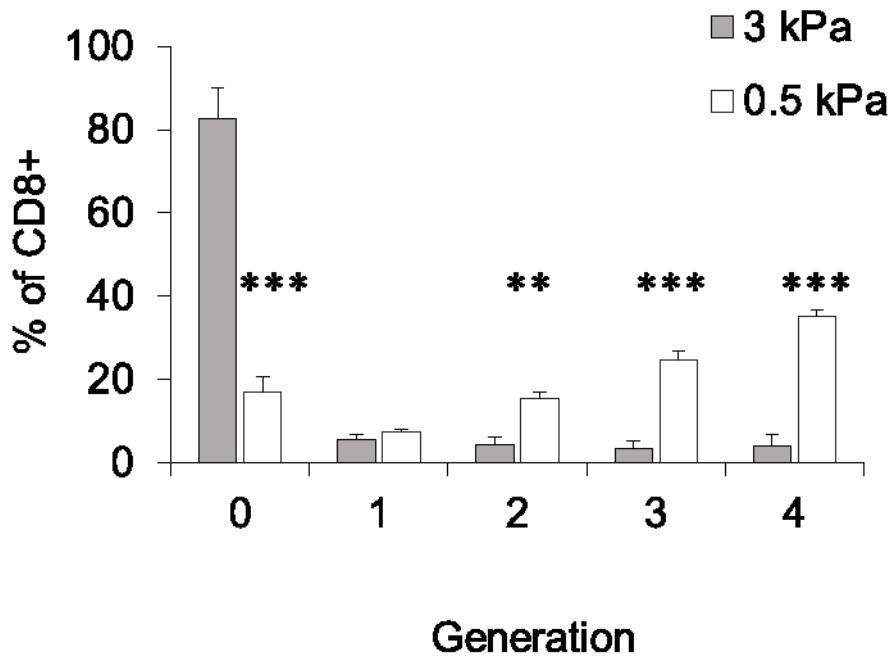

Figure 6-7: CD8+ T cell fold expansion measured after three days of stimulation of the T cells on aTMs with varying stiffness (error bars show s.e.m.; *p < 0.05, **p < 0.005, n = 4-12, one-way ANOVA with Tukey's post test).

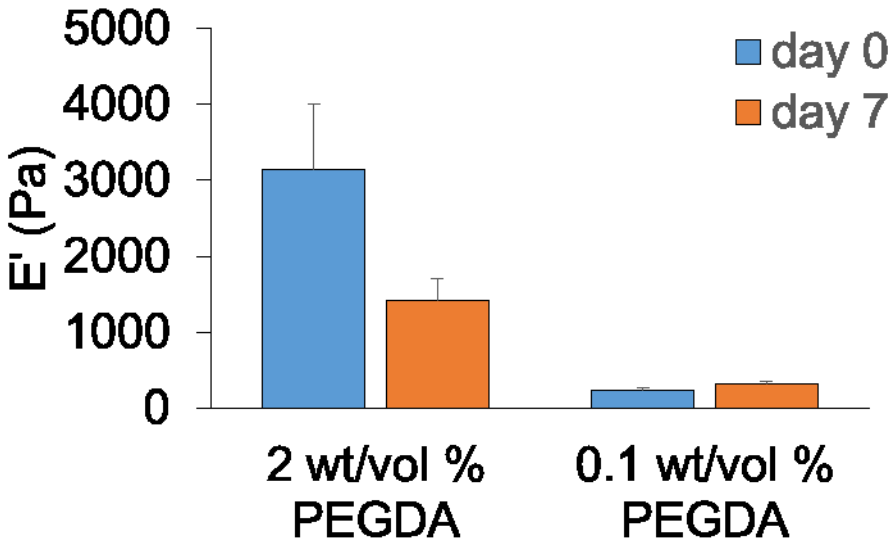

Figure 6-8: Stiffness of aTM hydrogels measured both on day 0 and after 7 days of culture with CD8+ T cells (error bars show s.e.m.; not significant, two-tailed Student's t-test).

It was surprising to observe such a dramatic increase in T cell expansion at stiffness below 1 kPa. We hypothesized that this expansion was a result of stiffness-dependent TCR signaling through the conjugated stimulatory signals more so than T cell-ECM interactions, as mechano-transduction may play a role in TCR signaling due to the motile nature of interacting cognate T cells and antigen presenting cells[135–138,492].

To evaluate our hypothesis of the role of mechanotransduction of TCR stimulating signals, we performed additional experiments where we confirmed similar antibody conjugations to the hydrogel, utilized myosin inhibitors, decoupled signaling components from the hydrogel, macro and microscale visualized cellular attachment, and added further cell-adhesive molecules. First, we confirmed that similar densities of stimulatory signal were conjugated to the surface of the different stiffness aTM through fluorescent secondary antibody staining (**Figure 6-9**). Second, we added a blebbistatin, a myosin II inhibitor important in the role of T cell mechanotransduction[360,493], to the culture of a 0.5-kPa aTM.

In the presence of the inhibitor, CD8+ T cell expansion is abolished even with the same amount of stimulatory ligand present (**Figure 6-5**E).

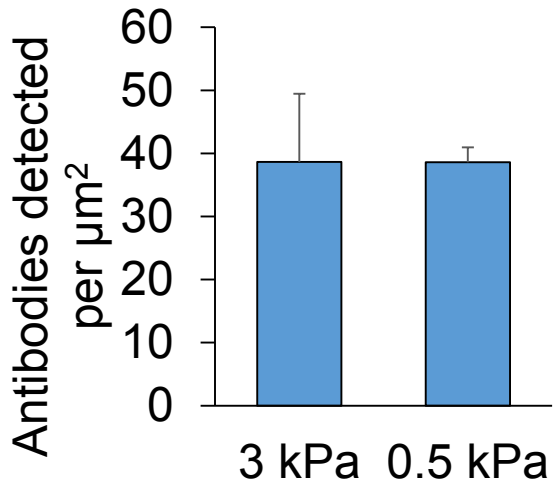

Figure 6-9: Similar densities of antibody are detected on both 3 kPa and 0.5 kPa aTM through secondary fluorescent staining (error bars show s.e.m.; n = 6-7).

Third, we decoupled the stimulatory agent from the matrix and stimulated with cognate artificial antigen presenting cells (aAPC) on different stiffness of hydrogels. The nanoparticle aAPC contain both Signals necessary for CD8+ T cell activation—Signal 1: peptide loaded major histocompatibility complex (pMHC) and Signal 2: anti-CD28 costimulatory antibody (**Figure 6-10**). There were no differences in the CFSE proliferation assay or in resultant cell phenotype between soft (0.5 kPa) and stiff (3 kPa) HA hydrogels (**Figure 6-5**F, **Figure 6-11**). This demonstrates that the mechanotransduction is independent of ECM-cell adhesion receptor interactions traditionally investigated, but instead dependent upon TCR signaling when stimulatory ligands are attached to HA hydrogels.

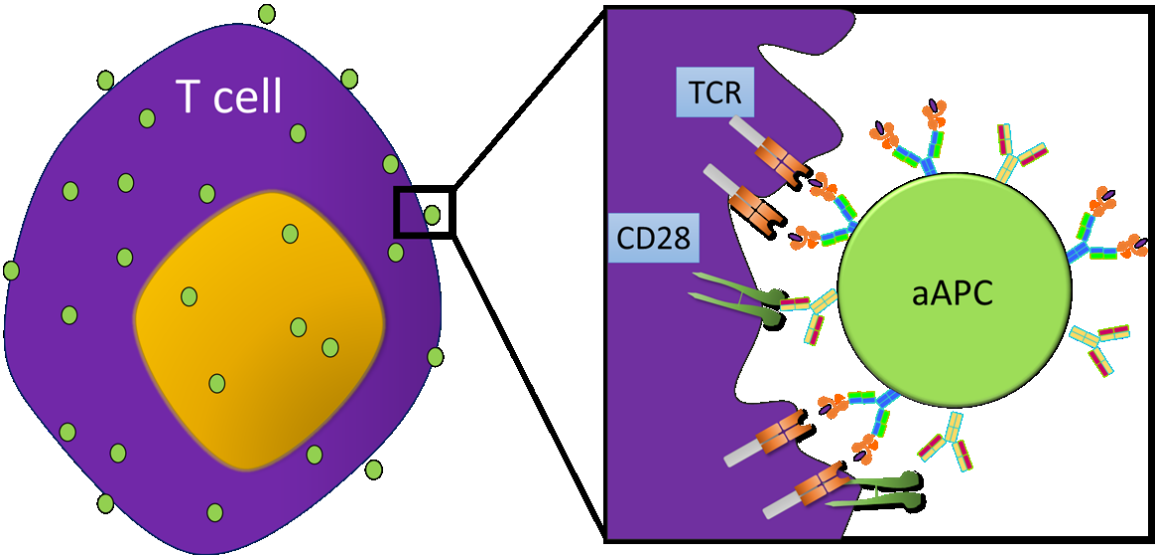

Figure 6-10: Schematic of artificial antigen-presenting cell (aAPC) with Signal 1 (pMHC) and Signal 2 (aCD28) attached to a particle platform.

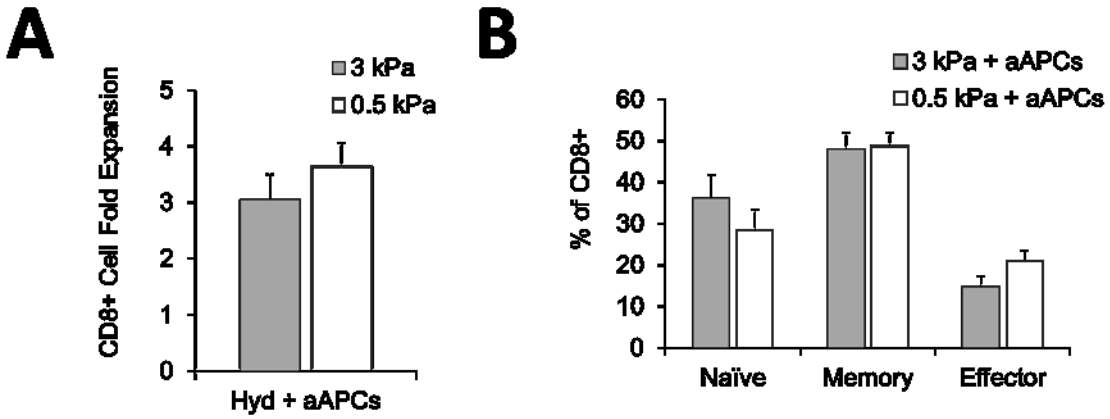

Figure 6-11: Activation of CD8+ T cells is not changed by surface stiffness when stimulus is decoupled from the surface. (A) CD8+ T cell fold expansion from T cells stimulated by aAPC on different hydrogel stiffness (0.5 kPa, 3 kPa) (error bars show s.e.m., n= 14-15). (B) Phenotypic markers (CD62L, CD44) measured by flow cytometry after 7 days of stimulation an (error bars show s.e.m.; n = 18, Student's t-test).

Fourth, we visualized the interaction of the T cells and the aTM hydrogels or HA hydrogels (without Signals 1 and 2) with light video microscopy (**Figure 6-12**). After 24 hours, only CD8+ T cells remained attached to the soft (0.5 kPa) aTM hydrogel with both

stimulatory signals conjugated. Whereas CD8+ T cells did not attach to stiff aTM (3 kPa) or soft (0.5 kPa) hydrogels without Signals 1 and 2 attached. Fifth, by doing super resolution microscopy we observed significant differences in the CD3 clustering on T cells cultured on the soft (0.5 kPa) aTM versus the stiff (3 kPa) aTM with little difference in actin co-localization (**Figure 6-5**G). Indeed by analyzing the CD3 cluster size, T cells cultured on the soft aTM had significantly greater CD3 cluster area of 0.05 μm^2 compared to 0.02 μm^2 for that of the T cells stimulated on the stiff aTM (**Figure 6-5**H).

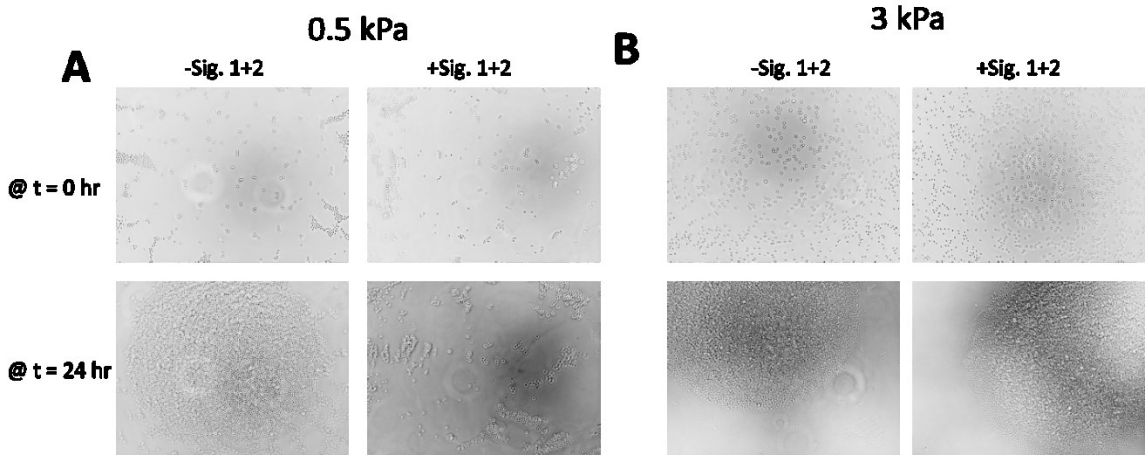

Figure 6-12: T cells attach to aTMs when Signals 1 and 2 are conjugated and are soft (0.5 kPa). Light video microscopy over a period of 24 hours was done to track cell movement and attachment to the aTMs of (A) 0.5 kPa (B) 3 kPa both with and without Signals 1 and 2 at time points of t=0 and t=24 hr.

Sixth, adding cell-adhesive ligands has been shown to increase cell attachment to surfaces[494]. We included additional ECM-binding proteins to the aTM scaffold such as laminin and cyclic RGD, a sequence derived from ECM-binding proteins to determine whether this might improve engagement and stimulation on stiff hydrogels. Even providing cell-adhesive ligands did not help stiff aTMs (3 kPa) stimulate antigen-specific PMEL CD8+ T cells, whereas RGD further increased T cell proliferation on soft (0.5 kPa) aTM surfaces resulting in effective expansion (**Figure 6-5**I, **Figure 6-13**).

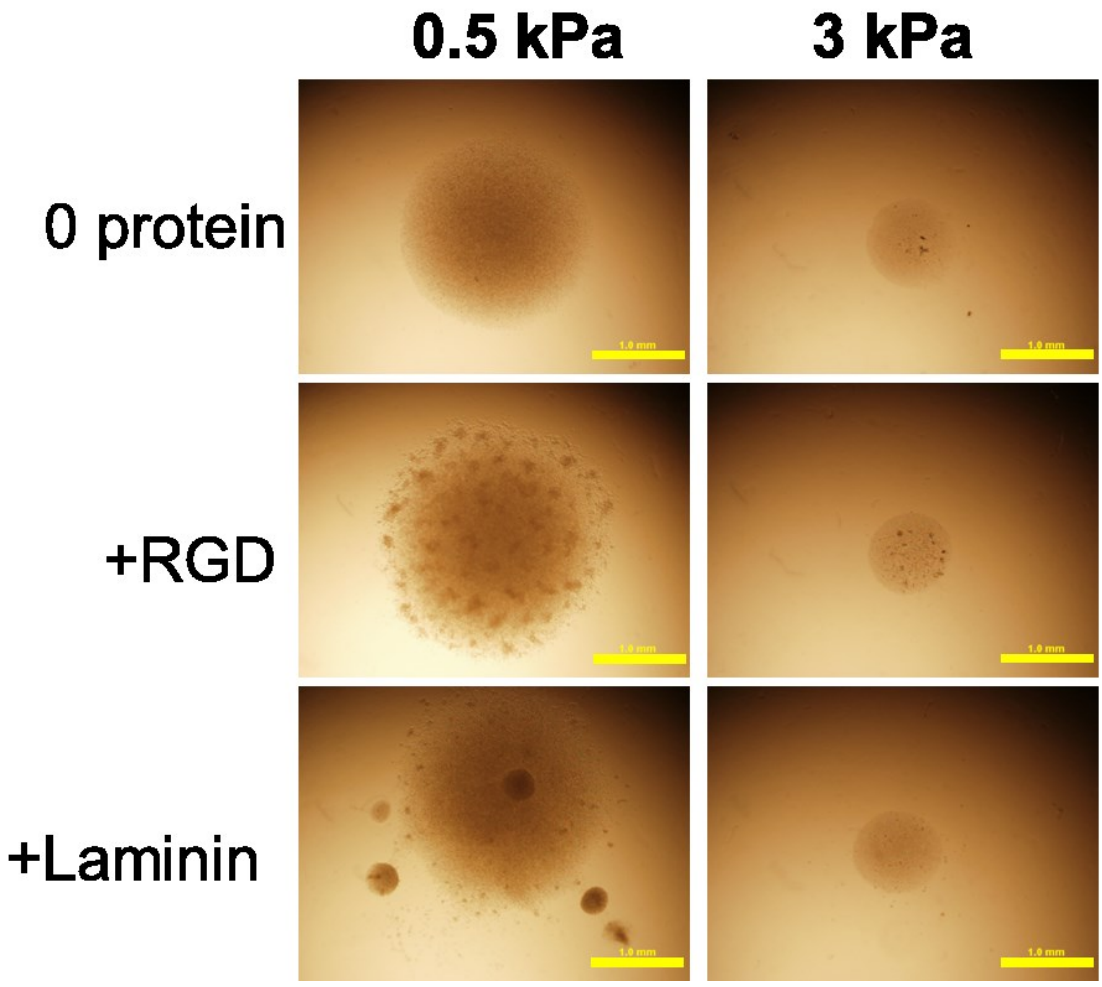

Figure 6-13: Light microscopy images of T cell cultures on aTMs at day 3 with different stiffness (0.5, 3 kPa) and proteins (cyclic RGD, laminin) attached (scale bar = 1 mm).

Taken together, these data indicate that the role of mechanical stimulation is mediated through the TCR and the stimulatory ligands conjugated to the matrix, yet cannot be overcome with adding additional cell-attachment sequences. This enhanced mechanotransduction at lower stiffness could be due to a number of reasons. First, softer hydrogels which are more compliant and may enable enhanced clustering of neighboring attached Signal 1 molecules on the hydrogel—shown to promote superior TCR signaling, which we observe[103,495]. Second, traditionally T cells are stimulated by surfaces which have

stimulatory signals non-specifically adsorbed to surfaces, whereas our signals are chemically attached to the matrix, which may contribute to more effective mechanotransduction. Third, the stiffness range of the aTM more closely matches the stiffness of the secondary lymphoid tissue. To our knowledge this represents the lowest stiffness of a surface, orders of magnitude less than T cells have been stimulated with, where traditionally the surface is a stiff (~MPa) plastic[359,360]. At softer hydrogel surfaces, we are approaching the appropriate level of resistance that a T cell may observe at a cellular level, where researchers have shown that the minimum adhesion strength to antigen presenting cells to be around 90 Pa[136,496]. In conclusion the stiffness of the aTM is critical to enhance mechano-transduction TCR signaling for effective T cell expansion.

6.2.3 Extracellular Matrix Provides Additional Signaling and Phenotype Skewing

Beyond biophysical cues such as stiffness, the ECM can provide molecular signaling cues via cellular receptor activation. We were particularly curious to how the base HA hydrogel affects both T cell functionality and phenotype, as T cells express CD44—a ligand specific for HA[483,497]. For T cells, CD44 has primarily been utilized as a marker for cellular phenotype and not examined as a co-stimulatory molecule[498–501]. To investigate how the HA hydrogel contributes to T cell activation and signaling, we decoupled the other unique biophysical variable—having the T cell stimulatory signals attached to the surface—by utilizing aAPC for T cell stimulation. In this manner we could mechanistically study differences in T cell signaling directly due to the HA hydrogel.

To examine the influence of stimulatory environment, transgenic PMEL CD8+ T cells and cognate aAPC were co-incubated and then either plated onto ECM-mimic hydrogels (HA) or the traditional tissue culture plate (TCP) wells (**Figure 6-14**A). Interestingly, CD8+ T cells that were cultured on HA hydrogel surfaces demonstrate much higher antigen-specific T cell proliferation as indicated by CFSE dilution after three days of culture (**Figure 6-14**B). In fact, there are significantly more T cells that have reached the second, third, and fourth generations when compared to the T cells cultured on traditional tissue culture plates, where the majority of the cells have not yet divided (**Figure 6-15**). There was no inherent signaling or activation without stimulatory aAPC with no effects on cell viability on the HA surface (**Figure 6-16**). Moreover, including soluble HA also increased the percent of CD8+ T cells to divide (~35%) as compared to the tissue culture plate without hydrogel (~15%), but not as much when it is crosslinked into a hydrogel (~65%) (**Figure 6-14**C). Therefore, the benefit of the HA to early CD8+ T cell proliferation is partially mediated through direct interaction with crosslinked HA in combination with TCR signaling.

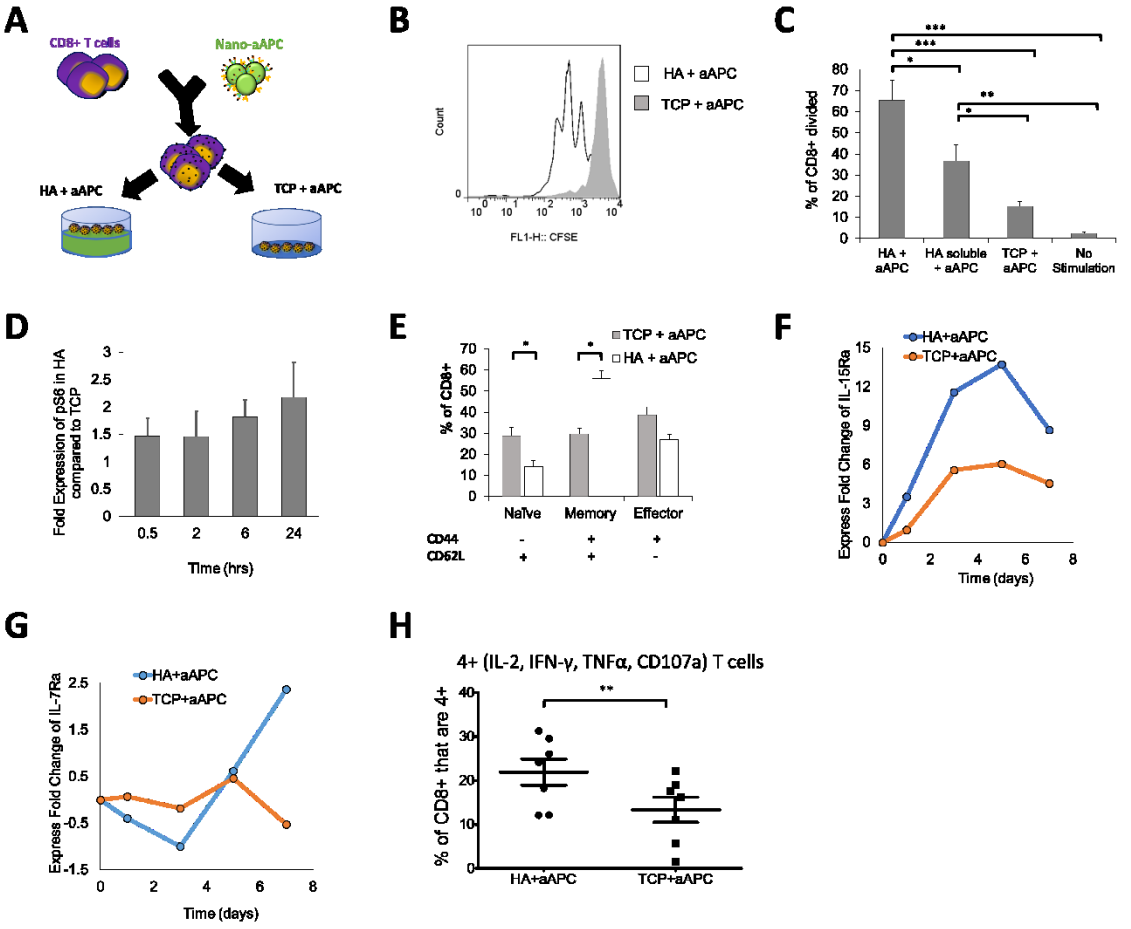

Figure 6-14: Stimulated T cells are influenced by additional signaling from the HA hydrogel. (A) Schematic showing experimental setup testing the difference between activating antigen-specific CD8+ T cells with nanoparticle artificial antigens presenting cells (aAPC) on HA hydrogel versus a tissue culture plate (TCP). (B) CFSE proliferation dye dilution measured after 3 days of stimulation of antigen-specific T cells stimulated by the same dose of aAPC on either TCP or on HA hydrogel surface. (C) Percent of CD8+ T cells that have divided by day 3 as measured by CFSE proliferation dye dilution (error bars show s.e.m., *$p < 0.05$, **$p < 0.005$, ***$p < 0.0005$ n = 7, one-way ANOVA with Tukey's post test). (D) Time course experiment using p-S6 (S240/S244) as the read out for mTORC1 activation. This relative fold-change pattern represents three independent experiments using phospho-flow cytometry. (E) Phenotypic markers (CD62L, CD44) measured by flow cytometry after 7 days of stimulation with aAPC on different surfaces (error bars show s.e.m.; *$p < 0.05$, n = 7, Student's t-test, two-tailed). (F, G) Time course experiment detecting fold change of (F) IL15Ra (CD215) and (G) IL7Ra (CD127). Geometric means of each data point are compared first with their isotype controls followed by the baseline control. Data represents two independent experiments. (H) T cells positive for all four cytokine and functional molecules (IL-2, IFN-γ, TNFα, CD107a) were measured by flow cytometry after 7 days of stimulation (error bars show s.e.m.; *$p < 0.05$, n = 7, Paired t-test, two-tailed).

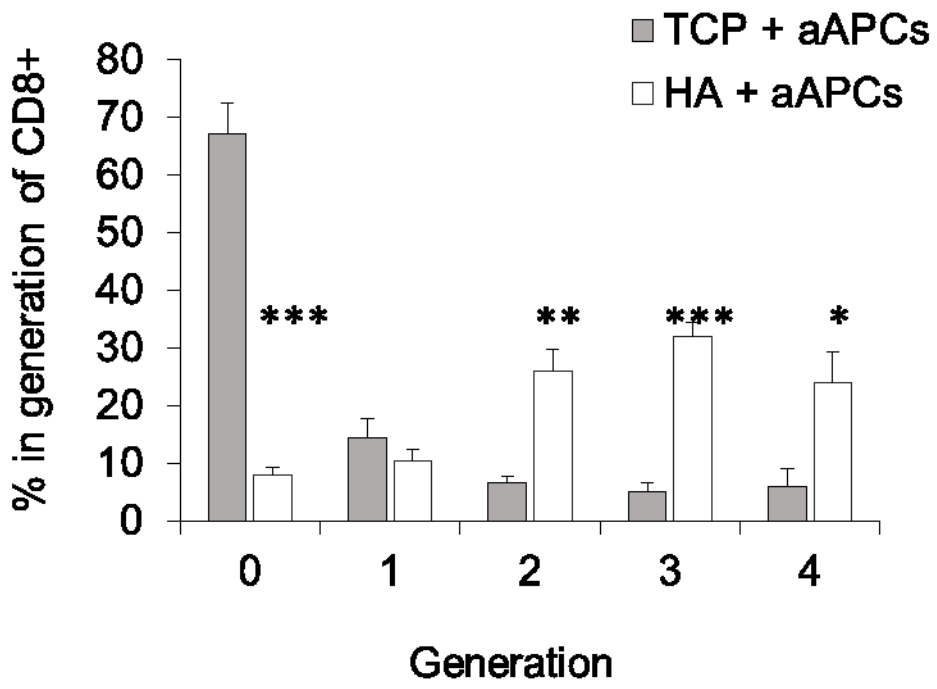

Figure 6-15: Quantitation of percentage of T cells in each divisional generation based on CFSE proliferation dye dilution for the experiment described in Figure 3B (error bars show s.e.m.; *$p < 0.05$, **$p < 0.005$, ***$p < 0.0005$, $n = 5$, Student's t-test).

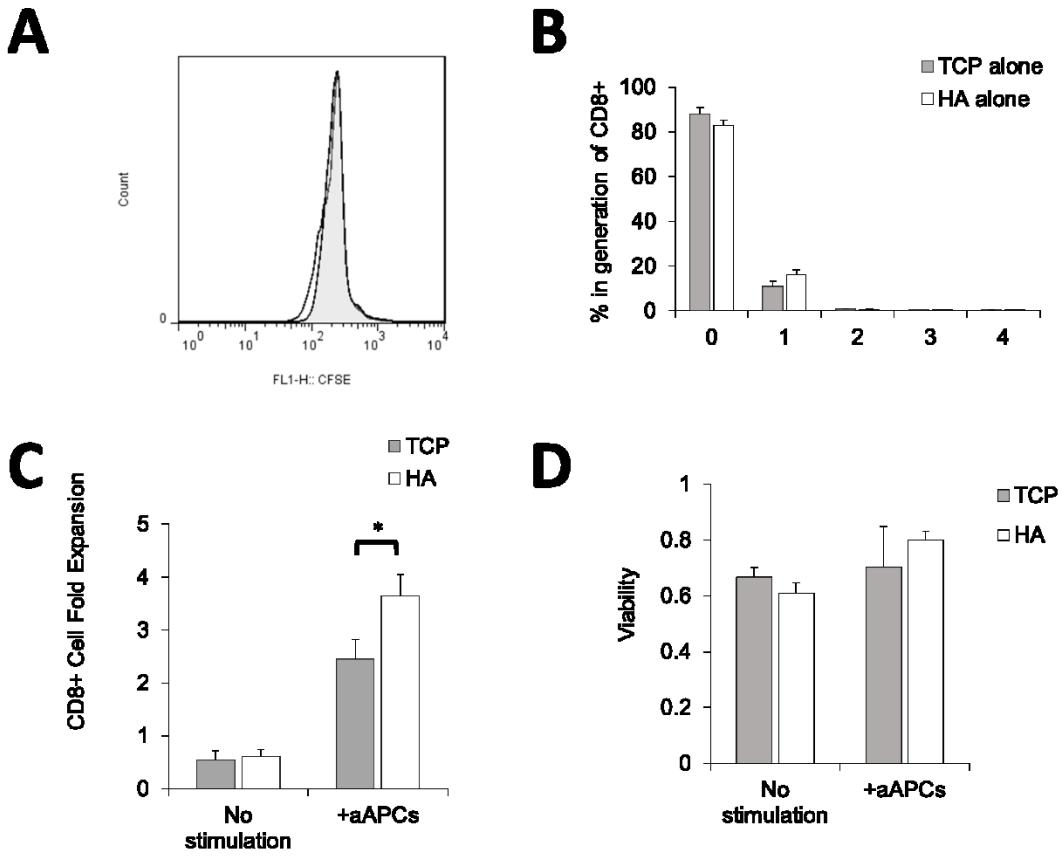

Figure 6-16: The HA hydrogel environment does not provide any inherent stimulation for T cell proliferation. (A) CFSE proliferation dye dilution measured after 3 days of culture of T cells on either tissue culture plates (TCPs) or on hyaluronic acid hydrogels (HA) without stimulatory signals present. (B) Quantitation of percentage of T cells in each divisional generation based on CFSE proliferation dye dilution (error bars show s.e.m., n=15). (C) CD8+ T cell fold proliferation (error bars show s.e.m.; *$p < 0.05$, n = 7, Student's t-test) and (D) viability (error bars show s.e.m., n=8-11) measured after seven days of stimulation of the antigen-specific T cells on the hydrogels with or without aAPC.

We investigated the role of HA in signaling and inducing greater early expansion of CD8+ T cells in the hydrogel condition. Exploring key signaling pathways related to T cell activation and proliferation, we identified a significant increased expression of p-S6K1 and p-S6 (**Figure 6-14**D, **Figure 6-17**), consistent with upregulation of mTORC1 (mammalian target of rapamycin complex 1), and a downregulation of p-AKT (indicative of mTORC2) under the HA culture condition compared to the TCP condition (**Figure**

6-17). Furthermore, CD44-signaling has been shown to trigger Ras-Erk signaling in other cell types[484], and Ras-Erk and PI3K-mTOR pathways have been shown to crosstalk and compensate each other in T cells[502]. Indeed we observe a significant amount of p-S6 signal may come from CD44-induced Ras-Erk signaling (**Figure 6-18**A,B). CD44 has also been shown to directly interact with Src family proteins like Lck[503]. Lck is involved in early phosphorylation the ITAM domains of TCRζ chain and CD3 complex for T cell activation upstream of both Ras-Erk and PI3k-mTOR signaling[504]. We observe higher phosphorylation of p-Src family protein at Y416 (which includes Y934 in p-Lck as an activation signal), with equal amounts of inhibiting signal and total protein—p-Lck Y505 and total Lck, respectively (**Figure 6-19**). Taken together, the interaction of T cells with HA critically influences early T cell priming and activation with noted contributions of enhanced Lck phosphorylation and potential crosstalk between Ras-Erk and PI3K-mTOR pathways, where mTOR is an important integrator of immune cues for robust T cell activation and phenotype skewing[505].

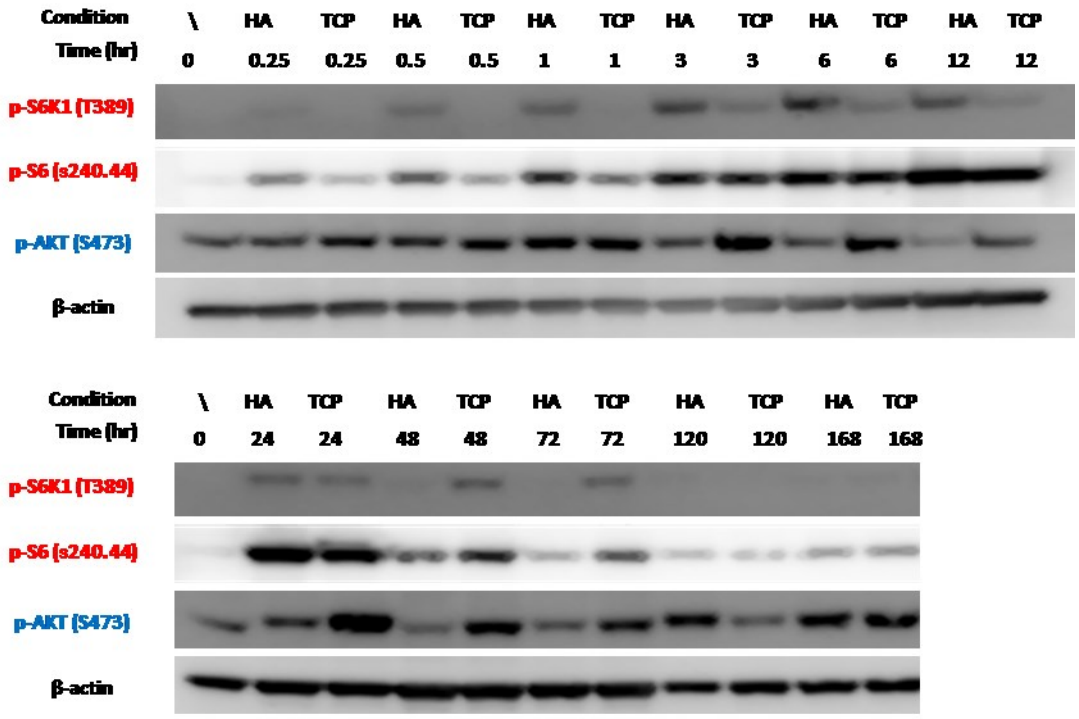

Figure 6-17: Time course experiment for T cell activation on HA surfaces compared to TCP surfaces for mTOR signaling. Cells were collected for western blot at designated time points after activation. Read out for mTORC1: p-S6K1 (T389) and p-S6 (S240/244); read out for mTORC2: p-AKT (S473). These images represent five independent experiments.

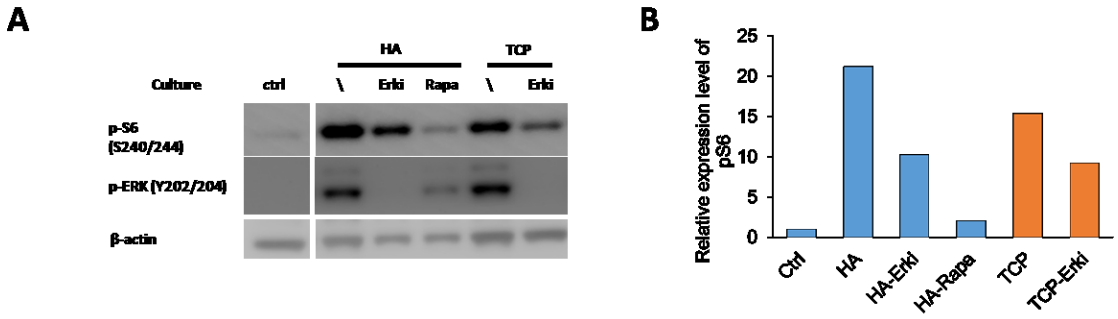

Figure 6-18: HA-CD44 signaling induces CD8+ T cell expansion through crosstalk between Ras-Erk and PI3K-mTOR pathways. (A) Isolated CD8+ T cells were treated with different drug conditions. Erki = U0126, an inhibitor that specifically targets Erk1/2; Rapa = Rapamycin, an inhibitor that specifically targets mTORC1. Image represents three independent experiments. (B) Quantified data from western blot representing levels of expression of mTORC1 24 hours after activation, using p-S6 (S240/244) as a readout. The fold change pattern represents three independent experiments.

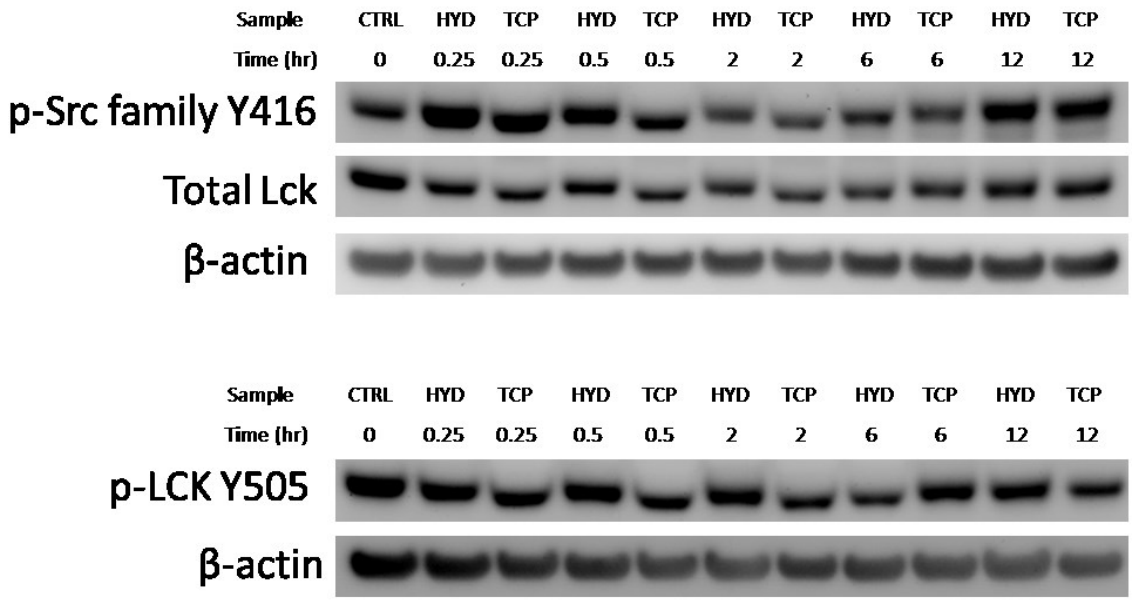

Figure 6-19: HA-CD44 signaling induces CD8+ T cell expansion by early (15 min – 30 min) phosphorylation of Src family kinases for early T cell activation, but not changes in Total Lck protein or phosphorylation of LCK inhibition sites (p-LCK Y505), and no changes in beta actin. Phospho-Src family Y416 is equivalent to phospho-Lck Y394, which serves as an activation site of Lck activity.

To investigate the long-term role of ECM-mimic hydrogels in enhancing CD8+ T cell expansion and hemostasis, we looked at the expression of CD44 after stimulation on the two different surfaces. CD44 is expressed by CD8+ T cells in concordance with changes in phenotype, where CD44 remains upregulated in activated and memory cells[498–501]. We also stained for CD62L to separate CD8+ T cell phenotypes influenced by the HA hydrogel—naïve, memory, and effector.

Stimulation on the HA hydrogel resulted in significantly higher percentage of CD44+ T cells (**Figure 6-14**E). This increase was associated with nearly double the percentage of memory T cells (CD62L+, CD44+) and a decrease in effector T cells though not statistically significant. Consistent with an increase in memory-like cells, we observed a global upregulation of IL-15Ra (**Figure 6-14**F) and a conditional upregulation of IL-7Ra

(**Figure 6-14**G) at late contraction phases under HA condition, confirmed at the mRNA level (**Figure 6-20**). Both IL-7Ra and IL-15Ra are receptors for cytokines that trigger memory T cell homeostasis[506], and thus an upregulation of both receptors may induce memory T cell formation. In conclusion, this both informs that HA can contribute to increased proliferation, and also demonstrates that the ECM hydrogel surface influences the final phenotype of the cells.

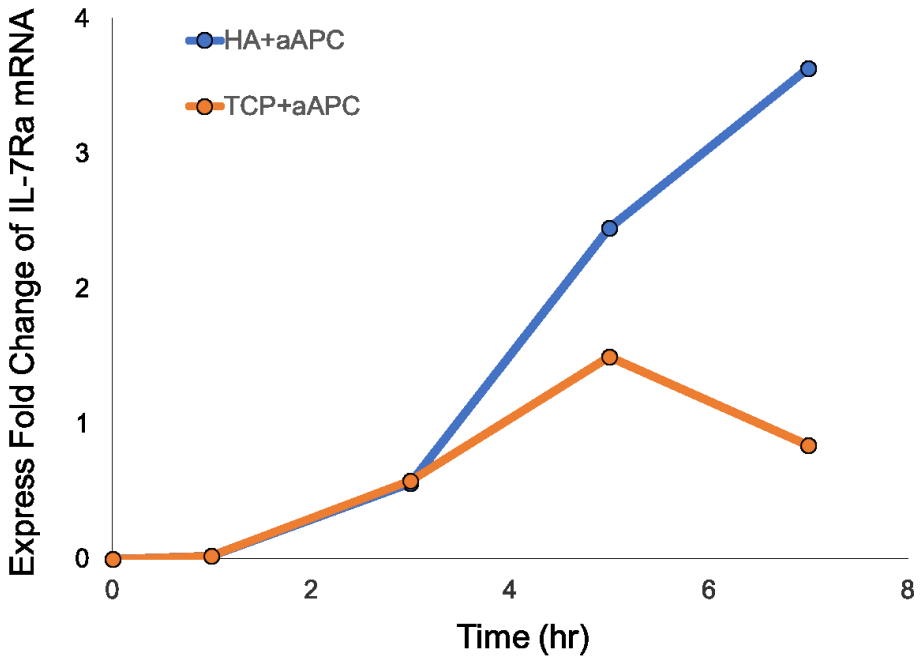

Figure 6-20: Quantified rt-PCR data of IL7Ra mRNA collected cells at different time points post activation in either HA+aAPC or TCP+aAPC conditions. Data are collected using ΔΔCT method. The pattern of mRNA matches relatively with the protein fold change level.

Memory T cells have an increased persistence and potential for proliferation, with stem-cell like qualities[426], and have been shown effective in anti-cancer responses for ACT[507]. To test the function and quality of the resultant CD8+ T cells *in vitro,* we examined how well they co-produced multiple cytokines and cytolytic molecules[41], which is associated with successful immune responses in infection and cancer[39,435,436,462]. In chronic

infections and after extended stimulations such as in ACT and in the cancer microenvironment, CD8+ T cells will continue to differentiate and become "exhausted" or less potent[37,462,508,509]. We observed a higher percentage of CD8+ T cells that are co-positive for all functionality markers—IFN-γ, TNF-α, IL-2, and CD107a—on the HA hydrogel, when compared to the TCP condition (**Figure 6-14**H). Thus, the HA hydrogel ECM environment enhances early cell proliferation, memory cell induction, and functional T cell generation.

6.2.4 aTM Stimulates and Polarizes Human CD8+ T Cells

To show that aTM is also capable of stimulating human CD8+ T cells, we attached anti-human CD3 (Signal 1) and anti-human CD28 (Signal 2) to the HA hydrogels. We observed a similar increase in the fold expansion when increasing the density of the Signal 1 and 2 to 4 μg/mL (~25 fold CD8+ T cell expansion in 1 week) on 0.5-kPa aTM, but beyond this value, the fold proliferation of the cells dramatically decreased where little to no expansion was detected in the 25 μg/mL condition (**Figure 6-21**A), with minimal CFSE dilution (**Figure 6-22**). Nevertheless, phenotypic studies revealed that the cells are still proliferating at this dose, albeit at lower frequency (**Figure 6-21**B). Interestingly, this indicates control over phenotype independent of cell proliferation. Additionally, we verified the interaction of the T cells with the aTM at higher densities through light video microscopy where there is a higher fraction of cells bound to the aTM matrix over the first hour of attachment, similar to what we have observed with murine T cells (**Figure 6-23**). After 3 days we observed macroscopically more punctate, smaller cell clusters in the 25 μg/mL aTMs than in the 4 μg/mL condition, potentially indicating the antibody density

may prevent beneficial multi-cellular interactions from forming due to an inhibition of migration necessary for expansion (**Figure 6-24**).

Similar matrix stiffness-dependent effects were observed where more effective stimulation (>20 fold expansion in 1 week) is observed on aTM hydrogels with an elastic modulus less than 1 kPa (**Figure 6-21**C,D, **Figure 6-25**, **Figure 6-26**). By changing the stiffness of the aTM, we observed differences in phenotype even within conditions that have similar fold expansions (**Figure 6-21**E). For example, the 0.5 kPa and 1 kPa aTMs both provided nearly 20-fold expansion, but the 1 kPa aTM generated a more balanced ratio of central memory to effector memory CD8+ T cells than the 0.5 kPa aTM. In summary, this demonstrates that we can create an aTM that stimulates and polarizes human CD8+ T cells for potential ACT therapy.

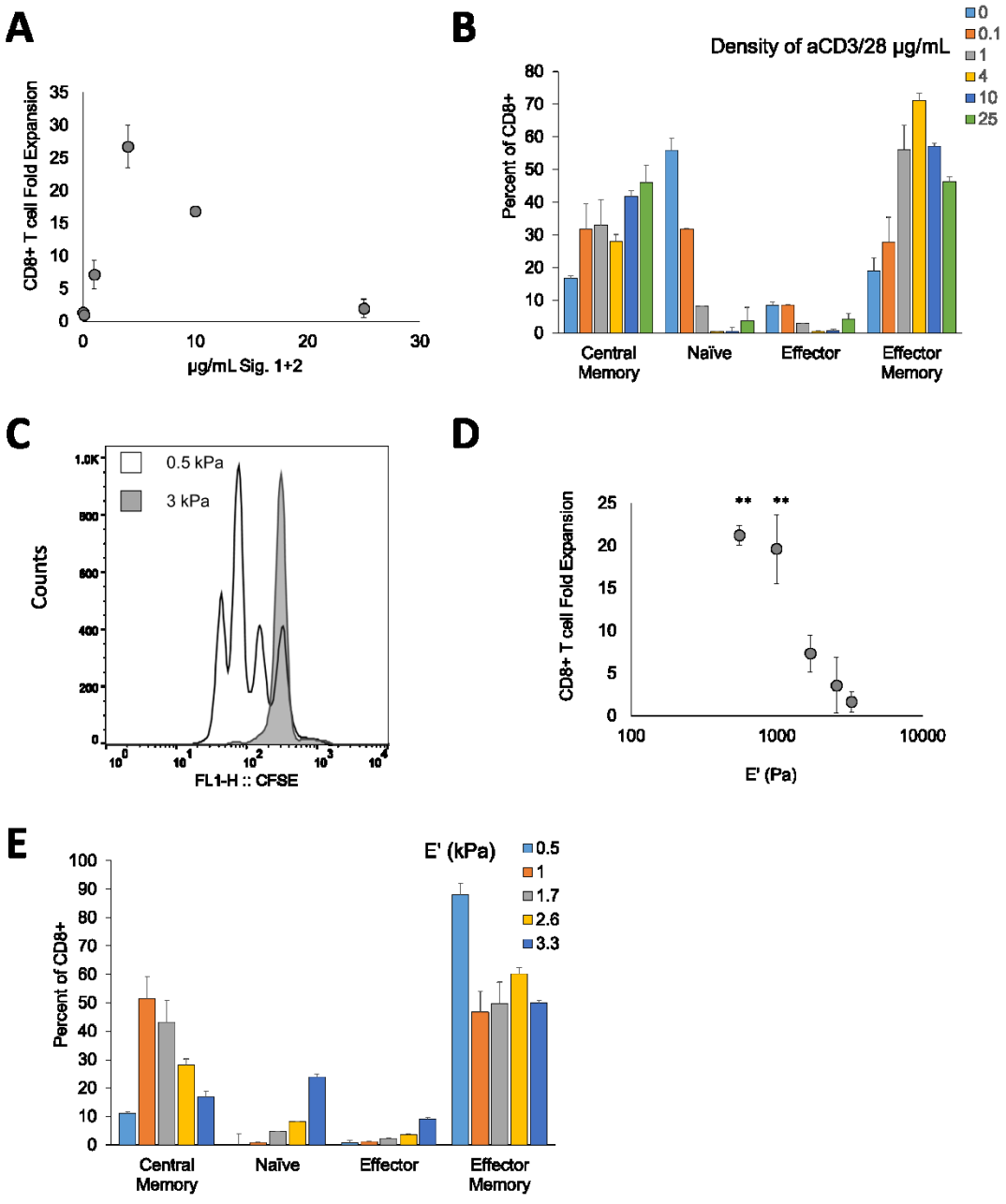

Figure 6-21: Artificial T cell stimulating matrix hydrogels provide effective stimulation to human CD8+ T cells. (A) CD8+ T cell fold expansion measured after seven days of stimulation by aTM with Signals 1+2 (anti-CD3 and anti-CD28) conjugated at varying amounts, n = 3 independent donors. (B) Phenotype of CD8+ T cells after culture on aTM surfaces of varying Signals 1+2 amounts defined by CD45RA and CD62L (error bars show s.e.m). (C) CFSE proliferation dye dilution measured after 3 days of stimulation of CD8+ T cells comparing a stiff (3 kPa) and soft (0.5 kPa) aTM, n = 3 independent donors. (D) CD8+ T cell fold expansion measured after seven days of stimulation on aTMs with varying stiffness (error bars show s.e.m.; **p < 0.01, n = 3 independent donors, one-way ANOVA with Dunnett's post test comparing to 3 kPa condition). (E) Phenotype of CD8+ T cells after culture on aTM surfaces of varying stiffness defined by CD45RA and CD62L (error bars show s.e.m) n = 3 independent donors.

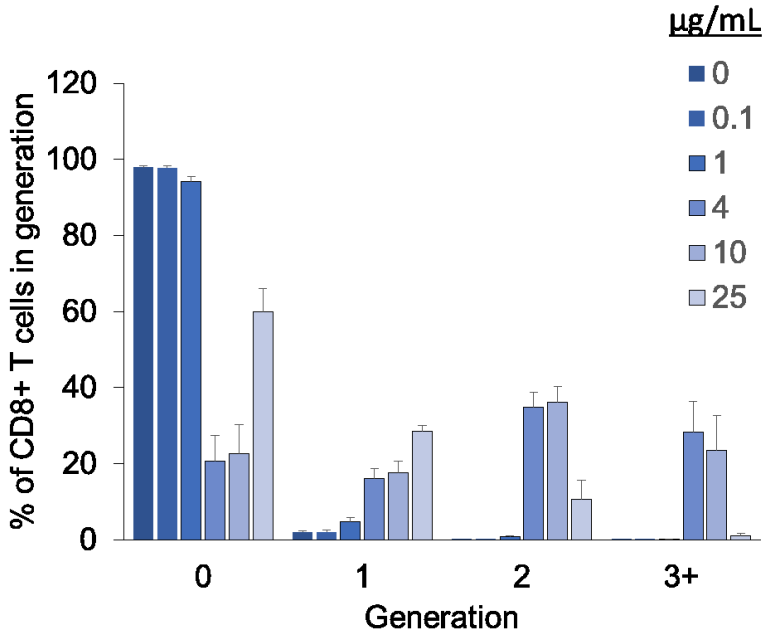

Figure 6-22: Quantitation of percentage of human CD8+ T cells in each divisional generation based on CFSE proliferation dye dilution with T cells stimulated on aTM with different density of anti-human CD3/CD28 (error bars show s.e.m, n = 3 independent donors).

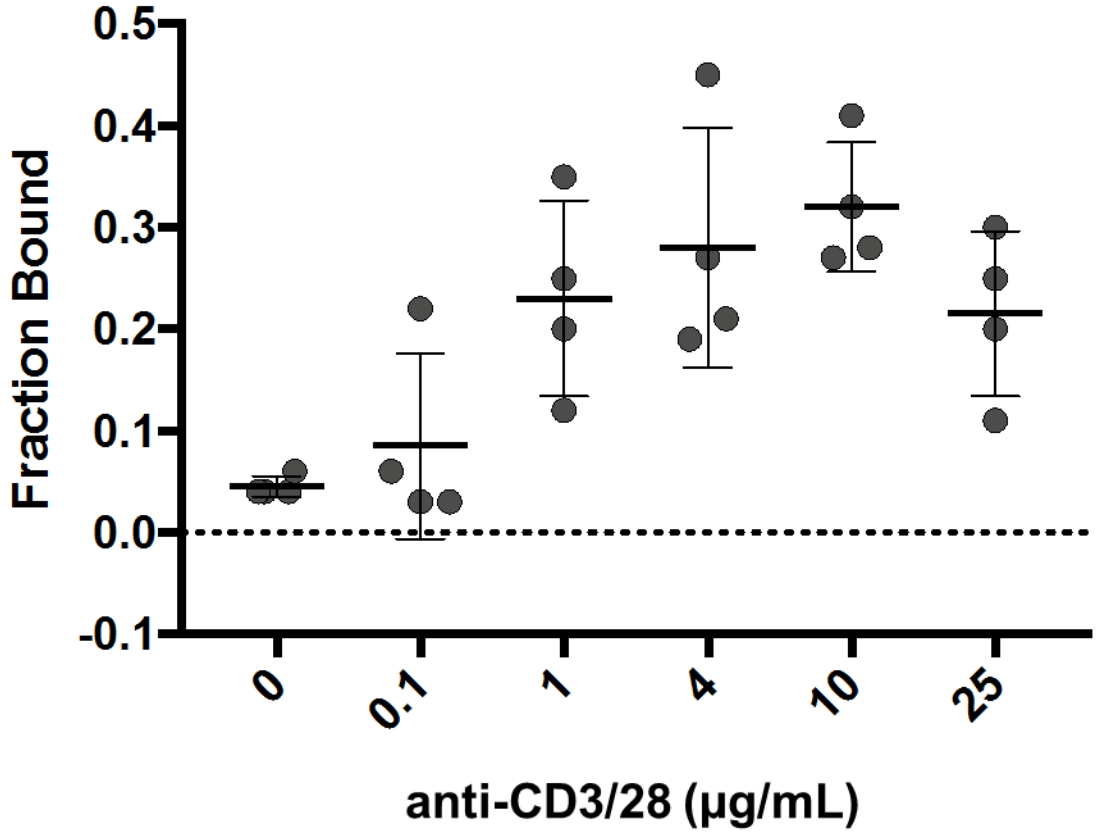

Figure 6-23: Quantitation of fraction of human CD8+ T cells bound to aTM hydrogels of different anti-CD3 and anti-CD28 concentrations after 1 hour of imaging.

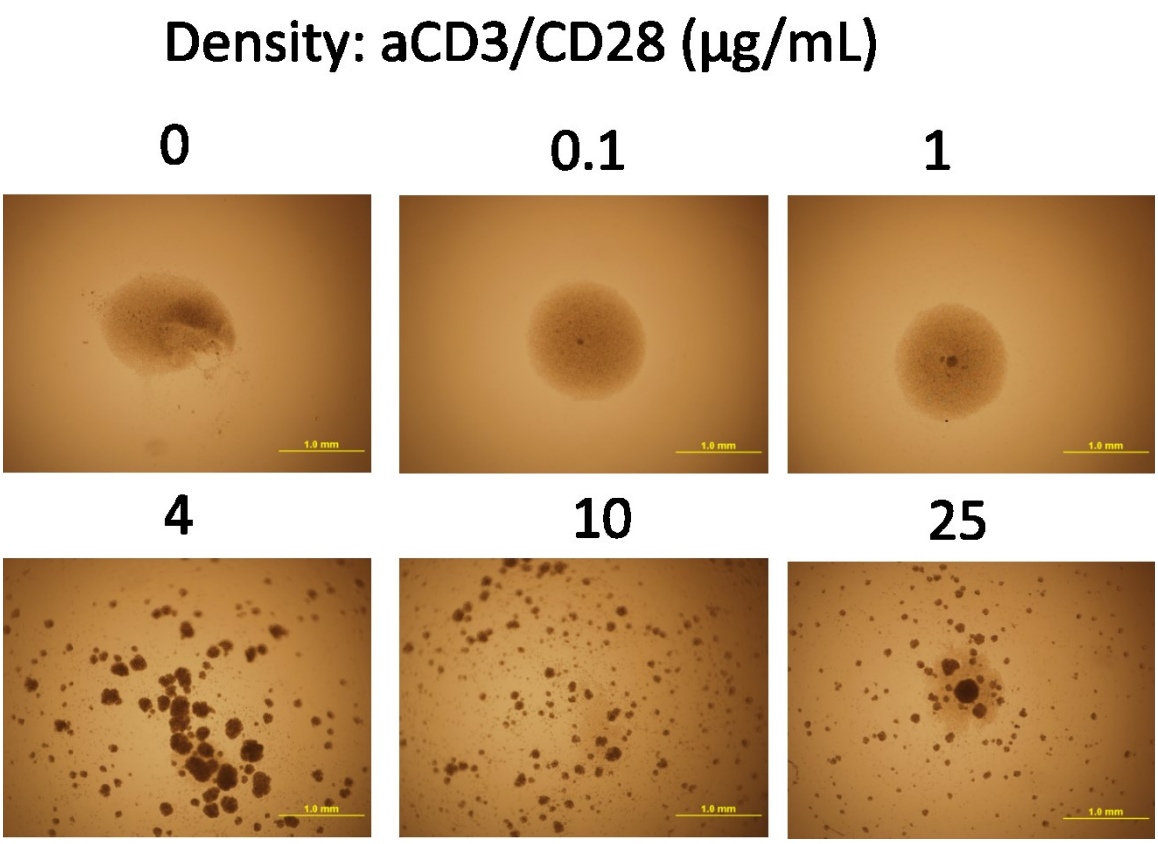

Figure 6-24: Representative light microscopy images of T cell cultures on aTMs with different density of aCD3/CD28 attached (0, 0.1, 1, 4, 10, and 25 µg/mL) (scale bar = 1mm).

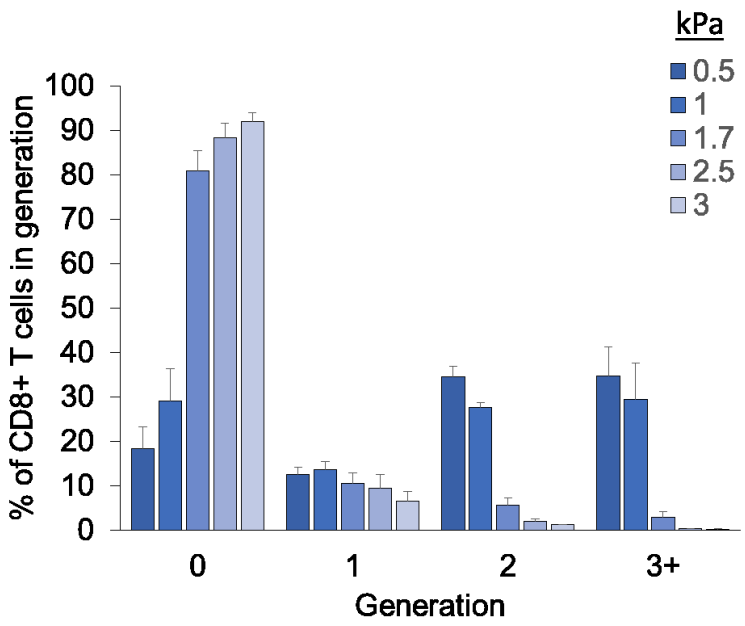

Figure 6-25: Quantitation of percentage of human CD8+ T cells in each divisional generation based on CFSE proliferation dye dilution with T cells stimulated on aTM with different stiffness with 4 µg/mL anti-CD3/CD28 (error bars show s.e.m, n = 3 independent donors).

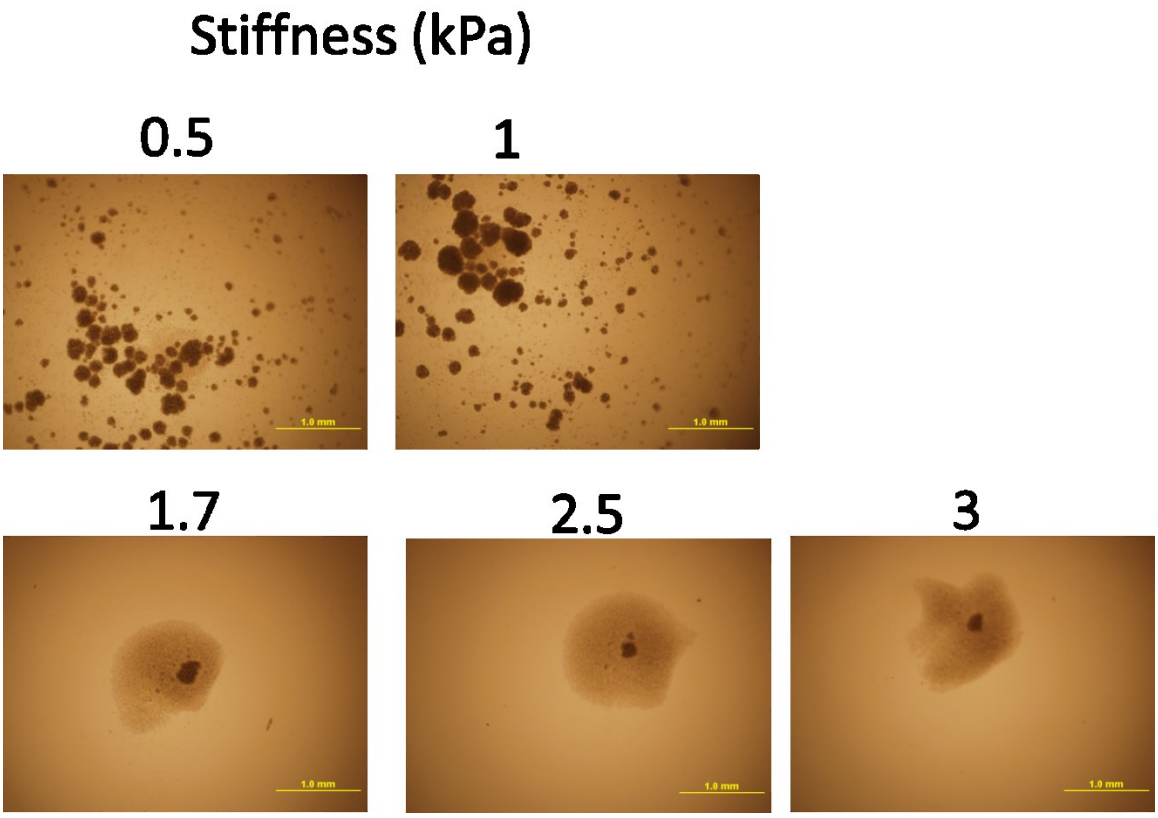

Figure 6-26: Representative light microscopy images of T cell cultures on aTMs with different stiffness (0.5, 1, 1.7, 2.5, 3 kPa) (scale bar = 1mm).

6.2.5 aTM-stimulated Endogenous, Antigen-specific T Cells Inhibit Established Tumor Growth

A main goal of ACT is to be able expand rare (frequency of 1 in 10^5 to 10^6 CD8+ T cells), antigen-specific CD8+ T cells to high numbers that are functional. Because of the difficulty in obtaining and activating these cells, most studies investigate the antigen-specific activation of T cells from transgenic mice or the non-specific activation of endogenous T cells. This limits clinical relevance because of lack of translatability and the monoclonality of these T cells. On the other hand, we investigated an optimized version of

the aTM in the setting of activating rare antigen-specific CD8+ T cells. Thus, instead of using non-specific Signal 1 (anti-CD3) we conjugate antigen-specific Signal 1 (pMHC: Kb-SIY) to aTM with costimulatory anti-CD28, and compared stimulating conditions similar to those used with T cells mixed with aAPC cultured on HA hydrogel or TCP surface.

After seven days of stimulation, we determined the antigen-specificity of the cultures and found that an average of 22% of the CD8+ T cells were antigen-specific from aTM cultures (**Figure 6-27**A). Indeed, we observed more than double the percentage of antigen-specific cells and more than quadruple the total number of antigen-specific cells expanded on aTM (**Figure 6-27**B, C). This highlights the importance of studying endogenous T cell activation where now differences are much larger between groups than when studying with transgenic cells or in non-specific activation. Such a drastic increase in cell number, even between the aTM and HA + aAPC groups where the only difference was the location of the stimulatory signals, is quite surprising. Therefore, the combination of both engaging the TCRs and CD28 from stimulatory signals conjugated to the soft hydrogel and direct interaction with the hyaluronic acid ECM hydrogel surface represents important progress in activating antigen-specific T cells effectively.

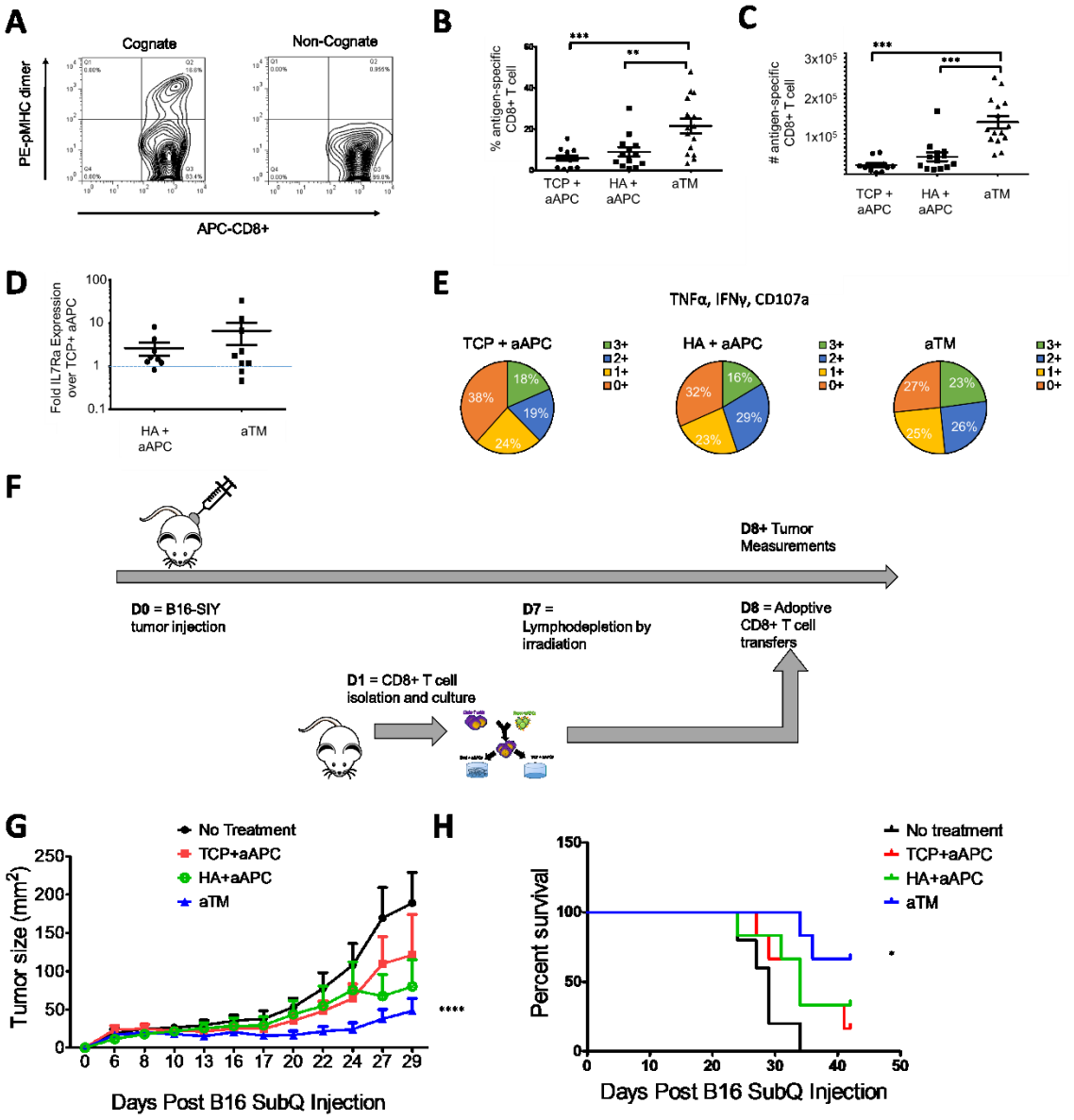

Figure 6-27: aTM stimulates a greater number and percent of functional antigen-specific CD8+ T cells that provide more effective tumor treatment. (A, B) Percentage of antigen-specific T cells after 7 days of stimulation is determined by staining with cognate and non-cognate antigen-loaded peptide major histocompatibility complex (pMHC) and anti-CD8a. (B, C) Percentages (B) and numbers (C) of antigen-specific CD8+ T cells stimulated by aTM, or by aAPC on either TCP or HA hydrogel surface (error bars show s.e.m.; $^{**}p < 0.01$, $^{***}p < 0.001$, n = 12-15, one-way ANOVA with Tukey's post test). (D) Fold IL7Ra expression on antigen-specific CD8+ T cells from HA+ aAPC and aTM compared to IL7Ra expression on antigen-specific CD8+ T cells from TCP + aAPC (error bars show s.e.m., n = 8–9). (E) T cell functionality was measured by the number of functional molecules co-expressed by each antigen-specific cell (IFN-γ, TNFα, CD107a) after 7 days of stimulation (n = 5–7). (F) Murine melanoma therapeutic in vivo model for adoptively transferred cells. (G) Tumor size measurements indicate that adoptive T cells from aTM stimulation significantly delayed tumor growth. Significance measured by two-way ANOVA with Bonferroni post-test ($p < 0.0001$) and (H) significantly extended survival. Significance measured by log-rank test ($p = 0.05$, n = 5–6).

Since we had observed differences in the IL7Ra expression and functionality of the CD8+ T cells cultured on the HA hydrogel, we also probed antigen-specific cells after seven days of stimulation for these markers. We again observed an increase in both the IL7Ra (**Figure 6-27**D) and the functionality associated with an increase in the percent of SIY+ T cells that were positive for multiple cytokines and degranulation markers (**Figure 6-27**E, **Figure 6-28**), and was confirmed by an *in vitro* killing assay (**Figure 6-29**). This is significant, because it shows that aTM is capable of generating higher numbers of functional antigen-specific CD8+ T cells. We also confirmed that these findings were consistent with CD8+ T cells isolated from mice with established tumors (**Figure 6-30**), and that we could expand human antigen-specific T cells with aTM specific for CMV+ CD8+ human T cells (**Figure 6-31**).

Figure 6-28: Intracellular cytokine and functionality staining of antigen-specific CD8+ T cells on day 7 reveals that aTM stimulations provide functional cells by (A) CD107a, (B) IFNγ, (C) TNFα staining (n=5-7, error bars represent s.e.m.).

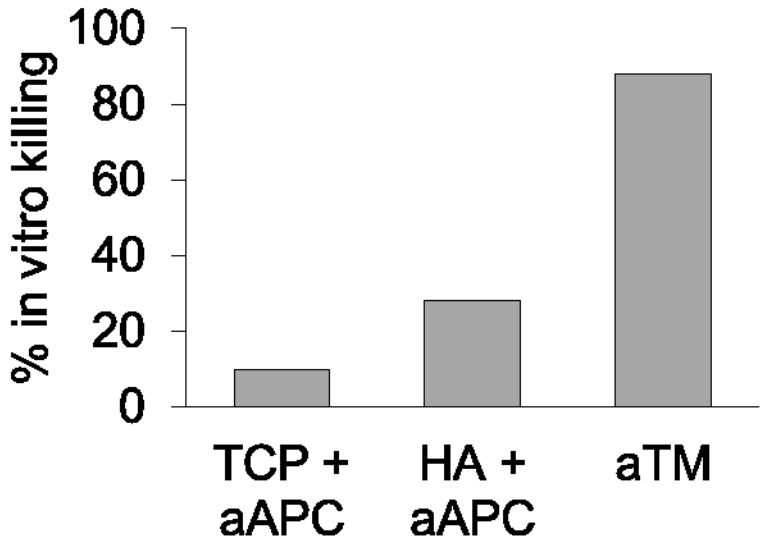

Figure 6-29: In vitro killing assay demonstrates that aTM-stimulated antigen-specific CD8+ T cells are most effective at killing target cells.

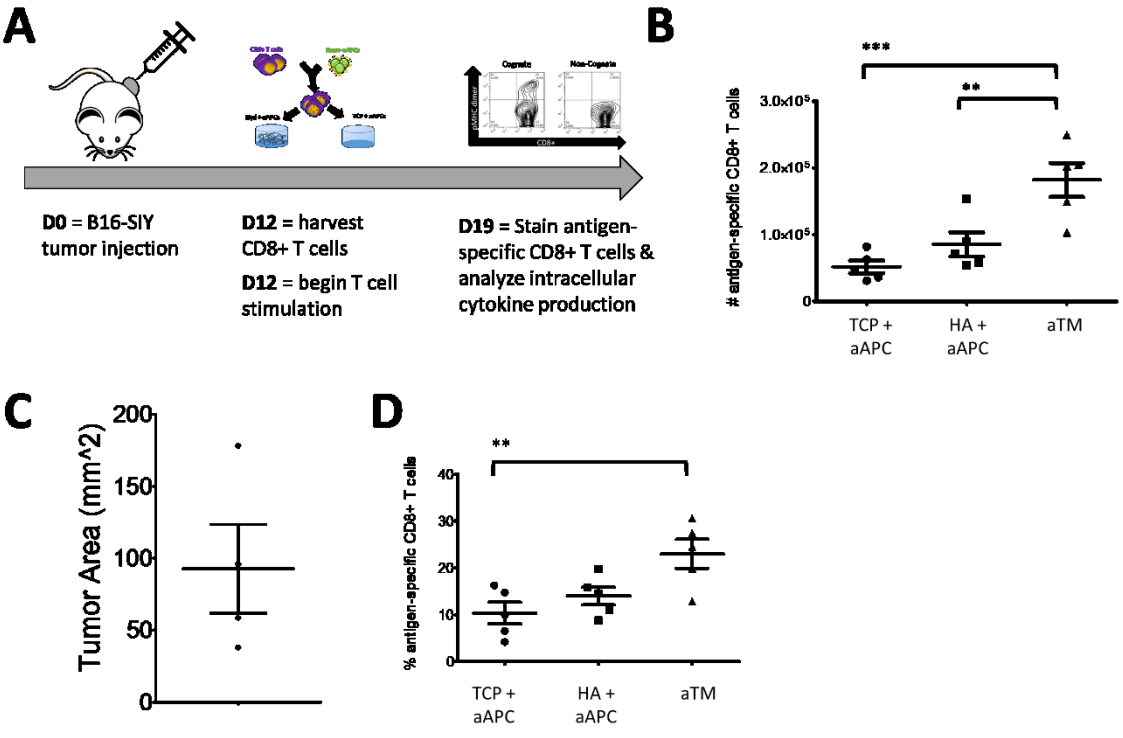

Figure 6-30: aTM provides an effective stimulation from tumor-experienced antigen-specific cells. (A) Schematic of experimental set up to test if aTM can provide additional support to stimulate tumor-experienced antigen-specific T cells. (B) Number of antigen-specific CD8+ T cells at day 7 of culture as measured by hemocytometry and cognate dimer staining by flow cytometry (error bars show s.e.m.; *p <

0.05, **p < 0.01, n = 5, one-way ANOVA with Tukey's post test). (C) Size of B16-SIY tumors at day 12 post-injection (n=4). (D) Percent of antigen-specific CD8+ T cells at day 7 of culture as measured by cognate dimer staining by flow cytometry (error bars show s.e.m.; **p < 0.01, n = 5, one-way ANOVA with Tukey's post test).

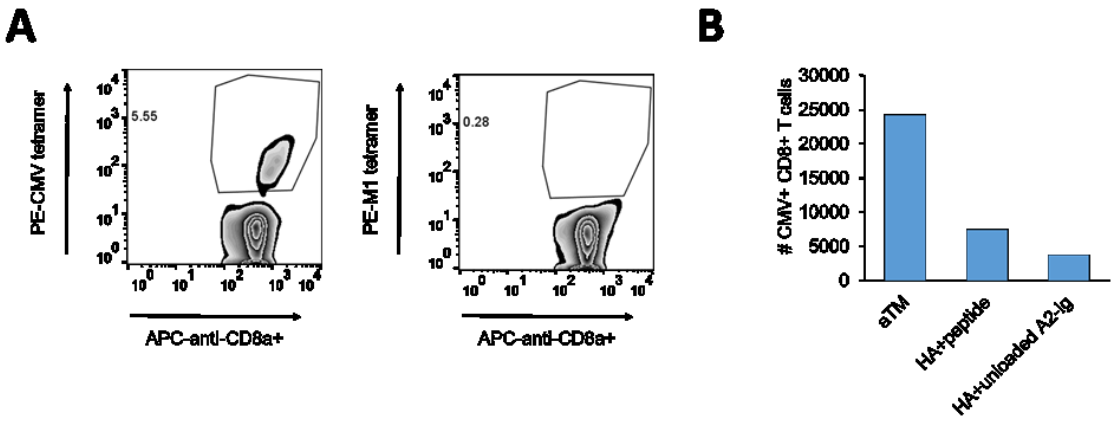

Figure 6-31: aTM can stimulate antigen-specific human CD8+ T cells. (A) aTM-stimulated CMV+, CD8+ T cells were stained on day 7 of culture with cognate CMV-tetramer and non-cognate M1-tetramer to determine the percentage of antigen-specific T cells. (B) aTM produce more than four times as many CMV+, CD8+ T cells by day 7 than controls: peptide pulsing without Signal 1 and 2 attached or no-peptide with Signal 1 and 2 attached (n = 1).

Finally, we tested the *in vivo* activity of aTM-stimulated and expanded T cells in an ACT model where T cells were transferred into mice with established B16-SIY melanoma tumors (**Figure 6-27**F). T cells stimulated by aTM significantly reduced tumor growth as compared to T cells on other surfaces and no treatment controls. Even on day 29, tumors in the group receiving aTM-stimulated T cells were stable below 50 mm^2 (**Figure 6-27**G, **Figure 6-32**). This treatment also resulted in improved survival rate. By day 40, none among the no treatment group, 16% of TCP + aAPC treated mice, 33% of HA+ aAPC treated group survived, in contrast, 66% of mice survived after receiving aTM-stimulated T cells at the same dose (**Figure 6-27**H). Furthermore, there was no significant difference in the percentage of transferred cells 21 days after transfer (**Figure 6-33**). Thus, T cells

stimulated on the aTM had significantly increased efficacy compared to those stimulated with traditional methods. In conclusion, the aTM offers a unique combination of an ECM cue and stiffness-mediated mechanical signaling through the TCR. It was only when these two parameters were combined and optimized which resulted in effective antigen-specific expansion, phenotype skewing, and effective control of an established, aggressive, immunosuppressive murine melanoma.

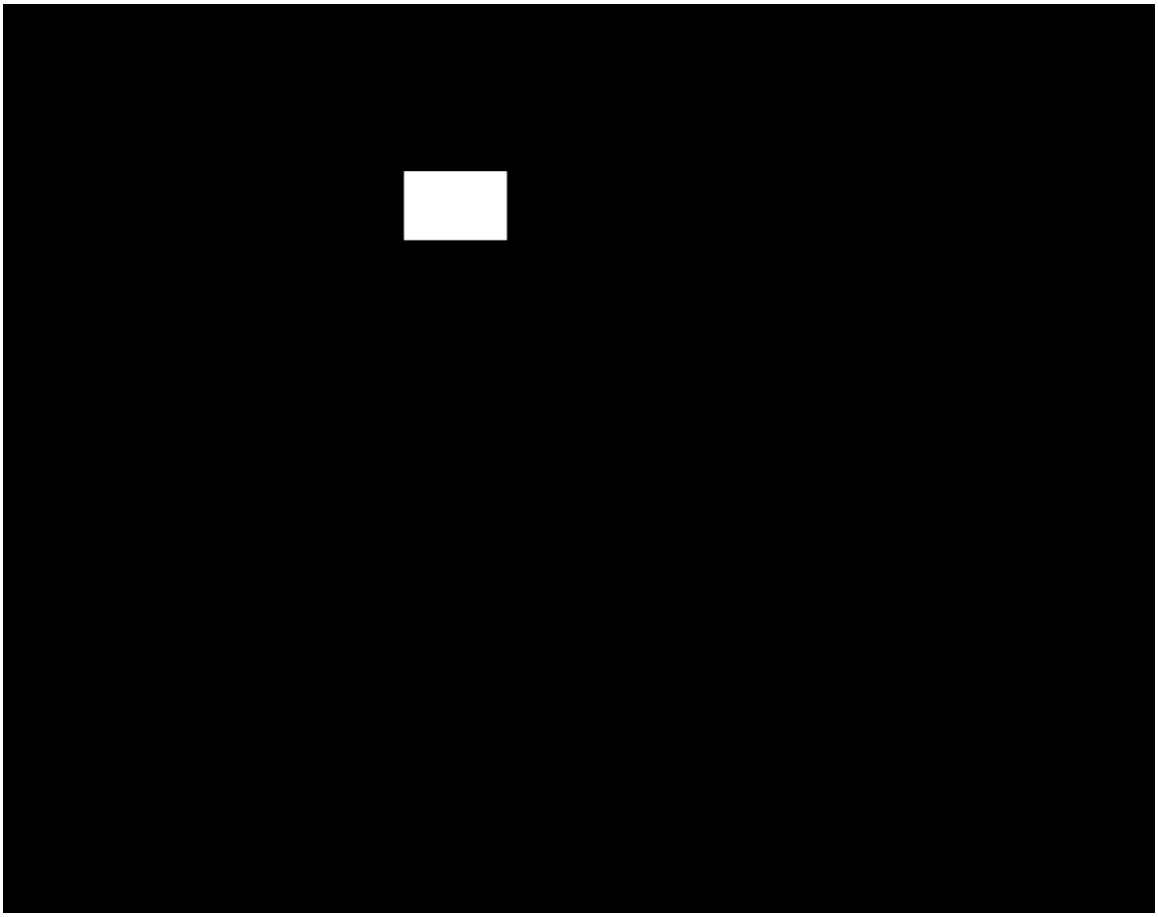

Figure 6-32: Individual growth curves from mice with tumors for each treatment group (A) No treatment (B) TCP+aAPC (C) HA+aAPC (D) aTM.

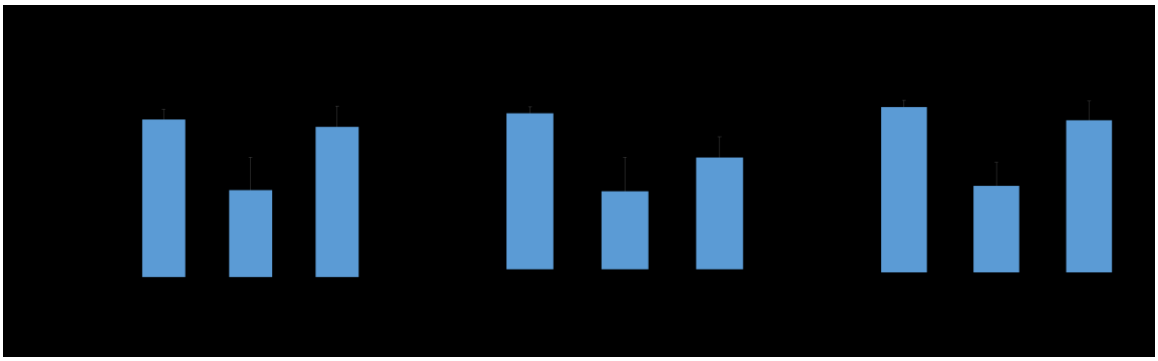

Figure 6-33: Percentage of Thy1.1+ (adoptively transferred CD8+ T cells) on day 21 after adoptive transfer. No significant differences were observed between groups in the (A) Spleen, (B) lymph nodes, or (C) blood compartments by flow cytometry (error bars show s.e.m., n=3).

6.3 Conclusion

Herein we have engineered an artificial T cell stimulating matrix (aTM). By considering the native T cell biology we designed the aTM through mimicking critical features of both the natural extracellular matrix (ECM) and the antigen presenting cells. We conjugated T-cell stimulating molecules to develop the first ECM-based T cell activation biomaterial. The density of the signal attached and stiffness were key biophysical parameters engineered that influenced the ability for both murine and human CD8+ T cells to interact and be stimulated by the aTM. Additionally, we utilized a hyaluronic acid (HA) as an ECM molecule and found that it provides an additional signaling component influencing both the activation and polarization of T cells. By fine-tuning these biophysical properties, the aTM produced four times as many functional, therapeutic antigen-specific CD8+ T cells than current stimulation materials—resulting in more effective tumor inhibition. Additional work will need to be done to continue to study the underlying signaling implications for why biophysical properties of the aTM confer improved T cell activation. This has implications for adoptive T cell and CAR T cell therapies, where large numbers of high quality antigen-specific T cells are needed[306,510,511]. Engineering the

environment with ECM modulation represents a new approach to control T cell activation, where previously researchers have focused on cytokine cocktails, and generating artificial cells using particles or scaffolds instead of environmental cues[103,267,368]. Finally, besides creating an *ex vivo* environment for T cell activation, the aTM has the potential to be applied for direct T cell activation *in vivo,* thus eliminating the need for *ex vivo* T cell manipulation[367].

6.4 Experimental Section

Mice

B6, 2C, and PMEL transgenic mice were maintained per guidelines approved by the Johns Hopkins University's Institutional Review Board.

Reagents

Soluble MHC-Ig dimers loaded with peptides (pMHC-Ig) and artificial antigen presenting cells (aAPC) were produced in-house as described[103,250].

Hydrogel Preparation

Thiol-modified hyaluronic acid (HA) (ESI BIO, Alameda, CA, USA) was resuspended with 1 mL sterile dH_2O and incubated at 37 °C for 30 minutes until completely dissolved to form 1% HA solution in 1× PBS. To form hydrogels, HA was plated immediately after getting mixed with polyethylene glycol diacrylate (PEGDA) with a molecular weight of 3400 (Laysan Bio, Arab, AL) crosslinker at a 4:1 volume ratio to fully cover the well. Plated hydrogels were incubated for a minimum of 1 hour prior to cell culture.

Preparation of aTM

HA solution was prepared as previously described. Anti-CD3 and anti-CD28 antibodies were purchased respectively from BioXCell (145-2C11; West Lebanon, NH, USA) and BioLegend (37.51; San Diego, CA, USA). Antibody and MHC-Ig dimers were partially reduced with 100 mM dithiothreitol (DTT) for 30 minutes at room temperature to expose free thiol groups and thoroughly washed through a centrifugation filtration with a 50-kDa MWCO filter. PEGDA crosslinker was added to reduced MHC-Ig dimers, anti-CD3 and anti-CD28 antibody solutions to a final concentration of 0.5% PEGDA for preparation for

crosslinking. This results in at least a 200-fold excess of PEGDA to antibody ratio, which prevents thiol oxidation and long-term storage of antibody-PEGDA conjugates and that antibody can be attached effectively to the thiolated HA hydrogel. Prior to hydrogel formation, MHC-Ig dimers or anti-CD3 antibodies and anti-CD28 co-stimulatory signals with 0.5% PEGDA were added to the HA solution to directly attach signals on HA through thiol-diene chemistry. The HA-antibody solution was then mixed with PEGDA crosslinker at a 4:1 ratio to be plated. The aTM was allowed to form within flat-bottomed tissue culture plates to form a complete layer for at least 1 hour prior to washing 3 times with 1× PBS to remove any unbound stimulatory signal and cells were subsequently plated. To investigate the effects of extracellular matrix (ECM) protein attachment, cyclic RGD (sequence: CCRRGDWLC), which was synthesized by solid phase methods as described previously[512] or laminin (ThermoFisher) were added to make a HA solution with protein concentration of respectively 100 μM and 20 μg/mL, prior to the hydrogel formation. To investigate the stiffness effects of aTMs, we changed the PEGDA crosslinker concentration from a final concentration of 0.05 wt/vol% to 2 wt/vol%.

Characterization of aTM

To evaluate the mechanical stiffness of aTMs, elastic moduli of hydrogels were measured using Ares G2 oscillatory shear rheometer. First, HA solution was mixed with varying PEGDA crosslinker concentrations to a final volume of 200 μL and placed immediately on the stationary lower plate of the rheometer. The shear storage modulus, G', and the sheer loss modulus, G", were recorded during in situ hydrogel formation over one hour at 37 °C. The elastic modulus, E', was calculated by $E' = 2G'(1+\gamma)$ where γ is the Poisson's ratio. For HA hydrogels, we assumed γ to be 0.5 because the Poisson's ratio of

incompressible materials is approximately 0.5 and the hydrogels are used under low strain conditions[488].

For scanning electron microscopy (SEM), hydrogels were cross-linked overnight at 37^{0}C and subsequently flash frozen in liquid nitrogen for 5 minutes. Samples were placed in the FreeZone 4.5 Benchtop (LABCONCO) freeze dry system for 72 hours for complete dehydration of samples. Samples were coated using a Desk III (Denton Vacuum) Au/Pd sputter coater for 2 mins at 25mA before imaging in LEO 435 VP SEM.

To evaluate the conjugation to the surface of the hydrogel, we stained both HA hydrogels with no antibodies attached and HA hydrogels with 10 μg/mL anti-CD3, anti-CD28 in black 96-well half area wells. We stained with FITC-anti-Armenian and Syrian Hamster IgG, clone G192-1 and FITC-anti-Armenian and Syrian Hamster IgG1, clone G94-56 (BD Pharminogen) for 5 minutes at 4 °C. Then the surfaces of the hydrogels were washed 5 times with PBS and then the fluorescence per well was read on a fluorescent plate reader and compared to a standard curve of the fluorescent antibodies titrated down the plate. To estimate the density of the ligand on the surface of the aTM, the thickness observed by cells was assumed to be 1 μm, and then the density was calculated based off the total mass of Signal 1 and 2 within this slab and then dividing by the surface area.

CD8+ T Lymphocyte Isolation

Murine cells were obtained from adult mouse lymph nodes and spleens. Obtained cells were treated with ACK lysing buffer to lyse red blood cells and filtered through cell strainers to isolate splenocytes. PBMCs from healthy donors were isolated by Ficoll-Paque PLUS gradient centrifugation (GE Healthcare). CD8+ T lymphocytes were then isolated from splenocytes or PBMCs by negative selection using CD8+ isolation kits and

magnetic columns from Miltenyi Biotech (Auburn, CA, USA) according to the manufacturer's protocol. PBMCs were obtained from blood drawn from healthy males and females per JHU IRB approved protocols.

Ex Vivo T Cell Culture and Activation

For *ex vivo* T cell expansion, isolated CD8+ T cells were cultured in the T cell culture media (RPMI supplemented with L-glutamine, non- essential amino acids, vitamin solution, sodium pyruvate, β-mercaptoethanol, 10% fetal bovine serum, ciproflaxin, and a cocktail of T cell growth factors as described previously[513]). In the case of human T cell expansion, 10% AB serum was used instead of 10% fetal bovine serum. On day 3 or 4 of culture, cells were fed with half the volume of the initial T cell culture media with twice the concentration of T cell growth factor cocktail.

For activation with aAPC, T cells were co-cultured with a concentration of 75 pM-bound pMHC-Ig on the aAPC and then plated on respective surfaces. For stimulation on the aTM, cells were plated on the surfaces aTM with concentrations of the stimulatory antibody (either anti-CD3 and anti-CD28 or pMHC-Ig and anti-CD28) conjugated to the HA hydrogel.

T Cell Proliferation Assay

CD8+ T cells were isolated as previous described and resuspended in 1 mL T cell culture media. Cells were mixed with 1 μL CellTrace™ carboxyfluorescein succinimidyl ester (CFSE) dye (ThermoFisher) in 1 mL T cell culture media per 3 million cells and incubated at 37 °C for 20 minutes. CFSE stained cells were washed with 50 mL T cell culture media to remove unstained dye and plated. On day 3 of culture, cells were harvested and stained with a 1:100 PBS solution of APC-conjugated rat anti-mouse

CD8a, clone 53-6.7 (BD Pharmingen) for 15 minutes at 4 °C. The CFSE fluorescence intensity was measured using BD FACSCalibur flow cytometer. Cell proliferation was analyzed using FlowJo with diluted CFSE fluorescence peaks signifying population after each round of cell division. A subset of the cells were allowed to expand for 7 days and viable cells were counted with a hemocytometer to determine fold expansion. Images of cell cultures were taken with an Olympus IX71 inverted light microscope at a 4× magnification on day 3 of cultures.

Time Course Experiments

Two million purified CD8+ T cells from either PMEL or 2C mice were cultured on HA or TCP conditions. The cells were collected at designated time points. These cells were frozen down in liquid nitrogen for western blots, stored in TRIzol for mRNA detection, or PFA fixed for phospho-flow. For drugs, the final concentration of rapamycin (mTORC1 inhibitor), U-0126 (Erk1/2 inhibitor), blebbistatin, and anti-CD44 (KM201) were 0.1 μM, 10 μM, 100 μM, and 5 μg/mL, respectively. Half-volumes of T cell culture media is added every other day to keep cells in good condition. For western blot and rt-PCR, live cells that have been cultured for more than 24 hours were first purified using Ficoll-Paque followed by the procedure mentioned above.

Western Blot

Frozen cells were lysed in a radioimmunoprecipitation assay (RIPA) buffer-based mixture containing proteinase inhibitor, PMSF (phenylmethane sulfonyl fluoride), sodium pyrophosphate, sodium fluoride, sodium orthovanadate, and β-glycerophosphate to inhibit phosphatases. Then, protein samples underwent standard western blot procedure with 1-2 hours of incubation in 5% milk, overnight incubation in primary

antibodies (in 4% BSA), and 1hr incubation in secondary antibodies. Films were imaged in a UVP BioSpectrum Imaging System, analyzed in UVP VisionWorks and quantified in ImageJ. Antibodies used include:

Target	Cat#	Vendor
p-S6 (S240/244)	2215	Cell Signaling
p-Erk (Y202/204)	4695	Cell Signaling
Beta-actin	4970	Cell Signaling
p-S6K1 (T389)	9234	Cell Signaling
p-AKT (S473)	3787	Cell Signaling
Total Lck	2752	Cell Signaling
p-Lck (Y505)	2751	Cell Signaling
p-Src (Y416)	2101	Cell Signaling

RT-PCR

Cells were kept in TRIzol in -80℃ for storage. mRNA was purified using Zymo Quick-RNA MiniPrep Kit. Then, reaction mix was prepared based on standard RT-PCR protocol. Probes were from TaqMan FAM/MGB probes with VIC/TAMRA Eukaryotic 18S rRNA as an endogenous control (ThermoFisher). Samples were run in quintuplicate in Applied Biosystems StepOnePlus Real-Time PCR system and analyzed using Excel.

Phosphorylation Flow Cytometry

Cells were first stained with Live/Dead stain and then were fixed using BD Phosflow Fix Buffer I at room temperature for 10 minutes. After washing, cells were permeabilized using ice cold BD Phosflow Perm Buffer II for 30 minutes on ice. Samples were then stained with a solution of FACS wash buffer with 1:50 PE conjugated rat anti mouse CD8a, clone 53 6.7 (BD Pharmingen) and a 1:100 Rabbit anti Phospho S6 Ribosomal Protein (Ser235/236), clone

D57.2.2E, or Rabbit IgG Isotype Control, clone DA1E (Cell Signaling Technology, Danvers, Massachusetts) for 45 minutes at room temperature. Samples were then washed with FACS wash buffer and then stained with a solution of FACS wash buffer with 1:250 of Alexa Fluor 647-conjugated Goat S22 anti Rabbit IgG, polyclonal (ThermoFisher) for 45 minutes at room temperature. Samples were washed and resuspended with FACS wash buffer and read on a BD FACSCalibur.

T Cell Phenotype Assay

On day 7 of culture, the numbers of cells were counted using hemocytometer. After counting, less than 500,000 cells were collected and stained with a 1:100 PBS solution of APC-conjugated rat anti-mouse CD8a, clone 53-6.7 (BD Pharmingen), PE-conjugated rat anti-mouse CD62L, clone MEL-14 (BD Pharmingen), PerCP-conjugated rat anti-mouse CD44, clone IM7 (Biolegend), and 1:1000 of LIVE/DEAD® Fixable Green Dead Cell Stain (ThermoFisher) for 15 minutes at 4 °C. Cells were then washed with FACS wash buffer to be read on BD FACSCalibur flow cytometer and analyzed using FlowJo to measure the population of naïve T cells (CD62L+CD44-), effector T cells (CD62L-CD44+), and memory T cells (CD62L+CD44+). For human phenotype experiments, the same protocol was used except, the cells were instead stained with a 1:100 PBS solution of APC-conjugated anti-human CD45RA, Clone HI100 (Biolegend), PE-conjugated anti-human CD62L, clone DREG-56 (Biolegend), PerCP-conjugated anti-human CD8a, clone SK-1 (Biolegend), and 1:1000 of LIVE/DEAD® Fixable Green Dead Cell Stain for 15 minutes at 4 °C. Cells were then washed with FACS wash buffer to be read on BD FACSCalibur flow cytometer and analyzed using FlowJo to measure the population of

naïve T cells (CD62L-CD45RA-), effector T cells (CD62L-CD45RA+), central memory T cells (CD62L+CD45RA-), and effector memory T cells (CD62L-CD45RA-).

For analysis of IL-7Ra and IL-15Ra expression on cells, on day 7 of culture, the numbers of cells were counted using hemocytometer. After counting, samples were divided into four tubes (less than 500,000 cells per tube) and stained with a 1:100 PBS solution of APC-conjugated rat anti-mouse CD8a, clone 53-6.7 (BD Pharmingen), 1:1000 of LIVE/DEAD® Fixable Green Dead Cell Stain (ThermoFisher), and either PE-conjugated rat anti-mouse IL7Ra, clone A7R34 (Biolegend), or isotype control PE-conjugated Rat IgG2a, κ Isotype Ctrl, clone RTK2758 (Biolegened), or PE-conjugated rat anti-mouse IL15Ra, clone DNT15Ra (eBioscience), or isotype control PE-conjugated Rat IgG1, κ Isotype Ctrl, clone eBRG1 (eBioscience), for 15 minutes at 4 °C. Cells were then washed with FACS wash buffer to be read on BD FACSCalibur flow cytometer and analyzed using FlowJo.

T Cell Cytokine Functionality Assay

On day 7 of culture, approximately 500,000 CD8+ T cells were isolated from each condition and separated into restimulation and no-stimulation groups in 100 µL T cell culture media. To inhibit protein transport, 10 µL solution of 1:50 FITC anti-CD107a, 1:350 BD GolgiStop Protein Transport Inhibitor (BD Biosciences), and 1:350 BD GolgiPlug Protein Transport Inhibitor (BD Biosciences) in PBS was added to the samples. For the restimulation group, microparticle Dyanl-based aAPC were added at a 1:1 ratio. Both groups were incubated at 37 °C for 6 hours. After incubation, cells were washed and stained with 1:100 PBS solution of PerCP-conjugated anti-mouse CD8a, clone 53-6.7 (Biolegend) and 1:1000 of LIVE/DEAD® AmCyan Fixable Aqua Dead Cell

Stain (ThermoFisher) at 4 °C for 30 minutes. Cells were then fixed and permeabilized with 100 μL BD Cytofix/Cytoperm Fixation and Permeabilization Solution (BD Biosciences) overnight. To analyze intracellular cytokines, cells were washed with 1x BD PERM/Wash buffer with 2% BSA the following day and stained with 1:100 solution of PE-conjugated rat anti-mouse IFN-γ, clone XMG1.2 (BD Pharmingen), APC-conjugated rat anti-mouse IL2, clone JES6-5H4 (BD Pharmingen), and PE-Cy7-conjugated rat anti-mouse TNFα, clone MP6-XT22 (Biolegend) in PERM/Wash buffer with 2% BSA at 4 °C for 1 hour. Stained cells were read on BD LSR II flow cytometer and analyzed by subtracting cytokine positive cells in the no-stimulation group from the re-stimulation group using FlowJo.

For antigen-specific cells a similar assay was used with the following modifications. Instead of a restimulation, cells were simply stained with 1 μg of either cognate or non-cognate biotinylated pMHC-Ig dimer for 1 hour at 4°C. After washing, samples were stained with a 1:350 ratio of PE-labeled streptavidin (BD Pharmingen). Then 10 μL solution of 1:50 FITC anti-CD107a, 1:350 BD GolgiStop Protein Transport Inhibitor (BD Biosciences), and 1:350 BD GolgiPlug Protein Transport Inhibitor (BD Biosciences) in PBS was added to the samples and incubated for 37 °C for 6 hours. Cells were then washed and stained with 1:100 PBS solution of PerCP-conjugated anti-mouse CD8a, clone 53-6.7 (Biolegend) and 1:1000 of LIVE/DEAD® AmCyan Fixable Aqua Dead Cell Stain (ThermoFisher) at 4 °C for 30 minutes. Cells were then fixed and permeabilized with 100 μL BD Cytofix/Cytoperm Fixation and Permeabilization Solution (BD Biosciences) overnight. Cells were then washed with 1x BD PERM/Wash buffer with 2% BSA and stained with 1:100 solution of APC-conjugated rat anti-mouse IFN-γ, clone

XMG1.2 (BD Pharmingen) and PE-Cy7-conjugated rat anti-mouse TNFα, clone MP6-XT22 (Biolegend) in PERM/Wash buffer with 2% BSA at 4 °C for 1 hour. Stained cells were read on BD LSR II flow cytometer.

In Situ Staining and Super-resolution Microscopy

CD8+ T cells were added to the surface of the aTM hydrogels and allowed to culture at 37 °C for 1 hour. Gels were fixed with 4% PFA for 20 minutes at room temperature, followed by permeabilization, and staining with Alexafluor phalloidin-564 and CD3 (Novus Biologicals). The secondary antibody used was Alexafluor-488. Gels were mounted on coverslips and imaged using the Zeiss 800 confocal microscope equipped with an AiryScan detector. Airyscan super-resolution images were processed using Zen software. Quantification of CD3 spot area was performed in FIJI/ImageJ using the analyze particles function.

Expansion of Rare Antigen-Specific T cells

B6 CD8+ T cells were stimulated on aTM surfaces as described previously for 7 days. To detect antigen-specific CD8+ T cells, cells were stained with 1 µg of either cognate or non-cognate biotinylated pMHC-Ig dimer, with a 1:100 ratio of APC-conjugated rat anti-mouse CD8a, clone 53-6.7 (BD Pharmingen) in FACS wash buffer for 1 hour at 4°C. Samples were washed and then stained with a 1:350 ratio of PE-labeled streptavidin (BD Pharmingen) and a 1:1000 ratio of LIVE/DEAD™ Fixable Green Dead Cell Stain (ThermoFisher) in PBS for 15 minutes at 4°C. Cells were then washed and read on a BD FACSCalibur. Percent antigen-specific cells were calculated by subtracting the percent gated in cognate stained CD8+ T cells from non-cognate stained CD8+ T cells. Number of antigen-specific cells was determined from multiplying the percent of antigen-specific

cells by the number counted following cell harvest. Detection of antigen-specific human cells was done similarly, except instead of staining with biotynlated dimer, the antigen-specific cells were stained with purchased PE-labeled tetramer (MBL International, Woburn, MA) for 30 minutes at room temperature, then washed and stained with APC-conjugated anti-human CD8a, clone SK-1 (Biolegend), and 1:1000 of LIVE/DEAD® Fixable Green Dead Cell Stain for 15 minutes at 4 °C.

For expansion of rare T cells from tumor-experienced mice, mice were injected with 2×10^6 B16-SIY melanoma tumor cells expressing the SIY antigen and tumors were allowed to grow until on average were around 100 mm^2. CD8+ T cells were then harvested from the lymph nodes and spleens as previously described and expansion and detection were performed as previously described.

For analysis of IL7Ra of antigen-specific T cells, a similar process was used. Cells were stained with 1 μg of either cognate or non-cognate biotinylated pMHC-Ig dimer, with a 1:100 ratio of PerCP-conjugated rat anti-mouse CD8a, clone 53-6.7 (BD Pharmingen) in FACS wash buffer for 1 hour at 4°C. Samples were washed and then stained with a 1:350 ratio of PE-labeled streptavidin (BD Pharmingen), either APC-conjugated rat anti-mouse IL7Ra, clone A7R34 (Biolegend) or isotype control APC-conjugated Rat IgG2a, κ Isotype Ctrl, clone RTK2758 (Biolegend), and a 1:1000 ratio of LIVE/DEAD™ Fixable Green Dead Cell Stain (ThermoFisher) in PBS for 15 minutes at 4°C.

In Vitro Killing Assay

Target cells were harvested from splenocytes of B6 mice. 20 x 10^6 splenocytes were labeled with a high concentration of CFSE (5 μM) and another was labeled with a low concentration of CFSE (0.05 μM) in 1 mL of PBS at 37°C for 10 min (Invitrogen,

Eugene, OR). Media with FBS was added to quench the reaction and allowed to incubate at 37°C for another 5 min and then washed with media. The CFSE-high cells were then incubated at 37°C for 1 hour with 1 μM SIY peptide in media without serum. The cells were then washed and mixed at a 1:1 ratio with control non-target, CFSE-low splenocytes. This mixed population was added to CD8+ T cells which had been stimulated for 7 days at a 1:1 ratio and allowed to incubate for 18 hours at 37°C in a cell incubator. Then cells were washed, stained with a 1:1000 of LIVE/DEAD® AmCyan Fixable Aqua Dead Cell Stain (ThermoFisher) at 4 °C for 30 minutes. The cells were washed and read on a BD LSRII flow cytometer. The percent killing was calculated as follows: % of in vivo killing = 100 − ([(% specific peptide pulsed cells in treatment/% unspecific B6 cells in treatment)/(% specific peptide pulsed in no treatment controls/% unspecific B6 cells in no treatment controls)] × 100).

Therapeutic Adoptive Transfer of T Cells

On day 0, B6 mice were injected with 2×10^6 B16-SIY melanoma tumor cells expressing the SIY antigen. On day 1, CD8+ T cells were isolated from wildtype B6 mice and cultured for 7 days to produce stimulated T cells for adoptive transfer. On day 7, mice were given a central dose of 500 cGy, which induces transient lymphopenia similar standard approaches within adoptive immunotherapy[514]. On day 8, T cells cultured *ex vivo* were harvested and adoptively transferred intravenously in volumes of 100 μL. For every 3 mice receiving treatment, 1 B6 spleen was used for CD8+ T cell isolation and stimulation. This resulted in each mouse receiving 500,000 stimulated CD8+ T cells. Tumor sizes were measured using calipers and multiplying the longest measured length by the perpendicular direction of the tumor. Mice were sacrificed once tumors grew

larger than 200 mm^2. For studies involving persistence of cells, Thy1.1+ B6 donor mice were used. On day 21 blood, spleen, and lymph nodes were harvested from recipient mice and stained with a 1:100 ratio of APC-conjugated rat anti-mouse CD8a, clone 53-6.7 (BD Pharmingen) and 1:100 ratio of Alexa Fluor 488-conjugated mouse anti-mouse CD90.1 (Thy1.1), clone OX-7 (Biolegend) in FACS wash buffer for 15 minutes at 4°C.

Chapter 7. Contributions to Additional Research

7.1 Introduction

I was fortunate to be able to participate in a variety of research projects ancillary to the goals of the lab and my overall thesis goals in controlling biomaterial properties to understand and control T cell responses. Here I will only briefly summarize our major findings with these projects as these were not the focus of my PhD thesis. First, I will describe the projects I have contributed to for creating biodegradable aAPCs. Second, I will describe the projects I have contributed to towards other students in our lab. Finally, I will briefly mention some of the projects I have started, but did not progress at the rate that I had intended so they were eventually dropped or stopped.

7.2 Biodegradable aAPCs[4]

Biomimetic materials that target the immune system and generate an anti-tumor responses hold promise in augmenting cancer immunotherapy. These synthetic materials can be engineered and optimized for their biodegradability, physical parameters such as shape and size, and controlled release of immune-modulators. As these new platforms enter the playing field, it is imperative to understand their interaction with existing immunotherapies since single-targeted approaches have limited efficacy. Here, we investigated the synergy between a PLGA-based artificial antigen presenting cell (aAPC) and a checkpoint blockade molecule, anti-PD1 monoclonal antibody (mAb). The

[4] Sections of this chapter are reprinted (adapted) with permission from “Kosmides, A. K., et al. "Biomimetic biodegradable artificial antigen presenting cells synergize with PD-1 blockade to treat melanoma." Biomaterials 118 (2017): 16-26.” Copyright 2017 Elsevier.

combination of antigen-specific aAPC-based activation and anti-PD-1 mAb checkpoint blockade induced the greatest IFN-γ secretion by CD8+ T cells in vitro. Combination treatment also acted synergistically in an *in vivo* murine melanoma model to result in delayed tumor growth and extended survival, while either treatment alone had no effect. This was shown mechanistically to be due to decreased PD-1 expression and increased antigen-specific proliferation of CD8+ T cells within the tumor microenvironment and spleen. Thus, biomaterial-based therapy can synergize with other immunotherapies and motivates the translation of biomimetic combinatorial treatments[257]. Here my specific contribution was to complete the *in vivo* efficacy of the combination therapy and also evaluate the mechanism of action by further analyzing immune cells both within the tumor and other immune related organs like the lymph node and spleen.

We have also recently found that modulation of the base polymer which forms the aAPC can significantly increase the efficiency of binding and expansion of cognate T-cells. By incorporating a poly(beta-amino ester) (PBAE) into the PLGA-based microparticles, we have discovered that the resultant microparticles can bind in a targeted fashion to cognate T-cells with much greater efficiency than PLGA particles alone. Furthermore, this binding demonstrates a much higher capacity to stimulate cognate T cells for expansion at 100's-fold lower particle doses and is able to effectively stimulate endogenous antigen-specific T cell responses, something which previous biodegradable PLGA aAPCs were unable to do. We found that the PLGA/PBAE aAPCs absorb/conjugate a much higher amount of dimer and anti-CD28 potentially pointing to this as the mechanism of action of increased functionality. Consequently, we further tested these PLGA/PBAE aAPC formulation for activating the endogenous antigen-

specific T cells *in vivo*, where previous therapies were always in combination with transgenic CD8+ T adoptive T cell responses. From this preliminary trial we saw both a reduction in tumor burden and increase in overall survival.

We have also investigated the differences in particle shape when activating T cells because of the polymer flexibility and ability to be shaped when heated. Building off the group's previous work with microparticle aAPCs, we have looked at spherical, 1D-stretched, and 2D-stretched aAPCs. Interestingly, 1D-stretched aAPCs show most *in vivo* efficacy, while 2D-stretched aAPCs and spherical aAPCs have been less effective, although the 2D-stretched aAPCs have been just as effective as 1D-stretched aAPCs *in vitro*. Therefore, the shape of the aAPC influences not only the binding of the aAPC with cognate T cells, but also the biodistribution of the particles *in vivo* potentially causing differential *in vivo* effects.

7.3 Contributions to other Schneck lab projects[5]

T cell activation requires the coordination of a variety of signaling molecules including T cell receptor-specific signals and costimulatory signals. Altering the composition and distribution of costimulatory molecules during stimulation greatly affects T cell functionality for applications such as adoptive cell therapy (ACT), but the large diversity in these molecules complicates these studies. Here, we develop and validate a reductionist T cell activation platform that enables streamlined customization of stimulatory conditions. This platform is useful for the optimization of ACT protocols

[5] Sections of this chapter are reprinted (adapted) with permission from "Kosmides, Alyssa K., et al. "Separating T Cell Targeting Components onto Magnetically Clustered Nanoparticles Boosts Activation." Nano letters 18.3 (2018): 1916-1924." Copyright 2018 American Chemical Society.

as well as the more general study of immune T cell activation. Rather than decorating particles with both signal 1 antigen and signal 2 costimulus, we use distinct, monospecific, paramagnetic nanoparticles, which are then clustered on the cell surface by a magnetic field. This allows for rapid synthesis and characterization of a small number of single-signal nanoparticles which can be systematically combined to explore and optimize T cell activation. By increasing cognate T cell enrichment and incorporating additional costimulatory molecules using this platform, we find significantly higher frequencies and numbers of cognate T cells stimulated from an endogenous population. The magnetic field-induced association of separate particles thus provides a tool for optimizing T cell activation for adoptive immunotherapy and other immunological studies. Involved directly in engineering nanoparticle aAPCs and its properties, I worked closely with Alyssa Kosmides as well on her project in creating nanoparticle aAPCs which had separated signal 1 and signal 2 aAPCs[250].

Engineering the aAPC and the system of enrichment and expansion, I created a JoVE (Journal of Visualized Experiments) video protocol for the process[515] and was involved in Ami Bessell's project with understanding cross-reactive gut microbiota antigen-specific T cell responses. Here we used the aAPC process to enrich and expand both SIY (foreign/tumor model antige) and SVY (gut microbiota derived protein)-reactive T cells and understand the influence of the presence of the microbiota on this antigen-specific T cell response in the context of tumor immunotherapy. Specifically, we also looked at the enrichment of antigen-specific T cells on day 0 with the fluorescent magnetic beads I had developed in Chapter 5.

7.4 Incomplete Projects

This section serves to be a dump for those projects which met dead-ends, yet were a significant part of my research during my PhD. First, I tried to give my first undergraduate Fernando a project to make a MHC-array detection chip. This was to improve upon the work Dr. Schneck had done with Mike Paulitis and try to improve antigen-specific CD8+ T cell detection in high throughput. We were able to get antigen-specific binding on the spots that we printed; however, the sensitivity was not improved over that of flow cytometry, so we decided to abandon this project in favor of further development of the aAPC for the same purpose.

Another project included one where I worked with another PhD student in the Neuroscience department to create EGFR-targeted magnetic nanoparticles and attempted to use a magnetic field to cluster receptors on neural cells to enable magnetic control of neuron activity. Unfortunately, the student showed little signal above background and as this was a side project, it was discarded without much troubleshooting.

I have also tested many other parameters with the hydrogel-T cell culture system. First, I obtained decellularized ECM from the Elisseeff lab and incorporated it into the stimulation mixture. After several stimulations it did not seem to have major effects on the activation, except if there was too high of a concentration of dECM in the hydrogel, then this would eliminate any CD8+ T cell activation. Similar results were seen when I would add gelatin and heparin at various ratios. I added gelatin to decrease the stiffness of the gel and increase CD8+ T cell migration in 3D gels; however, all experiments with 3D stimulation in these gels did not work because the cells would not move in these gels, while they would move very quickly through collagen 3D gels. The reason I was

interested in adding heparin is because the heparin is known to bind to cytokines and chemokines and keep them as a depot in the ECM. This can provide extended signaling and preservation of the cytokines for longer periods of time, and I hypothesized this would work for T cell cytokines and further enhance T cell activation.

Also, towards the goal of doing 3D stimulation of the T cells *ex vivo*, I tried to use polymeric nanofibers produced through electrospinning as a component to reinforce the hydrogel while increasing the porosity. I was able to get this composite material to also stimulate antigen-specific CD8+ T cells in 2D effectively, but never get migration or expansion in 3D. Optimizing gel properties for 3D stimulation has taken a large portion of my time and yielded little success, which is why we have decided to go with producing microparticle hydrogels instead. Along the lines of the composite material, I also looked at the difference of stimulating CD8+ T cells on fiber mats with different diameter fibers. At similar conjugation efficiencies, I did not observe any differential activation of the antigen-specific T cells, though I observed effective activation.

Chapter 8. Conclusions

8.1 Summary of work

I have successfully addressed many of the challenges facing T cell immunotherapies by systematically engineering novel biomaterials such as magnetic nanoparticles and ECM hydrogels (**Figure 8-1**). Both will be immediate tools to researchers and clinicians to use in detecting in high-throughput and controlling the expansion and phenotype of rare antigen-specific T cells that will advance our understanding of antigen-specific responses. Already they have improved our understanding of T cell biology where changing the size of the aAPC demonstrated the importance of clustered cognate recognition events needed for T cell activation. Additionally, changing the mechanical strength of the aTM elucidated the strict mechanical requirements of the T cell receptor needs for effective activation. Further demonstrating that the environment influences the cellular therapeutic product is paradigm-shifting and delineates the importance of the ECM, providing a case study of how to engineer ECM-materials for therapeutic immune stimulation in the future. Finally, besides creating an ex vivo environment for T cell activation, the aTM has the potential to be applied for direct T cell activation *in vivo*, thus eliminating the need for *ex vivo* T cell manipulation entirely.

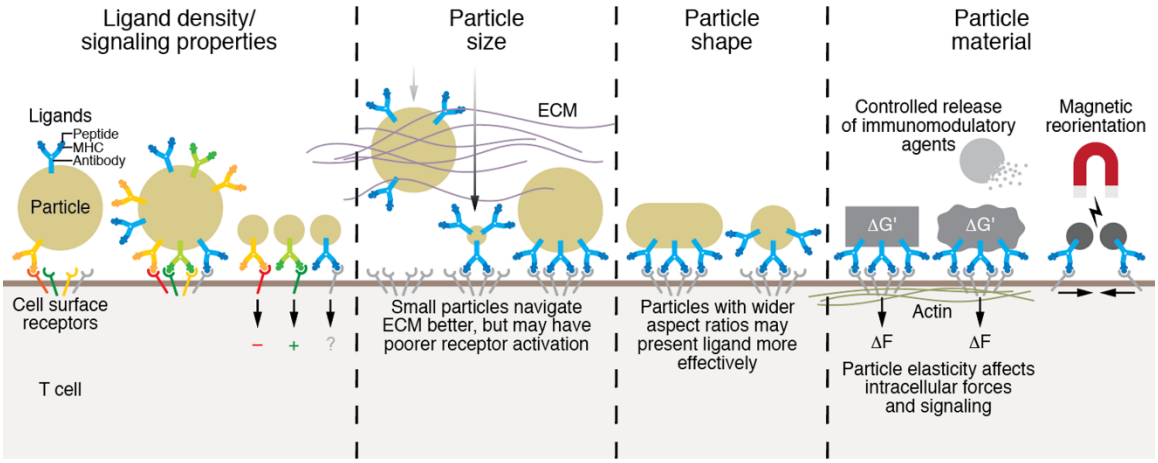

Figure 8-1: Schematic of biomaterials properties I engineered to solve problems facing T cell immunotherapies during my PhD thesis.

8.2 Future directions

The work in Chapters 3-5 have mostly been developed with mouse CD8+ T cells. Thus, true translation and utility will be the use of these aAPC tools in human CD8+ T cells. I will finish out my PhD attempting to translate our findings to human CD8+ T cells. Finally, I hope to continue to work with Mekha to understand the role of CD4+ T cells in our splenocyte cultures as she is in a lab where they are able to do signle cell fluorescent imaging with transgenic mice that express fluorescent phosphorylated ERK. Furthermore, other students in the lab will begin to look at some of these engineering parameters within the development of Class II aAPCs for CD4+ T cells.

Chapter 6 mostly focused on the *ex vivo* stimulation of antigen-specific CD8+ T cells. The original main goal for this project was to develop "artificial lymph nodes" or *in vivo* hydrogel activation hubs for antigen-specific CD8+ T cells. Already I have made progress towards this goal where we create injectable microparticle hydrogels by passing the gel through a stainless steel mesh. Furthermore, we are able to attach

immunocytokines or antibody-binding cytokines to the surface of the hydrogel for a signal 3 because of the lack of cytokine support *in vivo*. Next steps are to finish optimizing the combination of the three signals and perform *in vivo* T cell activation and tumor models to demonstrate efficacy.

Similar to the aAPCs, in addition to the use of the aTM *in vivo*, CD4+ T cell activation can be probed on the surface of the hydrogel. CD4+ T cells are much more phenotypically sensitive and may prove different in terms of activation and phenotype from the HA hydrogels. This also points to another new direction the project could go. Here we only extensively investigated one ECM component, HA, but there are dozens more that may also differentially influence T cell activation, studying them further could improve our overall design of the aTM and also provide more clues to how the environment influences T cell activation.

Bibliography

1. Smith-Garvin, J. E.; Koretzky, G. A.; Jordan, M. S. T Cell Activation. *Annu. Rev. Immunol.* **2009**, *27*, 591–619.
2. Cannons, J. L.; Lau, P.; Ghumman, B.; DeBenedette, M. A.; Yagita, H.; Okumura, K.; Watts, T. H. 4-1BB Ligand Induces Cell Division, Sustains Survival, and Enhances Effector Function of CD4 and CD8 T Cells with Similar Efficacy. *J. Immunol.* **2001**, *167*, 1313–1324.
3. Buchan, S. L.; Manzo, T.; Flutter, B.; Rogel, A.; Edwards, N.; Zhang, L.; Sivakumaran, S.; Ghorashian, S.; Carpenter, B.; Bennett, C. L.; Freeman, G. J.; Sykes, M.; Croft, M.; Al-Shamkhani, A.; Chakraverty, R. OX40- and CD27-Mediated Costimulation Synergizes with Anti-PD-L1 Blockade by Forcing Exhausted CD8+ T Cells to Exit Quiescence. *J. Immunol.* **2015**, *194*, 125–133.
4. Zeng, W.; Su, M.; Anderson, K. S.; Sasada, T. Artificial Antigen-Presenting Cells Expressing CD80, CD70, and 4-1BB Ligand Efficiently Expand Functional T Cells Specific to Tumor-Associated Antigens. *Immunobiology* **2014**, *219*, 583–592.
5. Chacon, J. A.; Wu, R. C.; Sukhumalchandra, P.; Molldrem, J. J.; Sarnaik, A.; Pilon-Thomas, S.; Weber, J.; Hwu, P.; Radvanyi, L. Co-Stimulation through 4-1BB/CD137 Improves the Expansion and Function of CD8(+) Melanoma Tumor-Infiltrating Lymphocytes for Adoptive T-Cell Therapy. *PLoS One* **2013**, *8*, e60031.
6. Zhang, H.; Snyder, K. M.; Suhoski, M. M.; Maus, M. V; Kapoor, V.; June, C. H.; Mackall, C. L. 4-1BB Is Superior to CD28 Costimulation for Generating CD8+ Cytotoxic Lymphocytes for Adoptive Immunotherapy. *J. Immunol.* **2007**, *179*, 4910–4918.
7. Oh, H. S.; Choi, B. K.; Kim, Y. H.; Lee, D. G.; Hwang, S.; Lee, M. J.; Park, S. H.; Bae, Y.-S.; Kwon, B. S. 4-1BB Signaling Enhances Primary and Secondary Population Expansion of CD8+ T Cells by Maximizing Autocrine IL-2/IL-2 Receptor Signaling. *PLoS One* **2015**, *10*, e0126765.
8. Rudolf, D.; Silberzahn, T.; Walter, S.; Maurer, D.; Engelhard, J.; Wernet, D.; Bühring, H.-J.; Jung, G.; Kwon, B. S.; Rammensee, H.-G.; Stevanović, S. Potent Costimulation of Human CD8 T Cells by Anti-4-1BB and Anti-CD28 on Synthetic Artificial Antigen Presenting Cells. *Cancer Immunol.*

Immunother. **2008**, *57*, 175–183.

9. Zheng, G.; Wang, B.; Chen, A. The 4-1BB Costimulation Augments the Proliferation of CD4+CD25+ Regulatory T Cells. *J. Immunol.* **2004**, *173*, 2428–2434.
10. Resta, R.; Thompson, L. F. T Cell Signalling through CD73. *Cell Signal* **1997**, *9*, 131–139.
11. Debenedette, M. A.; Shahinian, A.; Mak, T. W.; Watts, T. H. Costimulation of CD28- T Lymphocytes by 4-1BB Ligand. *J. Immunol.* **1997**, *158*, 551–559.
12. Curtsinger, J. M.; Mescher, M. F. Inflammatory Cytokines as a Third Signal for T Cell Activation Julie. *Curr Opin Immunol* **2011**, *22*, 333–340.
13. Lillemeier, B. F.; Mörtelmaier, M. A.; Forstner, M. B.; Huppa, J. B.; Groves, J. T.; Davis, M. M. TCR and Lat Are Expressed on Separate Protein Islands on T Cell Membranes and Concatenate during Activation. *Nat. Immunol.* **2010**, *11*, 90–96.
14. Hashimoto-Tane, A.; Saito, T. Dynamic Regulation of TCR-Microclusters and the Microsynapse for T Cell Activation. *Front. Immunol.* **2016**, *7*, 1–8.
15. Yokosuka, T.; Kobayashi, W.; Sakata-Sogawa, K.; Takamatsu, M.; Hashimoto-Tane, A.; Dustin, M. L.; Tokunaga, M.; Saito, T. Spatiotemporal Regulation of T Cell Costimulation by TCR-CD28 Microclusters and Protein Kinase C Translocation. *Immunity* **2008**, *29*, 589–601.
16. Saito, T.; Yokosuka, T.; Hashimoto-Tane, A. Dynamic Regulation of T Cell Activation and Co-Stimulation through TCR-Microclusters. *FEBS Lett.* **2010**, *584*, 4865–4871.
17. Dustin, M. L.; Depoil, D. New Insights into the T Cell Synapse from Single Molecule Techniques. *Nat. Rev. Immunol.* **2011**, *11*, 672–684.
18. Bashour, K. T.; Tsai, J.; Shen, K.; Lee, J.-H.; Sun, E.; Milone, M. C.; Dustin, M. L.; Kam, L. C. Cross Talk between CD3 and CD28 Is Spatially Modulated by Protein Lateral Mobility. *Mol. Cell. Biol.* **2014**, *34*, 955–964.
19. Zhu, J. T Helper Cell Differentiation, Heterogeneity, and Plasticity. *Cold Spring Harb. Perspect. Biol.* **2017**, a030338.
20. Luckheeram, R. V.; Zhou, R.; Verma, A. D.; Xia, B. CD4+T Cells: Differentiation and Functions. *Clin. Dev. Immunol.* **2012**, *2012*.
21. Tesmer, L. A.; Lundy, S. K.; Sarkar, S.; Fox, D. A. Th17 Cells in Human Disease. *Immunol Rev*

2008, *223*, 87–113.

22. Josefowicz, S. Z.; Lu, L.-F.; Rudensky, A. Y. Regulatory T Cells: Mechanisms of Differentiation and Function. *Annu. Rev. Immunol.* **2012**, *30*, 531–564.

23. Zhang, N.; Bevan, M. J. CD8+ T Cells: Foot Soldiers of the Immune System. *Immunity* **2011**, *35*, 161–168.

24. Schumacher, T. N.; Schreiber, R. D. Neoantigens in Cancer Immunotherapy. *Science (80-.).* **2015**, *348*, 69–74.

25. Bobisse, S.; Foukas, P. G.; Coukos, G.; Harari, A. Neoantigen-Based Cancer Immunotherapy. *Ann. Transl. Med.* **2016**, *4*, 262–262.

26. Vigneron, N. Review Article Human Tumor Antigens and Cancer Immunotherapy. *Hindawi* **2015**, *2015*, 1–17.

27. Vasievich, E. a; Huang, L. The Suppressive Tumor Microenvironment: A Challenge in Cancer Immunotherapy. *Mol. Pharm.* **2011**, *8*, 635–641.

28. Chen, D. S.; Mellman, I. Oncology Meets Immunology: The Cancer-Immunity Cycle. *Immunity* **2013**, *39*, 1–10.

29. Snyder, A.; Makarov, V.; Merghoub, T.; Yuan, J.; Zaretsky, J. M.; Desrichard, A.; Walsh, L. a.; Postow, M. a.; Wong, P.; Ho, T. S.; Hollmann, T. J.; Bruggeman, C.; Kannan, K.; Li, Y.; Elipenahli, C.; Liu, C.; Harbison, C. T.; Wang, L.; Ribas, A.; *et al.* Genetic Basis for Clinical Response to CTLA-4 Blockade in Melanoma. *N. Engl. J. Med.* **2014**, *371*, 2189–2199.

30. Mcgranahan, N.; Furness, A. J. S.; Rosenthal, R.; Ramskov, S.; Lyngaa, R.; Saini, S. K.; Jamal-hanjani, M.; Wilson, G. A.; Birkbak, N. J.; Hiley, C. T.; Watkins, T. B. K.; Shafi, S.; Murugaesu, N.; Mitter, R.; Akarca, A. U.; Linares, J.; Marafioti, T.; Henry, J. Y.; Allen, E. M. Van. Clonal Neoantigens Elicit T Cell Immunoreactivity and Sensitivity to Immune Checkpoint Blockade. *Science (80-.).* **2016**, *351*, 1463–1469.

31. Germano, G.; Lamba, S.; Rospo, G.; Barault, L.; Magrì, A.; Maione, F.; Russo, M.; Crisafulli, G.; Bartolini, A.; Lerda, G.; Siravegna, G.; Mussolin, B.; Frapolli, R.; Montone, M.; Morano, F.; de Braud, F.; Amirouchene-Angelozzi, N.; Marsoni, S.; D'Incalci, M.; *et al.* Inactivation of DNA Repair Triggers Neoantigen Generation and Impairs Tumour Growth. *Nature* **2017**, *552*, 116–120.

32. Rabinovich, G. a; Gabrilovich, D.; Sotomayor, E. M. Immunosuppressive Strategies That Are Mediated by Tumor Cells. *Annu. Rev. Immunol.* **2007**, *25*, 267–296.

33. Garrido, F.; Algarra, I. MHC Antigens and Tumor Escape from Immune Surveillance. *Adv. Cancer Res.* **2001**, *83*, 117–158.

34. Baghdadi, M.; Jinushi, M. The Impact of the TIM Gene Family on Tumor Immunity and Immunosuppression. *Cell. Mol. Immunol.* **2014**, *11*, 41–48.

35. Wang, Q.; Liu, F.; Liu, L. Prognostic Significance of PD-L1 in Solid Tumor: An Updated Meta-Analysis. *Medicine (Baltimore).* **2017**, *96*.

36. Speiser, D. E.; Utzschneider, D. T.; Oberle, S. G.; Münz, C.; Romero, P.; Zehn, D. T Cell Differentiation in Chronic Infection and Cancer: Functional Adaptation or Exhaustion? *Nat. Rev. Immunol.* **2014**, *14*, 768.

37. Wherry, E. J. T Cell Exhaustion. *Nat. Immunol.* **2011**, *131*, 492–499.

38. Wherry, E. J.; Kurachi, M. Molecular and Cellular Insights into T Cell Exhaustion. *Nat. Rev. Immunol.* **2015**, *15*, 486.

39. Almeida, J. R.; Price, D. a; Papagno, L.; Arkoub, Z. A.; Sauce, D.; Bornstein, E.; Asher, T. E.; Samri, A.; Schnuriger, A.; Theodorou, I.; Costagliola, D.; Rouzioux, C.; Agut, H.; Marcelin, A.-G.; Douek, D.; Autran, B.; Appay, V. Superior Control of HIV-1 Replication by CD8+ T Cells Is Reflected by Their Avidity, Polyfunctionality, and Clonal Turnover. *J. Exp. Med.* **2007**, *204*, 2473–2485.

40. Barber, D. L.; Wherry, E. J.; Masopust, D.; Zhu, B.; Allison, J. P.; Sharpe, A. H.; Freeman, G. J.; Ahmed, R. Restoring Function in Exhausted CD8 T Cells during Chronic Viral Infection. *Nature* **2006**, *439*, 682–687.

41. Chiu, Y.-L. L.; Shan, L.; Huang, H.; Haupt, C.; Bessell, C.; Canaday, D. H.; Zhang, H.; Ho, Y. C.; Powell, J. D.; Oelke, M.; Margolick, J. B.; Blankson, J. N.; Griffin, D. E.; Schneck, J. P. Sprouty-2 Regulates HIV-Specific T Cell Polyfunctionality. *J. Clin. Invest.* **2014**, *124*, 198–208.

42. Buckner, J. H. Mechanisms of Impaired Regulation by CD4+ CD25+ FOXP3+ Regulatory T Cells in Human Autoimmune Diseases. *Nat. Rev. Immunol.* **2010**, *10*, 849.

43. Theofilopoulos, A. N.; Kono, D. H.; Baccala, R. The Multiple Pathways to Autoimmunity. *Nat.*

Immunol. **2017**, *18*, 716.

44. Wing, K.; Sakaguchi, S. Regulatory T Cells Exert Checks and Balances on Self Tolerance and Autoimmunity. *Nat. Immunol.* **2010**, *11*, 7.

45. Rosenblum, M. D.; Gratz, I. K.; Paw, J. S.; Abbas, A. K. Treating Human Autoimmunity: Current Practice and Future Prospects. *Sci. Transl. Med.* **2012**, *4*, 125sr1-125sr1.

46. Perica, K.; Kosmides, A. K.; Schneck, J. P. Linking Form to Function: Biophysical Aspects of Artificial Antigen Presenting Cell Design. *Biochim. Biophys. Acta* **2015**, *1853*, 781–790.

47. Birnbaum, M. E.; Berry, R.; Hsiao, Y.-S.; Chen, Z.; Shingu-Vazquez, M. A.; Yu, X.; Waghray, D.; Fischer, S.; McCluskey, J.; Rossjohn, J.; Walz, T.; Garcia, K. C. Molecular Architecture of the Aβ T Cell Receptor–CD3 Complex. *Proc. Natl. Acad. Sci.* **2014**, *111*, 17576–17581.

48. Chen, L.; Flies, D. B. Molecular Mechanisms of T Cell Co-Stimulation and Co-Inhibition. *Nat. Rev. Immunol.* **2013**, *13*, 227–242.

49. Shuford, W. W.; Klussman, K.; Tritchler, D. D.; Loo, D. T.; Chalupny, J.; Siadak, a W.; Brown, T. J.; Emswiler, J.; Raecho, H.; Larsen, C. P.; Pearson, T. C.; Ledbetter, J. a; Aruffo, A.; Mittler, R. S. 4-1BB Costimulatory Signals Preferentially Induce CD8+ T Cell Proliferation and Lead to the Amplification in Vivo of Cytotoxic T Cell Responses. *J. Exp. Med.* **1997**, *186*, 47–55.

50. Okazaki, T.; Chikuma, S.; Iwai, Y.; Fagarasan, S.; Honjo, T. A Rheostat for Immune Responses: The Unique Properties of PD-1 and Their Advantages for Clinical Application. *Nat. Immunol.* **2013**, *14*, 1212–1218.

51. Postow, M. A.; Chesney, J.; Pavlick, A. C.; Robert, C.; Grossmann, K.; McDermott, D.; Linette, G. P.; Meyer, N.; Giguere, J. K.; Agarwala, S. S.; Shaheen, M.; Ernstoff, M. S.; Minor, D.; Salama, A. K.; Taylor, M.; Ott, P. A.; Rollin, L. M.; Horak, C.; Gagnier, P.; *et al.* Nivolumab and Ipilimumab versus Ipilimumab in Untreated Melanoma. *N. Engl. J. Med.* **2015**, *372*, 2006–2017.

52. Callahan, M. K.; Wolchok, J. D. At the Bedside: CTLA-4- and PD-1-Blocking Antibodies in Cancer Immunotherapy. *J. Leukoc. Biol.* **2013**, *94*, 41–53.

53. Spranger, S.; Koblish, H. K.; Horton, B.; Scherle, P. a; Newton, R.; Gajewski, T. F. Mechanism of Tumor Rejection with Doublets of CTLA-4, PD-1/PD-L1, or IDO Blockade Involves Restored IL-2 Production and Proliferation of CD8(+) T Cells Directly within the Tumor Microenvironment. *J.*

Immunother. cancer **2014**, *2*, 3.

54. Chen, S.; Lee, L.-F.; Fisher, T. S.; Jessen, B.; Elliott, M.; Evering, W.; Logronio, K.; Tu, G. H.; Tsaparikos, K.; Li, X.; Wang, H.; Ying, C.; Xiong, M.; VanArsdale, T.; Lin, J. C. Combination of 4-1BB Agonist and PD-1 Antagonist Promotes Antitumor Effector/Memory CD8 T Cells in a Poorly Immunogenic Tumor Model. *Cancer Immunol. Res.* **2014**, *3*, 149–160.

55. Shindo, Y.; Yoshimura, K.; Kuramasu, A.; Watanabe, Y.; Ito, H. H.; Kondo, T.; Oga, A.; Ito, H. H.; Yoshino, S.; Hazama, S.; Tamada, K.; Yagita, H.; Oka, M. Combination Immunotherapy with 4-1BB Activation and PD-1 Blockade Enhances Antitumor Efficacy in a Mouse Model of Subcutaneous Tumor. *Anticancer Res* **2015**, *35*, 129–136.

56. Vezys, V.; Penaloza-macmaster, P.; Barber, D. L.; Ha, S.-J.; Konieczny, B.; Freeman, G. J.; Mittler, R. S.; Ahmed, R. 4-1BB Signaling Synergizes with Programmed Death Ligand 1 Blockade to Augment CD8 T Cell Responses during Chronic Viral Infection. *J. Immunol.* **2011**, *187*, 1634–1642.

57. Doh, J.; Irvine, D. J. Immunological Synapse Arrays: Patterned Protein Surfaces That Modulate Immunological Synapse Structure Formation in T Cells. *Proc. Natl. Acad. Sci. U. S. A.* **2006**, *103*, 5700–5705.

58. Delcassian, D.; Depoil, D.; Rudnicka, D.; Liu, M.; Davis, D. M.; Dustin, M. L.; Dunlop, I. E. Nanoscale Ligand Spacing Influences Receptor Triggering in T Cells and NK Cells. *Nano Lett.* **2013**, *13*, 5608–5614.

59. Matic, J.; Deeg, J.; Scheffold, A.; Goldstein, I.; Spatz, J. P. Fine Tuning and Efficient T Cell Activation with Stimulatory ACD3 Nanoarrays. *Nano Lett.* **2013**, *13*, 5090–5097.

60. Deeg, J.; Axmann, M.; Matic, J.; Liapis, A.; Depoil, D.; Afrose, J.; Curado, S.; Dustin, M. L.; Spatz, J. P. T Cell Activation Is Determined by the Number of Presented Antigens. *Nano Lett.* **2013**, *13*, 5619–5626.

61. Yokosuka, T.; Takamatsu, M.; Kobayashi-Imanishi, W.; Hashimoto-Tane, A.; Azuma, M.; Saito, T. Programmed Cell Death 1 Forms Negative Costimulatory Microclusters That Directly Inhibit T Cell Receptor Signaling by Recruiting Phosphatase SHP2. *J. Exp. Med.* **2012**, *209*, 1201–1217.

62. Hui, E.; Cheung, J.; Zhu, J.; Su, X.; Taylor, M. J.; Wallweber, H. A.; Sasmal, D. K.; Huang, J.;

Kim, J. M.; Mellman, I.; Vale, R. D. T Cell Costimulatory Receptor CD28 Is a Primary Target for PD-1–mediated Inhibition. *Science (80-.).* **2017**, *355*, 1428–1433.

63. Stephan, M. T.; Ponomarev, V.; Brentjens, R. J.; Chang, A. H.; Dobrenkov, K. V; Heller, G.; Sadelain, M. T Cell-Encoded CD80 and 4-1BBL Induce Auto- and Transcostimulation, Resulting in Potent Tumor Rejection. *Nat. Med.* **2007**, *13*, 1440–1449.

64. Tsai, S.; Shameli, A.; Yamanouchi, J.; Clemente-Casares, X.; Wang, J.; Serra, P.; Yang, Y.; Medarova, Z.; Moore, A.; Santamaria, P. Reversal of Autoimmunity by Boosting Memory-like Autoregulatory T Cells. *Immunity* **2010**, *32*, 568–580.

65. Fooksman, D. R.; Vardhana, S.; Vasiliver-Shamis, G.; Liese, J.; Blair, D. A.; Waite, J.; Sacristán, C.; Victora, G. D.; Zanin-Zhorov, A.; Dustin, M. L. Functional Anatomy of T Cell Activation and Synapse Formation. *Annu. Rev. Immunol.* **2009**, *28*, 79–105.

66. Varma, R.; Campi, G.; Yokosuka, T.; Saito, T.; Dustin, M. L. T Cell Receptor-Proximal Signals Are Sustained in Peripheral Microclusters and Terminated in the Central Supramolecular Activation Cluster. *Immunity* **2006**, *25*, 117–127.

67. Fahmy, T. M.; Bieler, J. G.; Edidin, M.; Schneck, J. P. Increased TCR Avidity after T Cell Activation: A Mechanism for Sensing Low-Density Antigen. *Immunity* **2001**, *14*, 135–143.

68. Bosch, B.; Heipertz, E. L.; Drake, J. R.; Roche, P. A. Major Histocompatibility Complex (MHC) Class II-Peptide Complexes Arrive at the Plasma Membrane in Cholesterol-Rich Microclusters. *J. Biol. Chem.* **2013**, *288*, 13236–13242.

69. Hwang, J.; Gheber, L. A.; Margolis, L.; Edidin, M. Domains in Cell Plasma Membranes Investigated by Near-Field Scanning Optical Microscopy. *Biophys. J.* **1998**, *74*, 2184–2190.

70. Ferez, M.; Castro, M.; Alarcon, B.; van Santen, H. M. Cognate Peptide–MHC Complexes Are Expressed as Tightly Apposed Nanoclusters in Virus-Infected Cells to Allow TCR Crosslinking. *J. Immunol.* **2014**, *192*, 52–58.

71. Lu, X.; Gibbs, J. S.; Hickman, H. D.; David, A.; Dolan, B. P.; Jin, Y.; Kranz, D. M.; Bennink, J. R.; Yewdell, J. W.; Varma, R. Endogenous Viral Antigen Processing Generates Peptide-Specific MHC Class I Cell-Surface Clusters. *Proc. Natl. Acad. Sci.* **2012**, *109*, 15407–15412.

72. Matsui, K.; Boniface, J. J.; Reay, P. A.; Schild, H.; Groth, B. F. de S.; Davis, M. M. Low Affinity

Interaction of Peptide-MHC Complexes with T Cell Receptors. *Science (80-.).* **1991**, *254*, 1788–1792.

73. Lever, M.; Maini, P. K.; van der Merwe, P. A.; Dushek, O. Phenotypic Models of T Cell Activation. *Nat. Rev. Immunol.* **2014**, *14*, 619–629.

74. Bousso, P. T-Cell Activation by Dendritic Cells in the Lymph Node: Lessons from the Movies. *Nat. Rev. Immunol.* **2008**, *8*, 675–684.

75. Huppa, J. B.; Gleimer, M.; Sumen, C.; Davis, M. M. Continuous T Cell Receptor Signaling Required for Synapse Maintenance and Full Effector Potential. *Nat. Immunol.* **2003**, *4*, 749–755.

76. Iezzi, G.; Karjalainen, K.; Lanzavecchia, A. The Duration of Antigenic Stimulation Determines the Fate of Naive and Effector T Cells. *Immunity* **1998**, *8*, 89–95.

77. Celli, S.; Lemaître, F.; Bousso, P. Real-Time Manipulation of T Cell-Dendritic Cell Interactions in Vivo Reveals the Importance of Prolonged Contacts for CD4+ T Cell Activation. *Immunity* **2007**, *27*, 625–634.

78. Fooksman, D. R.; Grönvall, G. K.; Tang, Q.; Edidin, M. Clustering Class I MHC Modulates Sensitivity of T Cell Recognition. *J. Immunol.* **2006**, *176*, 6673–6680.

79. Bullock, T. N. J.; Mullins, D. W.; Engelhard, V. H. Antigen Density Presented by Dendritic Cells in Vivo Differentially Affects the Number and Avidity of Primary, Memory, and Recall CD8+ T Cells. *J. Immunol.* **2003**, *170*, 1822–1829.

80. Manz, B. N.; Jackson, B. L.; Petit, R. S.; Dustin, M. L.; Groves, J. T-Cell Triggering Thresholds Are Modulated by the Number of Antigen within Individual T-Cell Receptor Clusters. *Proc. Natl. Acad. Sci.* **2011**, *108*, 9089–9094.

81. Bromley, S. K.; Iaboni, A.; Davis, S. J.; Whitty, A.; Green, J. M.; Shaw, A. S.; Weiss, A.; Dustin, M. L. The Immunological Synapse and CD28-CD80 Interactions. *Nat. Immunol.* **2001**, *2*, 1159–1166.

82. Hickey, J. W.; Santos, J. L.; Williford, J.-M.; Mao, H.-Q. Control of Polymeric Nanoparticle Size to Improve Therapeutic Delivery. *J. Control. Release* **2015**, *219*, 536–547.

83. Monopoli, M. P.; Åberg, C.; Salvati, A.; Dawson, K. A. Biomolecular Coronas Provide the Biological Identity of Nanosized Materials. *Nat. Nanotechnol.* **2012**, *7*, 779–786.

84. Nel, A. E.; Mädler, L.; Velegol, D.; Xia, T.; Hoek, E. M. V; Somasundaran, P.; Klaessig, F.; Castranova, V.; Thompson, M. Understanding Biophysicochemical Interactions at the Nano–bio Interface. *Nat. Mater.* **2009**, *8*, 543–557.

85. Tenzer, S.; Docter, D.; Kuharev, J.; Musyanovych, A.; Fetz, V.; Hecht, R.; Schlenk, F.; Fischer, D.; Kiouptsi, K.; Reinhardt, C. Rapid Formation of Plasma Protein Corona Critically Affects Nanoparticle Pathophysiology. *Nat. Nanotechnol.* **2013**, *8*, 772–781.

86. Albanese, A.; Tang, P. S.; Chan, W. C. W. The Effect of Nanoparticle Size, Shape, and Surface Chemistry on Biological Systems. *Annu. Rev. Biomed. Eng.* **2012**, *14*, 1–16.

87. Shang, L.; Nienhaus, K.; Nienhaus, G. U. Engineered Nanoparticles Interacting with Cells: Size Matters. *J. Nanobiotechnology* **2014**, *12*, 5.

88. Gratton, S. E. a; Ropp, P. a; Pohlhaus, P. D.; Luft, J. C.; Madden, V. J.; Napier, M. E.; DeSimone, J. M. The Effect of Particle Design on Cellular Internalization Pathways. *Proc. Natl. Acad. Sci. U. S. A.* **2008**, *105*, 11613–11618.

89. Shann, S. Y.; Lau, C. M.; Thomas, S. N.; Jerome, W. G.; Maron, D. J.; Dickerson, J. H.; Hubbell, J. A.; Giorgio, T. D. Size-and Charge-Dependent Non-Specific Uptake of PEGylated Nanoparticles by Macrophages. *Int. J. Nanomedicine* **2012**, *7*, 799.

90. Yuan, H.; Li, J.; Bao, G.; Zhang, S. Variable Nanoparticle-Cell Adhesion Strength Regulates Cellular Uptake. *Phys. Rev. Lett.* **2010**, *105*, 138101.

91. Lai, S. K.; Hida, K.; Man, S. T.; Chen, C.; Machamer, C.; Schroer, T. A.; Hanes, J. Privileged Delivery of Polymer Nanoparticles to the Perinuclear Region of Live Cells via a Non-Clathrin, Non-Degradative Pathway. *Biomaterials* **2007**, *28*, 2876–2884.

92. Rejman, J.; Oberle, V.; Zuhorn, I. S.; Hoekstra, D. Size-Dependent Internalization of Particles via the Pathways of Clathrin- and Caveolae-Mediated Endocytosis. *Biochem. J.* **2004**, *377*, 159–169.

93. Kettiger, H.; Schipanski, A.; Wick, P.; Huwyler, J. Engineered Nanomaterial Uptake and Tissue Distribution: From Cell to Organism. *Int. J. Nanomedicine* **2013**, *8*, 3255.

94. Conner, S. D.; Schmid, S. L. Regulated Portals of Entry into the Cell. *Nature* **2003**, *422*, 37–44.

95. Zauner, W.; Farrow, N. A.; Haines, A. M. R. In Vitro Uptake of Polystyrene Microspheres: Effect of Particle Size, Cell Line and Cell Density. *J. Control. Release* **2001**, *71*, 39–51.

96. Choi, J.-S.; Cao, J.; Naeem, M.; Noh, J.; Hasan, N.; Choi, H.-K.; Yoo, J.-W. Size-Controlled Biodegradable Nanoparticles: Preparation and Size-Dependent Cellular Uptake and Tumor Cell Growth Inhibition. *Colloids Surfaces B Biointerfaces* **2014**, *122*, 545–551.

97. Gao, H.; Shi, W.; Freund, L. B. Mechanics of Receptor-Mediated Endocytosis. *Proc. Natl. Acad. Sci. U. S. A.* **2005**, *102*, 9469–9474.

98. Zhang, S.; Li, J.; Lykotrafitis, G.; Bao, G.; Suresh, S. Size-dependent Endocytosis of Nanoparticles. *Adv. Mater.* **2009**, *21*, 419–424.

99. Narayanan, K.; Yen, S. K.; Dou, Q.; Padmanabhan, P.; Sudhaharan, T.; Ahmed, S.; Ying, J. Y.; Selvan, S. T. Mimicking Cellular Transport Mechanism in Stem Cells through Endosomal Escape of New Peptide-Coated Quantum Dots. *Sci. Rep.* **2013**, *3*.

100. Jung, Y.; Park, H.-J.; Kim, P.-H.; Lee, J.; Hyung, W.; Yang, J.; Ko, H.; Sohn, J.-H.; Kim, J.-H.; Huh, Y.-M. Retargeting of Adenoviral Gene Delivery via Herceptin–PEG–adenovirus Conjugates to Breast Cancer Cells. *J. Control. release* **2007**, *123*, 164–171.

101. Smith, T. T.; Stephan, S. B.; Moffett, H. F.; McKnight, L. E.; Ji, W.; Reiman, D.; Bonagofski, E.; Wohlfahrt, M. E.; Pillai, S. P. S.; Stephan, M. T. In Situ Programming of Leukaemia-Specific T Cells Using Synthetic DNA Nanocarriers. *Nat. Nanotechnol.* **2017**, *12*, 813.

102. Oelke, M.; Maus, M. V; Didiano, D.; June, C. H.; Mackensen, A.; Schneck, J. P. Ex Vivo Induction and Expansion of Antigen-Specific Cytotoxic T Cells by HLA-Ig-Coated Artificial Antigen-Presenting Cells. *Nat. Med.* **2003**, *9*, 619–624.

103. Hickey, J. W.; Vicente, F. P.; Howard, G. P.; Mao, H.-Q.; Schneck, J. P. Biologically Inspired Design of Nanoparticle Artificial Antigen-Presenting Cells for Immunomodulation. *Nano Lett.* **2017**, *17*.

104. Franz, S.; Rammelt, S.; Scharnweber, D.; Simon, J. C. Immune Responses to Implants–a Review of the Implications for the Design of Immunomodulatory Biomaterials. *Biomaterials* **2011**, *32*, 6692–6709.

105. Veiseh, O.; Doloff, J. C.; Ma, M.; Vegas, A. J.; Tam, H. H.; Bader, A. R.; Li, J.; Langan, E.; Wyckoff, J.; Loo, W. S. Size-and Shape-Dependent Foreign Body Immune Response to Materials Implanted in Rodents and Non-Human Primates. *Nat. Mater.* **2015**, *14*, 643–651.

106. Gong, C.; Linderman, J. J.; Kirschner, D. Harnessing the Heterogeneity of T Cell Differentiation Fate to Fine-Tune Generation of Effector and Memory T Cells. *Front. Immunol.* **2014**, *5*.

107. Jain, R. K.; Stylianopoulos, T. Delivering Nanomedicine to Solid Tumors. *Nat. Rev. Clin. Oncol.* **2010**, *7*, 653–664.

108. Irvine, D. J.; Swartz, M. A.; Szeto, G. L. Engineering Synthetic Vaccines Using Cues from Natural Immunity. *Nat. Mater.* **2013**, *12*, 978–990.

109. Reddy, S. T.; Van Der Vlies, A. J. A. J.; Simeoni, E.; Angeli, V.; Randolph, G. J.; O'Neil, C. P.; Lee, L. K.; Swartz, M. A.; Hubbell, J. A. Exploiting Lymphatic Transport and Complement Activation in Nanoparticle Vaccines. *Nat. Biotechnol.* **2007**, *25*, 1159–1164.

110. Hirosue, S.; Dubrot, J. Modes of Antigen Presentation by Lymph Node Stromal Cells and Their Immunological Implications. *Front. Immunol.* **2015**, *6*.

111. Norris, D. A.; Puri, N.; Sinko, P. J. The Effect of Physical Barriers and Properties on the Oral Absorption of Particulates. *Adv. Drug Deliv. Rev.* **1998**, *34*, 135–154.

112. Champion, J. a; Mitragotri, S. Role of Target Geometry in Phagocytosis. *Proc. Natl. Acad. Sci. U. S. A.* **2006**, *103*, 4930–4934.

113. Sharma, G.; Valenta, D. T.; Altman, Y.; Harvey, S.; Xie, H.; Mitragotri, S.; Smith, J. W. Polymer Particle Shape Independently Influences Binding and Internalization by Macrophages. *J. Control. Release* **2010**, *147*, 408–412.

114. Yoo, J.-W.; Mitragotri, S. Polymer Particles That Switch Shape in Response to a Stimulus. *Proc. Natl. Acad. Sci. U. S. A.* **2010**, *107*, 11205–11210.

115. Barua, S.; Yoo, J.-W.; Kolhar, P.; Wakankar, A.; Gokarn, Y. R.; Mitragotri, S. Particle Shape Enhances Specificity of Antibody-Displaying Nanoparticles. *Proc. Natl. Acad. Sci. U. S. A.* **2013**, *110*, 3270–3275.

116. Sunshine, J. C.; Perica, K.; Schneck, J. P.; Green, J. J. Particle Shape Dependence of CD8+ T Cell Activation by Artificial Antigen Presenting Cells. *Biomaterials* **2014**, *35*, 269–277.

117. Meyer, R. a.; Sunshine, J. C.; Perica, K.; Kosmides, A. K.; Aje, K.; Schneck, J. P.; Green, J. J. Biodegradable Nanoellipsoidal Artificial Antigen Presenting Cells for Antigen Specific T-Cell Activation. *Small* **2014**, *11*, 1519–1525.

118. Andorko, J. I.; Jewell, C. M. Designing Biomaterials with Immunomodulatory Properties for Tissue Engineering and Regenerative Medicine. *Bioeng. Transl. Med.* **2017**, *2*, 139–155.

119. Torchilin, V. P.; Trubetskoy, V. S. Which Polymers Can Make Nanoparticulate Drug Carriers Long-Circulating? *Adv. Drug Deliv. Rev.* **1995**, *16*, 141–155.

120. Cheng, J.; Teply, B. A.; Sherifi, I.; Sung, J.; Luther, G.; Gu, F. X.; Levy-Nissenbaum, E.; Radovic-Moreno, A. F.; Langer, R.; Farokhzad, O. C. Formulation of Functionalized PLGA–PEG Nanoparticles for in Vivo Targeted Drug Delivery. *Biomaterials* **2007**, *28*, 869–876.

121. Xu, Q.; Ensign, L. M.; Boylan, N. J.; Schön, A.; Gong, X.; Yang, J.-C.; Lamb, N. W.; Cai, S.; Yu, T.; Freire, E. Impact of Surface Polyethylene Glycol (PEG) Density on Biodegradable Nanoparticle Transport in Mucus Ex Vivo and Distribution in Vivo. *ACS Nano* **2015**, *9*, 9217–9227.

122. Duncan, R. Polymer Conjugates as Anticancer Nanomedicines. *Nat. Rev. cancer* **2006**, *6*, 688.

123. Safra, T.; Muggia, F.; Jeffers, S.; Tsao-Wei, D. D.; Groshen, S.; Lyass, O.; Henderson, R.; Berry, G.; Gabizon, A. Pegylated Liposomal Doxorubicin (Doxil): Reduced Clinical Cardiotoxicity in Patients Reaching or Exceeding Cumulative Doses of 500 Mg/M2. *Ann. Oncol.* **2000**, *11*, 1029–1033.

124. Torchilin, V. P. Recent Advances with Liposomes as Pharmaceutical Carriers. *Nat. Rev. Drug Discov.* **2005**, *4*, 145.

125. Hu, C.-M. J.; Zhang, L.; Aryal, S.; Cheung, C.; Fang, R. H.; Zhang, L. Erythrocyte Membrane-Camouflaged Polymeric Nanoparticles as a Biomimetic Delivery Platform. *Proc. Natl. Acad. Sci.* **2011**, *108*, 10980–10985.

126. Fang, R. H.; Hu, C.-M. J.; Luk, B. T.; Gao, W.; Copp, J. A.; Tai, Y.; O'Connor, D. E.; Zhang, L. Cancer Cell Membrane-Coated Nanoparticles for Anticancer Vaccination and Drug Delivery. *Nano Lett.* **2014**, *14*, 2181–2188.

127. Parodi, A.; Quattrocchi, N.; Van De Ven, A. L.; Chiappini, C.; Evangelopoulos, M.; Martinez, J. O.; Brown, B. S.; Khaled, S. Z.; Yazdi, I. K.; Enzo, M. V. Synthetic Nanoparticles Functionalized with Biomimetic Leukocyte Membranes Possess Cell-like Functions. *Nat. Nanotechnol.* **2013**, *8*, 61.

128. Oldenborg, P.-A.; Zheleznyak, A.; Fang, Y.-F.; Lagenaur, C. F.; Gresham, H. D.; Lindberg, F. P.

Role of CD47 as a Marker of Self on Red Blood Cells. *Science (80-.).* **2000**, *288*, 2051–2054.

129. Rodriguez, P. L.; Harada, T.; Christian, D. A.; Pantano, D. A.; Tsai, R. K.; Discher, D. E. Minimal" Self" Peptides That Inhibit Phagocytic Clearance and Enhance Delivery of Nanoparticles. *Science (80-.).* **2013**, *339*, 971–975.

130. Liu, H.; Moynihan, K. D.; Zheng, Y.; Szeto, G. L.; Li, A. V.; Huang, B.; Van Egeren, D. S.; Park, C.; Irvine, D. J. Structure-Based Programming of Lymph-Node Targeting in Molecular Vaccines. *Nature* **2014**, *507*, 519–522.

131. Burdick, J. A.; Anseth, K. S. Photoencapsulation of Osteoblasts in Injectable RGD-Modified PEG Hydrogels for Bone Tissue Engineering. *Biomaterials* **2002**, *23*, 4315–4323.

132. Discher, D. E.; Mooney, D. J.; Zandstra, P. W. Growth Factors, Matrices, and Forces Combine and Control Stem Cells. *Science (80-.).* **2009**, *324*, 1673–1677.

133. Humphrey, J. D.; Dufresne, E. R.; Schwartz, M. A. Mechanotransduction and Extracellular Matrix Homeostasis. *Nat. Rev. Mol. cell Biol.* **2014**, *15*, 802.

134. Jaalouk, D. E.; Lammerding, J. Mechanotransduction Gone Awry. *Nat. Rev. Mol. cell Biol.* **2009**, *10*, 63.

135. Huse, M. Mechanical Forces in the Immune System. *Nat. Rev. Immunol.* **2017**, *17*, 679.

136. Kim, S. T.; Takeuchi, K.; Sun, Z.-Y. J.; Touma, M.; Castro, C. E.; Fahmy, A.; Lang, M. J.; Wagner, G.; Reinherz, E. L. The Aβ T Cell Receptor Is an Anisotropic Mechanosensor. *J. Biol. Chem.* **2009**, *284*, 31028–31037.

137. Liu, B.; Chen, W.; Evavold, B. D.; Zhu, C. Accumulation of Dynamic Catch Bonds between TCR and Agonist Peptide-MHC Triggers T Cell Signaling. *Cell* **2014**, *157*, 357–368.

138. Das, D. K.; Feng, Y.; Mallis, R. J.; Li, X.; Keskin, D. B.; Hussey, R. E.; Brady, S. K.; Wang, J.-H.; Wagner, G.; Reinherz, E. L. Force-Dependent Transition in the T-Cell Receptor β-Subunit Allosterically Regulates Peptide Discrimination and PMHC Bond Lifetime. *Proc. Natl. Acad. Sci.* **2015**, *112*, 1517–1522.

139. Basu, R.; Huse, M. Mechanical Communication at the Immunological Synapse. *Trends Cell Biol.* **2017**, *27*, 241–254.

140. Comrie, W. A.; Li, S.; Boyle, S.; Burkhardt, J. K. The Dendritic Cell Cytoskeleton Promotes T Cell

Adhesion and Activation by Constraining ICAM-1 Mobility. *J Cell Biol* **2015**, *208*, 457–473.

141. Andorko, J. I.; Hess, K. L.; Pineault, K. G.; Jewell, C. M. Intrinsic Immunogenicity of Rapidly-Degradable Polymers Evolves during Degradation. *Acta Biomater.* **2016**, *32*, 24–34.

142. Lu, Y.; Aimetti, A. A.; Langer, R.; Gu, Z. Bioresponsive Materials. *Nat. Rev. Mater.* **2017**, *2*, 16075.

143. Baeza, A.; Colilla, M.; Vallet-Regí, M. Advances in Mesoporous Silica Nanoparticles for Targeted Stimuli-Responsive Drug Delivery. *Expert Opin. Drug Deliv.* **2015**, *12*, 319–337.

144. Meng, F.; Hennink, W. E.; Zhong, Z. Reduction-Sensitive Polymers and Bioconjugates for Biomedical Applications. *Biomaterials* **2009**, *30*, 2180–2198.

145. Callmann, C. E.; Barback, C. V; Thompson, M. P.; Hall, D. J.; Mattrey, R. F.; Gianneschi, N. C. Therapeutic Enzyme-Responsive Nanoparticles for Targeted Delivery and Accumulation in Tumors. *Adv. Mater.* **2015**, *27*, 4611–4615.

146. Mura, S.; Nicolas, J.; Couvreur, P. Stimuli-Responsive Nanocarriers for Drug Delivery. *Nat. Mater.* **2013**, *12*, 991.

147. Korin, N.; Kanapathipillai, M.; Matthews, B. D.; Crescente, M.; Brill, A.; Mammoto, T.; Ghosh, K.; Jurek, S.; Bencherif, S. A.; Bhatta, D. Shear-Activated Nanotherapeutics for Drug Targeting to Obstructed Blood Vessels. *Science (80-.).* **2012**, 1217815.

148. Schmaljohann, D. Thermo-and PH-Responsive Polymers in Drug Delivery. *Adv. Drug Deliv. Rev.* **2006**, *58*, 1655–1670.

149. Chertok, B.; Moffat, B. A.; David, A. E.; Yu, F.; Bergemann, C.; Ross, B. D.; Yang, V. C. Iron Oxide Nanoparticles as a Drug Delivery Vehicle for MRI Monitored Magnetic Targeting of Brain Tumors. *Biomaterials* **2008**, *29*, 487–496.

150. Kumar, C. S. S. R.; Mohammad, F. Magnetic Nanomaterials for Hyperthermia-Based Therapy and Controlled Drug Delivery. *Adv. Drug Deliv. Rev.* **2011**, *63*, 789–808.

151. Tong, R.; Hemmati, H. D.; Langer, R.; Kohane, D. S. Photoswitchable Nanoparticles for Triggered Tissue Penetration and Drug Delivery. *J. Am. Chem. Soc.* **2012**, *134*, 8848–8855.

152. Han, G.; You, C.; Kim, B.; Turingan, R. S.; Forbes, N. S.; Martin, C. T.; Rotello, V. M. Light-regulated Release of DNA and Its Delivery to Nuclei by Means of Photolabile Gold Nanoparticles.

Angew. Chemie **2006**, *118*, 3237–3241.

153. Javadi, M.; Pitt, W. G.; Belnap, D. M.; Tsosie, N. H.; Hartley, J. M. Encapsulating Nanoemulsions inside ELiposomes for Ultrasonic Drug Delivery. *Langmuir* **2012**, *28*, 14720–14729.

154. Wang, C.-H.; Kang, S.-T.; Lee, Y.-H.; Luo, Y.-L.; Huang, Y.-F.; Yeh, C.-K. Aptamer-Conjugated and Drug-Loaded Acoustic Droplets for Ultrasound Theranosis. *Biomaterials* **2012**, *33*, 1939–1947.

155. De Jong, W. H.; Borm, P. J. A. Drug Delivery and Nanoparticles: Applications and Hazards. *Int. J. Nanomedicine* **2008**, *3*, 133.

156. Bobo, D.; Robinson, K. J.; Islam, J.; Thurecht, K. J.; Corrie, S. R. Nanoparticle-Based Medicines: A Review of FDA-Approved Materials and Clinical Trials to Date. *Pharm. Res.* **2016**, *33*, 2373–2387.

157. Aguado, B. A.; Grim, J. C.; Rosales, A. M.; Watson-Capps, J. J.; Anseth, K. S. Engineering Precision Biomaterials for Personalized Medicine. *Sci. Transl. Med.* **2018**, *10*, eaam8645.

158. Lurie, N.; Slater, J.; McGovern, P.; Ekstrum, J.; Quam, L.; Margolis, K. A Progress Report on the Treatment of 157 Patients with Advanced Cancer Using Lymphokine-Activated Killer Cells and Interleukin-2 of High-Dose Interleukin-2 Alone. *N. Engl. J. Med.* **1993**, *329*, 478–482.

159. Rosenberg, S. A. IL-2: The First Effective Immunotherapy for Human Cancer. *J. Immunol.* **2014**, *192*, 5451–5458.

160. Malek, T. R.; Castro, I. Interleukin-2 Receptor Signaling: At the Interface between Tolerance and Immunity. *Immunity* **2010**, *33*, 153–165.

161. Krieg, C.; Letourneau, S.; Pantaleo, G.; Boyman, O. Improved IL-2 Immunotherapy by Selective Stimulation of IL-2 Receptors on Lymphocytes and Endothelial Cells. *Proc. Natl. Acad. Sci.* **2010**, *107*, 11906–11911.

162. Levin, A. M.; Bates, D. L.; Ring, A. M.; Krieg, C.; Lin, J. T.; Su, L.; Moraga, I. L.; Raeber, M. E.; Bowman, G. R.; Novick, P.; Pande, V. S.; Fathman, C. G.; Boyman, O.; Garcia, K. C.; Vijay, S.; Fathman, C. G.; Boyman, O.; Garcia, K. C. Exploiting a Natural Conformational Switch to Engineer an Interleukin-2 "Superkine." *Nature* **2012**, *484*, 529–533.

163. Mitra, S.; Ring, A. M.; Amarnath, S.; Spangler, J. B.; Li, P.; Ju, W.; Fishcer, S.; Oh, J.; Spolski, R.; Weiskopf, K.; Kohrt, H.; Foley, J. E.; Rajagopalan, S.; Long, E. O.; Fowler, D. H.; Waldmann, T.

A.; Garcia, K. C.; Leonard, W. J. Interleukin-2 Activity Can Be Fine-Tuned with Engineered Receptor Signaling Clamps. *Immunity* **2015**, *42*, 826–838.

164. Mishra, A.; Sullivan, L.; Caligiuri, M. A. Molecular Pathways: Interleukin-15 Signaling in Health and in Cancer. *Clin Cancer Res* **2014**, *20*, 2044–2050.

165. Rubinstein, M. P.; Kovar, M.; Purton, J. F.; Cho, J.-H.; Boyman, O.; Surh, C. D.; Sprent, J. Converting IL-15 to a Superagonist by Binding to Soluble IL-15Ra. *Proc. Natl. Acad. Sci. U. S. A.* **2006**, *103*, 9166–9171.

166. Zhu, X.; Marcus, W. D.; Xu, W.; Lee, H.-I.; Han, K.; Egan, J. O.; Yovandich, J. L.; Rhode, P. R.; Wong, H. c. Novel Human Interleukin-15 Agonists. *J Immunol* **2009**, *183*, 1–27.

167. Bailey, C. P.; Budak-Alpdogan, T.; Sauter, C. T.; Panis, M. M.; Buyukgoz, C.; Jeng, E. K.; Wong, H. C.; Flomenberg, N.; Alpdogan, O. New Interleukin-15 Superagonist (IL-15SA) Significantly Enhances Graft-versus-Tumor Activity. *Oncotarget* **2017**, *8*, 44366–44378.

168. Neri, D.; Sondel, P. M. Immunocytokines for Cancer Treatment: Past, Present and Future. *Curr Opin Immunol* **2016**, *40*, 96–102.

169. Müller, D. Antibody-Cytokine Fusion Proteins for Cancer Immunotherapy: An Update on Recent Developments. *BioDrugs* **2014**, *28*, 123–131.

170. Carnemolla, B.; Borsi, L.; Balza, E.; Castellani, P.; Meazza, R.; Berndt, A.; Ferrini, S.; Kosmehl, H.; Neri, D.; Zardi, L. Enhancement of the Antitumor Properties of Interleukin-2 by Its Targeted Delivery to the Tumor Blood Vessel Extracellular Matrix Enhancement of the Antitumor Properties of Interleukin-2 by Its Targeted Delivery to the Tumor Blood Vessel Extracellular Matr. **2013**, *99*, 1659–1665.

171. Liu, B.; Kong, L.; Han, K.; Hong, H.; Marcus, W. D.; Chen, X.; Jeng, E. K.; Alter, S.; Zhu, X.; Rubinstein, M. P.; Shi, S.; Rhode, P. R.; Cai, W.; Wong, H. C. A Novel Fusion of ALT-803 (Interleukin (IL)-15 Superagonist) with an Antibody Demonstrates Antigen-Specific Antitumor Responses. *J. Biol. Chem.* **2016**, *291*, 23869–23881.

172. Vincent, M.; Teppaz, G.; Lajoie, L.; Solé, V.; Bessard, A.; Maillasson, M.; Loisel, S.; Béchard, D.; Clémenceau, B.; Thibault, G.; Garrigue-Antar, L.; Jacques, Y.; Quéméner, A. Highly Potent Anti-CD20-RLI Immunocytokine Targeting Established Human B Lymphoma in SCID Mouse. *MAbs*

2014, *6*, 1026–1037.

173. Kawalkowska, J. Z.; Hemmerle, T.; Pretto, F.; Matasci, M.; Neri, D.; Williams, R. O. Targeted IL-4 Therapy Synergizes with Dexamethasone to Induce a State of Tolerance by Promoting Treg Cells and Macrophages in Mice with Arthritis. *Eur. J. Immunol.* **2016**, *46*, 1246–1257.

174. Fallon, J. K.; Vandeveer, A. J.; Schlom, J.; Greiner, J. W. Enhanced Antitumor Effects by Combining an IL-12/Anti-DNA Fusion Protein with Avelumab, an Anti-PD-L1 Antibody. *Oncotarget* **2017**, *8*, 20558–20571.

175. Chen, X.; Xu, J.; Guo, Q.; Wang, L.; Yang, Y.; Guo, H.; Gu, N.; Zhang, D.; Qian, W.; Hou, S.; Li, J.; Dai, J.; Guo, Y.; Wang, H. Therapeutic Efficacy of an Anti-PD-L1 Antibody Based Immunocytokine in a Metastatic Mouse Model of Colorectal Cancer. *Biochem. Biophys. Res. Commun.* **2016**, *480*, 160–165.

176. Kamath, A. V. Translational Pharmacokinetics and Pharmacodynamics of Monoclonal Antibodies. *Drug Discov. Today Technol.* **2016**, *21–22*, 75–83.

177. Almagro, J. C.; Daniels-wells, T. R.; Perez-tapia, S. M.; Penichet, M. L. Progress and Challenges in the Design and Clinical Development of Antibodies for Cancer Therapy. *Front. Immunol.* **2018**, *8*.

178. Chiu, M. L.; Gilliland, G. L. Engineering Antibody Therapeutics. *Curr. Opin. Struct. Biol.* **2016**, *38*, 163–173.

179. Sanchez-Martin, D.; Sorensen, M. D.; Lykkemark, S.; Sanz, L.; Kristensen, P.; Ruoslahti, E.; Alvarez-Vallina, L. Selection Strategies for Anti-Cancer Antibody Discovery: Searching off the Beaten Path. *Trends Biotechnol.* **2015**, *33*, 292–301.

180. Mahoney, K. M.; Rennert, P. D.; Freeman, G. J. Combination Cancer Immunotherapy and New Immunomodulatory Targets. *Nat. Rev. Drug Discov.* **2015**, *14*, 561–584.

181. Beers, S. A.; Glennie, M. J.; White, A. L. Influence of Immunoglobulin Isotype on Therapeutic Antibody Function. *Blood* **2016**, *127*, 1097–1101.

182. Wang, W.; Erbe, A. K.; Hank, J. A.; Morris, Z. S.; Sondel, P. M. NK Cell-Mediated Antibody-Dependent Cellular Cytotoxicity in Cancer Immunotherapy. *Front. Immunol.* **2015**, *6*.

183. Taylor, R. P.; Lindorfer, M. A. Cytotoxic Mechanisms of Immunotherapy: Harnessing Complement in the Action of Anti-Tumor Monoclonal Antibodies. *Semin. Immunol.* **2016**, *28*,

309–316.

184. Gong, Q.; Hazen, M.; Marshall, B.; Crowell, S. R.; Ou, Q.; Wong, A. W.; Phung, W.; Vernes, J. M.; Meng, Y. G.; Tejada, M.; Andersen, D.; Kelley, R. F. Increased in Vivo Effector Function of Human IgG4 Isotype Antibodies through Afucosylation. *MAbs* **2016**, *8*, 1098–1106.

185. Harding, F. A.; Stickler, M. M.; Razo, J.; DuBridge, R. B. The Immunogenicity of Humanized and Fully Human Antibodies: Residual Immunogenicity Resides in the CDR Regions. *MAbs* **2010**, *2*, 256–265.

186. Hamid, O.; Robert, C.; Daud, A.; Hodi, F. S.; Hwu, W.-J.; Kefford, R.; Wolchok, J. D.; Hersey, P.; Joseph, R. W.; Weber, J. S.; Dronca, R.; Gangadhar, T. C.; Patnaik, A.; Zarour, H.; Joshua, A. M.; Gergich, K.; Elassaiss-Schaap, J.; Algazi, A.; Mateus, C.; *et al.* Safety and Tumor Responses with Lambrolizumab (Anti-PD-1) in Melanoma. *N. Engl. J. Med.* **2013**, *369*, 134–144.

187. Chen, L.; Han, X. Anti – PD-1 / PD-L1 Therapy of Human Cancer : Past , Present , and Future. *J. Clin. Invest.* **2015**, *125*.

188. Larkin, J.; Chiarion-Sileni, V.; Gonzalez, R.; Grob, J. J.; Cowey, C. L.; Lao, C. D.; Schadendorf, D.; Dummer, R.; Smylie, M.; Rutkowski, P.; Ferrucci, P. F.; Hill, A.; Wagstaff, J.; Carlino, M. S.; Haanen, J. B.; Maio, M.; Marquez-Rodas, I.; McArthur, G. A.; Ascierto, P. A.; *et al.* Combined Nivolumab and Ipilimumab or Monotherapy in Untreated Melanoma. *N. Engl. J. Med.* **2015**, *373*, 23–34.

189. Pedicord, V. a; Montalvo, W.; Leiner, I. M.; Allison, J. P. Single Dose of Anti – CTLA-4 Enhances CD8 + T-Cell Memory Formation , Function , and Maintenance. *PNAS* **2011**, *108*, 266–271.

190. Hugo, W.; Zaretsky, J. M.; Sun, L.; Song, C.; Moreno, B. H.; Hu-Lieskovan, S.; Berent-Maoz, B.; Pang, J.; Chmielowski, B.; Cherry, G.; Seja, E.; Lomeli, S.; Kong, X.; Kelley, M. C.; Sosman, J. A.; Johnson, D. B.; Ribas, A.; Lo, R. S. Genomic and Transcriptomic Features of Response to Anti-PD-1 Therapy in Metastatic Melanoma. *Cell* **2016**, *165*, 35–44.

191. Van Allen, E. M.; Miao, D.; Schilling, B.; Shukla, S. A.; Blank, C.; Zimmer, L.; Sucker, A.; Hillen, U.; Geukes Foppen, M. H.; Goldinger, S. M.; Utikal, J.; Hassel, J. C.; Weide, B.; Kaehler, K. C.; Loquai, C.; Mohr, P.; Gutzmer, R.; Dummer, R.; Gabriel, S.; *et al.* Genomic Correlates of Response to CTLA-4 Blockade in Metastatic Melanoma. *Science (80-.).* **2015**, *350*, 207–211.

192. Jahan, N.; Talat, H.; Curry, W. T. Agonist OX40 Immunotherapy Improves Survival in Glioma-Bearing Mice and Is Complementary with Vaccination with Irradiated GM-CSF–expressing Tumor Cells. *Neuro. Oncol.* **2017**, *20*, 44–54.

193. Tyrsin, D.; Chuvpilo, S.; Matskevich, A.; Nemenov, D.; Römer, P. S.; Tabares, P.; Hünig, T. From TGN1412 to TAB08: The Return of CD28 Superagonist Therapy to Clinical Development for the Treatment of Rheumatoid Arthritis. *Clin. Exp. Rheumatol.* **2016**, *34*, 45–48.

194. Polu, K. R.; Lowman, H. B. Probody Therapeutics for Targeting Antibodies to Diseased Tissue. *Expert Opin. Biol. Ther.* **2014**, *14*, 1049–1053.

195. Kermer, V.; Hornig, N.; Harder, M.; Bondarieva, A.; Kontermann, R. E.; Muller, D. Combining Antibody-Directed Presentation of IL-15 and 4-1BBL in a Trifunctional Fusion Protein for Cancer Immunotherapy. *Mol. Cancer Ther.* **2014**, *13*, 112–121.

196. Yasunaga, M.; Manabe, S.; Matsumura, Y. Immunoregulation by IL-7R-Targeting Antibody-Drug Conjugates: Overcoming Steroid-Resistance in Cancer and Autoimmune Disease. *Sci. Rep.* **2017**, *7*, 1–14.

197. Lerner, R. A. Combinatorial Antibody Libraries: New Advances, New Immunological Insights. *Nature Reviews Immunology*, 2016, *16*, 498–508.

198. Packer, M. S.; Liu, D. R. Methods for the Directed Evolution of Proteins. *Nature Reviews Genetics*, 2015, *16*, 379–394.

199. Holliger, P.; Hudson, P. J. Engineered Antibody Fragments and the Rise of Single Domains. *Nature Biotechnology*, 2005, *23*, 1126–1136.

200. Owens, B. Faster, Deeper, Smaller—the Rise of Antibody-like Scaffolds. *Nat. Biotechnol.* **2017**, *35*, 602–603.

201. Xie, J. H.; Yamniuk, A. P.; Borowski, V.; Kuhn, R.; Susulic, V.; Rex-Rabe, S.; Yang, X. X.; Zhou, X. D.; Zhang, Y. F.; Gillooly, K.; Brosius, R.; Ravishankar, R.; Waggie, K.; Mink, K.; Price, L.; Rehfuss, R.; Tamura, J.; An, Y.; Cheng, L.; *et al.* Engineering of a Novel Anti-CD40L Domain Antibody for Treatment of Autoimmune Diseases. *J. Immunol.* **2014**, *192*, 4083–4092.

202. Strohl, W. R. Current Progress in Innovative Engineered Antibodies. *Protein Cell* **2017**, *9*, 1–35.

203. Chelius, D.; Ruf, P.; Gruber, P.; Plöscher, M.; Liedtke, R.; Gansberger, E.; Hess, J.; Wasiliu, M.;

Lindhofer, H.; Chelius, D.; Ruf, P.; Gruber, P.; Plöscher, M.; Liedtke, R.; Gansberger, E.; Hess, J.; Wasiliu, M.; Structural, H. L.; Chelius, D.; *et al.* Structural and Functional Characterization of the Trifunctional Antibody Catumaxomab Structural and Functional Characterization of the Trifunctional Antibody Catumaxomab. **2016**, *0862*, 309–319.

204. Huehls, A. M.; Coupet, T. A.; Sentman, C. L. Bispecific T Cell Engagers for Cancer Immunotherapy. *Immunol. Cell Biol.* **2015**, *93*, 290–296.

205. Klinger, M.; Brandl, C.; Zugmaier, G.; Hijazi, Y.; Bargou, R. C.; Topp, M. S.; Gökbuget, N.; Neumann, S.; Goebeler, M.; Viardot, A.; Stelljes, M.; Hoelzer, D.; Degenhard, E.; Nagorsen, D.; Baeuerle, P. a; Wolf, A.; Kufer, P.; Dc, W.; Go, N. Immunopharmacologic Response of Patients with B-Lineage Acute Lymphoblastic Leukemia to Continuous Infusion of T Cell − Engaging Immunopharmacologic Response of Patients with B-Lineage Acute Lymphoblastic Leukemia to Continuous Infusion of T Cell – Engagi. **2013**, *119*, 6226–6233.

206. Yuraszeck, T.; Kasichayanula, S.; Benjamin, J. E. Translation and Clinical Development of Bispecific T-Cell Engaging Antibodies for Cancer Treatment. *Clin. Pharmacol. Ther.* **2017**, *101*, 634–645.

207. Lee, K. J.; Chow, V.; Weissman, A.; Tulpule, S.; Aldoss, I.; Akhtari, M. Clinical Use of Blinatumomab for B-Cell Acute Lymphoblastic Leukemia in Adults. *Ther. Clin. Risk Manag.* **2016**, *12*, 1301–1310.

208. Kantarjian, H.; Stein, A.; Gökbuget, N.; Fielding, A. K.; Schuh, A. C.; Ribera, J.-M.; Wei, A.; Dombret, H.; Foà, R.; Bassan, R.; Arslan, Ö.; Sanz, M. A.; Bergeron, J.; Demirkan, F.; Lech-Maranda, E.; Rambaldi, A.; Thomas, X.; Horst, H.-A.; Brüggemann, M.; *et al.* Blinatumomab versus Chemotherapy for Advanced Acute Lymphoblastic Leukemia. *N. Engl. J. Med.* **2017**, *376*, 836–847.

209. Mack, M.; Riethmuller, G.; Kufer, P. A Small Bispecific Antibody Construct Expressed as a Functional Single-Chain Molecule with High Tumor Cell Cytotoxicity. *Proc. Natl. Acad. Sci.* **1995**, *92*, 7021–7025.

210. Hipp, S.; Tai, Y. T.; Blanset, D.; Deegen, P.; Wahl, J.; Thomas, O.; Rattel, B.; Adam, P. J.; Anderson, K. C.; Friedrich, M. A Novel BCMA/CD3 Bispecific T-Cell Engager for the Treatment

of Multiple Myeloma Induces Selective Lysis in Vitro and in Vivo. *Leukemia* **2017**, *31*, 1743–1751.

211. Iwahori, K.; Kakarla, S.; Velasquez, M. P.; Yu, F.; Yi, Z.; Gerken, C.; Song, X.-T.; Gottschalk, S. Engager T Cells: A New Class of Antigen-Specific T Cells That Redirect Bystander T Cells. *Mol. Ther.* **2014**.

212. Ross, S. L.; Sherman, M.; McElroy, P. L.; Lofgren, J. A.; Moody, G.; Baeuerle, P. A.; Coxon, A.; Arvedson, T. Bispecific T Cell Engager (BiTE®) Antibody Constructs Can Mediate Bystander Tumor Cell Killing. *PLoS One* **2017**, *12*, 1–24.

213. Ryan, J. M.; Mittal, P.; Menoret, A.; Svedova, J.; Wasser, J. S.; Adler, A. J.; Vella, A. T. A Novel Biologic Platform Elicits Profound T Cell Costimulatory Activity and Antitumor Immunity in Mice. *Cancer Immunol. Immunother.* **2018**, *0*, 0.

214. Chen, Y.; Xu, Y. Pharmacokinetics of Bispecific Antibody. *Current Pharmacology Reports*, 2017, *3*, 126–137.

215. Sedykh, S. E.; Prinz, V. V.; Buneva, V. N.; Nevinsky, G. A. Bispecific Antibodies: Design, Therapy, Perspectives. *Drug Design, Development and Therapy*, 2018, *12*, 195–208.

216. Fischer, J. A. A.; Hueber, A. J.; Wilson, S.; Galm, M.; Baum, W.; Kitson, C.; Auer, J.; Lorenz, S. H.; Moelleken, J.; Bader, M.; Tissot, A. C.; Tan, S.-L.; Seeber, S.; Schett, G. Combined Inhibition of Tumor Necrosis Factor α and Interleukin-17 As a Therapeutic Opportunity in Rheumatoid Arthritis: Development and Characterization of a Novel Bispecific Antibody. *Arthritis Rheumatol.* **2015**, *67*, 51–62.

217. Lyman, M.; Lieuw, V.; Richardson, R.; Timmer, A.; Stewart, C.; Granger, S.; Woods, R.; Silacci, M.; Grabulovski, D.; Newman, R. A Bispecific Antibody That Targets IL-6 Receptor and IL-17A for the Potential Therapy of Patients with Autoimmune and Inflammatory Diseases. *J. Biol. Chem.* **2018**, jbc-M117.

218. Huang, Y.; Yu, J.; Lanzi, A.; Yao, X.; Andrews, C. D.; Tsai, L.; Gajjar, M. R.; Sun, M.; Seaman, M. S.; Padte, N. N.; Ho, D. D. Engineered Bispecific Antibodies with Exquisite HIV-1-Neutralizing Activity. *Cell* **2016**, *165*, 1621–1631.

219. Steinhardt, J. J.; Guenaga, J.; Turner, H. L.; McKee, K.; Louder, M. K.; O'Dell, S.; Chiang, C. I.;

Lei, L.; Galkin, A.; Andrianov, A. K.; Doria-Rose, N. A.; Bailer, R. T.; Ward, A. B.; Mascola, J. R.; Li, Y. Rational Design of a Trispecific Antibody Targeting the HIV-1 Env with Elevated Anti-Viral Activity. *Nat. Commun.* **2018**, *9*.

220. Pang, X.; Ma, F.; Zhang, P.; Zhong, Y.; Zhang, J.; Wang, T.; Zheng, G.; Hou, X.; Zhao, J.; He, C. Treatment of Human B-Cell Lymphomas Using Minicircle DNA Vector Expressing Anti-CD3/CD20 in a Mouse Model. *Hum. Gene Ther.* **2017**, *28*, 216–225.

221. Oelke, M.; Schneck, J. P. Overview of a HLA-Ig Based "Lego-like System" for T Cell Monitoring, Modulation and Expansion. *Immunol. Res.* **2010**, *47*, 248–256.

222. Perica, K.; Kosmides, A. K.; Schneck, J. P. Linking Form to Function: Biophysical Aspects of Artificial Antigen Presenting Cell Design. *Biochim. Biophys. Acta (BBA)-Molecular Cell Res.* **2015**, *1853*, 781–790.

223. Dudley, M. E.; Rosenberg, S. a. Adoptive-Cell-Transfer Therapy for the Treatment of Patients with Cancer. *Nat. Rev. Cancer* **2003**, *3*, 666–675.

224. Rosenberg, S. A.; Restifo, N. P. Adoptive Cell Transfer as Personalized Immunotherapy for Human Cancer. *Science (80-.).* **2015**, *348*, 62–68.

225. Busch, D. H.; Fräßle, S. P.; Sommermeyer, D.; Buchholz, V. R.; Riddell, S. R. Role of Memory T Cell Subsets for Adoptive Immunotherapy. *Semin. Immunol.* **2016**, *28*, 28–34.

226. Della Bella, S.; Gennaro, M.; Vaccari, M.; Ferraris, C.; Nicola, S.; Riva, A.; Clerici, M.; Greco, M.; Villa, M. L. Altered Maturation of Peripheral Blood Dendritic Cells in Patients with Breast Cancer. *Br. J. Cancer* **2003**, *89*, 1463.

227. Satthaporn, S.; Robins, A.; Vassanasiri, W.; El-Sheemy, M.; Jibril, J. a; Clark, D.; Valerio, D.; Eremin, O. Dendritic Cells Are Dysfunctional in Patients with Operable Breast Cancer. *Cancer Immunol. Immunother.* **2004**, *53*, 510–518.

228. Ye, F.; Yu, Y.; Hu, Y.; Lu, W.; Xie, X. Alterations of Dendritic Cell Subsets in the Peripheral Circulation of Patients with Cervical Carcinoma. *J. Exp. Clin. Cancer Res.* **2010**, *29*, 78.

229. Curtsinger, J.; Deeths, M. J.; Pease, P.; Mescher, M. F. Artificial Cell Surface Constructs for Studying Receptor-Ligand Contributions to Lymphocyte Activation. *J. Immunol. Methods* **1997**, *209*, 47–57.

230. Mescher, M. F. Surface Contact Requirements for Activation of Cytotoxic T Lymphocytes. *J. Immunol.* **1992**, *149*, 2402–2405.

231. Oelke, M.; Maus, M. V; Didiano, D.; June, C. H.; Mackensen, A.; Schneck, J. P. Ex Vivo Induction and Expansion of Antigen-Specific Cytotoxic T Cells by HLA-Ig–coated Artificial Antigen-Presenting Cells. *Nat. Med.* **2003**, *9*, 619–625.

232. Tham, E. L.; Jensen, P. L.; Mescher, M. F. Activation of Antigen-Specific T Cells by Artificial Cell Constructs Having Immobilized Multimeric Peptide-Class I Complexes and Recombinant B7-Fc Proteins. *J. Immunol. Methods* **2001**, *249*, 111–119.

233. Motta, I.; Lone, Y. C.; Kourilsky, P. In Vitro Induction of Naive Cytotoxic T Lymphocytes with Complexes of Peptide and Recombinant MHC Class I Molecules Coated onto Beads: Role of TCR/Ligand Density. *Eur. J. Immunol.* **1998**, *28*, 3685–3695.

234. Hinrichs, C. S.; Borman, Z. a; Gattinoni, L.; Yu, Z.; Burns, W. R.; Klebanoff, C. a; Johnson, L. a; Kerkar, S. P.; Yang, S.; Muranski, P.; Palmer, D. C.; Scott, C. D.; Morgan, R. a; Robbins, P. F.; Rosenberg, S. a; Restifo, N. P.; Huang, J. Human Effector CD8 + T Cells Derived from Naive Rather than Memory Subsets Possess Superior Traits for Adoptive Immunotherapy. *October* **2011**, *117*, 808–814.

235. Steenblock, E. R.; Fahmy, T. M. A Comprehensive Platform for Ex Vivo T-Cell Expansion Based on Biodegradable Polymeric Artificial Antigen-Presenting Cells. *Mol. Ther.* **2008**, *16*, 765–772.

236. Perica, K.; De León Medero, A.; Durai, M.; Chiu, Y. L.; Bieler, J. G.; Sibener, L.; Niemöller, M.; Assenmacher, M.; Richter, A.; Edidin, M.; Oelke, M.; Schneck, J. Nanoscale Artificial Antigen Presenting Cells for T Cell Immunotherapy. *Nanomedicine* **2014**, *10*, 119–129.

237. Schamel, W. W. A.; Arechaga, I.; Risueño, R. M.; van Santen, H. M.; Cabezas, P.; Risco, C.; Valpuesta, J. M.; Alarcón, B. Coexistence of Multivalent and Monovalent TCRs Explains High Sensitivity and Wide Range of Response. *J. Exp. Med.* **2005**, *202*, 493–503.

238. Delcassian, D.; Depoil, D.; Rudnicka, D.; Liu, M.; Davis, D. M.; Dustin, M. L.; Dunlop, I. E. Nanoscale Ligand Spacing Influences Receptor Triggering in T Cells and NK Cells. *Nano Lett.* **2013**, *13*, 5608–5614.

239. Matic, J.; Deeg, J.; Scheffold, A.; Goldstein, I.; Spatz, J. P. Fine Tuning and Efficient T Cell

Activation with Stimulatory ACD3 Nanoarrays. *Nano Lett.* **2013**, *13*, 5090–5097.

240. Fang, J.; Nakamura, H.; Maeda, H. The EPR Effect: Unique Features of Tumor Blood Vessels for Drug Delivery, Factors Involved, and Limitations and Augmentation of the Effect. *Adv. Drug Deliv. Rev.* **2011**, *63*, 136–151.

241. Helle, M.; Rampazzo, E.; Monchanin, M.; Marchal, F.; Guillemin, F.; Bonacchi, S.; Salis, F.; Prodi, L.; Bezdetnaya, L. Surface Chemistry Architecture of Silica Nanoparticles Determine the Efficiency of in Vivo Fluorescence Lymph Node Mapping. *ACS Nano* **2013**, *7*, 8645–8657.

242. Astete, C. E.; Sabliov, C. M. Synthesis and Characterization of PLGA Nanoparticles. *J. Biomater. Sci. Polym. Ed.* **2006**, *17*, 247–289.

243. Danhier, F.; Ansorena, E.; Silva, J. M.; Coco, R.; Le Breton, A.; Préat, V. PLGA-Based Nanoparticles: An Overview of Biomedical Applications. *J. Control. Release* **2012**, *161*, 505–522.

244. Perica, K.; Tu, A.; Richter, A.; Bieler, J. G.; Edidin, M.; Schneck, J. P. Magnetic Field-Induced T Cell Receptor Clustering by Nanoparticles Enhances T Cell Activation and Stimulates Antitumor Activity. *ACS Nano* **2014**, *8*, 2252–2260.

245. Ye, Q.; Song, D.-G.; Poussin, M.; Yamamoto, T.; Best, A.; Li, C.; Coukos, G.; Powell, D. J. CD137 Accurately Identifies and Enriches for Naturally Occurring Tumor-Reactive T Cells in Tumor. *Clin. Cancer Res.* **2014**, *20*, 44–55.

246. Hernandez-chacon, J. A.; Li, Y.; Wu, R. C.; Bernatchez, C.; Weber, J.; Hwu, P.; Radvanyi, L. Co-Stimulation through the CD137/4-1BB Pathway Protects Human Melanoma Tumor-Infiltrating Lymphocytes from Activation-Induced Cell Death and Enhances Anti-Tumor Effector Function. **2012**, *34*, 236–250.

247. Zhang, H.; Snyder, K. M.; Suhoski, M. M.; Maus, M. V; Kapoor, V. 4-1BB Is Superior to CD28 Costimulation for Generating CD8+ Cytotoxic Lymphocytes for Adoptive Immunotherapy. **2013**, *179*, 4910–4918.

248. Tay, N. Q.; Lee, D. C. P.; Chua, Y. L.; Prabhu, N.; Gascoigne, N. R. J.; Kemeny, D. M. CD40L Expression Allows CD8+ T Cells to Promote Their Own Expansion and Differentiation through Dendritic Cells. *Front. Immunol.* **2017**, *8*.

249. Singh, M.; Vianden, C.; Cantwell, M. J.; Dai, Z.; Xiao, Z.; Sharma, M.; Khong, H.; Jaiswal, A. R.;

Faak, F.; Hailemichael, Y.; Janssen, L. M. E.; Bharadwaj, U.; Curran, M. A.; Diab, A.; Bassett, R. L.; Tweardy, D. J.; Hwu, P.; Overwijk, W. W. Intratumoral CD40 Activation and Checkpoint Blockade Induces T Cell-Mediated Eradication of Melanoma in the Brain. *Nat. Commun.* **2017**, *8*, 1–10.

250. Kosmides, A. K.; Necochea, K.; Hickey, J. W.; Schneck, J. P. Separating T Cell Targeting Components onto Magnetically Clustered Nanoparticles Boosts Activation. *Nano Lett.* **2018**, *18*.

251. Poon, I. K. H.; Lucas, C. D.; Rossi, A. G.; Ravichandran, K. S. Apoptotic Cell Clearance: Basic Biology and Therapeutic Potential. *Nat. Rev. Immunol.* **2014**, *14*, 166–180.

252. Bruns, H.; Bessell, C.; Varela, J. C.; Haupt, C.; Fang, J.; Pasemann, S.; Mackensen, A.; Oelke, M.; Schneck, J. P.; Schütz, C. CD47 Enhances in Vivo Functionality of Artificial Antigen-Presenting Cells. *Clin. Cancer Res.* **2015**, *21*, 2075–2083.

253. LEVINE, B. L.; COTTE, J.; SMALL, C. C.; CARROLL, R. G.; RILEY, J. L.; BERNSTEIN, W. B.; VAN EPPS, D. E.; HARDWICK, R. A.; JUNE, C. H. Large-Scale Production of CD4+ T Cells from HIV-1-Infected Donors after CD3/CD28 Costimulation. *J. Hematother.* **1998**, *7*, 437–448.

254. Perica, K.; Bieler, J. G.; Schütz, C.; Varela, J. C.; Douglass, J.; Skora, A.; Chiu, Y. L.; Oelke, M.; Kinzler, K.; Zhou, S. Enrichment and Expansion with Nanoscale Artificial Antigen Presenting Cells for Adoptive Immunotherapy. *ACS Nano* **2015**, *9*, 6861–6871.

255. Zhang, Q.; Wei, W.; Wang, P.; Zuo, L.; Li, F.; Xu, J.; Xi, X.; Gao, X.; Ma, G.; Xie, H. Biomimetic Magnetosomes as Versatile Artificial Antigen-Presenting Cells to Potentiate T-Cell-Based Anticancer Therapy. *ACS Nano* **2017**, *11*, 10724–10732.

256. Cheng, C. J.; Tietjen, G. T.; Saucier-Sawyer, J. K.; Saltzman, W. M. A Holistic Approach to Targeting Disease with Polymeric Nanoparticles. *Nat. Rev. Drug Discov.* **2015**, *14*, 239.

257. Kosmides, A. K. K.; Meyer, R. A. A.; Hickey, J. W. W.; Aje, K.; Cheung, K. N. N.; Green, J. J. J.; Schneck, J. P. P. Biomimetic Biodegradable Artificial Antigen Presenting Cells Synergize with PD-1 Blockade to Treat Melanoma. *Biomaterials* **2017**, *118*, 16–26.

258. Meyer, R. A.; Sunshine, J. C.; Perica, K.; Kosmides, A. K.; Aje, K.; Schneck, J. P.; Green, J. J. Biodegradable Nanoellipsoidal Artificial Antigen Presenting Cells for Antigen Specific T-cell Activation. *Small* **2015**, *11*, 1519–1525.

259. Janssen, E. M.; Lemmens, E. E.; Wolfe, T.; Christen, U.; von Herrath, M. G.; Schoenberger, S. P. CD4+ T Cells Are Required for Secondary Expansion and Memory in CD8+ T Lymphocytes. *Nature* **2003**, *421*, 852.

260. Malek, T. R. The Biology of Interleukin-2. *Annu. Rev. Immunol.* **2008**, *26*, 453–479.

261. Shedlock, D. J.; Shen, H. Requirement for CD4 T Cell Help in Generating Functional CD8 T Cell Memory. *Science (80-.).* **2003**, *300*, 337–339.

262. Steenblock, E. R.; Fadel, T.; Labowsky, M.; Pober, J. S.; Fahmy, T. M. An Artificial Antigen-Presenting Cell with Paracrine Delivery of IL-2 Impacts the Magnitude and Direction of the T Cell Response. *J. Biol. Chem.* **2011**, *286*, 34883–34892.

263. Yoo, J.-W.; Irvine, D. J.; Discher, D. E.; Mitragotri, S. Bio-Inspired, Bioengineered and Biomimetic Drug Delivery Carriers. *Nat. Rev. Drug Discov.* **2011**, *10*, 521.

264. Sun, X.; Han, X.; Xu, L.; Gao, M.; Xu, J.; Yang, R.; Liu, Z. Surface-Engineering of Red Blood Cells as Artificial Antigen Presenting Cells Promising for Cancer Immunotherapy. *Small* **2017**, *13*, 1–8.

265. Giannoni, F.; Barnett, J.; Bi, K.; Samodal, R.; Lanza, P.; Marchese, P.; Billetta, R.; Vita, R.; Klein, M. R.; Prakken, B. Clustering of T Cell Ligands on Artificial APC Membranes Influences T Cell Activation and Protein Kinase C θ Translocation to the T Cell Plasma Membrane. *J. Immunol.* **2005**, *174*, 3204–3211.

266. Ding, Q.; Chen, J.; Wei, X.; Sun, W.; Mai, J.; Yang, Y.; Xu, Y. RAFTsomes Containing Epitope-MHC-II Complexes Mediated CD4+ T Cell Activation and Antigen-Specific Immune Responses. *Pharm. Res.* **2013**, *30*, 60–69.

267. Fadel, T. R.; Sharp, F. A.; Vudattu, N.; Ragheb, R.; Garyu, J.; Kim, D.; Hong, E.; Li, N.; Haller, G. L.; Pfefferle, L. D.; Justesen, S.; Harold, K. C.; Fahmy, T. M. A Carbon Nanotube-Polymer Composite for T-Cell Therapy. *Nat. Nanotechnol.* **2014**, *9*, 639–647.

268. Clemente-Casares, X.; Blanco, J.; Ambalavanan, P.; Yamanouchi, J.; Singha, S.; Fandos, C.; Tsai, S.; Wang, J.; Garabatos, N.; Izquierdo, C.; Agrawal, S.; Keough, M. B.; Yong, V. W.; James, E.; Moore, A.; Yang, Y.; Stratmann, T.; Serra, P.; Santamaria, P. Expanding Antigen-Specific Regulatory Networks to Treat Autoimmunity. *Nature* **2016**, *530*, 434–440.

269. Singha, S.; Shao, K.; Yang, Y.; Clemente-Casares, X.; Solé, P.; Clemente, A.; Blanco, J.; Dai, Q.; Song, F.; Liu, S. W.; Yamanouchi, J.; Umeshappa, C. S.; Nanjundappa, R. H.; Detampel, P.; Amrein, M.; Fandos, C.; Tanguay, R.; Newbigging, S.; Serra, P.; *et al.* Peptide-MHC-Based Nanomedicines for Autoimmunity Function as T-Cell Receptor Microclustering Devices. *Nat. Nanotechnol.* **2017**, *12*, 701–710.

270. Shutz, C.; Varela, J. C.; Perica, K.; Haupt, C.; Oelke, M.; Schneck, J. P. Antigen-Specific T Cell Redirectors: A Nanoparticle Based Approach for Redirecting T Cells. *Oncotarget* **2016**, *7*, 68503–68512.

271. Kosmides, A. K. A. K.; Sidhom, J. W. J.-W.; Fraser, A.; Bessell, C. A. C. A.; Schneck, J. P. J. P. Dual Targeting Nanoparticle Stimulates the Immune System to Inhibit Tumor Growth. *ACS Nano* **2017**, *11*, 5417–5429.

272. Steinman, R. M. Decisions About Dendritic Cells: Past, Present, and Future. *Annu. Rev. Immunol.* **2012**, *30*, 1–22.

273. Bookstaver, M. L.; Tsai, S. J.; Bromberg, J. S.; Jewell, C. M. Improving Vaccine and Immunotherapy Design Using Biomaterials. *Trends in Immunology*, 2017.

274. Kantoff, P. W.; Higano, C. S.; Shore, N. D.; Berger, R.; Small, E. J.; Penson, D. F.; Redfern, C. H.; Ferrari, A. C.; Dreicer, R.; Sims, R. B.; Xu, Y.; Frohlich, M. W.; Schellhammer, P. F. Sipuleucel-T Immunotherapy for Castration-Resistant Prostate Cancer. *N. Engl. J. Med.* **2010**, *363*, 2373–2383.

275. Paller, C. J.; Antonarakis, E. S. Sipuleucel-T for the Treatment of Metastatic Prostate Cancer. *Hum. Vaccin. Immunother.* **2012**, *8*, 509–519.

276. Gu, L.; Mooney, D. J. Biomaterials and Emerging Anticancer Therapeutics: Engineering the Microenvironment. *Nat. Rev. Cancer* **2015**, *16*, 56–66.

277. Leleux, J.; Alexandra, A.; Roy, K. Engineering Immunity: Modulating Dendritic Cell Subsets and Lymph Node Response to Direct Immune-Polarization and Vaccine Efficacy. *J Control Release* **2015**, *219*, 610–621.

278. Fifis, T.; Gamvrellis, A.; Crimeen-Irwin, B.; Pietersz, G. A.; Li, J.; Mottram, P. L.; McKenzie, I. F. C.; Plebanski, M. Size-Dependent Immunogenicity: Therapeutic and Protective Properties of Nano-Vaccines against Tumors. *J. Immunol.* **2004**, *173*, 3148–3154.

279. Kuai, R.; Ochyl, L. J.; Bahjat, K. S.; Schwendeman, A.; Moon, J. J. Designer Vaccine Nanodiscs for Personalized Cancer Immunotherapy. *Nat. Mater.* **2016**, *1*, 1–10.

280. Manolova, V.; Flace, A.; Bauer, M.; Schwarz, K.; Saudan, P.; Bachmann, M. F. Nanoparticles Target Distinct Dendritic Cell Populations According to Their Size. *Eur. J. Immunol.* **2008**, *38*, 1404–1413.

281. Hess, K. L.; Oh, E.; Tostanoski, L. H.; Andorko, J. I.; Susumu, K.; Deschamps, J. R.; Medintz, I. L.; Jewell, C. M. Engineering Immunological Tolerance Using Quantum Dots to Tune the Density of Self-Antigen Display. *Adv. Funct. Mater.* **2017**, *27*.

282. Tostanoski, L. H.; Chiu, Y. C.; Andorko, J. I.; Guo, M.; Zeng, X.; Zhang, P.; Royal, W.; Jewell, C. M. Design of Polyelectrolyte Multilayers to Promote Immunological Tolerance. *ACS Nano* **2016**, *10*, 9334–9345.

283. Lewis, J. S.; Dolgova, N. V.; Zhang, Y.; Xia, C. Q.; Wasserfall, C. H.; Atkinson, M. A.; Clare-Salzler, M. J.; Keselowsky, B. G. A Combination Dual-Sized Microparticle System Modulates Dendritic Cells and Prevents Type 1 Diabetes in Prediabetic NOD Mice. *Clin. Immunol.* **2015**, *160*, 90–102.

284. Hunter, Z.; McCarthy, D. P.; Yap, W. T.; Harp, C. T.; Getts, D. R.; Shea, L. D.; Miller, S. D. A Biodegradable Nanoparticle Platform for the Induction of Antigen-Specific Immune Tolerance for Treatment of Autoimmune Disease. *ACS Nano* **2014**, *8*, 2148–2160.

285. Pishesha, N.; Bilate, A. M.; Wibowo, M. C.; Huang, N.-J.; Li, Z.; Dhesycka, R.; Bousbaine, D.; Li, H.; Patterson, H. C.; Dougan, S. K.; Maruyama, T.; Lodish, H. F.; Ploegh, H. L. Engineered Erythrocytes Covalently Linked to Antigenic Peptides Can Protect against Autoimmune Disease. *Proc. Natl. Acad. Sci.* **2017**, *114*, 3157–3162.

286. Lee, I. H.; Kwon, H. K.; An, S.; Kim, D.; Kim, S.; Yu, M. K.; Lee, J. H.; Lee, T. S.; Im, S. H.; Jon, S. Imageable Antigen-Presenting Gold Nanoparticle Vaccines for Effective Cancer Immunotherapy in Vivo. *Angew. Chemie - Int. Ed.* **2012**, *51*, 8800–8805.

287. Li, A. V; Moon, J. J.; Abraham, W.; Suh, H.; Seidman, M. A.; Yen, M.; Im, E.; Foley, M. H.; Dan, H. Generation of Effector Memory T Cell–Based Mucosal and Systemic Immunity with Pulmonary Nanoparticle Vaccination. *Sci Transl Med* **2014**, *5*, 204ra130.

288. Raghuwanshi, D.; Mishra, V.; Suresh, M. R.; Kaur, K. A Simple Approach for Enhanced Immune Response Using Engineered Dendritic Cell Targeted Nanoparticles. *Vaccine* **2012**, *30*, 7292–7299.

289. Cruz, L. J.; Rosalia, R. A.; Kleinovink, J. W.; Rueda, F.; Löwik, C. W. G. M.; Ossendorp, F. Targeting Nanoparticles to CD40, DEC-205 or CD11c Molecules on Dendritic Cells for Efficient CD8+T Cell Response: A Comparative Study. *J. Control. Release* **2014**, *192*, 209–218.

290. Scott, E. A.; Stano, A.; Gillard, M.; Maio-Liu, A. C.; Swartz, M. A.; Hubbell, J. A. Dendritic Cell Activation and T Cell Priming with Adjuvant- and Antigen-Loaded Oxidation-Sensitive Polymersomes. *Biomaterials* **2012**, *33*, 6211–6219.

291. Balmert, S. C.; Donahue, C.; Vu, J. R.; Erdos, G.; Falo, L. D.; Little, S. R. In Vivo Induction of Regulatory T Cells Promotes Allergen Tolerance and Suppresses Allergic Contact Dermatitis. *J. Control. Release* **2017**, *261*, 223–233.

292. Ratay, M. L.; Glowacki, A. J.; Balmert, S. C.; Acharya, A. P.; Polat, J.; Andrews, L. P.; Fedorchak, M. V.; Schuman, J. S.; Vignali, D. A. A.; Little, S. R. Treg-Recruiting Microspheres Prevent Inflammation in a Murine Model of Dry Eye Disease. *J. Control. Release* **2017**, *258*, 208–217.

293. Jhunjhunwala, S.; Raimondi, G.; Glowacki, A. J.; Hall, S. J.; Maskarinec, D.; Thorne, S. H.; Thomson, A. W.; Little, S. R. Bioinspired Controlled Release of CCL22 Recruits Regulatory T Cells in Vivo. *Adv. Mater.* **2012**, *24*, 4735–4738.

294. Glowacki, A. J.; Yoshizawa, S.; Jhunjhunwala, S.; Vieira, A. E.; Garlet, G. P.; Sfeir, C.; Little, S. R. Prevention of Inflammation-Mediated Bone Loss in Murine and Canine Periodontal Disease via Recruitment of Regulatory Lymphocytes. *Proc. Natl. Acad. Sci.* **2013**, *110*, 18525–18530.

295. Fahmy, T. M.; Schneck, J. P.; Saltzman, W. M. A Nanoscopic Multivalent Antigen-Presenting Carrier for Sensitive Detection and Drug Delivery to T Cells. *Nanomedicine* **2007**, *3*, 75–85.

296. Dinauer, N.; Balthasar, S.; Weber, C.; Kreuter, J.; Langer, K.; von Briesen, H. Selective Targeting of Antibody-Conjugated Nanoparticles to Leukemic Cells and Primary T-Lymphocytes. *Biomaterials* **2005**, *26*, 5898–5906.

297. Ramishetti, S.; Kedmi, R.; Goldsmith, M.; Leonard, F.; Sprague, A. G.; Godin, B.; Gozin, M.; Cullis, P. R.; Dykxhoorn, D. M.; Peer, D. Systemic Gene Silencing in Primary T Lymphocytes Using Targeted Lipid Nanoparticles. **2015**, 6706–6716.

298. Stephan, M. T.; Stephan, S. B.; Bak, P.; Chen, J.; Irvine, D. J. Synapse-Directed Delivery of Immunomodulators Using T-Cell-Conjugated Nanoparticles. *Biomaterials* **2012**, *33*, 5776–5787.

299. Jones, R. B.; Mueller, S.; Kumari, S.; Vrbanac, V.; Genel, S.; Tager, A. M.; Allen, T. M.; Walker, B. D.; Irvine, D. J. Antigen Recognition-Triggered Drug Delivery Mediated by Nanocapsule-Functionalized Cytotoxic T-Cells. *Biomaterials* **2017**, *117*, 44–53.

300. Zheng, Y.; Tang, L.; Mabardi, L.; Kumari, S.; Irvine, D. J. Enhancing Adoptive Cell Therapy of Cancer through Targeted Delivery of Small-Molecule Immunomodulators to Internalizing or Non-Internalizing Receptors. *ACS Nano* **2017**, acsnano.7b00078.

301. Ascierto, P. A.; Simeone, E.; Sznol, M.; Fu, Y. X.; Melero, I. Clinical Experiences with Anti-CD137 and Anti-PD1 Therapeutic Antibodies. *Semin. Oncol.* **2010**, *37*, 508–516.

302. Panelli, M. C.; White, R.; Foster, M.; Martin, B.; Wang, E.; Smith, K.; Marincola, F. M. Forecasting the Cytokine Storm Following Systematic Interleukin (IL)-2 Administration. *J. Transl. Med.* **2004**, *2*, 1–14.

303. Kwong, B.; Gai, S. A.; Elkhader, J.; Wittrup, K. D.; Irvine, D. J. Localized Immunotherapy via Liposome-Anchored Anti-CD137 + IL-2 Prevents Lethal Toxicity and Elicits Local and Systemic Antitumor Immunity. *Cancer Res.* **2013**, *73*, 1547–1558.

304. Zhang, Y.; Li, N.; Suh, H.; Irvine, D. J. Nanoparticle Anchoring Targets Immune Agonists to Tumors Enabling Anti-Cancer Immunity without Systemic Toxicity. *Nat. Commun.* **2018**, *9*, 6.

305. Butler, M. O.; Hirano, N. Human Cell-based Artificial Antigen-presenting Cells for Cancer Immunotherapy. *Immunol. Rev.* **2014**, *257*, 191–209.

306. Maus, M. V; Thomas, A. K.; Leonard, D. G. B.; Allman, D.; Addya, K.; Schlienger, K.; Riley, J. L.; June, C. H. Ex Vivo Expansion of Polyclonal and Antigen-Specific Cytotoxic T Lymphocytes by Artificial APCs Expressing Ligands for the T-Cell Receptor, CD28 and 4-1BB. *Nat. Biotechnol.* **2002**, *20*, 143.

307. Suhoski, M. M.; Golovina, T. N.; Aqui, N. a; Tai, V. C.; Varela-Rohena, A.; Milone, M. C.; Carroll, R. G.; Riley, J. L.; June, C. H. Engineering Artificial Antigen-Presenting Cells to Express a Diverse Array of Co-Stimulatory Molecules. *Mol. Ther.* **2007**, *15*, 981–988.

308. Singh, H.; Figliola, M. J.; Dawson, M. J.; Huls, H.; Olivares, S.; Switzer, K.; Mi, T.; Maiti, S.;

Kebriaei, P.; Lee, D. A. Reprogramming CD19-Specific T Cells with IL-21 Signaling Can Improve Adoptive Immunotherapy of B-Lineage Malignancies. *Cancer Res.* **2011**, *71*, 3516–3527.

309. Hasan, A. N.; Selvakumar, A.; Liu, X.-R.; Sadelain, M. W.; Riviere, I.; Dupont, B.; O'Reilly, R. J. IL-15 Enhances in-Vitro Expansion And Functional Activity Of Antigen-Specific Effector Memory T Cells (TEM) While Co-Expression Of IL-15 And IL-15 Rα On Antigen Presenting Cells Also Promotes Enrichment And Preferential Expansion Of Central Memory T-Cells. *Biol. Blood Marrow Transplant.* **2010**, *16*, S159.

310. Papanicolaou, G. A.; Latouche, J.-B.; Tan, C.; Dupont, J.; Stiles, J.; Pamer, E. G.; Sadelain, M. Rapid Expansion of Cytomegalovirus–specific Cytotoxic T Lymphocytes by Artificial Antigen-Presenting Cells Expressing a Single HLA Allele. *Blood* **2003**, *102*, 2498–2505.

311. Garnier, A.; Hamieh, M.; Drouet, A.; Leprince, J.; Vivien, D.; Frébourg, T.; Le Mauff, B.; Latouche, J.-B.; Toutirais, O. Artificial Antigen-Presenting Cells Expressing HLA Class II Molecules as an Effective Tool for Amplifying Human Specific Memory CD4+ T Cells. *Immunol. Cell Biol.* **2016**, *94*, 662.

312. Butler, M. O.; Lee, J.-S.; Ansén, S.; Neuberg, D.; Hodi, F. S.; Murray, A. P.; Drury, L.; Berezovskaya, A.; Mulligan, R. C.; Nadler, L. M.; Hirano, N. Long-Lived Antitumor CD8+ Lymphocytes for Adoptive Therapy Generated Using an Artificial Antigen-Presenting Cell. *Clin. Cancer Res.* **2007**, *13*, 1857–1867.

313. Dupont, J.; Latouche, J.-B.; Ma, C.; Sadelain, M. Artificial Antigen-Presenting Cells Transduced with Telomerase Efficiently Expand Epitope-Specific, Human Leukocyte Antigen-Restricted Cytotoxic T Cells. *Cancer Res.* **2005**, *65*, 5417–5427.

314. Fesnak, A. D.; June, C. H.; Levine, B. L. Engineered T Cells: The Promise and Challenges of Cancer Immunotherapy. *Nat. Rev. Cancer* **2016**, *16*, 566–581.

315. Kochenderfer, J. N.; Wilson, W. H.; Janik, J. E.; Dudley, M. E.; Stetler-Stevenson, M.; Feldman, S. A.; Maric, I.; Raffeld, M.; Nathan, D.-A. N.; Lanier, B. J. Eradication of B-Lineage Cells and Regression of Lymphoma in a Patient Treated with Autologous T Cells Genetically Engineered to Recognize CD19. *Blood* **2010**, *116*, 4099–4102.

316. Maude, S. L.; Frey, N.; Shaw, P. A.; Aplenc, R.; Barrett, D. M.; Bunin, N. J.; Chew, A.; Gonzalez,

V. E.; Zheng, Z.; Lacey, S. F. Chimeric Antigen Receptor T Cells for Sustained Remissions in Leukemia. *N. Engl. J. Med.* **2014**, *371*, 1507–1517.

317. Porter, D. L.; Levine, B. L.; Kalos, M.; Bagg, A.; June, C. H. Chimeric Antigen Receptor–modified T Cells in Chronic Lymphoid Leukemia. *N. Engl. J. Med.* **2011**, *365*, 725–733.

318. Prasad, V. Immunotherapy: Tisagenlecleucel—the First Approved Car-t-Cell Therapy: Implications for Payers and Policy Makers. *Nat. Rev. Clin. Oncol.* **2018**, *15*, 11.

319. Jethwa, H.; Adami, A. A.; Maher, J. Use of Gene-Modified Regulatory T-Cells to Control Autoimmune and Alloimmune Pathology: Is Now the Right Time? *Clinical Immunology*, 2014, *150*, 51–63.

320. Lim, W. A.; June, C. H. The Principles of Engineering Immune Cells to Treat Cancer. *Cell* **2017**, *168*, 724–740.

321. Srivastava, S.; Riddell, S. R. Engineering CAR-T Cells: Design Concepts. *Trends Immunol.* **2015**, *36*, 494–502.

322. Davila, M. L.; Riviere, I.; Wang, X.; Bartido, S.; Park, J.; Curran, K.; Chung, S. S.; Stefanski, J.; Borquez-Ojeda, O.; Olszewska, M. Efficacy and Toxicity Management of 19-28z CAR T Cell Therapy in B Cell Acute Lymphoblastic Leukemia. *Sci. Transl. Med.* **2014**, *6*, 224ra25-224ra25.

323. Kochenderfer, J. N.; Dudley, M. E.; Feldman, S. A.; Wilson, W. H.; Spaner, D. E.; Maric, I.; Stetler-Stevenson, M.; Phan, G. Q.; Hughes, M. S.; Sherry, R. M. B-Cell Depletion and Remissions of Malignancy along with Cytokine-Associated Toxicity in a Clinical Trial of Anti-CD19 Chimeric-Antigen-Receptor–transduced T Cells. *Blood* **2012**, *119*, 2709–2720.

324. Morgan, R. A.; Yang, J. C.; Kitano, M.; Dudley, M. E.; Laurencot, C. M.; Rosenberg, S. A. Case Report of a Serious Adverse Event Following the Administration of T Cells Transduced with a Chimeric Antigen Receptor Recognizing ERBB2. *Mol. Ther.* **2010**, *18*, 843–851.

325. Gargett, T.; Brown, M. P. The Inducible Caspase-9 Suicide Gene System as a "Safety Switch" to Limit on-Target, off-Tumor Toxicities of Chimeric Antigen Receptor T Cells. *Front. Pharmacol.* **2014**, *5*, 235.

326. Chekmasova, A. A.; Rao, T. D.; Nikhamin, Y.; Park, K. J.; Levine, D. A.; Spriggs, D. R.; Brentjens, R. J. Successful Eradication of Established Peritoneal Ovarian Tumors in SCID-Beige

Mice Following Adoptive Transfer of T Cells Genetically Targeted to the MUC16 Antigen. *Clin. Cancer Res.* **2010**, *16*, 3594–3606.

327. Hudecek, M.; Schmitt, T. M.; Baskar, S.; Lupo-Stanghellini, M. T.; Nishida, T.; Yamamoto, T. N.; Bleakley, M.; Turtle, C. J.; Chang, W.-C.; Greisman, H. A. The B-Cell Tumor–associated Antigen ROR1 Can Be Targeted with T Cells Modified to Express a ROR1-Specific Chimeric Antigen Receptor. *Blood* **2010**, *116*, 4532–4541.

328. Rapoport, A. P.; Stadtmauer, E. A.; Binder-Scholl, G. K.; Goloubeva, O.; Vogl, D. T.; Lacey, S. F.; Badros, A. Z.; Garfall, A.; Weiss, B.; Finklestein, J. NY-ESO-1–specific TCR–engineered T Cells Mediate Sustained Antigen-Specific Antitumor Effects in Myeloma. *Nat. Med.* **2015**, *21*, 914.

329. Oren, R.; Hod-Marco, M.; Haus-Cohen, M.; Thomas, S.; Blat, D.; Duvshani, N.; Denkberg, G.; Elbaz, Y.; Benchetrit, F.; Eshhar, Z. Functional Comparison of Engineered T Cells Carrying a Native TCR versus TCR-like Antibody–based Chimeric Antigen Receptors Indicates Affinity/Avidity Thresholds. *J. Immunol.* **2014**, *193*, 5733–5743.

330. Alonso-Camino, V.; Sánchez-Martín, D.; Compte, M.; Nuñez-Prado, N.; Diaz, R. M.; Vile, R.; Alvarez-Vallina, L. CARbodies: Human Antibodies against Cell Surface Tumor Antigens Selected from Repertoires Displayed on T Cell Chimeric Antigen Receptors. *Mol. Ther. - Nucleic Acids* **2013**, *2*.

331. Alonso-Camino, V.; Sánchez-Martín, D.; Compte, M.; Sanz, L.; Alvarez-Vallina, L. Lymphocyte Display: A Novel Antibody Selection Platform Based on T Cell Activation. *PLoS One* **2009**, *4*, e7174.

332. Kloss, C. C.; Condomines, M.; Cartellieri, M.; Bachmann, M.; Sadelain, M. Combinatorial Antigen Recognition with Balanced Signaling Promotes Selective Tumor Eradication by Engineered T Cells. *Nat. Biotechnol.* **2013**, *31*, 71.

333. Wilkie, S.; van Schalkwyk, M. C. I.; Hobbs, S.; Davies, D. M.; van der Stegen, S. J. C.; Pereira, A. C. P.; Burbridge, S. E.; Box, C.; Eccles, S. A.; Maher, J. Dual Targeting of ErbB2 and MUC1 in Breast Cancer Using Chimeric Antigen Receptors Engineered to Provide Complementary Signaling. *J. Clin. Immunol.* **2012**, *32*, 1059–1070.

334. Fedorov, V. D.; Themeli, M.; Sadelain, M. PD-1–and CTLA-4–based Inhibitory Chimeric Antigen

Receptors (ICARs) Divert off-Target Immunotherapy Responses. *Sci. Transl. Med.* **2013**, *5*, 215ra172-215ra172.

335. Wu, C.-Y.; Roybal, K. T.; Puchner, E. M.; Onuffer, J.; Lim, W. A. Remote Control of Therapeutic T Cells through a Small Molecule-Gated Chimeric Receptor. *Science (80-.).* **2015**, *350*, aab4077.

336. Caruso, H. G.; Hurton, L. V; Najjar, A.; Rushworth, D.; Ang, S.; Olivares, S.; Mi, T.; Switzer, K.; Singh, H.; Huls, H. Tuning Sensitivity of CAR to EGFR Density Limits Recognition of Normal Tissue While Maintaining Potent Antitumor Activity. *Cancer Res.* **2015**, *75*, 3505–3518.

337. Klebanoff, C. A.; Rosenberg, S. A.; Restifo, N. P. Prospects for Gene-Engineered T Cell Immunotherapy for Solid Cancers. *Nat. Med.* **2016**, *22*, 26–36.

338. Yarchoan, M.; Johnson III, B. A.; Lutz, E. R.; Laheru, D. A.; Jaffee, E. M. Targeting Neoantigens to Augment Antitumour Immunity. *Nat. Rev. Cancer* **2017**, *17*, 209.

339. Robbins, P. F.; Lu, Y.-C.; El-Gamil, M.; Li, Y. F.; Gross, C.; Gartner, J.; Lin, J. C.; Teer, J. K.; Cliften, P.; Tycksen, E. Mining Exomic Sequencing Data to Identify Mutated Antigens Recognized by Adoptively Transferred Tumor-Reactive T Cells. *Nat. Med.* **2013**, *19*, 747.

340. Tran, E.; Robbins, P. F.; Lu, Y.-C.; Prickett, T. D.; Gartner, J. J.; Jia, L.; Pasetto, A.; Zheng, Z.; Ray, S.; Groh, E. M. T-Cell Transfer Therapy Targeting Mutant KRAS in Cancer. *N. Engl. J. Med.* **2016**, *375*, 2255–2262.

341. Chong, E. A.; Melenhorst, J. J.; Lacey, S. F.; Ambrose, D. E.; Gonzalez, V.; Levine, B. L.; June, C. H.; Schuster, S. J. PD-1 Blockade Modulates Chimeric Antigen Receptor (CAR)–modified T Cells: Refueling the CAR. *Blood* **2017**, *129*, 1039–1041.

342. Rupp, L. J.; Schumann, K.; Roybal, K. T.; Gate, R. E.; Chun, J. Y.; Lim, W. A.; Marson, A. CRISPR/Cas9-Mediated PD-1 Disruption Enhances Anti-Tumor Efficacy of Human Chimeric Antigen Receptor T Cells. *Sci. Rep.* **2017**, *7*, 737.

343. Roybal, K. T.; Williams, J. Z.; Morsut, L.; Rupp, L. J.; Kolinko, I.; Choe, J. H.; Walker, W. J.; McNally, K. A.; Lim, W. A. Engineering T Cells with Customized Therapeutic Response Programs Using Synthetic Notch Receptors. *Cell* **2016**, *167*, 419–432. e16.

344. Grada, Z.; Hegde, M.; Byrd, T.; Shaffer, D. R.; Ghazi, A.; Brawley, V. S.; Corder, A.; Schönfeld, K.; Koch, J.; Dotti, G. TanCAR: A Novel Bispecific Chimeric Antigen Receptor for Cancer

Immunotherapy. *Mol. Ther. Acids* **2013**, *2*.

345. Eyquem, J.; Mansilla-Soto, J.; Giavridis, T.; Van Der Stegen, S. J. C.; Hamieh, M.; Cunanan, K. M.; Odak, A.; Gönen, M.; Sadelain, M. Targeting a CAR to the TRAC Locus with CRISPR/Cas9 Enhances Tumour Rejection. *Nature* **2017**, *543*, 113–117.

346. MacDonald, K. G.; Hoeppli, R. E.; Huang, Q.; Gillies, J.; Luciani, D. S.; Orban, P. C.; Broady, R.; Levings, M. K. Alloantigen-Specific Regulatory T Cells Generated with a Chimeric Antigen Receptor. *J. Clin. Invest.* **2016**, *126*, 1413–1424.

347. Tebas, P.; Stein, D.; Tang, W. W.; Frank, I.; Wang, S. Q.; Lee, G.; Spratt, S. K.; Surosky, R. T.; Giedlin, M. A.; Nichol, G. Gene Editing of CCR5 in Autologous CD4 T Cells of Persons Infected with HIV. *N. Engl. J. Med.* **2014**, *370*, 901–910.

348. Conklin, B. R.; Hsiao, E. C.; Claeysen, S.; Dumuis, A.; Srinivasan, S.; Forsayeth, J. R.; Guettier, J.-M.; Chang, W. C.; Pei, Y.; McCarthy, K. D. Engineering GPCR Signaling Pathways with RASSLs. *Nat. Methods* **2008**, *5*, 673.

349. Kawahara, M.; Ueda, H.; Nagamune, T. Engineering Cytokine Receptors to Control Cellular Functions. *Biochem. Eng. J.* **2010**, *48*, 283–294.

350. Allan, S. E.; Alstad, A. N.; Merindol, N.; Crellin, N. K.; Amendola, M.; Bacchetta, R.; Naldini, L.; Roncarolo, M. G.; Soudeyns, H.; Levings, M. K. Generation of Potent and Stable Human CD4+ T Regulatory Cells by Activation-Independent Expression of FOXP3. *Mol. Ther.* **2008**, *16*, 194–202.

351. Chai, J. G.; Xue, S. A.; Coe, D.; Addey, C.; Bartok, I.; Scott, D.; Simpson, E.; Stauss, H. J.; Hori, S.; Sakaguchi, S.; Dyson, J. Regulatory T Cells, Derived from Naive CD4+CD25- T Cells by in Vitro Foxp3 Gene Transfer, Can Induce Transplantation Tolerance. *Transplantation* **2005**, *79*, 1310–1316.

352. Andolfi, G.; Fousteri, G.; Rossetti, M.; Magnani, C. F.; Jofra, T.; Locafaro, G.; Bondanza, A.; Gregori, S.; Roncarolo, M.-G. Enforced IL-10 Expression Confers Type 1 Regulatory T Cell (Tr1) Phenotype and Function to Human CD4(+) T Cells. *Mol. Ther.* **2012**, *20*, 1778–1790.

353. Qian, Z.; Latham, K. a; Whittington, K. B.; Miller, D. C.; Brand, D. D.; Rosloniec, E. F. Engineered Regulatory T Cells Coexpressing MHC Class II:Peptide Complexes Are Efficient Inhibitors of Autoimmune T Cell Function and Prevent the Development of Autoimmune Arthritis.

J. Immunol. **2013**, *190*, 5382–5391.

354. Shen, K.; Thomas, V. K.; Dustin, M. L.; Kam, L. C. Micropatterning of Costimulatory Ligands Enhances CD4+ T Cell Function. *Proc. Natl. Acad. Sci.* **2008**, *105*, 7791–7796.

355. Spatz, J. P.; Mössmer, S.; Hartmann, C.; Möller, M.; Herzog, T.; Krieger, M.; Boyen, H.-G.; Ziemann, P.; Kabius, B. Ordered Deposition of Inorganic Clusters from Micellar Block Copolymer Films. *Langmuir* **2000**, *16*, 407–415.

356. Groves, J. T.; Dustin, M. L. Supported Planar Bilayers in Studies on Immune Cell Adhesion and Communication. *J. Immunol. Methods* **2003**, *278*, 19–32.

357. Mossman, K. D.; Campi, G.; Groves, J. T.; Dustin, M. L. Altered TCR Signaling from Geometrically Repatterned Immunological Synapses. *Science (80-.).* **2005**, *310*, 1191–1193.

358. Bashour, K. T.; Gondarenko, a; Chen, H.; Shen, K.; Liu, X.; Huse, M.; Hone, J. C.; Kam, L. C. CD28 and CD3 Have Complementary Roles in T-Cell Traction Forces. *Proc. Natl. Acad. Sci.* **2014**, *111*, 2241–2246.

359. Judokusumo, E.; Tabdanov, E.; Kumari, S.; Dustin, M. L.; Kam, L. C. Mechanosensing in T Lymphocyte Activation. *Biophys. J.* **2012**, *102*, L5–L7.

360. O'Connor, R. S.; Hao, X.; Shen, K.; Bashour, K.; Akimova, T.; Hancock, W. W.; Kam, L. C.; Milone, M. C. Substrate Rigidity Regulates Human T Cell Activation and Proliferation. *J. Immunol.* **2012**, *189*, 1330–1339.

361. Li, Y.; Strick-Marchand, H.; Lim, A. I.; Ren, J.; Masse-Ranson, G.; Jouvion, G.; Rogge, L.; Lucas, S.; Di Santo, J. P. Regulatory T Cells Control Toxicity in a Humanized Model of IL-2 Therapy. *Nat. Commun.* **2017**, *8*, 1762.

362. Hori, Y.; Winans, A. M.; Irvine, D. J. Modular Injectable Matrices Based on Alginate Solution/Microsphere Mixtures That Gel in Situ and Co-Deliver Immunomodulatory Factors. *Acta Biomater.* **2009**, *5*, 969–982.

363. Ali, O. A.; Huebsch, N.; Cao, L.; Dranoff, G.; Mooney, D. J. Infection-Mimicking Materials to Program Dendritic Cells in Situ. *Nat. Mater.* **2009**, *8*, 151–158.

364. Hori, Y.; Winans, A. M.; Huang, C. C.; Horrigan, E. M.; Irvine, D. J. Injectable Dendritic Cell-Carrying Alginate Gels for Immunization and Immunotherapy. *Biomaterials* **2008**, *29*, 3671–3682.

365. Graham, J. G.; Zhang, X.; Goodman, A.; Pothoven, K.; Houlihan, J.; Wang, S.; Gower, R. M.; Luo, X.; Shea, L. D. PLG Scaffold Delivered Antigen-Specific Regulatory T Cells Induce Systemic Tolerance in Autoimmune Diabetes. *Tissue Eng. Part A* **2013**, *19*, 1465–1475.

366. Smith, T. T.; Moffett, H. F.; Stephan, S. B.; Opel, C. F.; Dumigan, A. G.; Jiang, X.; Pillarisetty, V. G.; Pillai, S. P. S.; Wittrup, K. D.; Stephan, M. T. Biopolymers Codelivering Engineered T Cells and STING Agonists Can Eliminate Heterogeneous Tumors. *J. Clin. Invest.* **2017**, *127*, 2176–2191.

367. Stephan, S. B.; Taber, A. M.; Jileaeva, I.; Pegues, E. P.; Sentman, C. L.; Stephan, M. T. Biopolymer Implants Enhance the Efficacy of Adoptive T-Cell Therapy. *Nat. Biotechnol.* **2015**, *33*, 97.

368. Cheung, A. S.; Zhang, D. K. Y.; Koshy, S. T.; Mooney, D. J. Scaffolds That Mimic Antigen-Presenting Cells Enable Ex Vivo Expansion of Primary T Cells. *Nat. Biotechnol.* **2018**, *36*, 160–169.

369. Fatehullah, A.; Tan, S. H.; Barker, N. Organoids as an in Vitro Model of Human Development and Disease. *Nat. Cell Biol.* **2016**, *18*, 246.

370. Giese, C.; Demmler, C. D.; Ammer, R.; Hartmann, S.; Lubitz, A.; Miller, L.; Müller, R.; Marx, U. A Human Lymph Node in Vitro—Challenges and Progress. *Artif. Organs* **2006**, *30*, 803–808.

371. Stachowiak, A. N.; Irvine, D. J. Inverse Opal Hydrogel-collagen Composite Scaffolds as a Supportive Microenvironment for Immune Cell Migration. *J. Biomed. Mater. Res. Part A* **2008**, *85*, 815–828.

372. Kobayashi, Y.; Watanabe, T. Gel-Trapped Lymphorganogenic Chemokines Trigger Artificial Tertiary Lymphoid Organs and Mount Adaptive Immune Responses in Vivo. *Front. Immunol.* **2016**, *7*, 316.

373. Okamoto, N.; Chihara, R.; Shimizu, C.; Nishimoto, S.; Watanabe, T. Artificial Lymph Nodes Induce Potent Secondary Immune Responses in Naive and Immunodeficient Mice. *J. Clin. Invest.* **2007**, *117*, 997–1007.

374. Suematsu, S.; Watanabe, T. Generation of a Synthetic Lymphoid Tissue–like Organoid in Mice. *Nat. Biotechnol.* **2004**, *22*, 1539.

375. Clark, R. A.; Yamanaka, K.; Bai, M.; Dowgiert, R.; Kupper, T. S. Human Skin Cells Support

Thymus-Independent T Cell Development. *J. Clin. Invest.* **2005**, *115*, 3239–3249.

376. Poznansky, M. C.; Evans, R. H.; Foxall, R. B.; Olszak, I. T.; Piascik, A. H.; Hartman, K. E.; Brander, C.; Meyer, T. H.; Pykett, M. J.; Chabner, K. T. Efficient Generation of Human T Cells from a Tissue-Engineered Thymic Organoid. *Nat. Biotechnol.* **2000**, *18*, 729.

377. Pilon-Thomas, S.; Mackay, A.; Vohra, N.; Mulé, J. J. Blockade of Programmed Death Ligand 1 Enhances the Therapeutic Efficacy of Combination Immunotherapy against Melanoma. *J. Immunol.* **2010**, *184*, 3442–3449.

378. Li, B.; Vanroey, M.; Wang, C.; Chen, T. H. T.; Korman, A.; Jooss, K. Anti-Programmed Death-1 Synergizes with Granulocyte Macrophage Colony-Stimulating Factor-Secreting Tumor Cell Immunotherapy Providing Therapeutic Benefit to Mice with Established Tumors. *Clin. Cancer Res.* **2009**, *15*, 1623–1634.

379. Vilgelm, A. E.; Johnson, D. B.; Richmond, A. Combinatorial Approach to Cancer Immunotherapy: Strength in Numbers. *J. Leukoc. Biol.* **2016**, *100*.

380. Chandra, R. A.; Wilhite, T. J.; Balboni, T. A.; Alexander, B. M.; Spektor, A.; Ott, P. A.; Ng, A. K.; Hodi, F. S.; Schoenfeld, J. D. A Systematic Evaluation of Abscopal Responses Following Radiotherapy in Patients with Metastatic Melanoma Treated with Ipilimumab. *Oncoimmunology* **2015**, *4*, 1–7.

381. Rudqvist, N.-P.; Pilones, K. A.; Lhuillier, C.; Wennerberg, E.; Sidhom, J.-W.; Emerson, R. O.; Robins, H. S.; Schneck, J.; Formenti, S. C.; Demaria, S. Radiotherapy and CTLA-4 Blockade Shape the TCR Repertoire of Tumor-Infiltrating T Cells. *Cancer Immunol. Res.* **2017**, canimm.0134.2017.

382. Victor, C. T.-S.; Rech, A. J.; Maity, A.; Rengan, R.; Pauken, K. E.; Stelekati, E.; Benci, J. L.; Xu, B.; Dada, H.; Odorizzi, P. M.; Herati, R. S.; Mansfield, K. D.; Patsch, D.; Amaravadi, R. K.; Schuchter, L. M.; Ishwaran, H.; Mick, R.; Pryma, D. a.; Xu, X.; *et al.* Radiation and Dual Checkpoint Blockade Activate Non-Redundant Immune Mechanisms in Cancer. *Nature* **2015**, *520*, 373–377.

383. Zamarin, D.; Holmgaard, R. B.; Subudhi, S. K.; Park, J. S.; Mansour, M.; Palese, P.; Merghoub, T.; Wolchok, J. D.; Allison, J. P. Localized Oncolytic Virotherapy Overcomes Systemic Tumor

Resistance to Immune Checkpoint Blockade Immunotherapy. *Sci Transl Med* **2014**, *6*, 226ra32.

384. Butte, M. J.; Keir, M. E.; Phamduy, T. B.; Sharpe, A. H.; Freeman, G. J.; Sharpe, H. PD-L1 Interacts Specifically with B7-1 to Inhibit T Cell Proliferation. *Immunity* **2009**, *27*, 111–122.

385. Rollins, M. R.; Gibbons Johnson, R. M. CD80 Expressed by CD8 + T Cells Contributes to PD-L1-Induced Apoptosis of Activated CD8 + T Cells. *J. Immunol. Res.* **2017**, *2017*, 1–6.

386. Ostrand-Rosenberg, S.; Horn, L. A.; Alvarez, J. A. Novel Strategies for Inhibiting PD-1 Pathway-Mediated Immune Suppression While Simultaneously Delivering Activating Signals to Tumor-Reactive T Cells. *Cancer Immunol. Immunother.* **2015**, *64*, 1287–1293.

387. Messenheimer, D. J.; Jensen, S. M.; Afentoulis, M. E.; Wegmann, K. W.; Feng, Z.; Friedman, D. J.; Gough, M. J.; Urba, W. J.; Fox, B. A. Timing of PD-1 Blockade Is Critical to Effective Combination Immunotherapy with Anti-OX40. *Clin. Cancer Res.* **2017**, *23*, 6165–6177.

388. Mullard, A. IDO Takes a Blow, 2018.

389. Moynihan, K. D.; Opel, C. F.; Szeto, G. L.; Tzeng, A.; Zhu, E. F.; Engreitz, J. M.; Williams, R. T.; Rakhra, K.; Zhang, M. H.; Rothschilds, A. M. Eradication of Large Established Tumors in Mice by Combination Immunotherapy That Engages Innate and Adaptive Immune Responses. *Nat. Med.* **2016**, *22*, 1402.

390. Rosenberg, S. A.; Restifo, N. P.; Yang, J. C.; Morgan, R. A.; Dudley, M. E. Adoptive Cell Transfer: A Clinical Path to Effective Cancer Immunotherapy. *Nat. Rev. Cancer* **2008**, *8*, 299.

391. Perrault, S. D.; Walkey, C.; Jennings, T.; Fischer, H. C.; Chan, W. C. W. Mediating Tumor Targeting Efficiency of Nanoparticles through Design. *Nano Lett.* **2009**, *9*, 1909–1915.

392. Molnár, E.; Swamy, M.; Holzer, M.; Beck-García, K.; Worch, R.; Thiele, C.; Guigas, G.; Boye, K.; Luescher, I. F.; Schwille, P. Cholesterol and Sphingomyelin Drive Ligand-Independent T-Cell Antigen Receptor Nanoclustering. *J. Biol. Chem.* **2012**, *287*, 42664–42674.

393. Taylor, M. J.; Husain, K.; Gartner, Z. J.; Mayor, S.; Vale, R. D. A DNA-Based T Cell Receptor Reveals a Role for Receptor Clustering in Ligand Discrimination. *Cell* **2017**, *169*, 108–119.

394. Ruvinsky, I.; Sharon, N.; Lerer, T.; Cohen, H.; Stolovich-Rain, M.; Nir, T.; Dor, Y.; Zisman, P.; Meyuhas, O. Ribosomal Protein S6 Phosphorylation Is a Determinant of Cell Size and Glucose Homeostasis. *Genes Dev.* **2005**, *19*, 2199–2211.

395. Turner, M. S.; Kane, L. P.; Morel, P. A. Dominant Role of Antigen Dose in CD4+ Foxp3+ Regulatory T Cell Induction and Expansion. *J. Immunol.* **2009**, *183*, 4895–4903.

396. Katzman, S. D.; O'Gorman, W. E.; Villarino, A. V; Gallo, E.; Friedman, R. S.; Krummel, M. F.; Nolan, G. P.; Abbas, A. K. Duration of Antigen Receptor Signaling Determines T-Cell Tolerance or Activation. *Proc. Natl. Acad. Sci.* **2010**, 201010560.

397. Zheng, Y.; Collins, S. L.; Lutz, M. A.; Allen, A. N.; Kole, T. P.; Zarek, P. E.; Powell, J. D. A Role for Mammalian Target of Rapamycin in Regulating T Cell Activation versus Anergy. *J. Immunol.* **2007**, *178*, 2163–2170.

398. Zheng, Y.; Delgoffe, G. M.; Meyer, C. F.; Chan, W.; Powell, J. D. Anergic T Cells Are Metabolically Anergic. *J. Immunol.* **2009**, jimmunol-0803510.

399. Ugel, S.; Zoso, A.; De Santo, C.; Li, Y.; Marigo, I.; Zanovello, P.; Scarselli, E.; Cipriani, B.; Oelke, M.; Schneck, J. P. In Vivo Administration of Artificial Antigen-Presenting Cells Activates Low-Avidity T Cells for Treatment of Cancer. *Cancer Res.* **2009**, 8–5472.

400. Lanzavecchia, A.; Iezzi, G.; Viola, A. From TCR Engagement to T Cell Activation. *Cell* **1999**, *96*, 1–4.

401. Sykulev, Y.; Brunmark, A.; TsoMIDES, T. J.; Kageyama, S.; Jackson, M.; Peterson, P. A.; Eisen, H. N. High-Affinity Reactions between Antigen-Specific T-Cell Receptors and Peptides Associated with Allogeneic and Syngeneic Major Histocompatibility Complex Class I Proteins. *Proc. Natl. Acad. Sci.* **1994**, *91*, 11487–11491.

402. Brower, R. C.; England, R.; Takeshita, T.; Kozlowski, S.; Margulies, D. H.; Berzofsky, J. A.; Delisi, C. Minimal Requirements for Peptide Mediated Activation of CD8+ CTL. *Mol. Immunol.* **1994**, *31*, 1285–1293.

403. Christinck, E. R.; Luscher, M. A.; Barber, B. H.; Williams, D. B. Peptide Binding to Class I MHC on Living Cells and Quantitation of Complexes Required for CTL Lysis. *Nature* **1991**, *352*, 67.

404. Demotz, S.; Grey, H. M.; Sette, A. The Minimal Number of Class II MHC-Antigen Complexes Needed for T Cell Activation. *Science (80-.).* **1990**, *249*, 1028–1030.

405. Harding, C. V; Unanue, E. R. Quantitation of Antigen-Presenting Cell MHC Class II/Peptide Complexes Necessary for T-Cell Stimulation. *Nature* **1990**, *346*, 574.

406. Kimachi, K.; Croft, M.; Grey, H. M. The Minimal Number of Antigen-major Histocompatibility Complex Class II Complexes Required for Activation of Naive and Primed T Cells. *Eur. J. Immunol.* **1997**, *27*, 3310–3317.

407. Purbhoo, M. A.; Irvine, D. J.; Huppa, J. B.; Davis, M. M. T Cell Killing Does Not Require the Formation of a Stable Mature Immunological Synapse. *Nat. Immunol.* **2004**, *5*, 524.

408. Reay, P. A.; Matsui, K.; Haase, K.; Wulfing, C.; Chien, Y.-H.; Davis, M. M. Determination of the Relationship between T Cell Responsiveness and the Number of MHC-Peptide Complexes Using Specific Monoclonal Antibodies. *J. Immunol.* **2000**, *164*, 5626–5634.

409. Sykulev, Y.; Joo, M.; Vturina, I.; Tsomides, T. J.; Eisen, H. N. Evidence That a Single Peptide–MHC Complex on a Target Cell Can Elicit a Cytolytic T Cell Response. *Immunity* **1996**, *4*, 565–571.

410. Bray, D.; Levin, M. D.; Morton-Firth, C. J. Receptor Clustering as a Cellular Mechanism to Control Sensitivity. *Nature* **1998**, *393*, 85.

411. Recouvreux, P.; Lenne, P.-F. Molecular Clustering in the Cell: From Weak Interactions to Optimized Functional Architectures. *Curr. Opin. Cell Biol.* **2016**, *38*, 18–23.

412. Aleksic, M.; Dushek, O.; Zhang, H.; Shenderov, E.; Chen, J.-L.; Cerundolo, V.; Coombs, D.; van der Merwe, P. A. Dependence of T Cell Antigen Recognition on T Cell Receptor-Peptide MHC Confinement Time. *Immunity* **2010**, *32*, 163–174.

413. Huang, J.; Zarnitsyna, V. I.; Liu, B.; Edwards, L. J.; Jiang, N.; Evavold, B. D.; Zhu, C. The Kinetics of Two-Dimensional TCR and PMHC Interactions Determine T-Cell Responsiveness. *Nature* **2010**, *464*, 932.

414. Huppa, J. B.; Axmann, M.; Mörtelmaier, M. A.; Lillemeier, B. F.; Newell, E. W.; Brameshuber, M.; Klein, L. O.; Schütz, G. J.; Davis, M. M. TCR–peptide–MHC Interactions in Situ Show Accelerated Kinetics and Increased Affinity. *Nature* **2010**, *463*, 963.

415. Lee, K.-H.; Holdorf, A. D.; Dustin, M. L.; Chan, A. C.; Allen, P. M.; Shaw, A. S. T Cell Receptor Signaling Precedes Immunological Synapse Formation. *Science (80-.).* **2002**, *295*, 1539–1542.

416. Jenkins, M. K.; Moon, J. J. The Role of Naive T Cell Precursor Frequency and Recruitment in Dictating Immune Response Magnitude. *J. Immunol.* **2012**, *188*, 4135–4140.

417. Restifo, N. P.; Dudley, M. E.; Rosenberg, S. A. Adoptive Immunotherapy for Cancer: Harnessing the T Cell Response. *Nat. Rev. Immunol.* **2012**, *12*, 269.

418. Hurwitz, A. A.; Watkins, S. K. Immune Suppression in the Tumor Microenvironment: A Role for Dendritic Cell-Mediated Tolerization of T Cells. *Cancer Immunol. Immunother.* **2012**, *61*, 289–293.

419. Ma, Y.; Shurin, G. V; Gutkin, D. W.; Shurin, M. R. Tumor Associated Regulatory Dendritic Cells. In *Seminars in cancer biology*; Elsevier, 2012; Vol. 22, pp. 298–306.

420. Mosser, D. M.; Edwards, J. P. Exploring the Full Spectrum of Macrophage Activation. *Nat. Rev. Immunol.* **2008**, *8*, 958.

421. Chapuis, A. G.; Ragnarsson, G. B.; Nguyen, H. N.; Chaney, C. N.; Pufnock, J. S.; Schmitt, T. M.; Duerkopp, N.; Roberts, I. M.; Pogosov, G. L.; Ho, W. Y. Transferred WT1-Reactive CD8+ T Cells Can Mediate Antileukemic Activity and Persist in Post-Transplant Patients. *Sci. Transl. Med.* **2013**, *5*, 174ra27-174ra27.

422. Dudley, M. E.; Wunderlich, J.; Nishimura, M. I.; Yu, D.; Yang, J. C.; Topalian, S. L.; Schwartzentruber, D. J.; Hwu, P.; Marincola, F. M.; Sherry, R. Adoptive Transfer of Cloned Melanoma-Reactive T Lymphocytes for the Treatment of Patients with Metastatic Melanoma. *J. Immunother.* **2001**, *24*, 363–373.

423. Mackensen, A.; Meidenbauer, N.; Vogl, S.; Laumer, M.; Berger, J.; Andreesen, R. Phase I Study of Adoptive T-Cell Therapy Using Antigen-Specific CD8+ T Cells for the Treatment of Patients with Metastatic Melanoma. *J. Clin. Oncol.* **2006**, *24*, 5060–5069.

424. Fang, R. H.; Zhang, L. Nanoparticle-Based Modulation of the Immune System. *Annu. Rev. Chem. Biomol. Eng.* **2016**, *7*, 305–326.

425. Durai, M.; Krueger, C.; Ye, Z.; Cheng, L.; Mackensen, A.; Oelke, M.; Schneck, J. P. In Vivo Functional Efficacy of Tumor-Specific T Cells Expanded Using HLA-Ig Based Artificial Antigen Presenting Cells (AAPC). *Cancer Immunol. Immunother.* **2009**, *58*, 209–220.

426. Berger, C.; Jensen, M. C.; Lansdorp, P. M.; Gough, M.; Elliott, C.; Riddell, S. R. Adoptive Transfer of Effector CD8+ T Cells Derived from Central Memory Cells Establishes Persistent T Cell Memory in Primates. *J. Clin. Invest.* **2008**, *118*, 294–305.

427. Rizzuto, G. A.; Merghoub, T.; Hirschhorn-Cymerman, D.; Liu, C.; Lesokhin, A. M.; Sahawneh, D.; Zhong, H.; Panageas, K. S.; Perales, M.-A.; Altan-Bonnet, G. Self-Antigen–specific CD8+ T Cell Precursor Frequency Determines the Quality of the Antitumor Immune Response. *J. Exp. Med.* **2009**, *206*, 849–866.

428. Cai, H.; Muller, J.; Depoil, D.; Mayya, V.; Sheetz, M. P.; Dustin, M. L.; Wind, S. J. Full Control of Ligand Positioning Reveals Spatial Thresholds for T Cell Receptor Triggering. *Nat. Nanotechnol.* **2018**.

429. Stone, J. D.; Artyomov, M. N.; Chervin, A. S.; Chakraborty, A. K.; Eisen, H. N.; Kranz, D. M. Interaction of Streptavidin-Based Peptide–MHC Oligomers (Tetramers) with Cell-Surface TCRs. *J. Immunol.* **2011**, *187*, 6281–6290.

430. McCloskey, K. E.; Chalmers, J. J.; Zborowski, M. Magnetic Cell Separation: Characterization of Magnetophoretic Mobility. *Anal. Chem.* **2003**, *75*, 6868–6874.

431. Plouffe, B. D.; Murthy, S. K.; Lewis, L. H. Fundamentals and Application of Magnetic Particles in Cell Isolation and Enrichment: A Review. *Reports Prog. Phys.* **2014**, *78*, 16601.

432. Hammink, R.; Mandal, S.; Eggermont, L. J.; Nooteboom, M.; Willems, P. H. G. M.; Tel, J.; Rowan, A. E.; Figdor, C. G.; Blank, K. G. Controlling T-Cell Activation with Synthetic Dendritic Cells Using the Multivalency Effect. *ACS omega* **2017**, *2*, 937–945.

433. Cebecauer, M.; Guillaume, P.; Hozák, P.; Mark, S.; Everett, H.; Schneider, P.; Luescher, I. F. Soluble MHC-Peptide Complexes Induce Rapid Death of CD8+ CTL. *J. Immunol.* **2005**, *174*, 6809–6819.

434. Guillaume, P.; Legler, D. F.; Boucheron, N.; Doucey, M.-A.; Cerottini, J.-C.; Luescher, I. F. Soluble Major Histocompatibility Complex-Peptide Octamers with Impaired CD8 Binding Selectively Induce Fas-Dependent Apoptosis. *J. Biol. Chem.* **2003**, *278*, 4500–4509.

435. Rodrigue-Gervais, I. G.; Rigsby, H.; Jouan, L.; Sauvé, D.; Sékaly, R.-P.; Willems, B.; Lamarre, D. Dendritic Cell Inhibition Is Connected to Exhaustion of CD8+ T Cell Polyfunctionality during Chronic Hepatitis C Virus Infection. *J. Immunol.* **2010**, ji_0902522.

436. Ciuffreda, D.; Comte, D.; Cavassini, M.; Giostra, E.; Bühler, L.; Perruchoud, M.; Heim, M. H.; Battegay, M.; Genné, D.; Mulhaupt, B. Polyfunctional HCV-specific T-cell Responses Are

Associated with Effective Control of HCV Replication. *Eur. J. Immunol.* **2008**, *38*, 2665–2677.

437. Chithrani, B. D.; Ghazani, A. A.; Chan, W. C. W. Determining the Size and Shape Dependence of Gold Nanoparticle Uptake into Mammalian Cells. *Nano Lett.* **2006**, *6*, 662–668.

438. Jiang, W.; Kim, B. Y. S.; Rutka, J. T.; Chan, W. C. W. Nanoparticle-Mediated Cellular Response Is Size-Dependent. *Nat. Nanotechnol.* **2008**, *3*, 145.

439. Griffiths, G. M.; Tsun, A.; Stinchcombe, J. C. The Immunological Synapse: A Focal Point for Endocytosis and Exocytosis. *J. Cell Biol.* **2010**, *189*, 399–406.

440. Martínez-Martín, N.; Fernández-Arenas, E.; Cemerski, S.; Delgado, P.; Turner, M.; Heuser, J.; Irvine, D. J.; Huang, B.; Bustelo, X. R.; Shaw, A. T Cell Receptor Internalization from the Immunological Synapse Is Mediated by TC21 and RhoG GTPase-Dependent Phagocytosis. *Immunity* **2011**, *35*, 208–222.

441. Osborne, D. G.; Wetzel, S. A. Trogocytosis Results in Sustained Intracellular Signaling in CD4+ T Cells. *J. Immunol.* **2012**, 1201507.

442. Pollack, S. M.; Jones, R. L.; Farrar, E. A.; Lai, I. P.; Lee, S. M.; Cao, J.; Pillarisetty, V. G.; Hoch, B. L.; Gullett, A.; Bleakley, M. Tetramer Guided, Cell Sorter Assisted Production of Clinical Grade Autologous NY-ESO-1 Specific CD8+ T Cells. *J. Immunother. cancer* **2014**, *2*, 36.

443. Newell, E. W.; Davis, M. M. Beyond Model Antigens: High-Dimensional Methods for the Analysis of Antigen-Specific T Cells. *Nat. Biotechnol.* **2014**, *32*, 149.

444. Hickey, J. W.; Kosmides, A. K.; Schneck, J. P. Chapter Six - Engineering Platforms for T Cell Modulation. In *Biology of T Cells - Part A*; Galluzzi, L.; Rudqvist, N.-P. B. T.-I. R. of C. and M. B., Eds.; Academic Press, 2018; Vol. 341, pp. 277–362.

445. Tsai, S.; Shameli, A.; Yamanouchi, J.; Clemente-Casares, X.; Wang, J.; Serra, P.; Yang, Y.; Medarova, Z.; Moore, A.; Santamaria, P. Reversal of Autoimmunity by Boosting Memory-like Autoregulatory T Cells. *Immunity* **2010**, *32*, 568–580.

446. Ott, P. A.; Hu, Z.; Keskin, D. B.; Shukla, S. A.; Sun, J.; Bozym, D. J.; Zhang, W.; Luoma, A.; Giobbie-Hurder, A.; Peter, L.; Chen, C.; Olive, O.; Carter, T. A.; Li, S.; Lieb, D. J.; Eisenhaure, T.; Gjini, E.; Stevens, J.; Lane, W. J.; *et al.* An Immunogenic Personal Neoantigen Vaccine for Patients with Melanoma. *Nature* **2017**, *547*, 217.

447. Davis, M. M.; Bjorkman, P. J. T-Cell Antigen Receptor Genes and T-Cell Recognition. *Nature* **1988**, *334*, 395.

448. Altman, J. D.; Moss, P. A. H.; Goulder, P. J. R.; Barouch, D. H.; McHeyzer-Williams, M. G.; Bell, J. I.; McMichael, A. J.; Davis, M. M. Phenotypic Analysis of Antigen-Specific T Lymphocytes. *Science (80-.).* **1996**, *274*, 94–96.

449. Han, Q.; Bradshaw, E. M.; Nilsson, B.; Hafler, D. A.; Love, J. C. Multidimensional Analysis of the Frequencies and Rates of Cytokine Secretion from Single Cells by Quantitative Microengraving. *Lab Chip* **2010**, *10*, 1391–1400.

450. Betts, M. R.; Brenchley, J. M.; Price, D. A.; De Rosa, S. C.; Douek, D. C.; Roederer, M.; Koup, R. A. Sensitive and Viable Identification of Antigen-Specific CD8+ T Cells by a Flow Cytometric Assay for Degranulation. *J. Immunol. Methods* **2003**, *281*, 65–78.

451. Frentsch, M.; Arbach, O.; Kirchhoff, D.; Moewes, B.; Worm, M.; Rothe, M.; Scheffold, A.; Thiel, A. Direct Access to CD4+ T Cells Specific for Defined Antigens According to CD154 Expression. *Nat. Med.* **2005**, *11*, 1118.

452. Newell, E. W.; Sigal, N.; Bendall, S. C.; Nolan, G. P.; Davis, M. M. Cytometry by Time-of-Flight Shows Combinatorial Cytokine Expression and Virus-Specific Cell Niches within a Continuum of CD8+ T Cell Phenotypes. *Immunity* **2012**, *36*, 142–152.

453. Day, C. L.; Seth, N. P.; Lucas, M.; Appel, H.; Gauthier, L.; Lauer, G. M.; Robbins, G. K.; Szczepiorkowski, Z. M.; Casson, D. R.; Chung, R. T.; Bell, S.; Harcourt, G.; Walker, B. D.; Klenerman, P.; Wucherpfennig, K. W. Ex Vivo Analysis of Human Memory CD4 T Cells Specific for Hepatitis C Virus Using MHC Class II Tetramers. *J. Clin. Invest.* **2003**, *112*, 831–842.

454. Hickey, J. W.; Isser, A. Y.; Vicente, F. P.; Warner, S. B.; Mao, H.-Q.; Schneck, J. P. Efficient Magnetic Enrichment of Antigen-Specific T Cells by Engineering Particle Properties. *Biomaterials* **2018**.

455. Rodenko, B.; Toebes, M.; Hadrup, S. R.; Van Esch, W. J. E.; Molenaar, A. M.; Schumacher, T. N. M.; Ovaa, H. Generation of Peptide–MHC Class I Complexes through UV-Mediated Ligand Exchange. *Nat. Protoc.* **2006**, *1*, 1120.

456. Hadrup, S. R.; Bakker, A. H.; Shu, C. J.; Andersen, R. S.; Van Veluw, J.; Hombrink, P.;

Castermans, E.; thor Straten, P.; Blank, C.; Haanen, J. B. Parallel Detection of Antigen-Specific T-Cell Responses by Multidimensional Encoding of MHC Multimers. *Nat. Methods* **2009**, *6*, 520.

457. Newell, E. W.; Klein, L. O.; Yu, W.; Davis, M. M. Simultaneous Detection of Many T-Cell Specificities Using Combinatorial Tetramer Staining. *Nat. Methods* **2009**, *6*, 497.

458. Gee, M. H.; Han, A.; Lofgren, S. M.; Beausang, J. F.; Mendoza, J. L.; Birnbaum, M. E.; Bethune, M. T.; Fischer, S.; Yang, X.; Gomez-Eerland, R. Antigen Identification for Orphan T Cell Receptors Expressed on Tumor-Infiltrating Lymphocytes. *Cell* **2018**, *172*, 549–563.

459. Hickey, J. W.; Isser, A. Y.; Vicente, F. P.; Warner, S. B.; Mao, H.-Q.; Schneck, J. P. Efficient Magnetic Enrichment of Antigen-Specific T Cells by Engineering Particle Properties. *Biomaterials* **2018**, *187*, 105–116.

460. Abiko, K.; Matsumura, N.; Hamanishi, J.; Horikawa, N.; Murakami, R.; Yamaguchi, K.; Yoshioka, Y.; Baba, T.; Konishi, I.; Mandai, M. IFN-γ from Lymphocytes Induces PD-L1 Expression and Promotes Progression of Ovarian Cancer. *Br. J. Cancer* **2015**, *112*, 1501.

461. Sahin, U.; Derhovanessian, E.; Miller, M.; Kloke, B.-P.; Simon, P.; Lower, M.; Bukur, V.; Tadmor, A. D.; Luxemburger, U.; Schrors, B.; Omokoko, T.; Vormehr, M.; Albrecht, C.; Paruzynski, A.; Kuhn, A. N.; Buck, J.; Heesch, S.; Schreeb, K. H.; Muller, F.; *et al.* Personalized RNA Mutanome Vaccines Mobilize Poly-Specific Therapeutic Immunity against Cancer. *Nature* **2017**, *547*, 222–226.

462. Ahmadzadeh, M.; Johnson, L. A.; Heemskerk, B.; Wunderlich, J. R.; Dudley, M. E.; White, D. E.; Rosenberg, S. A. Tumor Antigen–specific CD8 T Cells Infiltrating the Tumor Express High Levels of PD-1 and Are Functionally Impaired. *Blood* **2009**, *114*, 1537–1544.

463. Wherry, E. J.; Teichgräber, V.; Becker, T. C.; Masopust, D.; Kaech, S. M.; Antia, R.; Von Andrian, U. H.; Ahmed, R. Lineage Relationship and Protective Immunity of Memory CD8 T Cell Subsets. *Nat. Immunol.* **2003**, *4*, 225.

464. Adams, J. C.; Watt, F. M. Fibronectin Inhibits the Terminal Differentiation of Human Keratinocytes. *Nature* **1989**, *340*, 307.

465. Watt, F. M. Terminal Differentiation of Epidermal Keratinocytes. *Curr. Opin. Cell Biol.* **1989**, *1*, 1107–1115.

466. Lynch, M. P.; Stein, J. L.; Stein, G. S.; Lian, J. B. The Influence of Type I Collagen on the Development and Maintenance of the Osteoblast Phenotype in Primary and Passaged Rat Calvarial Osteoblasts: Modification of Expression of Genes Supporting Cell Growth, Adhesion, and Extracellular Matrix Mineralizatio. *Exp. Cell Res.* **1995**, *216*, 35–45.

467. BISSELL, M. J.; BARCELLOS-HOFF, M. H. The Influence of Extracellular Matrix on Gene Expression: Is Structure the Message? *J Cell Sci* **1987**, *1987*, 327–343.

468. Gretz, J. E.; Anderson, A. O.; Shaw, S. Cords, Channels, Corridors and Conduits: Critical Architectural Elements Facilitating Cell Interactions in the Lymph Node Cortex. *Immunol. Rev.* **1997**, *156*, 11–24.

469. Ayroldi, E.; Cannarile, L.; Migliorati, G.; Bartoli, A.; Nicoletti, I.; Riccardi, C. CD44 (Pgp-1) Inhibits CD3 and Dexamethasone-Induced Apoptosis. *Blood* **1995**, *86*, 2672–2678.

470. Pozzi, A.; Wary, K. K.; Giancotti, F. G.; Gardner, H. A. Integrin A1β1 Mediates a Unique Collagen-Dependent Proliferation Pathway in Vivo. *J. Cell Biol.* **1998**, *142*, 587–594.

471. Petrie, H. T. Cell Migration and the Control of Post-Natal T-Cell Lymphopoiesis in the Thymus. *Nat. Rev. Immunol.* **2003**, *3*, 859.

472. Engler, A. J.; Sen, S.; Sweeney, H. L.; Discher, D. E. Matrix Elasticity Directs Stem Cell Lineage Specification. *Cell* **2006**, *126*, 677–689.

473. Trappmann, B.; Gautrot, J. E.; Connelly, J. T.; Strange, D. G. T.; Li, Y.; Oyen, M. L.; Stuart, M. A. C.; Boehm, H.; Li, B.; Vogel, V. Extracellular-Matrix Tethering Regulates Stem-Cell Fate. *Nat. Mater.* **2012**, *11*, 642.

474. Yeung, T.; Georges, P. C.; Flanagan, L. A.; Marg, B.; Ortiz, M.; Funaki, M.; Zahir, N.; Ming, W.; Weaver, V.; Janmey, P. A. Effects of Substrate Stiffness on Cell Morphology, Cytoskeletal Structure, and Adhesion. *Cell Motil. Cytoskeleton* **2005**, *60*, 24–34.

475. Fu, J.; Wang, Y.-K.; Yang, M. T.; Desai, R. A.; Yu, X.; Liu, Z.; Chen, C. S. Mechanical Regulation of Cell Function with Geometrically Modulated Elastomeric Substrates. *Nat. Methods* **2010**, *7*, 733.

476. DeLong, S. A.; Moon, J. J.; West, J. L. Covalently Immobilized Gradients of BFGF on Hydrogel Scaffolds for Directed Cell Migration. *Biomaterials* **2005**, *26*, 3227–3234.

477. Lee, S.-H.; Moon, J. J.; West, J. L. Three-Dimensional Micropatterning of Bioactive Hydrogels via

Two-Photon Laser Scanning Photolithography for Guided 3D Cell Migration. *Biomaterials* **2008**, *29*, 2962–2968.

478. Lutolf, M. P.; Lauer-Fields, J. L.; Schmoekel, H. G.; Metters, A. T.; Weber, F. E.; Fields, G. B.; Hubbell, J. A. Synthetic Matrix Metalloproteinase-Sensitive Hydrogels for the Conduction of Tissue Regeneration: Engineering Cell-Invasion Characteristics. *Proc. Natl. Acad. Sci.* **2003**, *100*, 5413–5418.

479. Kloxin, A. M.; Kasko, A. M.; Salinas, C. N.; Anseth, K. S. Photodegradable Hydrogels for Dynamic Tuning of Physical and Chemical Properties. *Science (80-.).* **2009**, *324*, 59–63.

480. Föger, N.; Marhaba, R.; Zöller, M. CD44 Supports T Cell Proliferation and Apoptosis by Apposition of Protein Kinases. *Eur. J. Immunol.* **2000**, *30*, 2888–2899.

481. Jackson, D. G. Immunological Functions of Hyaluronan and Its Receptors in the Lymphatics. *Immunol. Rev.* **2009**, *230*, 216–231.

482. Toole, B. P. Hyaluronan: From Extracellular Glue to Pericellular Cue. *Nat. Rev. Cancer* **2004**, *4*, 528.

483. Entwistle, J.; Hall, C. L.; Turley, E. A. HA Receptors: Regulators of Signalling to the Cytoskeleton. *J. Cell. Biochem.* **1996**, *61*, 569–577.

484. Ponta, H.; Sherman, L.; Herrlich, P. A. CD44: From Adhesion Molecules to Signalling Regulators. *Nat. Rev. Mol. cell Biol.* **2003**, *4*, 33.

485. Lei, Y.; Gojgini, S.; Lam, J.; Segura, T. The Spreading, Migration and Proliferation of Mouse Mesenchymal Stem Cells Cultured inside Hyaluronic Acid Hydrogels. *Biomaterials* **2011**, *32*, 39–47.

486. Shu, X. Z.; Ahmad, S.; Liu, Y.; Prestwich, G. D. Synthesis and Evaluation of Injectable, in Situ Crosslinkable Synthetic Extracellular Matrices for Tissue Engineering. *J. Biomed. Mater. Res. Part A* **2006**, *79*, 902–912.

487. Peattie, R. A.; Nayate, A. P.; Firpo, M. A.; Shelby, J.; Fisher, R. J.; Prestwich, G. D. Stimulation of in Vivo Angiogenesis by Cytokine-Loaded Hyaluronic Acid Hydrogel Implants. *Biomaterials* **2004**, *25*, 2789–2798.

488. Li, X.; Liu, X.; Cui, L.; Brunson, C.; Zhao, W.; Bhat, N. R.; Zhang, N.; Wen, X. Engineering an in

Situ Crosslinkable Hydrogel for Enhanced Remyelination. *FASEB J.* **2013**, *27*, 1127–1136.

489. Tan, H.; Ramirez, C. M.; Miljkovic, N.; Li, H.; Rubin, J. P.; Marra, K. G. Thermosensitive Injectable Hyaluronic Acid Hydrogel for Adipose Tissue Engineering. *Biomaterials* **2009**, *30*, 6844–6853.

490. Hirsch, S.; Guo, J.; Reiter, R.; Papazoglou, S.; Kroencke, T.; Braun, J.; Sack, I. MR Elastography of the Liver and the Spleen Using a Piezoelectric Driver, Single-shot Wave-field Acquisition, and Multifrequency Dual Parameter Reconstruction. *Magn. Reson. Med.* **2014**, *71*, 267–277.

491. Miyaji, K.; Furuse, A.; Nakajima, J.; Kohno, T.; Ohtsuka, T.; Yagyu, K.; Oka, T.; Omata, S. The Stiffness of Lymph Nodes Containing Lung Carcinoma Metastases: A New Diagnostic Parameter Measured by a Tactile Sensor. *Cancer Interdiscip. Int. J. Am. Cancer Soc.* **1997**, *80*, 1920–1925.

492. Li, Y.-C.; Chen, B.-M.; Wu, P.-C.; Cheng, T.-L.; Kao, L.-S.; Tao, M.-H.; Lieber, A.; Roffler, S. R. Cutting Edge: Mechanical Forces Acting on T Cells Immobilized via the TCR Complex Can Trigger TCR Signaling. *J. Immunol.* **2010**, ji_0900775.

493. Ilani, T.; Vasiliver-Shamis, G.; Vardhana, S.; Bretscher, A.; Dustin, M. L. T Cell Antigen Receptor Signaling and Immunological Synapse Stability Require Myosin IIA. *Nat. Immunol.* **2009**, *10*, 531.

494. Massia, S. P.; Hubbell, J. A. An RGD Spacing of 440 Nm Is Sufficient for Integrin Alpha V Beta 3-Mediated Fibroblast Spreading and 140 Nm for Focal Contact and Stress Fiber Formation. *J. Cell Biol.* **1991**, *114*, 1089–1100.

495. Chaudhuri, O.; Gu, L.; Darnell, M.; Klumpers, D.; Bencherif, S. A.; Weaver, J. C.; Huebsch, N.; Mooney, D. J. Substrate Stress Relaxation Regulates Cell Spreading. *Nat. Commun.* **2015**, *6*, 6365.

496. Wülfing, C.; Sjaastad, M. D.; Davis, M. M. Visualizing the Dynamics of T Cell Activation: Intracellular Adhesion Molecule 1 Migrates Rapidly to the T Cell/B Cell Interface and Acts to Sustain Calcium Levels. *Proc. Natl. Acad. Sci.* **1998**, *95*, 6302–6307.

497. Day, A. J.; Prestwich, G. D. Hyaluronan-Binding Proteins: Tying up the Giant. *J. Biol. Chem.* **2002**, *277*, 4585–4588.

498. Sanders, M. E.; Makgoba, M. W.; Sharrow, S. O.; Stephany, D.; Springer, T. A.; Young, H. A.; Shaw, S. Human Memory T Lymphocytes Express Increased Levels of Three Cell Adhesion Molecules (LFA-3, CD2, and LFA-1) and Three Other Molecules (UCHL1, CDw29, and Pgp-1)

and Have Enhanced IFN-Gamma Production. *J. Immunol.* **1988**, *140*, 1401–1407.

499. Graham, V. A.; Marzo, A. L.; Tough, D. F. A Role for CD44 in T Cell Development and Function during Direct Competition between CD44+ and CD44–cells. *Eur. J. Immunol.* **2007**, *37*, 925–934.

500. Budd, R. C.; Cerottini, J.-C.; MacDonald, H. R. Phenotypic Identification of Memory Cytolytic T Lymphocytes in a Subset of Lyt-2+ Cells. *J. Immunol.* **1987**, *138*, 1009–1013.

501. Budd, R. C.; Cerottini, J. C.; Horvath, C.; Bron, C.; Pedrazzini, T.; Howe, R. C.; MacDonald, H. R. Distinction of Virgin and Memory T Lymphocytes. Stable Acquisition of the Pgp-1 Glycoprotein Concomitant with Antigenic Stimulation. *J. Immunol.* **1987**, *138*, 3120–3129.

502. Mendoza, M. C.; Er, E. E.; Blenis, J. The Ras-ERK and PI3K-MTOR Pathways: Cross-Talk and Compensation. *Trends Biochem. Sci.* **2011**, *36*, 320–328.

503. Lefebvre, D. C.; Lai, J. C. Y.; Maeshima, N.; Ford, J. L.; Wong, A. S. L.; Cross, J. L.; Johnson, P. CD44 Interacts Directly with Lck in a Zinc-Dependent Manner. *Mol. Immunol.* **2010**, *47*, 1882–1889.

504. Rossy, J.; Williamson, D. J.; Gaus, K. How Does the Kinase Lck Phosphorylate the T Cell Receptor? Spatial Organization as a Regulatory Mechanism. *Front. Immunol.* **2012**, *3*, 167.

505. Pollizzi, K. N.; Patel, C. H.; Sun, I.-H.; Oh, M.-H.; Waickman, A. T.; Wen, J.; Delgoffe, G. M.; Powell, J. D. MTORC1 and MTORC2 Selectively Regulate CD8+ T Cell Differentiation. *J. Clin. Invest.* **2015**, *125*, 2090–2108.

506. Tan, J. T.; Ernst, B.; Kieper, W. C.; LeRoy, E.; Sprent, J.; Surh, C. D. Interleukin (IL)-15 and IL-7 Jointly Regulate Homeostatic Proliferation of Memory Phenotype CD8+ Cells but Are Not Required for Memory Phenotype CD4+ Cells. *J. Exp. Med.* **2002**, *195*, 1523–1532.

507. Klebanoff, C. A.; Gattinoni, L.; Torabi-Parizi, P.; Kerstann, K.; Cardones, A. R.; Finkelstein, S. E.; Palmer, D. C.; Antony, P. A.; Hwang, S. T.; Rosenberg, S. A. Central Memory Self/Tumor-Reactive CD8+ T Cells Confer Superior Antitumor Immunity Compared with Effector Memory T Cells. *Proc. Natl. Acad. Sci.* **2005**, *102*, 9571–9576.

508. Betts, M. R.; Nason, M. C.; West, S. M.; De Rosa, S. C.; Migueles, S. A.; Abraham, J.; Lederman, M. M.; Benito, J. M.; Goepfert, P. A.; Connors, M. HIV Nonprogressors Preferentially Maintain Highly Functional HIV-Specific CD8+ T Cells. *Blood* **2006**, *107*, 4781–4789.

509. Frebel, H.; Richter, K.; Oxenius, A. How Chronic Viral Infections Impact on Antigen-specific T-cell Responses. *Eur. J. Immunol.* **2010**, *40*, 654–663.

510. Rosenberg, S. A.; Spiess, P.; Lafreniere, R. A New Approach to the Adoptive Immunotherapy of Cancer with Tumor-Infiltrating Lymphocytes. *Science (80-.).* **1986**, *233*, 1318–1321.

511. Yee, C.; Thompson, J. A.; Byrd, D.; Riddell, S. R.; Roche, P.; Celis, E.; Greenberg, P. D. Adoptive T Cell Therapy Using Antigen-Specific CD8+ T Cell Clones for the Treatment of Patients with Metastatic Melanoma: In Vivo Persistence, Migration, and Antitumor Effect of Transferred T Cells. *Proc. Natl. Acad. Sci.* **2002**, *99*, 16168–16173.

512. Li, X.; Liu, X.; Josey, B.; Chou, C. J.; Tan, Y.; Zhang, N.; Wen, X. Short Laminin Peptide for Improved Neural Stem Cell Growth. *Stem Cells Transl. Med.* **2014**, *3*, 662–670.

513. Oelke, M.; Moehrle, U.; Chen, J.-L.; Behringer, D.; Cerundolo, V.; Lindemann, A.; Mackensen, A. Generation and Purification of CD8+ Melan-A-Specific Cytotoxic T Lymphocytes for Adoptive Transfer in Tumor Immunotherapy. *Clin. Cancer Res.* **2000**, *6*, 1997–2005.

514. Wrzesinski, C.; Paulos, C. M.; Kaiser, A.; Muranski, P.; Palmer, D. C.; Gattinoni, L.; Yu, Z.; Rosenberg, S. A.; Restifo, N. P. Increased Intensity Lymphodepletion Enhances Tumor Treatment Efficacy of Adoptively Transferred Tumor-Specific T Cells. *J. Immunother. (Hagerstown, Md. 1997)* **2010**, *33*, 1.

515. Hickey, J. W.; Schneck, J. P. Enrich and Expand Rare Antigen-Specific T Cells with Magnetic Nanoparticles. *JoVE (Journal Vis. Exp.* **2018**, e58640.

Curriculum Vitae

John W Hickey was born in 1988 in Mapleton, UT, USA.

John did his undergraduate work at Brigham Young University in the School of Engineering in Provo, UT in Chemical Engineering. At Brigham Young University, he conducted research in the lab of Dr. John Harb on methods to fabricate nanowires from DNA origami, in the lab of Dr. William Pitt on the effects of eye contact cleaning solutions on sorption of lipids and proteins, and in the lab of Dr. David Bearrs on the development of novel BRAF inhibitors for cancer therapy. John was awarded the most outstanding chemical engineering student award each year from his class of chemical engineering.

John began his Ph.D. in biomedical engineering at Johns Hopkins School of Medicine in 2013 and joined Dr. Jonathan Schneck's lab in 2014. During his Ph.D., he has co-authored several publications and presented at local and national conferences with 9 oral and 7 poster presentations. He mentored 6 graduate, 8 undergraduate, and 3 high school students, helping several receive research awards and present at national conferences. He developed 3 new university undergraduate and graduate classes and an Android/Apple-based education app. He was also Vice President of a Non-profit that facilitates and fosters interdisciplinary education, entrepreneurship, and medical innovation. John was also awarded an NSF graduate research fellowship, INBT CNTC fellowship, Discovery Award, ARCS fellowship, and was named a 2019 Siebel Scholar.